UNCLASSIFIED

AD NUMBER
AD813344
LIMITATION CHANGES
TO: **Approved for public release; distribution is unlimited.**
FROM: **Distribution authorized to U.S. Gov't. agencies and their contractors; Critical Technology; JAN 1967. Other requests shall be referred to Air Force Flight Dynamics Laboratory, ATTN: FDTE, Wright-Patterson AFB, OH 45433.**
AUTHORITY
AFFDL ltr dtd 8 Mar 1972

THIS PAGE IS UNCLASSIFIED

AD0813344

AFFDL-TR-66-113

A FEASIBILITY STUDY FOR THE DEVELOPMENT OF A FATIGUE DAMAGE INDICATOR

ROBERT S. HORNE

LOCKHEED-GEORGIA COMPANY

TECHNICAL REPORT AFFDL-TR-66-113

JANUARY 1967

20080815 154

This document is subject to special export controls and each transmittal to foreign governments or foreign nationals may be made only with prior approval of the Air Force Flight Dynamics Laboratory (AFSC), Wright-Patterson Air Force Base, Ohio 45433, ATTN: FDTE.

AIR FORCE FLIGHT DYNAMICS LABORATORY
RESEARCH AND TECHNOLOGY DIVISION
AIR FORCE SYSTEMS COMMAND
WRIGHT-PATTERSON AIR FORCE BASE, OHIO

NOTICES

When Government drawings, specifications, or other data are used for any purpose other than in connection with a definitely related Government procurement operation, the United States Government thereby incurs no responsibility nor any obligation whatsoever; and the fact that the Government may have formulated, furnished, or in any way supplied the said drawings, specifications, or other data, is not to be regarded by implication or otherwise as in any manner licensing the holder or any other person or corporation, or conveying any rights or permission to manufacture, use, or sell any patented invention that may in any way be related thereto.

Copies of this report should not be returned to the Research and Technology Division unless return is required by security considerations, contractual obligations, or notice on a specific document.

400 - March 1967 - CO192 - 27-606

AD 813344

A FEASIBILITY STUDY FOR THE DEVELOPMENT OF A FATIGUE DAMAGE INDICATOR

ROBERT S. HORNE

LOCKHEED-GEORGIA COMPANY

This document is subject to special export controls and each transmittal to foreign governments or foreign nationals may be made only with prior approval of the Air Force Flight Dynamics Laboratory (AFSC), Wright-Patterson Air Force Base, Ohio 45433, ATTN: FDTE.

FOREWORD

This feasibility study was performed by the Lockheed-Georgia Company of Marietta, Georgia under Air Force Contract No. 33(615)-2505. The contract was initiated under Project No. 1347 "Structural Testing of Flight Vehicles" and Task No. 134702 "Measurement of Structural Response".

The work was supervised and this report was prepared by Robert S. Horne, Project Engineer. This project was initiated by the Air Force Flight Dynamics Laboratory, Research and Technology Division and was administered under the technical coordination of Mr. James L. Mullineaux, FDTE.

The electronic equipment was designed and fabricated by the advanced Electronic Development Laboratory at Lockheed-Georgia Company. Acknowledgment is also given for the helpful assistance and technical guidance provided by Mr. O. L. Freyre, Specialist, Structural Methods Group and Mr. W. M. McGee, Specialist, Development Test Laboratory.

Many of the items compared in this report were commercial items that were not developed or manufactured to meet Government specifications, to withstand the tests to which they were subjected, or to operate as applied during this study. Any failure to meet the objectives of this study is no reflection on any of the commercial items discussed herein or on any manufacturer.

This document was submitted by the author in June, 1966 for publication as an RTD Technical Report.

This report covers work conducted from June, 1965 to June, 1966 and is the final report under Contract AF 33(615)-2505. The contractors report number is ER-7981.

This Technical Report has been reviewed and is approved.

James C. Horsley Jr

JAMES C. HORSLEY, JR., MAJOR, USAF
Chief, Experimental Mechanics Branch
Structures Division

ABSTRACT

The feasibility of developing a fatigue damage evaluation system was investigated. The investigations concern optimizing the behavior characteristics of a primary sensor, integrating it with an electronic system, and adapting both for usage on the primary structure of an aircraft. The primary detecting element selected has the appearance of a foil strain gage and is bonded to the structure in much the same manner as a strain gage. The major variation between the conventional strain gage and the fatigue sensor is the manner of conditioning the foil material and method of utilization. The investigation was logically divided into three laboratory test phases, that is (1) evaluation of fatigue sensors on coupons, (2) evaluation on typical aircraft structure, and (3) design and demonstration of a breadboard model. The objective of the first phase was to determine and optimize the behavior characteristics of the primary detecting element under a variety of environmental conditions. The practical application of the sensor was then evaluated on C-130E upper wing panels which were subjected to a specified number of simulated flight hours to produce a fatigue failure. Natural progression to a more complex structure consisted of installing and evaluating sensor capabilities on a full scale C-141 empennage and aft fuselage. This structure was subjected to simulated flight hours by spectrum loading with servo loading equipment. The electronic phase was designed as the final element of an electro-structural inspection system for determining the fatigue status of an airframe. This electronic hardware consists of a module for indicating the sensor's change in resistance. From the results obtained, it can be concluded that the system shows excellent promise as a method for determining an aircraft's degree of exposure to repeated load occurrences. For "long life" transport aircraft such as the C-5A, the system offers a much better means for determining the fatigue status of an airframe than simply stating its number of accumulated flight hours.

TABLE OF CONTENTS

		Page
I	Introduction	1
II	Basic Theory	3
III	Test Specimens, Test Equipment, Laboratory Test Methods & Procedures	5
	3.0 Test Specimens Phase I	5
	3.1 Test Equipment Phase I	10
	3.2 Test Equipment Phase II	12
	3.3 Test Instrumentation	12
	3.4 Laboratory Test Methods and Procedures	14
IV	Test Results	
	4.1 Phase I Coupon Tests	19
	4.1.1 Effect of Stress Ratio	19
	4.1.2 Threshold Sensitivity	50
	4.1.3 Weatherometry Effects	55
	4.1.4 Elevated Temperature Tests	58
	4.1.5 Low Temperature Tests	62
	4.1.6 Two load Level Tests	66
	4.1.7 Sonic Fatigue	69
	4.1.8 Summation of Irregularities	70
	4.1.9 Metallurgical Investigations	74
	4.1.10 Discussion of possible error sources	86

			PAGE
4.2	PHASE II TYPICAL AIRCRAFT STRUCTURE TESTS		90
	4.2.1	C-130E Panels	91
	4.2.2	C-141A Specimen "C"	107
	4.2.3	C-141A Specimen "B"	109
	4.2.4	K_t = 4 Splice Panels	117
4.3	PHASE III BREADBOARD MODEL		
	4.3.1	Test Specimen and Instrumentation	119
	4.3.2	Electronic Breadboard	119
	4.3.3	Mathematical Considerations	123
V.	SUMMARY AND CONCLUSION		
	5.1	Sensor Optimimization	125
	5.2	The Electronic Equipment	128
	5.3	Steps to Obtain Utilization on Fleet Aircraft	128
	5.4	Simplification of Fatigue Damage Analysis	129
VI	REFERENCES		133
VII	APPENDICES		135
	Appendix I	Installation of Fatigue Sensors	135
	Appendix II	Tabulation of Data Tables	138

LIST OF ILLUSTRATIONS

Figure		Page
1	Axial Load Fatigue Specimen With K_t = 1.0	6
2	Axial Load Fatigue Specimen With K_t = 2.72	7
3	Fatigue Damage Sensor Locations	8
4	Reversed Bending Specimen for Evaluation of Fatigue Sensors	9
5	Schematic Diagram of Axial-Load, Tuning Fork Type Fatigue Machines	11
6	Curves of Stress Level Versus Sensor Position	13
7	Tuning Fork Fatigue Machines Used for Testing Coupons	15
8	Loading Console For Loading and Monitoring of Tuning Fork Fatigue Machines	15
9	Slow Cycle Fatigue Machine Setup	16
10	Instrumentation for Controlling Loads on the Slow Cycle Machine and Measuring Fatigue Sensor Output	16
11	Temperature Control and Monitoring Equipment for Coupon Heaters	17
12	Typical Glass Rock and Quartz Lamp Heater for Elevated Temperature Tests	17
13	Instrumented Specimen With Companion Lateral Support Plates. Tension and Compression Loads are Applied Axially With Teflon Lined Support Plates to Prevent Bending	18
14	Typical Spiral Grid Installation, Centered Over the Hole Representing A K_t of 2.72 In The Specimen	18
15	Consolidation of Sensor No. 1 Curves for Various Specimen Fatigue Lives	21
16	Evaluation of Sensor Capability to Forecast Point of Failure	22
17	Evaluation of Two Types of Die Cut Sensors	23
18	Evaluation of Dentronic 204A-ST Die Cut Fatigue Sensor	24

LIST OF ILLUSTRATIONS

Figure		Page
19	Repeat of Previous Evaluations for Substantiating Data	25
20	Sensor Evaluation at a Lower Strain Level	26
21	Showing another Evaluation of Sensors with Nothing Changed Except Stress Level	27
22	Effect of Stress Ratio Upon End Resistance of Sensor	28
23	Evaluation of Sensor Repeatability	29
24	Comparison of Two Types of Sensors at a Low Stress Ratio	30
25	Sensor Evaluation at a Higher Cyclic Strain Level	31
26	Sensor Evaluation at High Strain Level and Low Frequency	32
27	Evaluation of Sensor on Specimen Fatigue Cycled in Plastic Region	33
28	Comparison of Acid Etch Gage and Die Cut Sensor	34
29	Evaluation of Sensors in Plastic Region of the Coupon	35
30	Performance Evaluation of Various Type Sensors	36
31	Sensor Behavior at a High Mean Strain Level	37
32	Evaluation at High Strain Level and Low Frequency	38
33	Sensor Evaluation at a High Strain Level and Low Frequency	39
34	Effect of Reversed Strain on Sensor End Resistance at Specimen Failure	40
35	S/N Curves of 7075-T6 @ Various Stress Ratios	41
36	Evaluation of Various Foils at a High Strain Level	42
37	Comparison of Various Types of Sensor Behavior at a High Strain Level	43
38	Comparison of High Elongation Gage & Fatigue Gage	44
39	Evaluation of Sensors Under Reversed Axial Strain	45
40	Effect of Specimen K_t = 2.72 Upon Sensor Output	46

LIST OF ILLUSTRATIONS

Figure		Page
41	Reversed Bending on Constant Strain Beam	47
42	Sensor Evaluation at a Higher Strain Level	48
43	Evaluation of 204DA-ST Sensor Under Reversed Bending	49
44A	Baldwin Spiral Grid Fatigue Sensor for Use Around Rivets	52
44B	Typical Sensor Installation on 7075-T6 Aluminum Shown After Specimen Failure. Sensor Bonded with Epy-150 and Moistureproofed with GW-1	52
45	Evaluation of Sensor After Exposure to Weatherometry	56
46	Specimen Exposed to 12 Months of Actual Georgia Weather	57
47	A Type HA204DA-ST Fatigue Sensor Installed on Titanium	60
48	Elevated Temperature Evaluation in Progress	60
49	Evaluation of Sensor on Titanium at Room Temperature	61
50	Low Temperature Evaluation of Sensor Behavior	63
51	Sensor Evaluation at -65°F	64
52	Evaluation of Sensors at -65°F	65
53	Sensor Response to Two Load Levels	67
54	Order of Loading Reversed From That Shown in Specimen No. 48	68
55	Typical Acid Etched Annealed Foil Gage Used as a Fatigue Sensor	71
56	Circles Indicate Irregularities in the Foil Strands Produced by the Acid Etching Process Visible at a Magnification of 24X.	71
57	Sequence of Oscilloscope Traces Showing the Progressive Stages of Sensor Grid Failure of Gage in Figure 58	76
58	S/N NA-01 Gage as Received from the Manufacturer Prior to Installation on the Constant Strain Beam of Figure 59	76
59	S/N Gage Mounted on Bending Specimen and Evaluated at ±1500 Micro In/In Until Gage Failure. Photo 2.2 Times Actual Size.	77

LIST OF ILLUSTRATIONS

Figure		Page
60	S/N NA-01 Strand at 1000X After Partial Removal of Epoxy Encapsulation. Armstrong Epoxy Stripper Used for Removal of Epoxy.	77
61	A Strand Section of the NA-01 S/N Gage at a Magnification of 1000X. Note the Severity of Undercutting of Strand Edge Due to Acid Etch Process of Fabrication	78
62	A Strand Failure in the Gage Shown in Figure 59 Note the Microscopic Crack Near the End Loop. The Surface Has Been Slightly Etched to Highlight The Grain Structure.	78
63	Micro Photo at 1000X of the No. 1 Sensor Used on Specimen No. 47. Crack Apparently Originated Near End Loop and Followed Grain Boundaries.	79
64	S/N Gage as Received From the Manufacturer. Photo Taken at 100X of the Bonding Side of the Gage. Shot Was Taken Through the Epoxy and Shows Bubbles in the Epoxy at Various Depths.	79
65	View of Unencapsulated Strands of Fatigue Gage at a Magnification of 50X. Oblique Lighting Used to Highlight Irregularities of the Surface. Gage in as Received Conditions Without Encapsulation.	80
66	View of Same Gage as Above at a Magnification of 200X. Gage in "As Received" Condition	80
67	Strand Photo at 500X of What Appears to be an Undesirable Area of the Strand Conductor. This Strand Shows a Variation in Foil Thickness, Transverse Scratches, and Grain Effect in the Flat Rolled Surface Plane.	81
68	View of the Same Strand at 1000X. Note the Change in Foil Thickness. Also the Appearance of Grain Effect, Although an Acid Etch Was not Used to Highlight the Grain	81
69	Photo of Fatigue Gage Strand as Received From the Manufacturer. Epoxy Encapsulation Removed by Armstrong Epoxy Stripper. Black Spots May Be Carbonized Oil, Since Oil is Sometimes Used in the Foil Rolling Process. Photo Made at 500X.	82

LIST OF ILLUSTRATIONS

Figure		Page
70	View of an Undesirable Strand Section of a 204DA-ST Sensor as Received from the Manufacturer. Although the 500X Magnification Shows Transverse Scratches, It Also Indicates the Sharp Edge Possible by Die Cutting	82
71	Photo Taken After A Fatigue Induced Failure of an NA-01 Gage. Possible Microscopic Crack in Lower Left Corner. Carapellas Reageant Used to Highlight Grain Structure.	83
72	Die Cut Foil Stock at 1500X. Surface Etched With Carapella Reageant to Obtain Relief Effect. Sub-grain Structure is Visible.	83
73	Average Installation of a 204A-ST Fatigue Sensor Shown Approximately 8 Times Actual Size. Although Excessive Solder Was Used on End Tabs, Sensor Endured 1,200,000 At ± 2100 U In/In On Coupon No. 30.	84
74	Micro Photo of Foil Stock As Used In the 204A-ST Sensor Shown at 500X. The Lines Are Finish Marks	84
75	Type 204A-ST Sensor Which Endured Over Two Million Cycles at 4000 Microstrain Before Failure. Note Radius at Strand End Loop. Magnification is 500X.	85
76	Grain Structure of a 204DA-ST At 1000X. Slight Etch With Carapellas Reagent to Emphasis Grain.	85
77	Temperature Effects Survey of 204A-ST Sensors Bonded to 7075-T6 Aluminum	88
78	Fatigue Sensor Readings on C-130E Filler Cap Panel Design I	98
79	C-130E Filler Cap Panel Design II Fatigue Sensor Readings	99
80	C-130E Filler Cap Panel Design II Fatigue Sensor Readings	100
81	C-130E Filler Cap Panel Design III Fatigue Sensor Readings	101
82	Redesign C-130E Filler Cap Panel Showing Cracks in the Riser Extension Adjacent to the Filler Cap	102

LIST OF ILLUSTRATIONS

Figure		Page
83	Other End of Riser Showing Cracks of a Similar Nature	102
84	Redesign C-130E Filler Cap Panel Showing a Crack Extending Out From a Rivet	103
85	Equipment Used for Recording Strain Gage Outputs During the Stress Survey	103
86	Redesign C-130E W.S. 1.5 Panel Showing Fatigue Crack at One Corner of the Access Door	104
87	Close Up View of Crack Which Runs From Door Fastener to the Rivet	104
88	C-130E W.S. 120 Filler Cutout	105
89	Sensor Installation on C-141 Specimen "B"	110
90	Empennage Fatigue Sensor Location	113
91	Laboratory Structural Integrity Specimen	115
92	Full Scale Laboratory Specimen Instrumented with Fatigue Sensors	116
93	Instrumentation of Constant Strain Beam (NAS 942) Theoretical $K_t = 1.9$	120
94	Block Diagram of Electronic Equipment	121
95	Electronic Phase of the Fatigue Evaluation System	122
96	Progressive Sequence of Activities to Obtain Utilization on Service Aircraft	131

LIST OF TABLES

TABLE		PAGE
I	TABULATION OF COUPON TESTS	138
II	SUMMARY OF FATIGUE SENSOR MATERIALS EVALUATED	146
III	TABULATION OF SENSOR DATA	148

SYMBOLS AND TERMINOLOGY

The following constitutes a list of terms and symbols used throughout the report. As far as possible, the terms used are compatible with those in MIL- HDBK-5. Some terms have been modified due to conflicts with terms recently coined in the laboratory.

Terminology

Acid Etch - A chemical process designed to dissolve or otherwise remove an unwanted portion of foil material leaving a particular grid configuration.

Alternating-Mean Ratio - Ratio of the alternating stress to the mean stress.

A of 1.000 = no gusts
A of 0.818 = high gusts
A of 0.333 = low gusts
A of ∞ = completely reversed loading

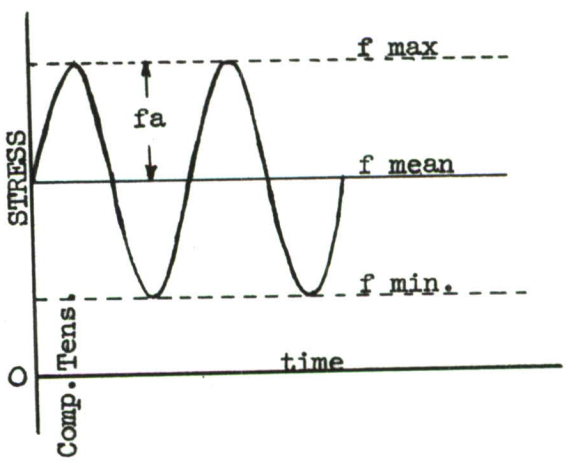

Constantan - Most common alloy used in the manufacture of strain gages. Known under various trade names the most common of which is "Advance" composed of 43% nickel and 57% copper.

Coupon; Specimen - Test article or structure; terms used interchangeably.

Discontinuity - Abrupt change in load path such as holes, notches, rivets or re-entrant corners.

Dislocations - Misfits in atomic spacing.

Gross Stress - Stress computed using overall dimensions without regard to internal discontinuities.

High Cycle Fatigue - Failure of specimen in more than 10^4 cycles.

Karma - Trade name for a Driver Harris material which is composed of 74% nickel, 20% chromium, 3% aluminum and 3% iron.

Low Cycle Fatigue	- Failure of specimen in less than 10^4 cycles.
Pass	- Sequence of cyclic load conditions which constitute a fixed number of simulated flight hours.
Prestrain	- Residual strain resulting from strain cycle above the porportional limit.
Sensor Grid	- That portion of the sensor which is most sensitive to mechanical forces and produces an electrical resistance change.
Slip	- Parallel displacements or translations of the crystal lattice elements.
Spectrum	- A predetermined grouping of fatigue loading conditions to be applied in sequence.
Supersensitivity	- Sophisticated way of saying the foil grid of a gage has failed. The failure consists of microscopic cracks in the strained portion of the foil which will intermittantly open and close. The phenomena is described in detail in Reference 7.
Threshold Sensitivity	- The endurance limit, or strain level at which the foil begins to yield, resulting in an increased electrical resistance change.
Zero Shift	- An increase in electrical resistance of the foil due to fatigue induced work hardening which is independent of the direction of strain.

SYMBOLS

A	-	Stress ratio of $\frac{fa}{f\ mean}$
CPM	-	Cycles per minute.
D	-	Damage ratio
E	-	Modulus of elasticity.
F	-	Frequency
G-A-G	-	Ground-air-ground
G.F.	-	Gage factor
KSI	-	Kips (1000 pounds) per square inch.
K_t	-	Theoretical stress concentration factor.
N	-	Number of cycles to fatigue failure.
P	-	Force or load in lbs.
Δ R	-	Permanent zero shift resistance change in the fatigue sensor (ohms, $\mu\epsilon$) due to fatigue induced strain hardening.
T	-	Temperature (^{o}F)
T.C.R	-	Temperature coefficient of resistance.
a, b,	-	Exponents
cps	-	Cycles per second
ϵ	-	Strain
fa	-	Alternating stress in KSI,
f max	-	Maximum stress in KSI, fatigue
f mean	-	Mean stress in KSI, fatigue
n	-	Number of cycles the specimen has endured at any stage of its fatigue life.
ppm	-	Parts per million

r	-	Radius in inches
t	-	Thickness of specimen in inches.
μ	-	Micro units or 10^{-6}
w	-	Width of specimen in inches
Δ	-	Incremental change

SECTION I

INTRODUCTION

Although many volumes have been written about structural fatigue, and laboratory test programs have provided much information regarding the statistical nature of fatigue failures, present state-of-the-art instrumentation does not permit a direct measurement of fatigue damage. Direct measurement of fatigue damage requires a determination of the metallurgical condition of the structure, and while this has been attempted by x-ray defraction, ultrasonic techniques, etc., these methods can only be successful under ideal laboratory conditions and at best, leaves something to be desired.

A desirable extension of the present state-of-the-art would be to measure directly a structures degree of exposure to repeated load occurrences. If this were done in a cumulative manner, a qualitative assessment of structural fatigue damage could be obtained. A measurement of this nature should provide a much better criteria for determining the fatigue status of an airframe than an expression of aircraft flight hours. The validity of using work hardenable foils as a device for totalizing repeated strains was previously investigated by Lockheed during a Company-funded project known as Research Authorization 3224. This Company-funded work was conducted concurrently with other test programs and indicated considerable more promise for assessing fatigue damage than any of a wide variety of methods previously investigated. The program resulted in a total system concept which was designated as a "Semi-Automatic Fatigue Evaluation"(SAFE)system. The feasibility of such a system was further investigated under an Air Force funded contract known as AF 33(615)-2505.

The user of foil strain gages during structural testing of components in a fatigue environment was often irritated by a "zero shift" in his gages. The phenomena is even more pronounced if one subjects a high elongation strain gage to a fatigue environment. Of course the manufacturer never designed his high elongation gage to be used for fatigue applications, however its response under repeated cyclic loading is of particular interest. This phenomena may be regarded as advantageous since anytime one variable changes in relation to another variable, the potential for a transducer exists.

In any planned system for the assessment of fatigue damage in an aircraft structure, it is very easy to select the detecting element as the most important part of the system. Consequently, a major effort was directed toward optimizing the sensor, since no amount of sophisticated end instrumentation can correct for an erroneous or inadequate sensing element. In general, without stating how high is high, or how low is low, it was desirable that the bonded fatigue detecting device should possess the following qualities.

1. High output
2. Low threshold sensitivity
3. High fatigue life

Generally speaking, a foil gage and a high fatigue life do not go together, especially at the higher strain levels. However, in a "trade off" one is often forced to accept a less desirable characteristic in order to obtain the more desirable ones.

At the onset of the R&D study, discussions among Lockheed personnel directly involved in the program produced two schools of thought in regard to utilizing the sensor on flight aircraft in a practical manner.

1. One concept was that if at structural failure the fatigue sensor end resistance was independent of stress ratio, environmental conditions, etc., one could approximate the K_t of the area under consideration and predetermine what the resistance of the sensor should be at structural failure.

2. Another philosophy, in case the first concept was not valid, was that a calibration could be performed on a laboratory specimen in order to obtain baseline data with which to forecast fatigue allowables for similar structure.

The laboratory test program was designed to realistically evaluate the capabilities of the fatigue sensor in regard to these two modes of utilization. It was felt that concept #1 could best be evaluated on coupons concurrent with optimization of the sensor, while concept # 2 would be evaluated on typical aircraft structure, operating under simulated aerodynamic conditions. In this respect, the C-130E wing panels were selected as structure representing a design which produced higher operating strain levels and the C-141 empennage laboratory fatigue specimen as a structure designed to operate at minimum strain levels.

In regard to concept #1, it is well known that many factors such as stress ratio, order of repeated load occurrences, temperature variations, corrosion and other environmental condition all affect the fatigue life of a structure.

It was not known what the end resistance of the fatigue sensor would be upon failure of a structure subjected to these variables, all other things being equal. The Phase I tests were designed to evaluate the effect of all of these variables one at a time. In this respect, simple tension-tension coupons seemed the logical choice; therefore, sixty some coupons, as shown in Table I, were used to evaluate and compare sensors under a variety of conditions.

The standard approach to a technical problem has in the past been established as; logical reasoning, experimental verification, and practical application. The same sequence of activities has been employed in this program.

SECTION II

BASIC THEORY

The fatigue sensors basic principle of operation involves metals or alloys which can be cold worked by strain hardening. Cold working requires a "moving of metal" and is usually mechanically induced. Any strain action will induce strain hardening into ductile metals which are hardenable by cold working. Dislocation theory in metallurgy contends that cold work in the metal lattice blocks the motion of the crystal boundaries by raising the stress level necessary to allow slip to occur, resulting in an electrical resistance change of the material. Basically, the physicists (Reference 2) seem to agree that a scattering of electrons as a result of dislocations causes a change in resistivity. With the above principal in mind fatigue sensors constructed of fully annealed constantan are bonded to a material or structure under surveillance. The phenomena utilized then, is the resistance change due to fatigue induced strain hardening of a thin foil sensor bonded to an article under investigation. The application of the fatigue sensor is predicated on the theory that correlation factors can be established which relates its change in resistance value (R) to the fatigue condition of the structure to which it is bonded.

The fatigue sensor does not function as a strain gage, in fact, the gage factor of the constantan foil is not considered, although one does exist. The configuration, electrical resistance, and bonding techniques are nearly identical with those of strain gages, however, this is a convenience rather than a necessity. The sensor utilizes its memory capacity to store the accumulated strain history as opposed to a strain gage which can only function as a device to measure instantaneous strain amplitudes. The objective is to take advantage of every material behavior phenomena which can be used to assist in determining the metallurgical condition of that material.

Experience with strain gages has led to the conclusion that a change in grid cross sectional area is associated with a change in electrical resistance. With the fatigue sensor, the total resistance change is greater than that created by the change in cross section.

Optical comparison of the bonded sensors BEFORE and AFTER strain hardening have shown no dimensional change, even though a relatively large resistance change has occurred. Lord Kelvin has stated that the following formula can be applied for determining the electrical resistance of a material.

$$R = \rho \frac{L}{A}$$

Where:

R = Resistance (ohms)
ρ = Specific resistance constant (ohms/cu. cm)
L = Length of conductor (cm)
A = Area of cross section (sq. cm)

Since "L" and "A" have not changed as indicated by the optical comparator, then it follows that the constant " ρ " must have experienced a permanent change. Further investigation reveals that if cold work due to strain hardening does not result in a reduction of cross section area to provide the resistance increase, it must have been caused by a scattering of electrons. Reference 2 indicates that the increase in resistivity is caused by a scattering of electrons as a result of dislocations due to plastic deformation of the foil. This is conceivable since the specimen is operated well below its elastic limit while the sensor material is operated well into its plastic region, as illustrated in the stress-strain curves shown below. Microphotographs taken of the foil before and after strain hardening have indicated no rotation or fold over of the grain structure.

The diagram below shows a somewhat unorthodox stress-strain curve for the constantan foil. The stress axis does not represent the stress level in the foil itself, but rather the stress in an aluminum specimen to produce the indicated strain output from the sensor. The stress level of 10 KSI, representing sensor threshold sensitivity is not the stress level in the constantan foil but stress present in the aluminum. Since the modulus of constantan is given as 23.3×10^6 PSI its stress level will be more than twice that of the aluminum. According to normal conventions, compression strain will yield stresses in the negative direction, however, the resistance change of the sensor will still be positive or the same direction as resistance changes resulting from tensile strains.

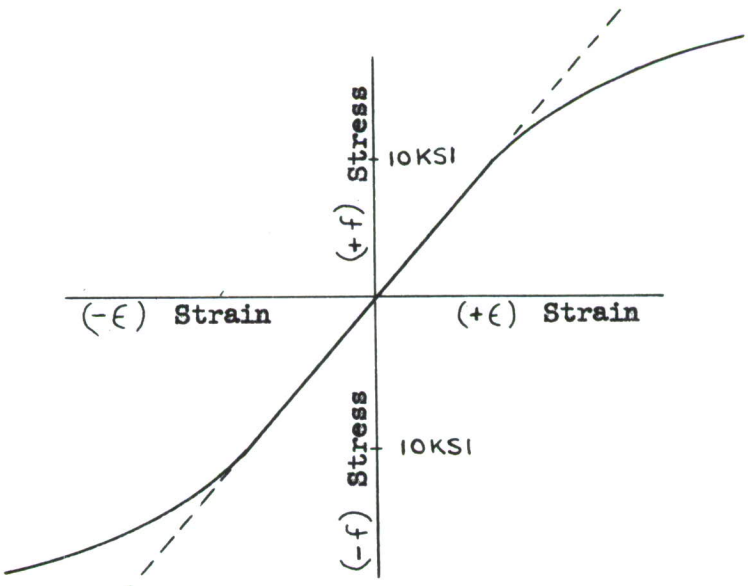

SECTION III

TEST EQUIPMENT, SPECIMENS, & PROCEDURES

3.0 TEST SPECIMENS - PHASE I

The test specimens used for Phase I are shown in Figures 1 through 4 and are fabricated from 7075-T6 bare aluminum and 8 Al - 1 Mo - 1V titanium alloy. Most designers of modern aircraft structures tend to utilize 7075-T6 aluminum as opposed to 2024-T4 or other alloys because wing applications are considered most significant and the higher compression allowables of 7075-T6 result in a lighter wing structure. The tensile strength of the 7075-T6 is also higher than most other aluminum alloys.

It is realized that the specimen shown in Figure 1 will have a strain gradient along it's test section, however the error along the 1/4 inch gage length of the sensor will be no greater than errors due to loading or misalignment of the sensor. This same condition could be present in an aircraft structure, but since the sensors are installed in the same location from coupon to coupon the validity of the sensor evaluation is not affected. The specimens as fabricated in accordance with the diagram of Figure 1 were "miked" and inspected for scratches or nicks in the test section. Any questionable specimens were rejected prior to instrumenting. Also some uninstrumented specimens were used for machine calibration, which accounts for some missing specimen numbers in the data section. All Phase I specimens, as shown in Figure 2 were checked for correct dimensions and an optical comparator used to insure a correct hole size for a calculated stress concentration factor (K_t) of 2.72. The object of this procedure is to insure optimum manufacturing tolerances and reduce scatter in the fatigue life of the specimens.

Although the majority of instrumented coupons were evaluated under axial loading conditions, a few constant moment bending beams were also evaluated in order to correlate the effect of bending strains versus axial strains upon the sensor.

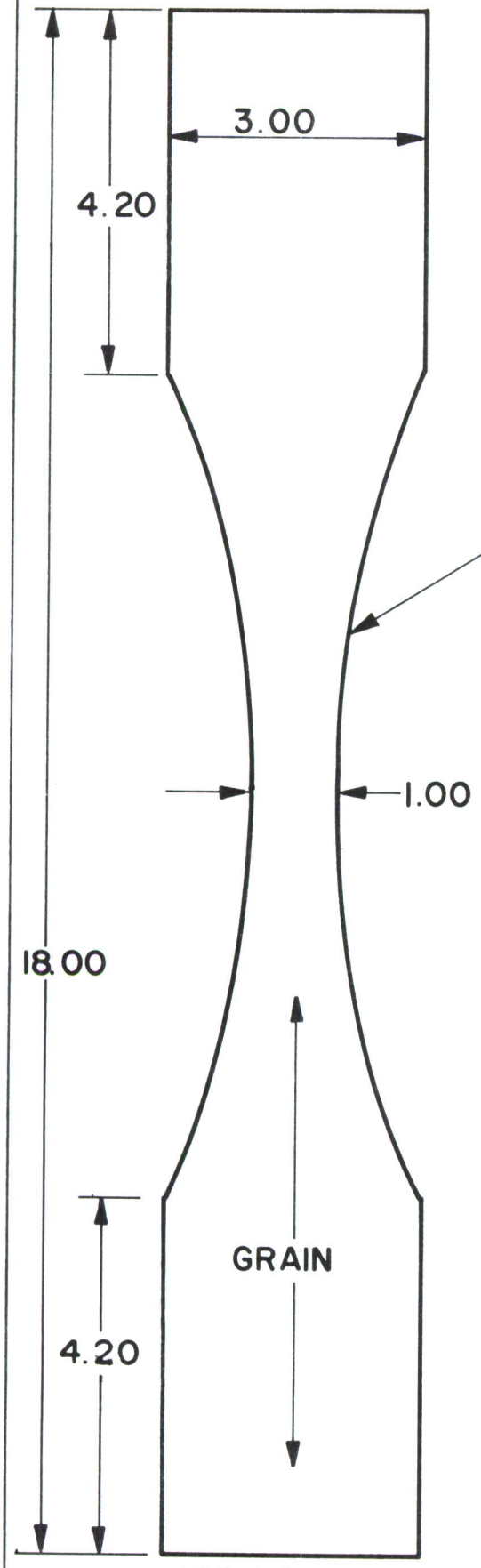

NOTE:

1. 1/2 SCALE
2. AVOID SURFACE SCRATCHES
3. 63 FINISH ON EDGES
4. SPECIMEN IDENTIFIED BY ELECTRO ETCH NUMBER ON EITHER END.

MATERIAL:

75 REQUIRED OF BARE 7075-T6 SHEET 0.100 THICK

8 REQUIRED OF Ti-8Al-1Mo-1V SHEET 0.060 THICK (AMS 4911)

FIG. 1 AXIAL LOAD FATIGUE SPECIMEN WITH $K_t = 1.0$

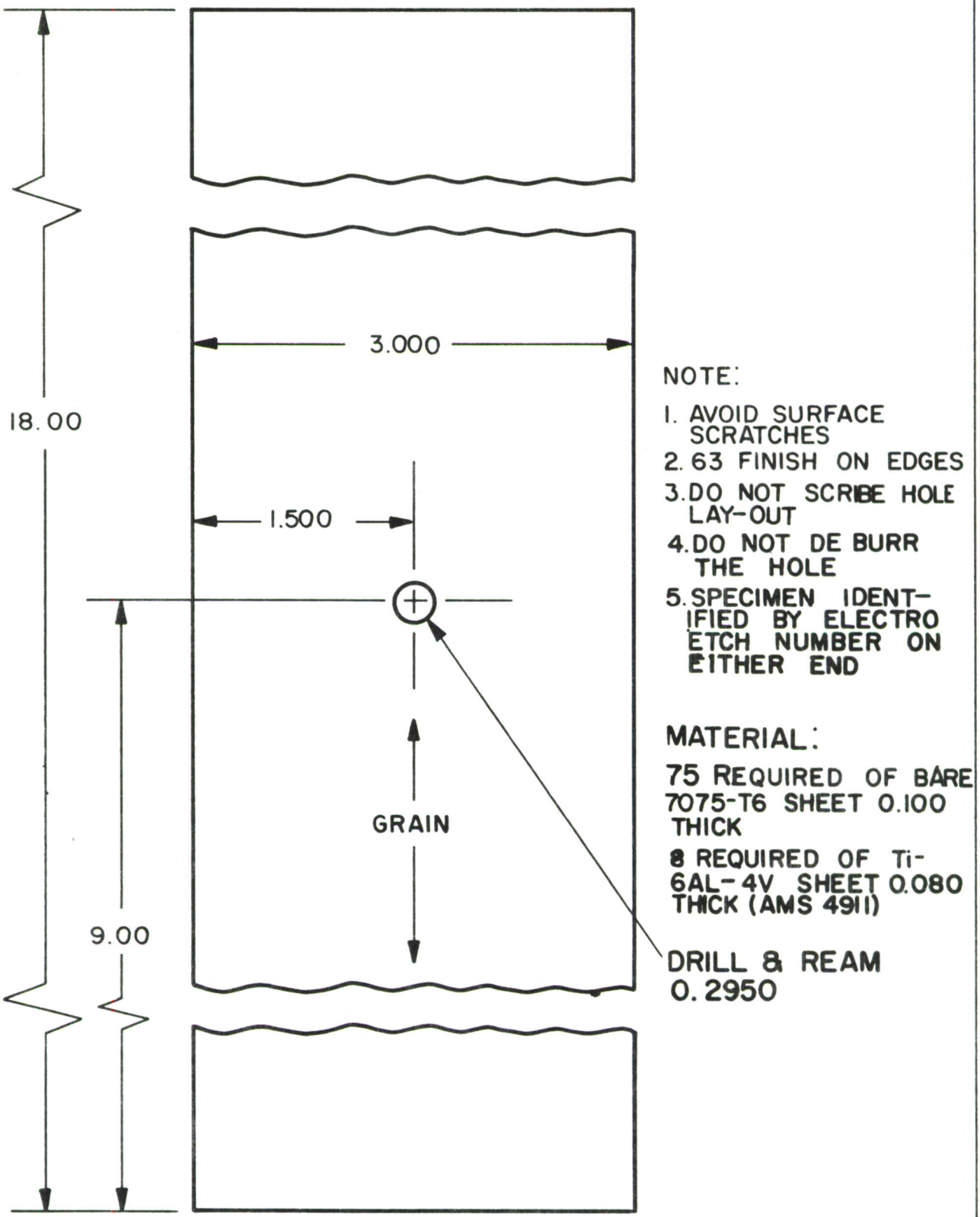

FIG. 2 AXIAL LOAD FATIGUE SPECIMEN WITH $K_t = 2.72$

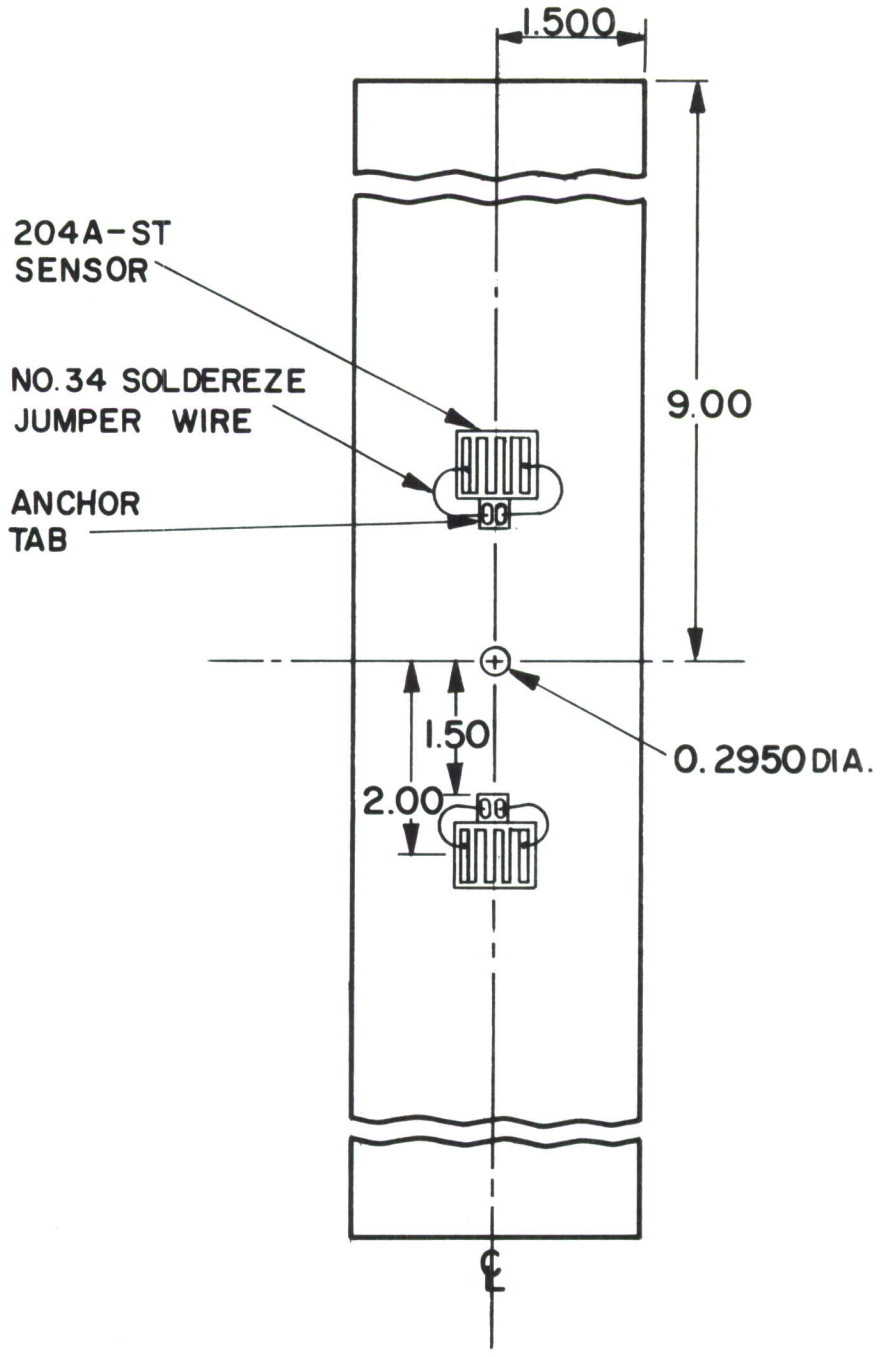

NOTES:

1. DO NOT SCRIBE SENSOR LOCATIONS
2. FOR COMPRESSION SPECIMENS, LEADS MUST EXTEND FROM THE TAB NORMAL TO THE PLAN OF SPECIMEN.
3. SENSORS MAY ALSO BE INSTALLED BACK TO BACK FOR A TOTAL OF FOUR PER SPECIMEN.

FIG. 3 FATIGUE DAMAGE SENSOR LOCATIONS

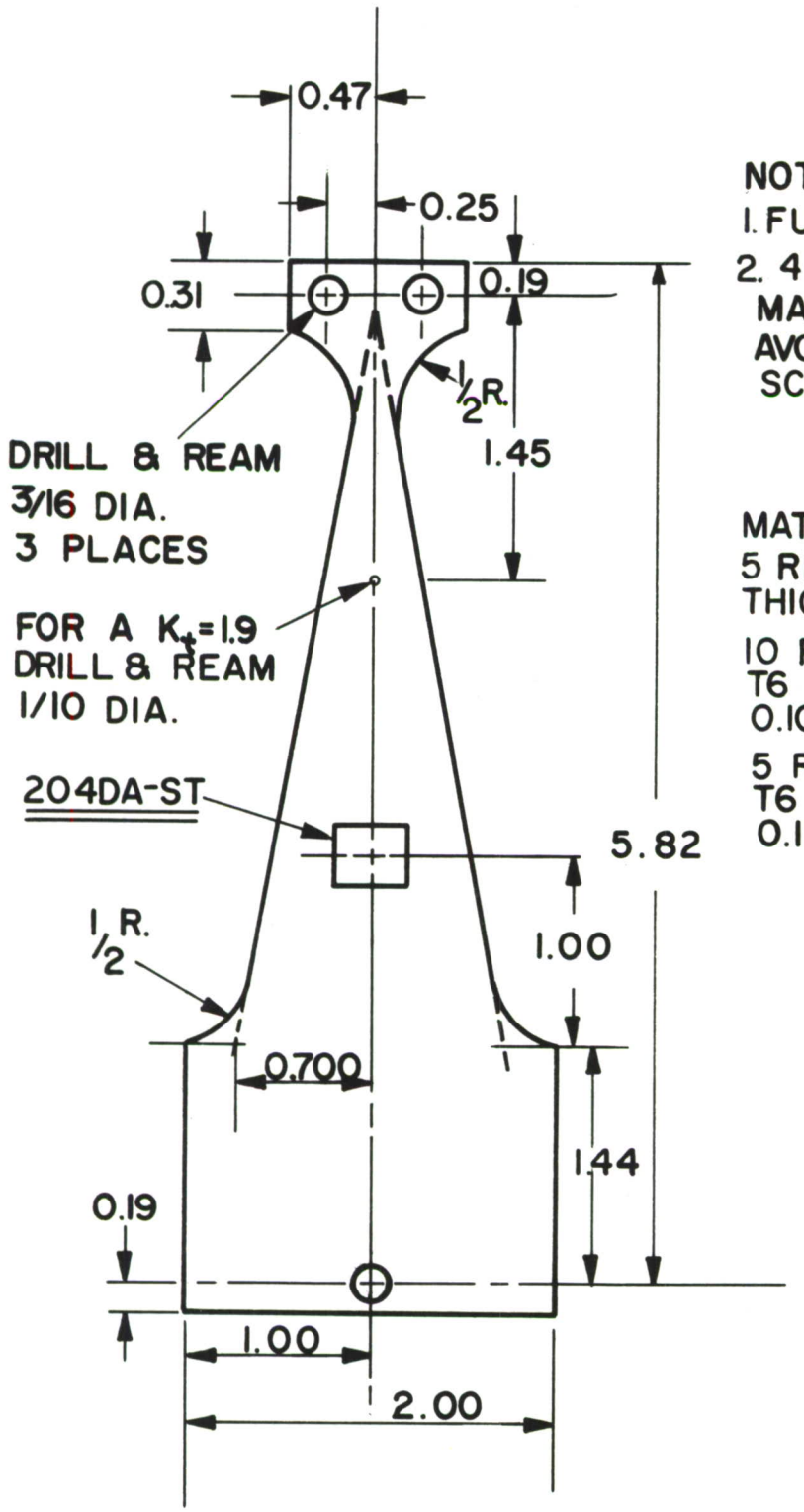

NOTE:
1. FULL SCALE
2. 40 FINISH ON MACHINED SURFACES, AVOID SURFACE SCRATCHES

MATERIALS:
5 REQUIRED OF 0.10 THICK INCONEL X(K_t=1.00)
10 REQUIRED OF 7075-T6 BARE ALUMINUM 0.100 THICK (K_t=1.90)
5 REQIRED OF 7075-T6 BARE ALUMINUM 0.100 THICK (K_t=1.00)

FIG. 4 REVERSED BENDING SPECIMEN FOR EVALUATION OF FATIGUE SENSORS

3.1 TEST EQUIPMENT PHASE I

Lockheed designed axial-load, tuning fork type fatigue machines were used for all Phase I axial loading tests. A schematic diagram of a typical machine with associated instrumentation appears in Figure 5. These machines have a static capacity of 15,000 pounds and a dynamic capacity of ± 10,000 pounds at a cycling rate of 1500 to 2200 cycles per minute. Specimen mean load is applied with a hydraulic actuator while sinusoidal alternating load is applied by a variable eccentric mass in the form of a wheel attached to one arm of the machine. The eccentric wheel is driven by a variable speed electric motor employing an automatic speed control device. Desired dynamic load is obtained by changing the rotational speed of the eccentric mass.

A mechanical counter, having a least reading of one thousand cycles and attached to the shaft of the eccentric wheel, records the number of cycles applied; and an automatic cut-off device stops the machine upon failure of the specimen.

A strain-gaged transducer placed in series with the test specimen, as shown in Figure 5, is used to sense the applied load. The transducer output is monitored with a dynamic strain analyzer consisting of calibrated balancing potentiometers, a three kilocycle carrier amplifier and an oscilloscope. The desired load is set on a calibrated potentiometer and the carrier wave is amplitude modulated by the transducer signal. The oscilloscope is used only as a null balance indicator. Maximum, minimum, and mean loads were monitored by this system. The complete load analyzing system was calibrated using a 20,000 pound capacity load cell which, in turn, was calibrated using a universal testing machine calibrated by proving rings certified by the National Bureau of Standards. The system provides an accuracy of ± 3 percent. The output of the sensor bonded to the test specimen is measured by use of a ten (10) channel SR-4 balance box and strain indicator. Data is recorded at convenient intervals, as indicated by the cyclic counter, and with no load on the specimen. Accessory equipment such as quartz lamp heaters, liquid nitrogen specimen enclosures and temperature recorders were used as required. All instrumentation equipment was calibrated and certified in accordance with MIL-C-45662A.

A Sonntag SF-2 fatigue machine was used for the bending beam tests of the specimens shown in Figure 4. This machine is primarily used for fatigue tests at or below the ± 1500 micro inch per inch strain level and will not permit cycling about a mean load. Since an eccentric weight is involved, the SF-2 machine must be calibrated dynamically.

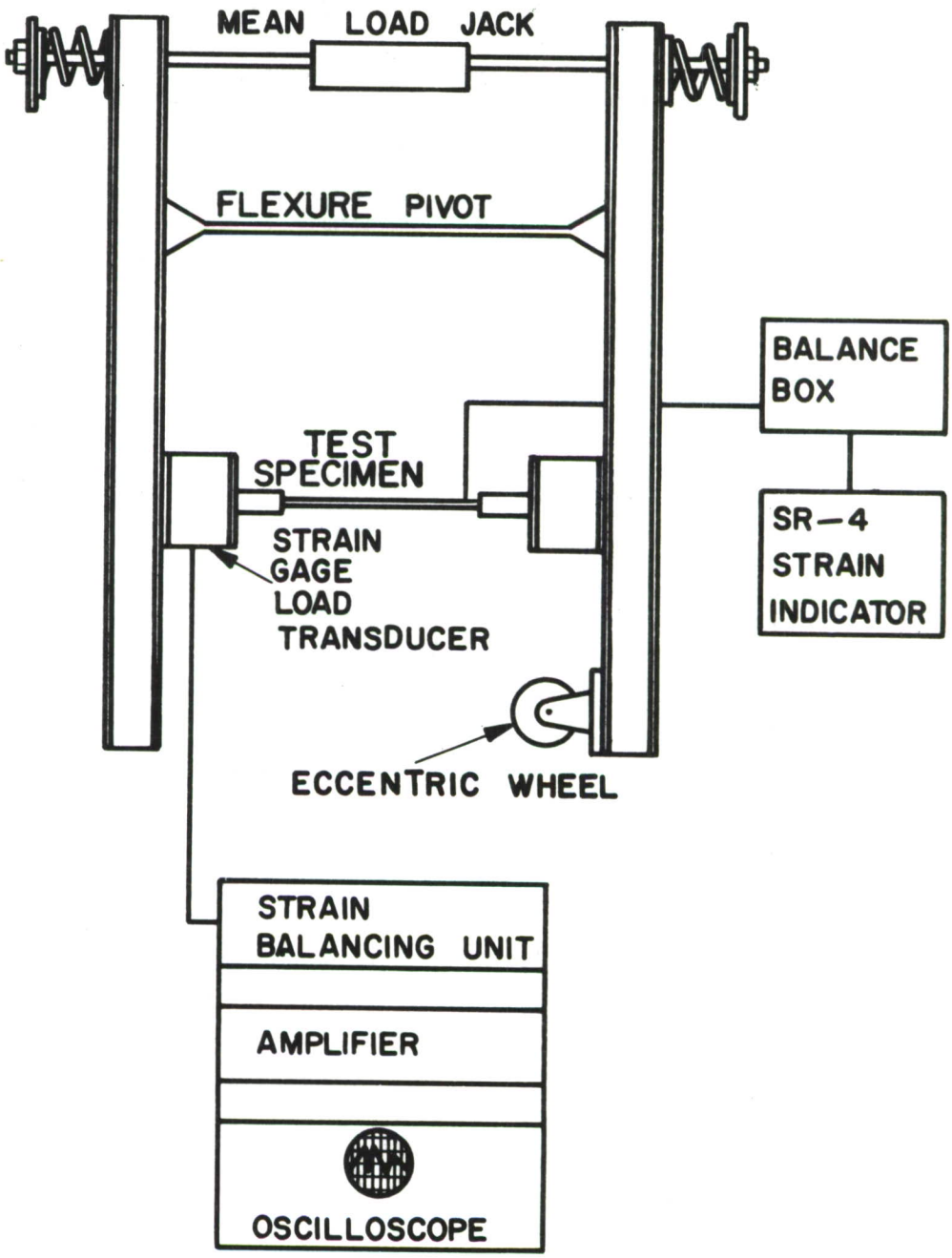

FIG.5 SCHEMATIC DIAGRAM OF AXIAL—LOAD, TUNING FORK TYPE FATIGUE MACHINES

3.2 TEST EQUIPMENT PHASE II

The evaluation of the fatigue sensor on typical aircraft structure required large capacity fatigue testing machines, since the C-130E wing specimens were 10 feet long and required peak loads of 250,000 pounds. Two (2) axial load machines having capacities up to ± 250,000 pounds mean load and ± 250,000 pounds alternating load were used. Calibrated load transducers were used to measure the cyclic loads, which were applied at a 6 CPM rate.

The fatigue sensors were also evaluated on full scale C-141A aircraft structure. This structure is better known as Specimen "C" or the C-141A aft fuselage empennage structure, and Specimen "B" a full wing and fuselage section. These specimens are fatigue cycled according to aircraft mission profiles by servo loading equipment. Some 79 channels of Research, Inc., Servac equipment are used to supply the simulated aerodynamic loads to the aircraft structure.

3.3 TEST INSTRUMENTATION

The change in resistance of the sensor can be measured by most any resistance measuring device, however, the higher the resolution the more accurate the measurement. A digital voltmeter, a wheatstone bridge, an SR-4 indicator, or most any conventional strain gage indicator could be used. The volumetric resistivity change of the foil material can reach a maximum of 8.7% or 10.4 ohms for a 120 ohm sensor. Therefore, a four decade wheatstone bridge could resolve 0.1 ohm or only one part in a 100 of the maximum possible change. This was considered inadequate for detecting the effects of temperature or time upon the zero shift of the sensor. By way of comparison the SR-4 strain indicator had a range coverage of 15 ohms change in 120 ohms, and a resolution of 10 parts out of 60,000. An SR-4 indicator set for a gage factor (G. F.) of 2.00 was used for the measurement of resistance changes of the sensor. The parameter which an SR-4 strain indicator measures is change in resistance and it can resolve micro ohms. The fact that the dial is calibrated in microinches per inch is merely a convenience in which the change in resistance can be related to micro-strain as a result of a particular gage factor setting. Especially for detecting low resistance changes in the fatigue sensor, a strain indicator should be substituted for a wheatstone bridge. The equivalent values are obtained in the manner shown below:

$$G.\,F. = \frac{\Delta R/R}{\Delta L/L} = \frac{\Delta R/R}{\epsilon}$$

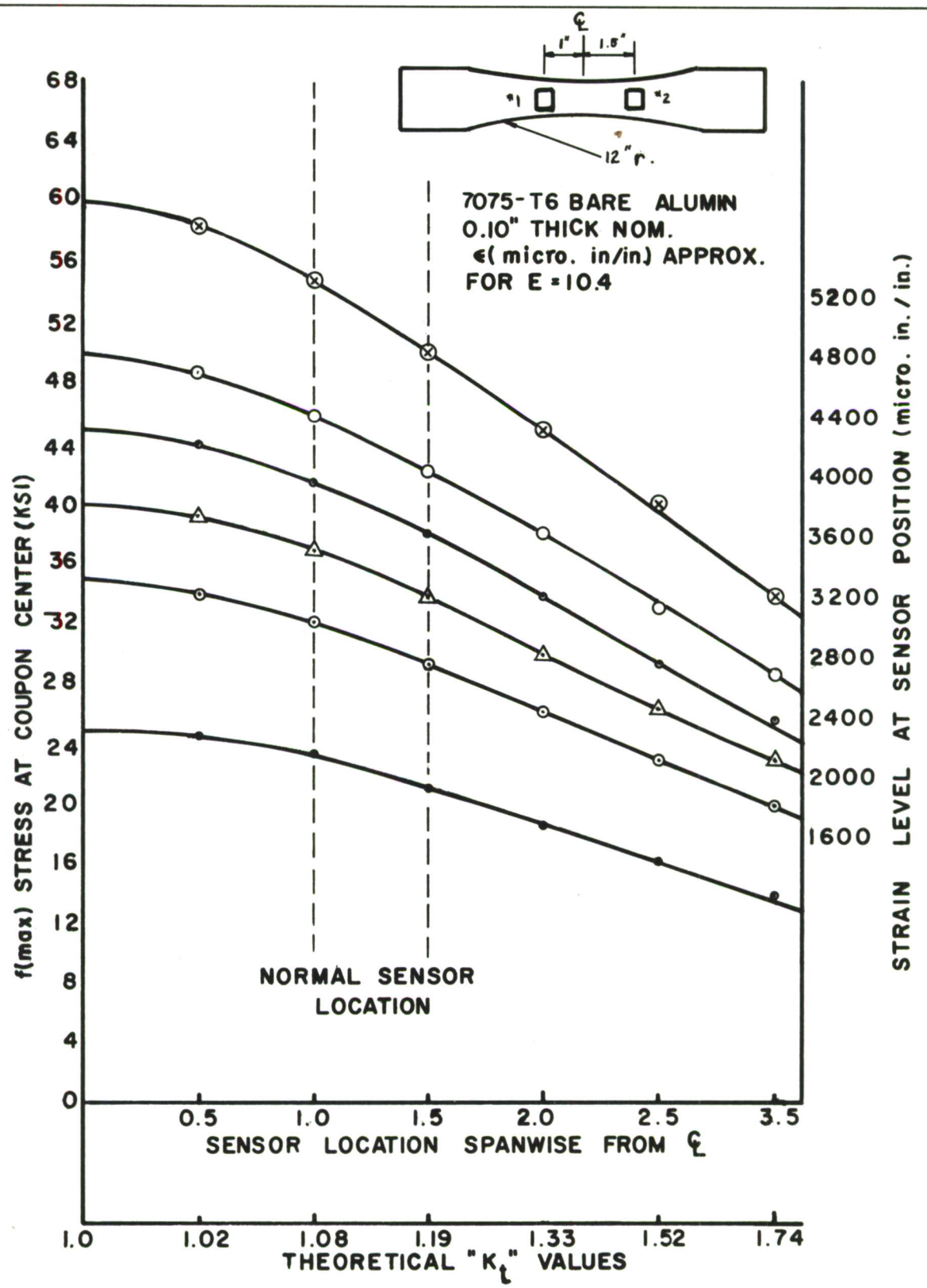

FIG. 6 CURVES OF STRESS LEVEL VERSUS SENSOR POSITION

Assuming a gage factor (G.F.) of 2 a value of $\mu\epsilon$ (micro-strain) is obtained for various Δ R's of the 120 ohm fatigue sensor, i.e., a 0.1 ohm change can be expressed in micro-strain and vice versa.

$$\epsilon = \frac{0.1\ \Omega}{/120\ \Omega} \times 10^6 = \frac{.000833}{2.00} \times 10^6$$

$$\epsilon = 416.6 \text{ micro-strain}$$

By the same token, a one (1) ohm resistance change in the 120 ohm fatigue sensor is the equivalent of 4166 micro-strain zero shift

3.4 LABORATORY TEST METHODS AND PROCEDURES

Basically the Phase I coupons were used only to establish the behavior characteristics of the annealed foil and to optimize the sensor in regard to configuration and output sensitivity. The sensor coupon data was never intended for correlation with fatigue damage allowables on typical aircraft structure, however, as much realism as possible was injected into the coupon sensor evaluations. Since an aircraft wing, for example, is subjected to differential bending resulting in axial loads on the upper and lower surfaces, the sensors are evaluated on specimens cycled by loading about a mean load. Theoretical K_t values and the various environmental conditions normally encountered by an aircraft structure were also simulated. The theoretical K_t values selected to represent typical stress concentrations are as follows:

K_t of 1.0 for a clean nominal area

K_t of 1.9 for a rivet filled hole

K_t of 2.72 for an unfilled hole

K_t of 4.00 for a load transferred across a splice joint

The basic coupon used, (Figure 1) will allow a specimen failure within a reasonable number of loading cycles and yet permit evaluation of the sensor at different stress levels on the same coupon. A narrow range of theroretical K_t values can be obtained by sensor location as shown in the Figure 6 curves.

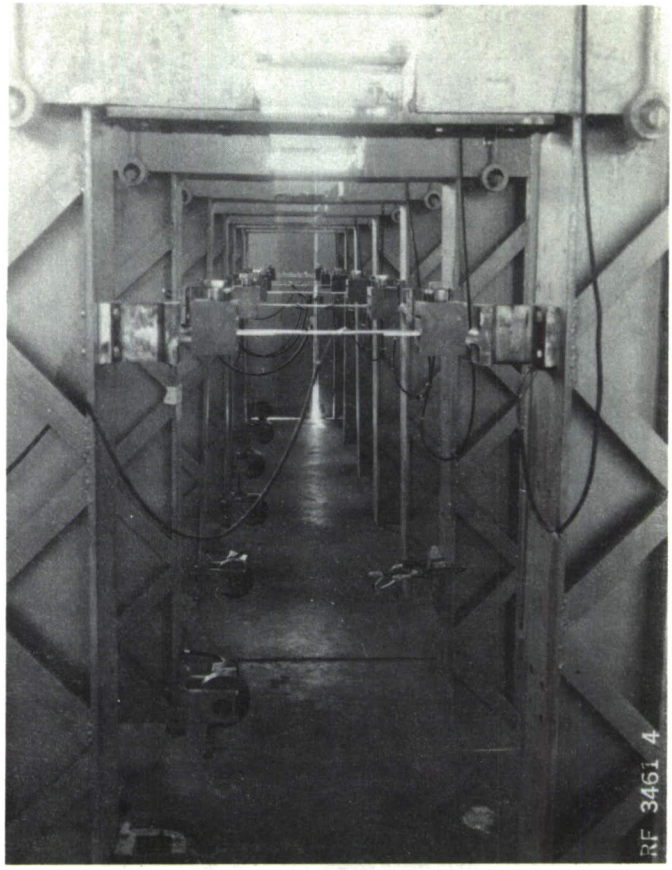

FIGURE 7 TUNING FORK FATIGUE MACHINES USED FOR TESTING COUPONS

FIGURE 8 LOADING CONSOLE FOR LOADING AND MONITORING OF TUNING FORK FATIGUE MACHINES

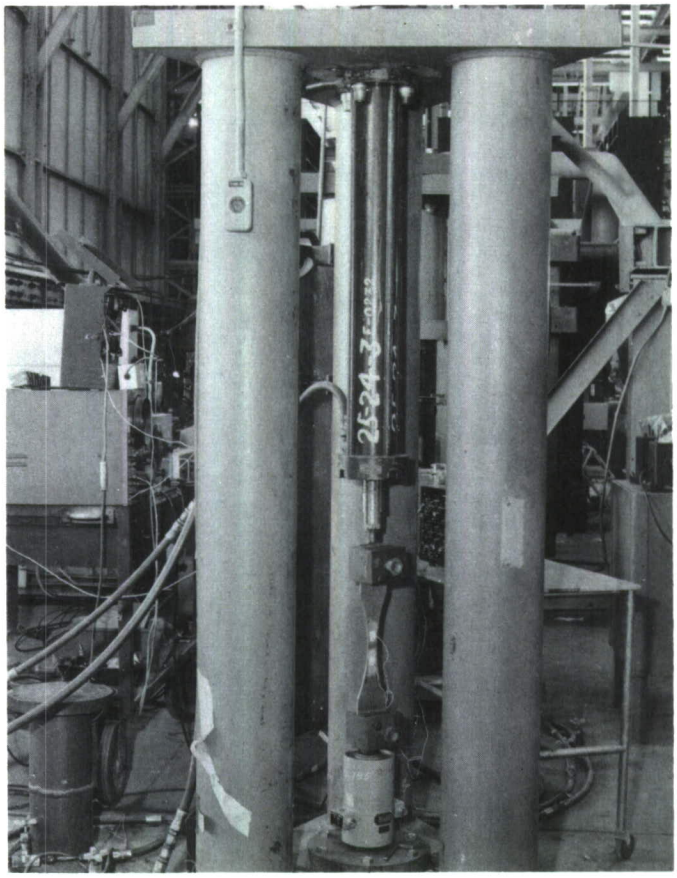

FIGURE 9 SLOW CYCLE FATIGUE MACHINE SETUP

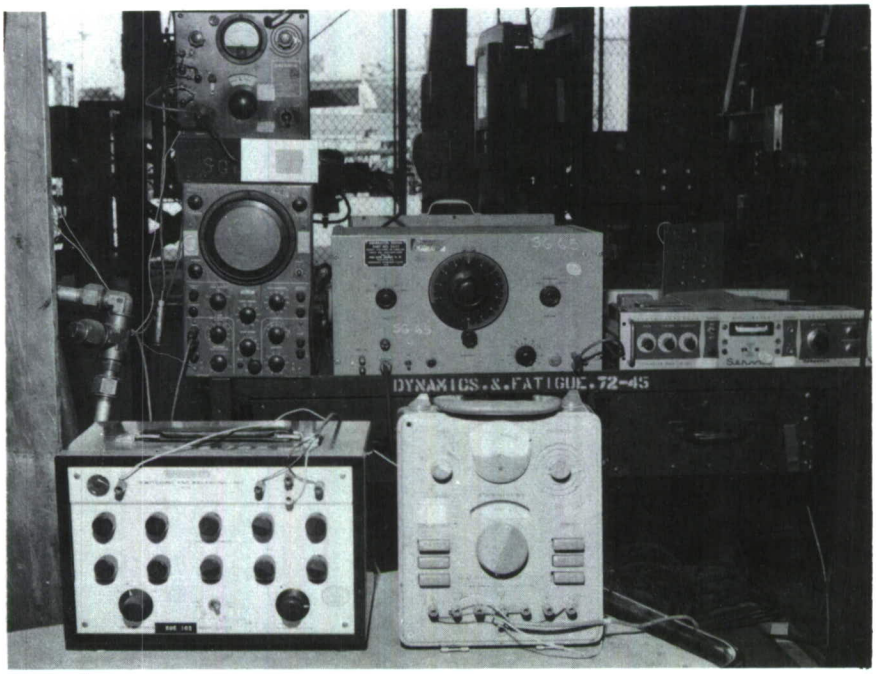

FIGURE 10 INSTRUMENTATION FOR CONTROLLING LOADS ON THE SLOW CYCLE MACHINE AND MEASURING FATIGUE SENSOR OUTPUT

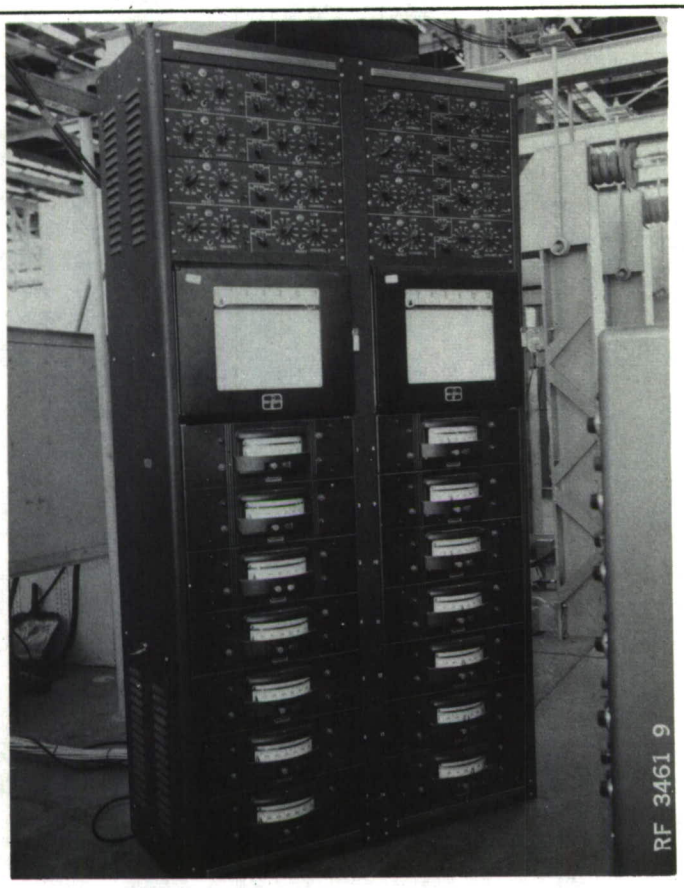

FIGURE 11 TEMPERATURE CONTROL AND MONITORING EQUIPMENT FOR COUPON HEATERS

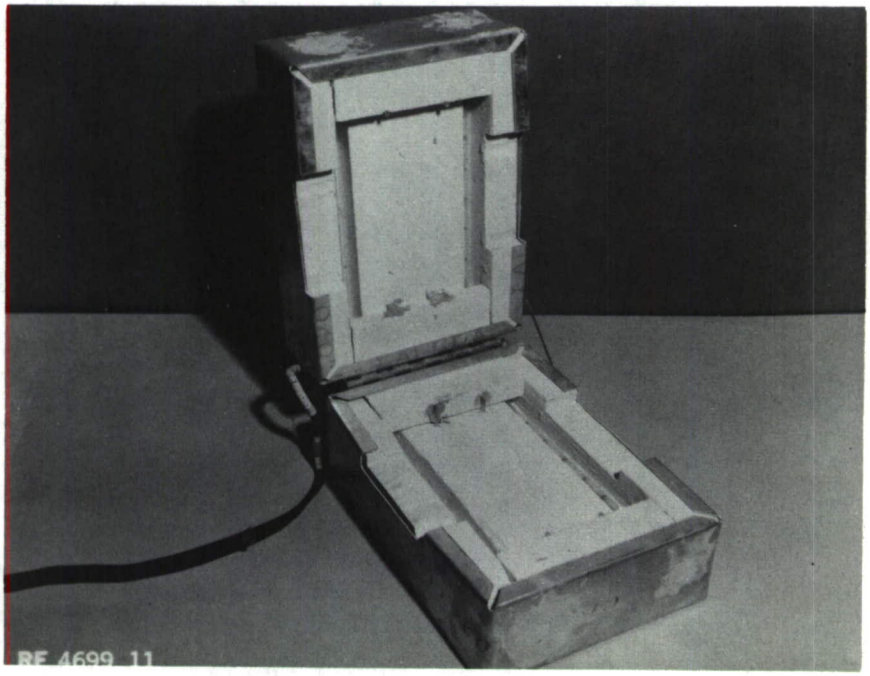

FIGURE 12 TYPICAL GLASS ROCK AND QUARTZ LAMP HEATER FOR ELEVATED TEMPERATURE TESTS

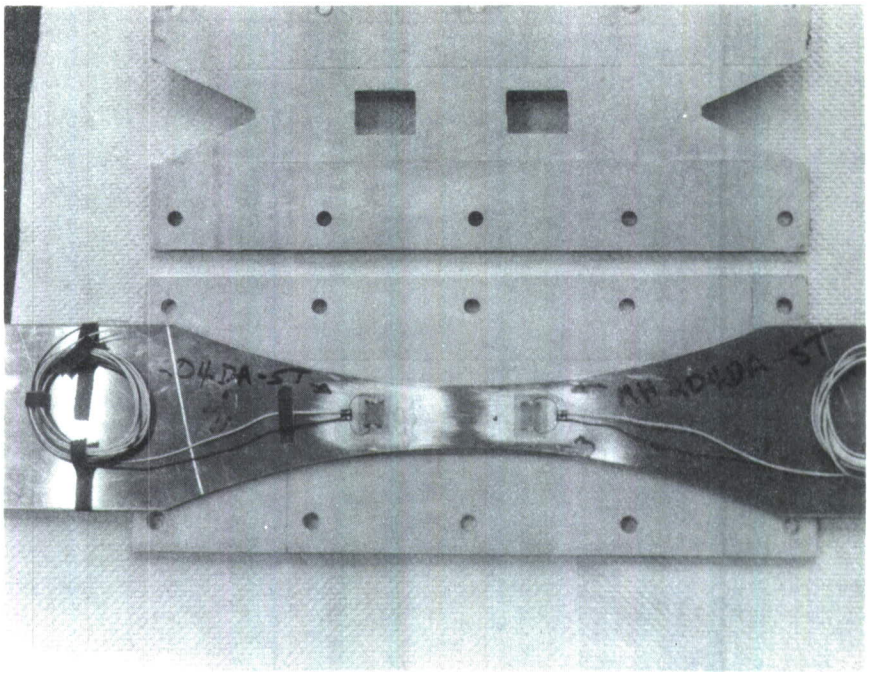

FIGURE 13 INSTRUMENTED SPECIMEN WITH COMPANION LATERAL SUPPORT PLATES. TENSION AND COMPRESSION LOADS ARE APPLIED AXIALLY WITH TEFLON LINED SUPPORT PLATES TO PREVENT BENDING.

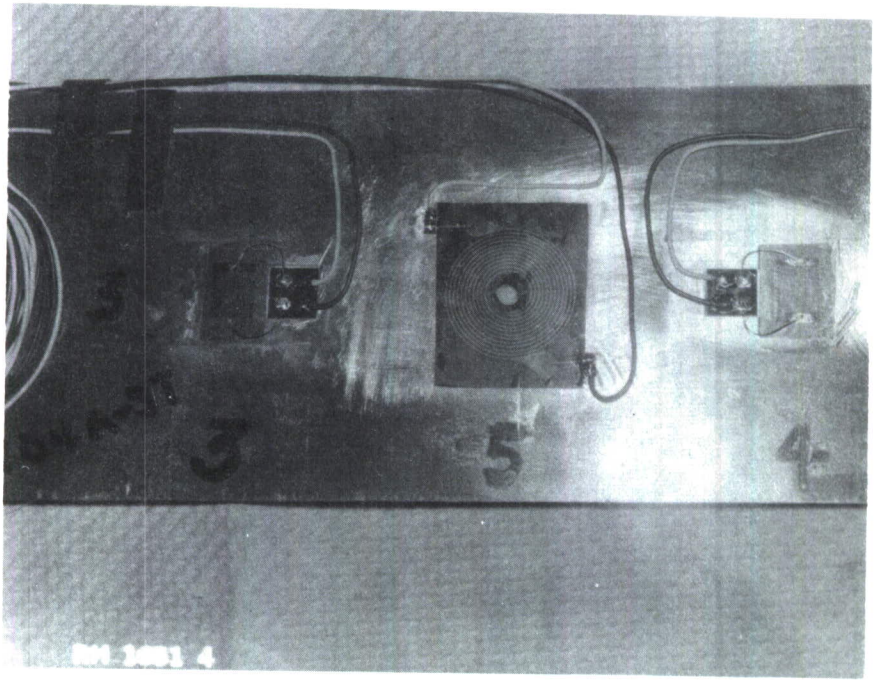

FIGURE 14 TYPICAL SPIRAL GRID INSTALLATION, CENTERED OVER THE HOLE REPRESENTING A K_t OF 2.72 IN THE SPECIMEN.

SECTION IV

TEST RESULTS

4.1 PHASE I COUPON TESTS

The phase I coupon tests were designed to evaluate the capabilities of the sensor over a wide range of structural variables and environmental conditions. The stress levels, stress ratios, environmental conditions, etc. would include the high extremes that an aircraft structure might encounter. Concurrent with evaluation and establishment of sensor behavior, the sensor construction and application would be optimized.

4.1.1 EFFECT OF STRESS RATIO

A series of instrumented test coupons were evaluated at different stress ratios to determine the effect of a specific stress ratio upon the end resistance of the sensor at specimen failure. Conventional stress ratios were selected; that is an A of 0.818, A of 0.333, and A = ∞. For any given coupon, the stress ratio and strain amplitude were held constant until failure of that coupon. Primarily the basic fatigue sensor used is the standard 204A-ST (noted as No. 1 and No. 2 location on the specimen with any experimental sensors installed as mirror images of these two and noted as No. 3 and No. 4.) Sensor No. 1 in most cases, is placed one inch from the specimen center line and sensor No. 2 is placed one and one-half inches from the center line. These locations were selected as most desirable as a result of earlier experiments, since a single specimen will provide data at two stress levels for any given f max. At the same time, the sensors ability to accumulate proportional fatigue damage and to indicate the location of failure was evaluated. Failure of the specimen occasionally occurs at locations other than its minimum width which may be reflected by the sensor reading. A pointed illustration of this is shown in the curves for specimen No. 3.

As indicated previously, the vertical scale can be shown as zero shift in microstrain units ($\mu\epsilon$), as resistance in ohms, or as a percentage resistance change if desired. Microstrain units were selected in order to obtain a higher resolution of resistance change as previously discussed in paragraph 3.2 of Section III. Specimen 10 also shows some variation in readings taken after the specimen failed. The departure of these points from the curve is caused by bending in the coupon, which will be indicated by the sensor since it is still strain sensitive. Curves and data are now shown for all specimen numbers listed in the tables, since some uninstrumented specimen were used to calibrate the machines and some were rejected because of scratches. The tables also show other coupons were tested but not plotted or otherwise evaluated since they indicated repetitive data.

The semi-log plots shown in the graph of Figure 14 represent a consolidation of the fatigue life of selected specimens versus sensor resistance readings at the time of failure. In all cases, the outputs (shown in Figure 15) represent the resistance of the No. 1 fatigue sensor which is located one inch from the specimen center. For specimens tested over a stress range of 35-40KSI and showing a fatigue life of from 46,000 cycles to 344,000 cycles (a ratio of approximately 8:1) the variation in sensor resistance reading at failure is approximately ± 12%. This is true only if data from selected specimens are plotted. It also appears that a constant end resistance at specimen failure does exist, but it should be noted that this is for only a constant stress ratio. As soon as the stress ratio is changed, i.e., Specimen No.'s 12, 13, 14, it is obvious that specimen failure occurs at a much different value of sensor end resistance.

Two different foil anneals were investigated during the early stages of the program. Namely the type designated as 204A-ST (single anneal) and 204DA-ST double anneal as shown in Table II, page 146. The curves from Specimens 5, 12, 13, 14, indicate that the output from the double anneal foil is definitely higher with an improvement in threshold sensitivity and no change in fatigue life.

Sensors on Specimens No. 30, 39, 42 and 43 were evaluated under the effects of completely reversed axial strain. These specimen were tested under axial loadings by using teflon lined lateral support plates to prevent bending of the coupon. To substantiate these data, sensors were also evaluated under reversed bending strains on Specimens 1C, 2C, and 4C. The preponderance of evidence indicates that the sensor end resistance at specimen failure is several orders of magnitude higher under reversed strain than cyclic strain about a mean level.

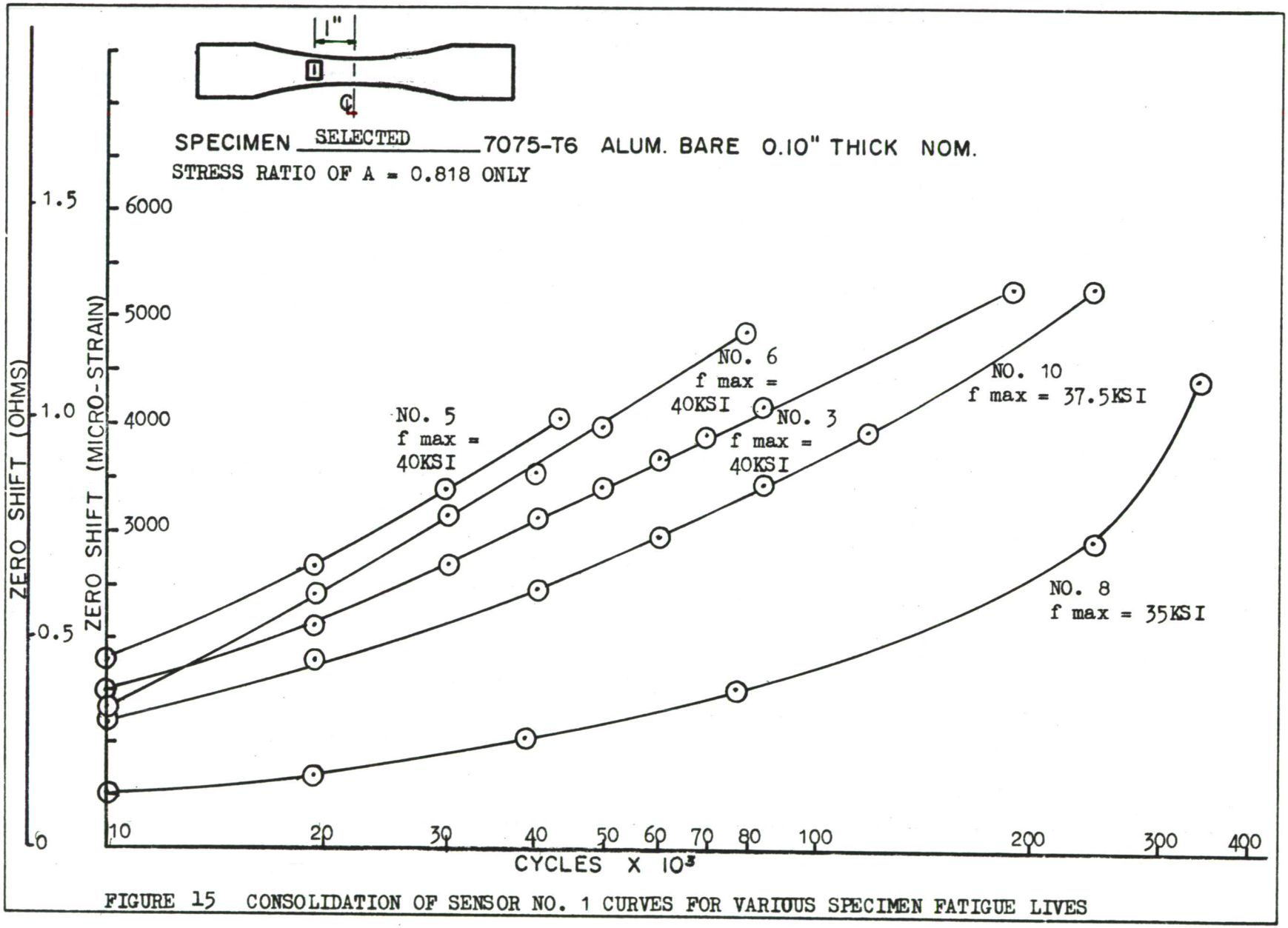

FIGURE 15 CONSOLIDATION OF SENSOR NO. 1 CURVES FOR VARIOUS SPECIMEN FATIGUE LIVES

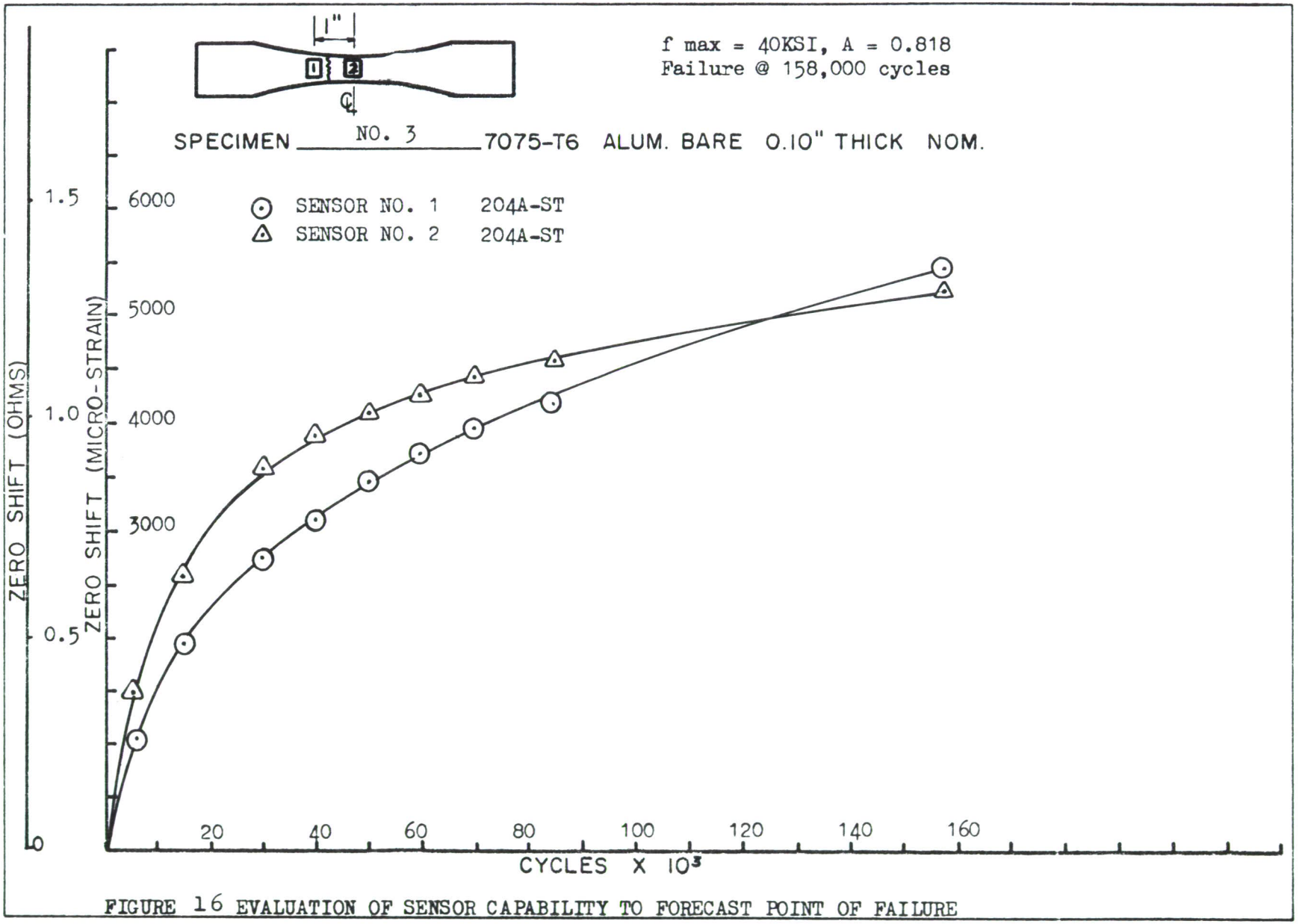

FIGURE 16 EVALUATION OF SENSOR CAPABILITY TO FORECAST POINT OF FAILURE

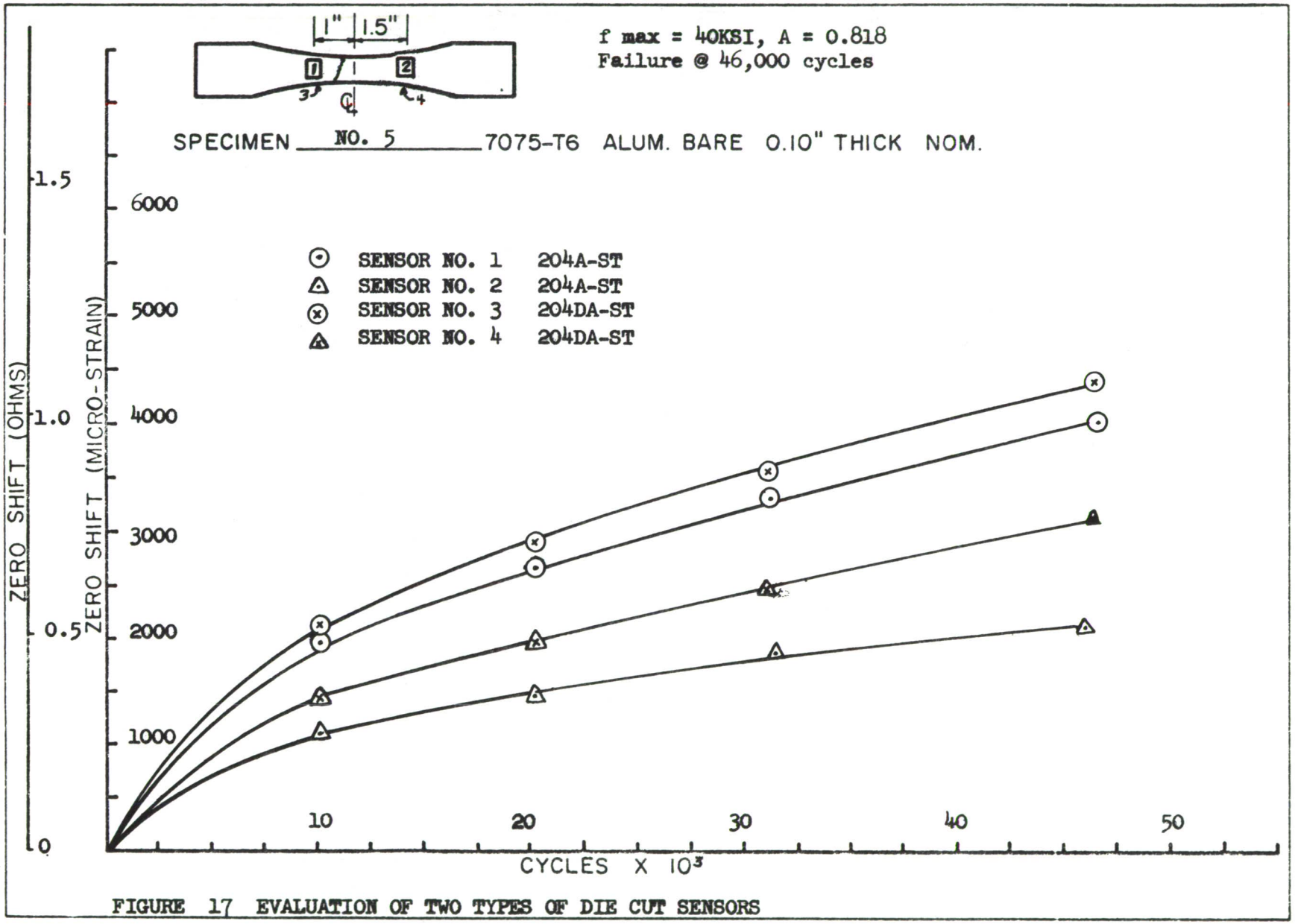

FIGURE 17 EVALUATION OF TWO TYPES OF DIE CUT SENSORS

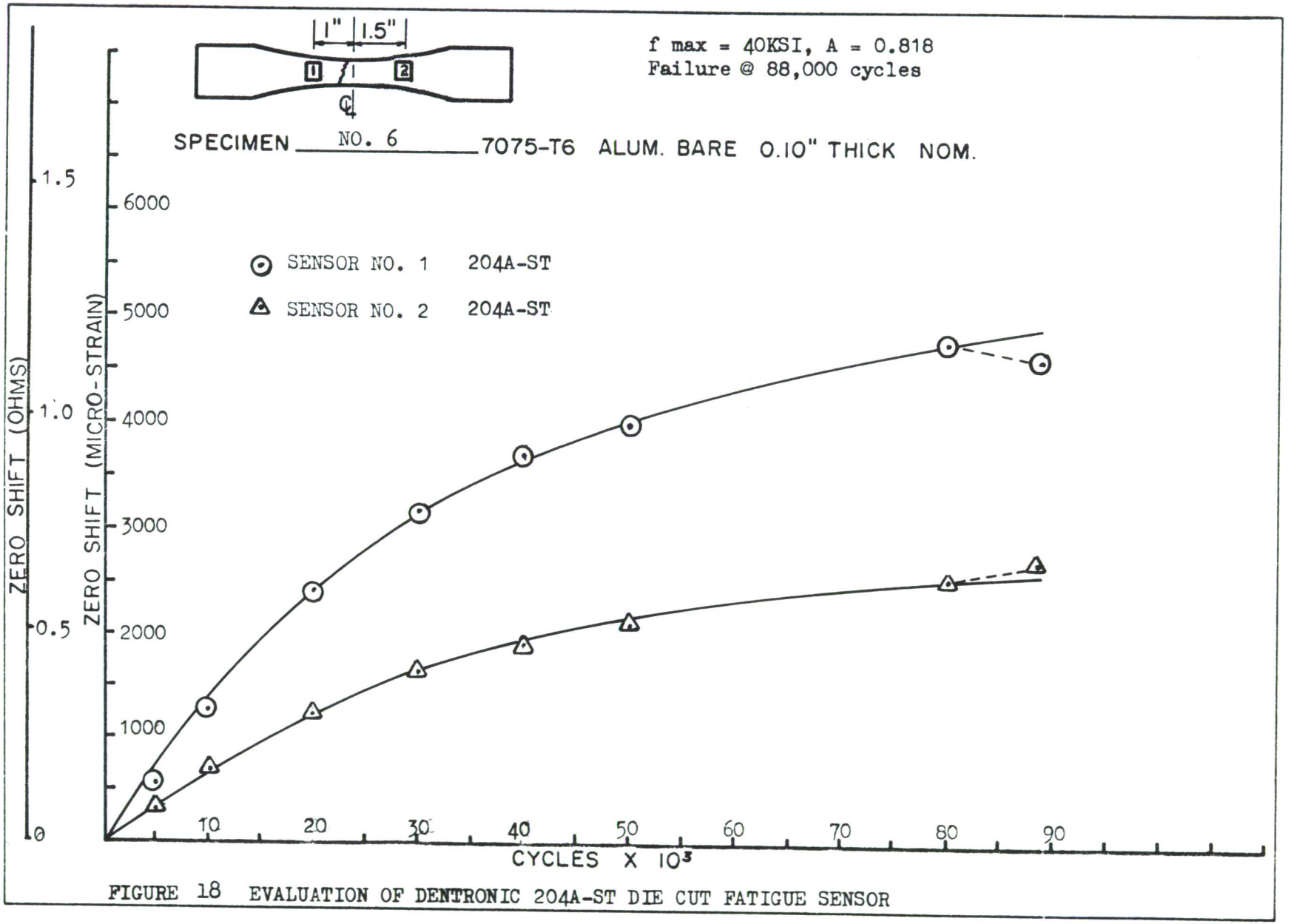

FIGURE 18 EVALUATION OF DENTRONIC 204A-ST DIE CUT FATIGUE SENSOR

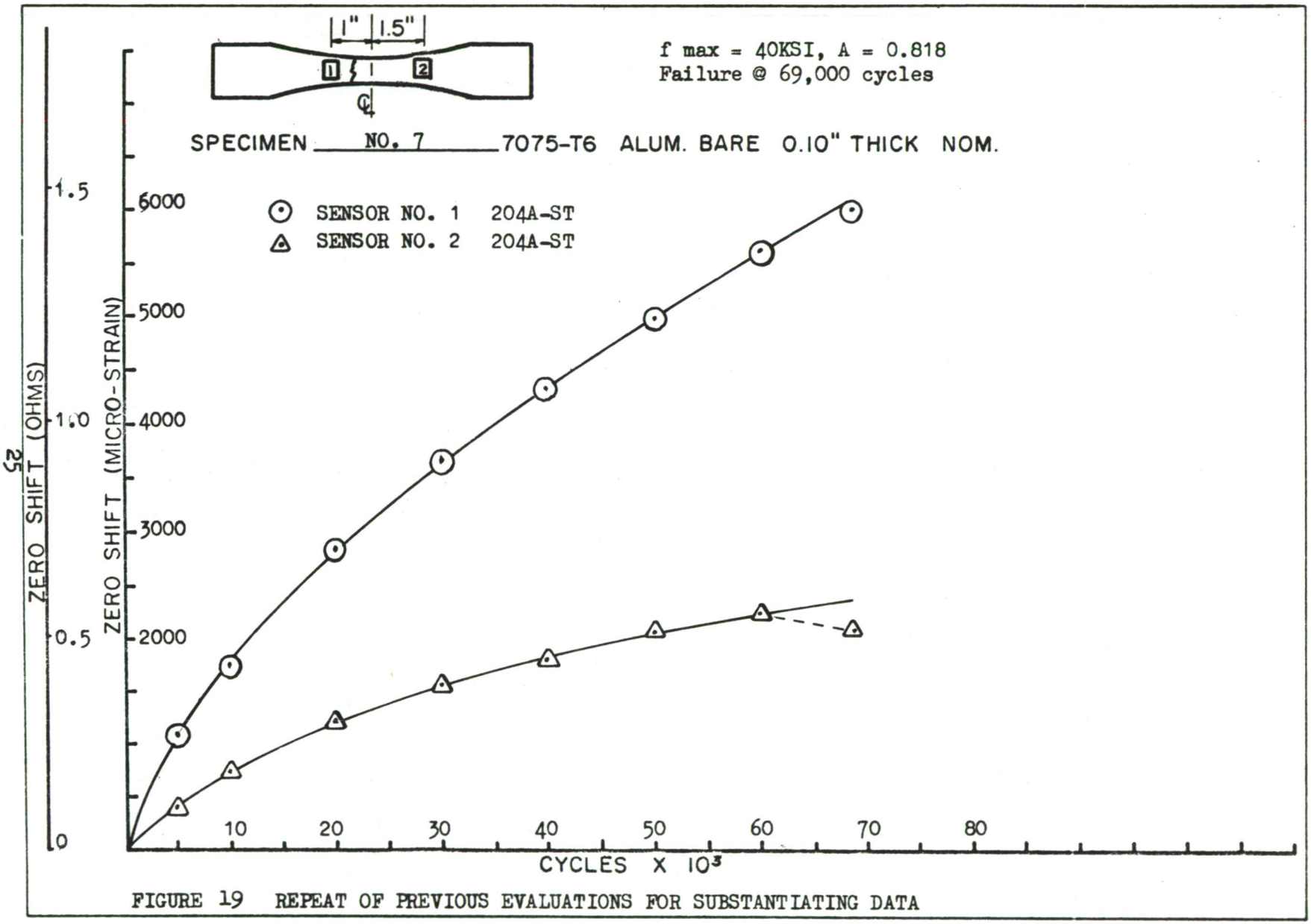

FIGURE 19 REPEAT OF PREVIOUS EVALUATIONS FOR SUBSTANTIATING DATA

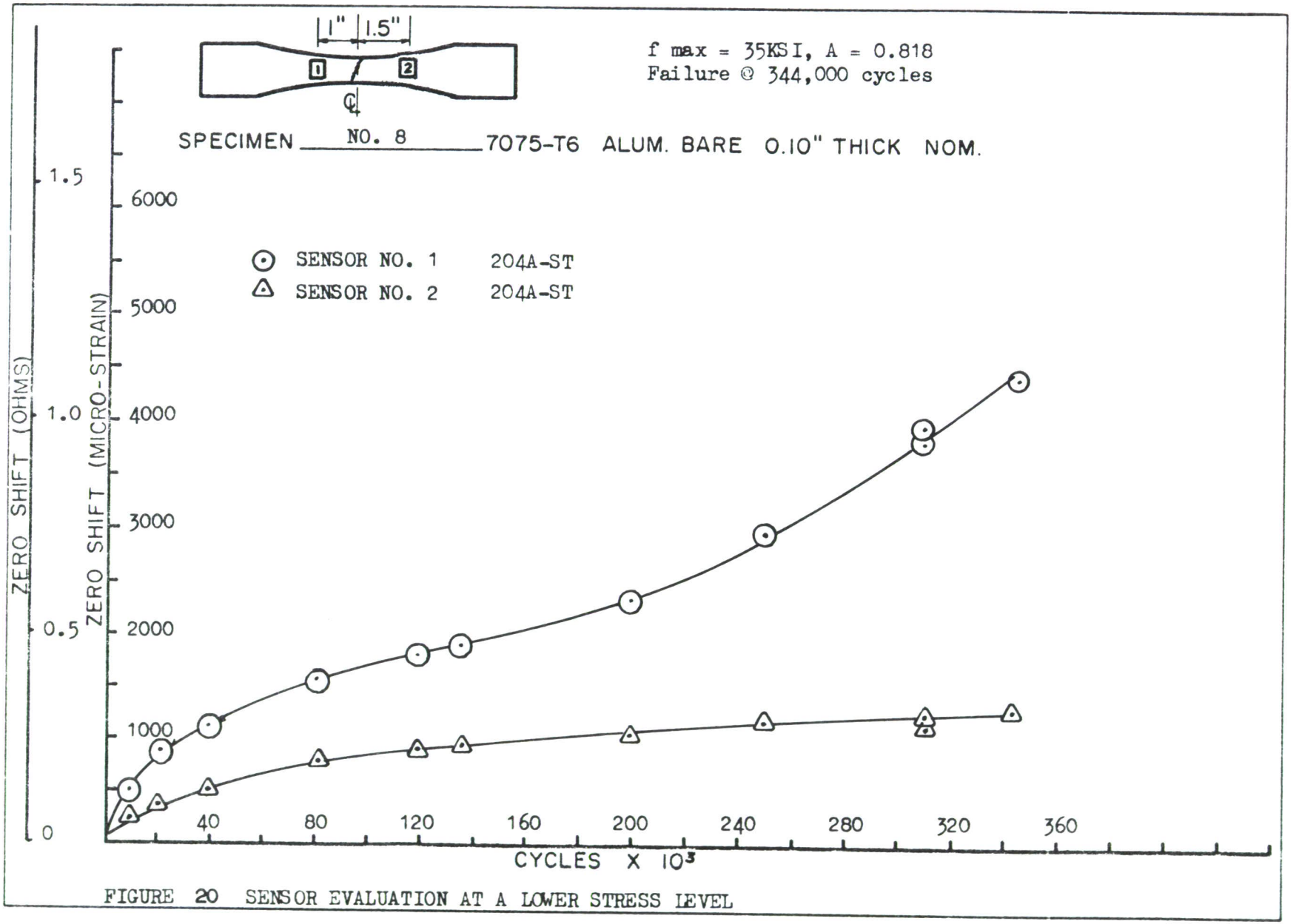

FIGURE 20 SENSOR EVALUATION AT A LOWER STRESS LEVEL

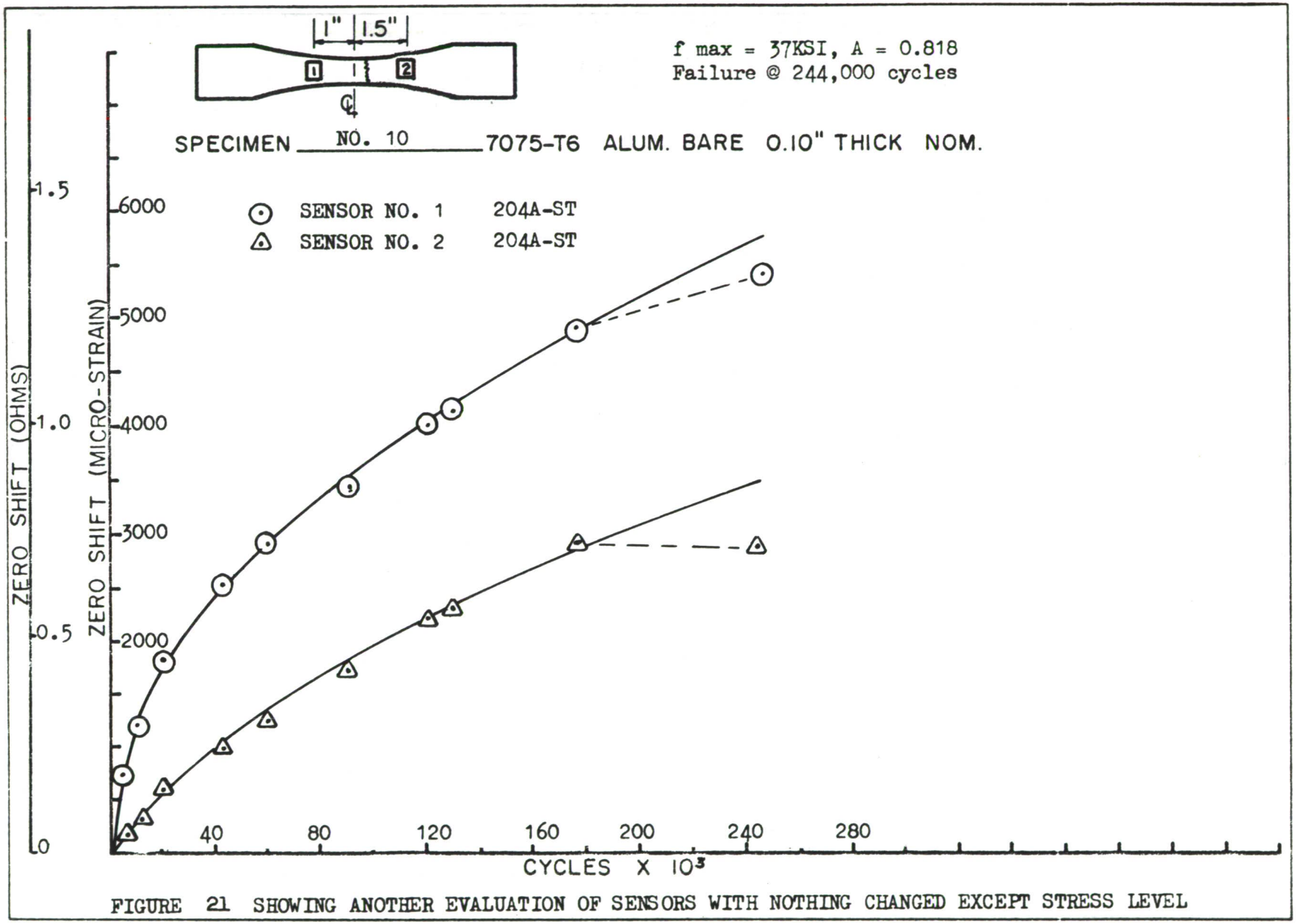

FIGURE 21 SHOWING ANOTHER EVALUATION OF SENSORS WITH NOTHING CHANGED EXCEPT STRESS LEVEL

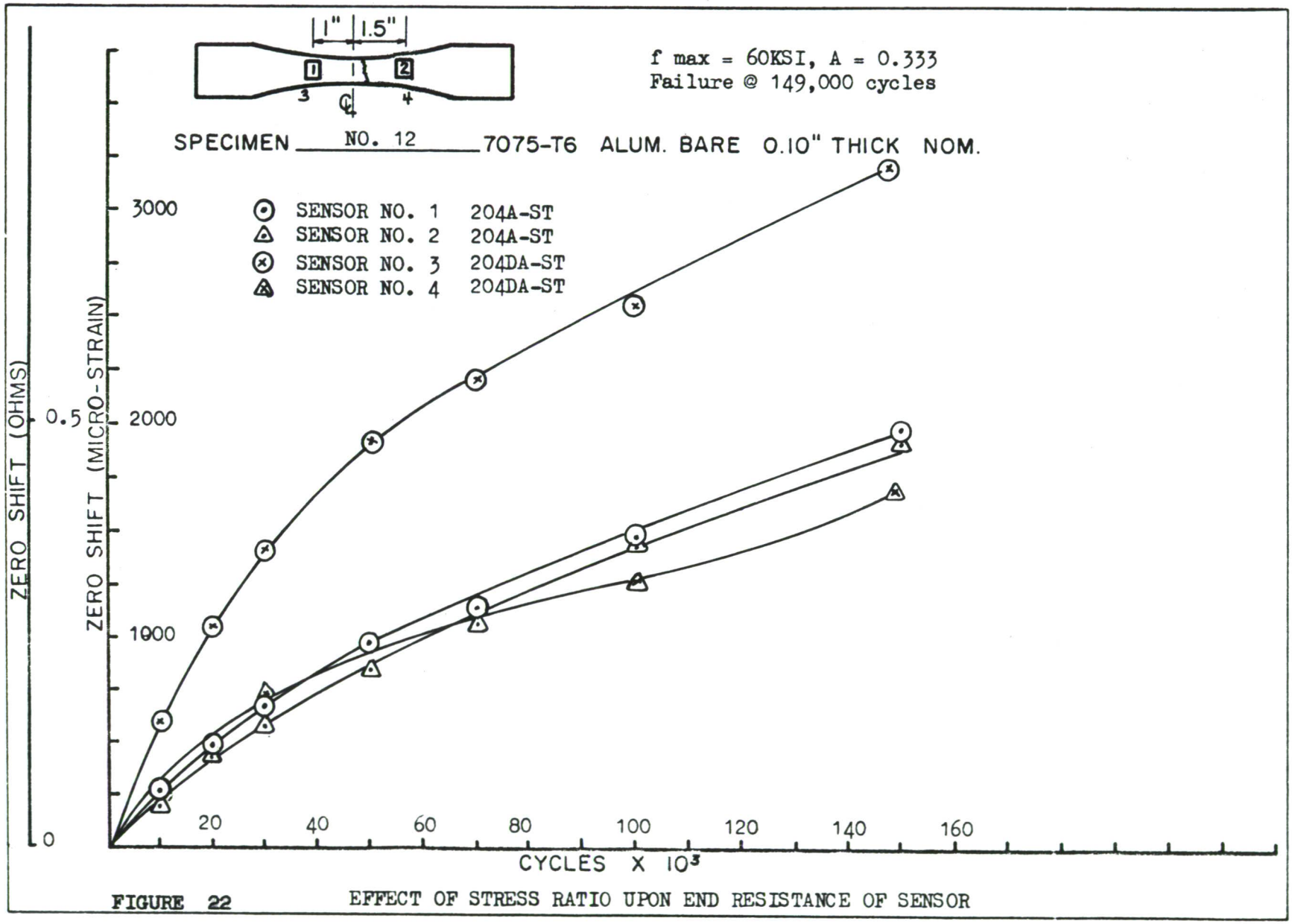

FIGURE 22 EFFECT OF STRESS RATIO UPON END RESISTANCE OF SENSOR

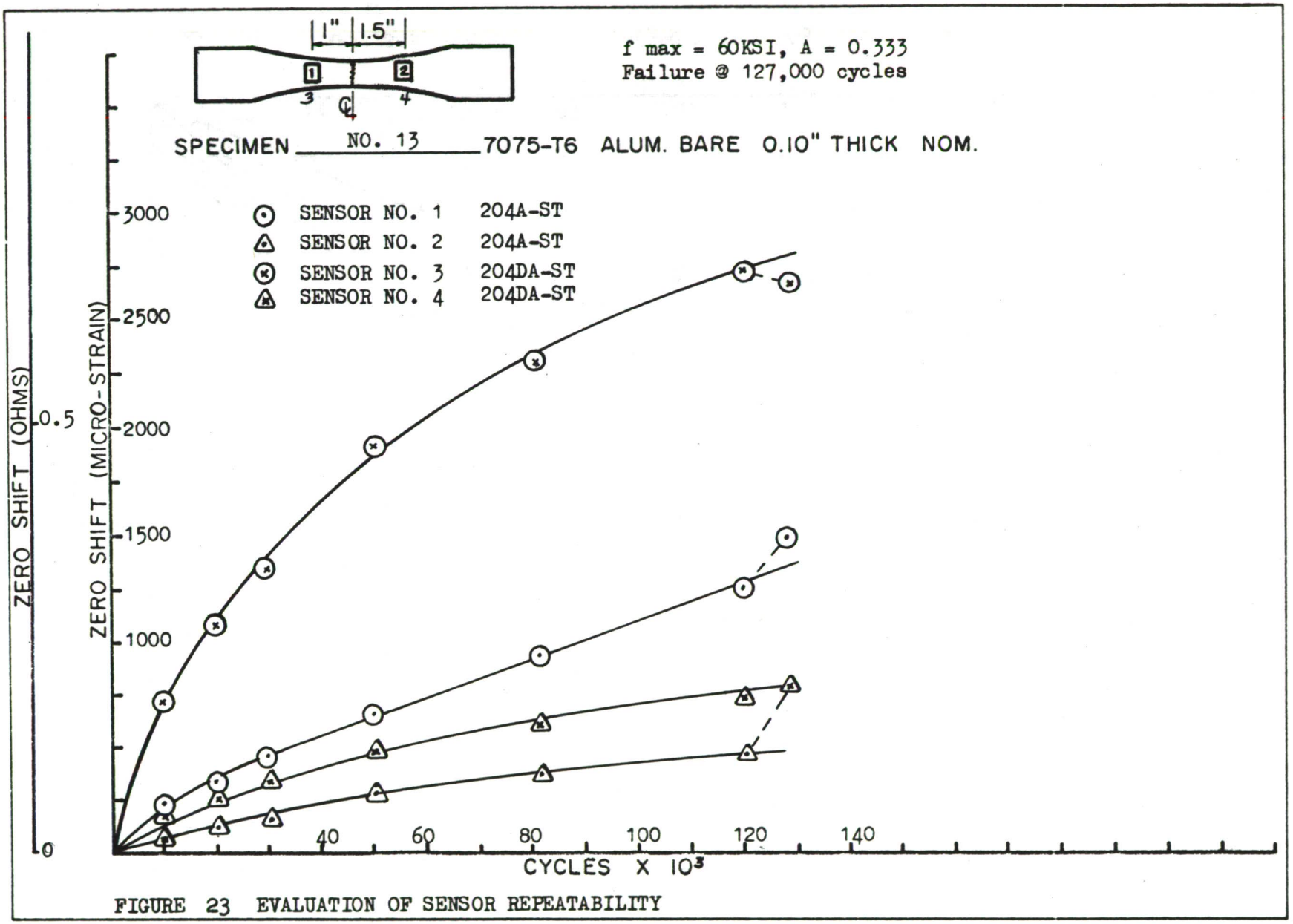

FIGURE 23 EVALUATION OF SENSOR REPEATABILITY

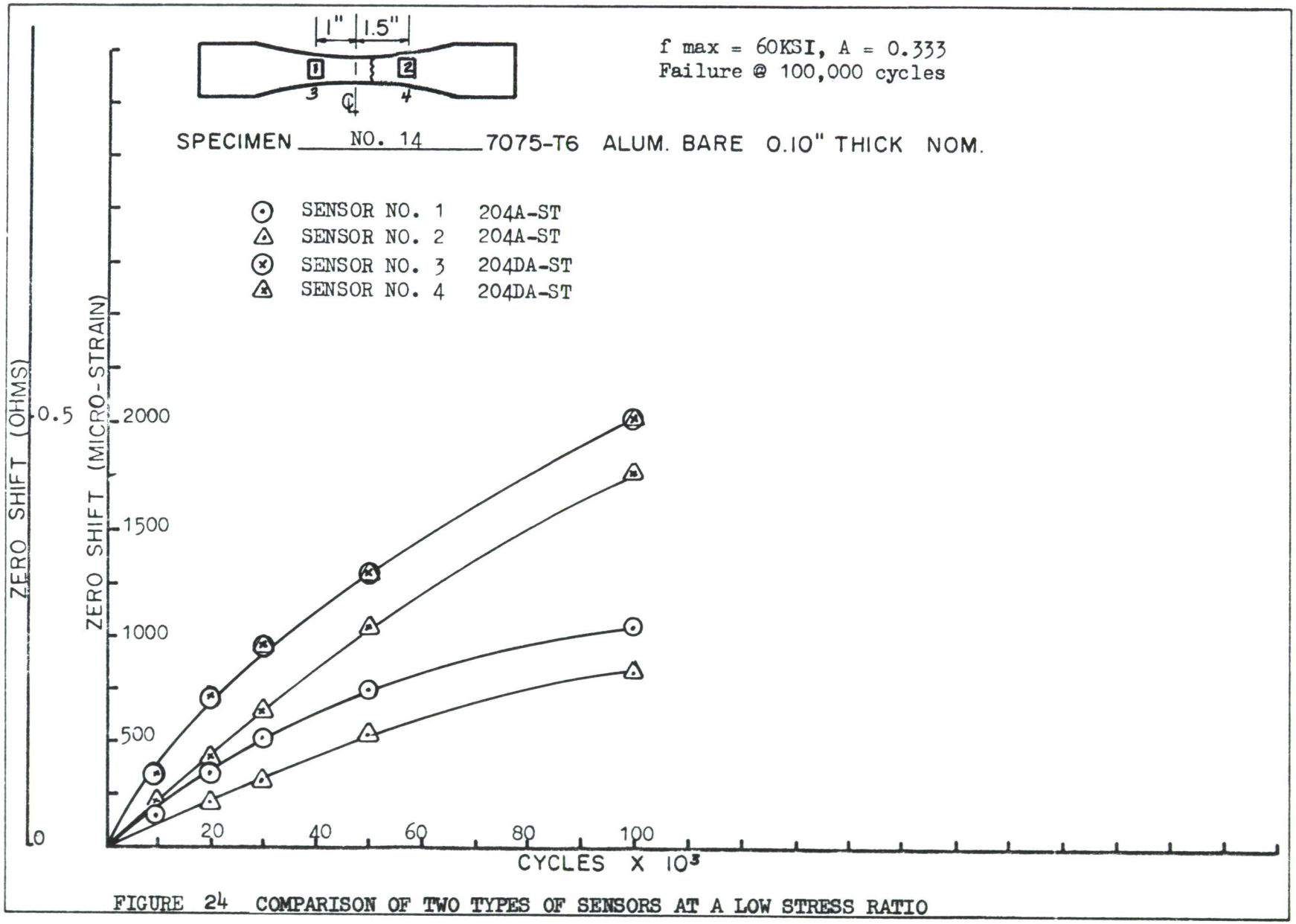

FIGURE 24 COMPARISON OF TWO TYPES OF SENSORS AT A LOW STRESS RATIO

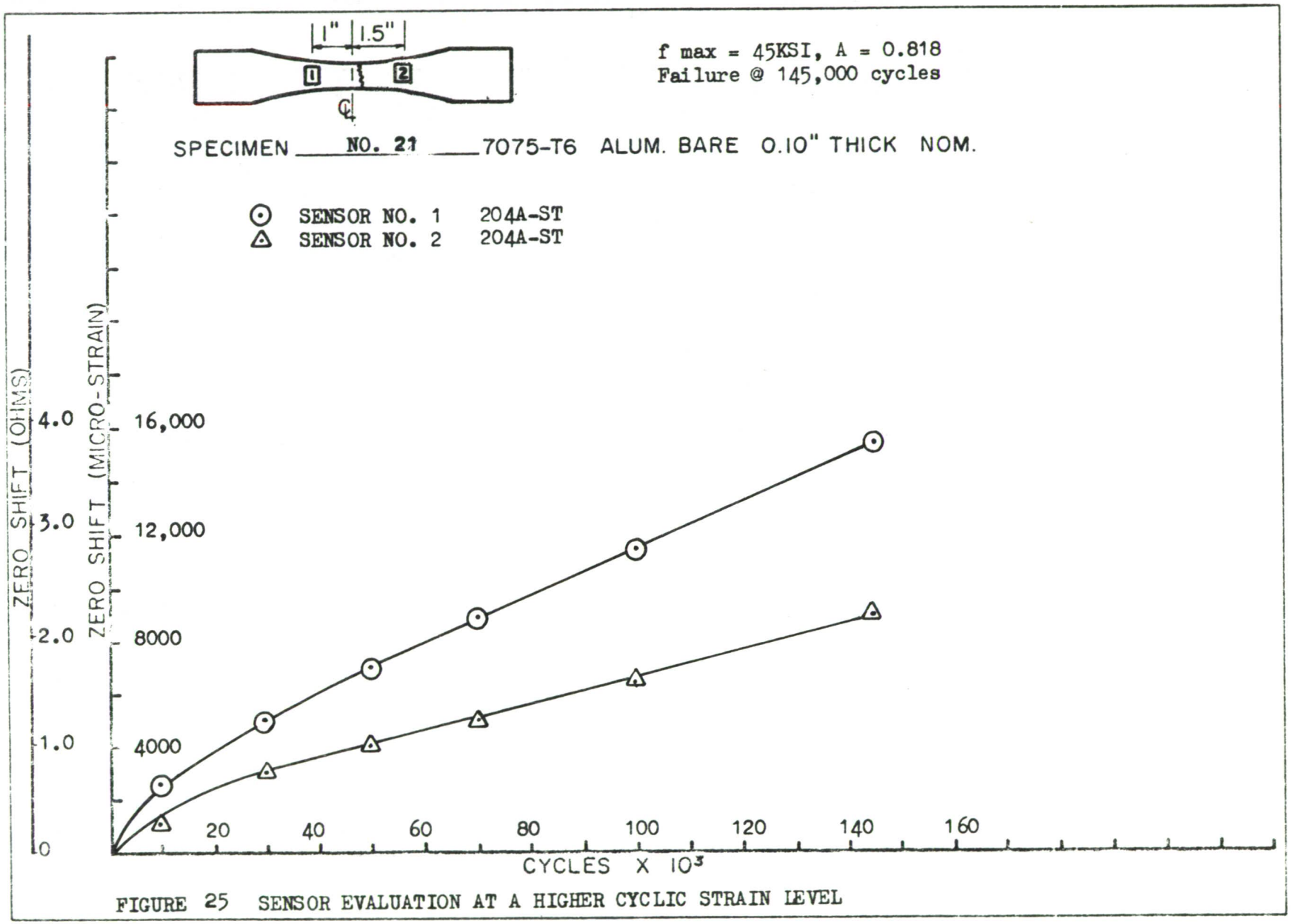

FIGURE 25 SENSOR EVALUATION AT A HIGHER CYCLIC STRAIN LEVEL

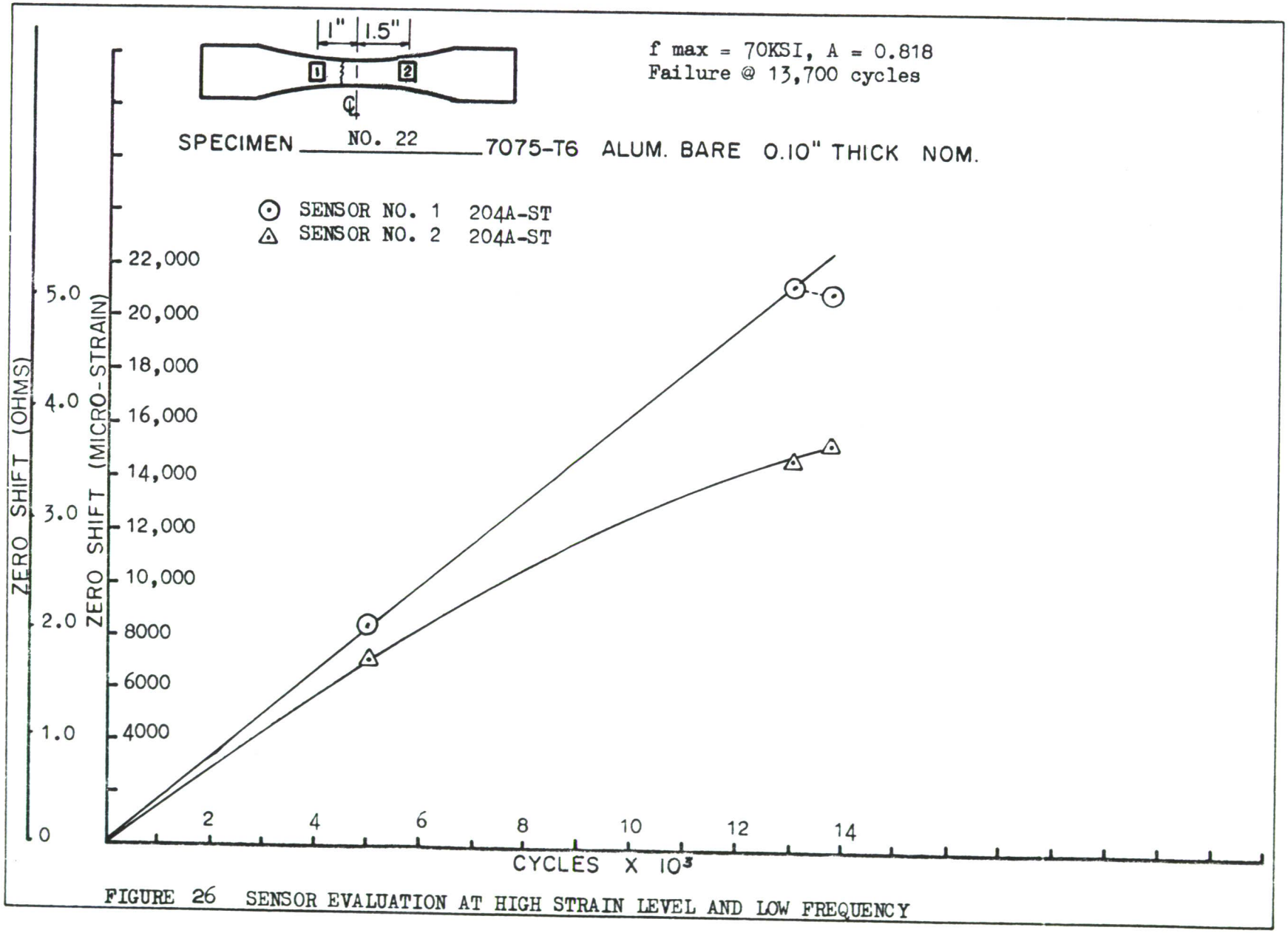

FIGURE 26 SENSOR EVALUATION AT HIGH STRAIN LEVEL AND LOW FREQUENCY

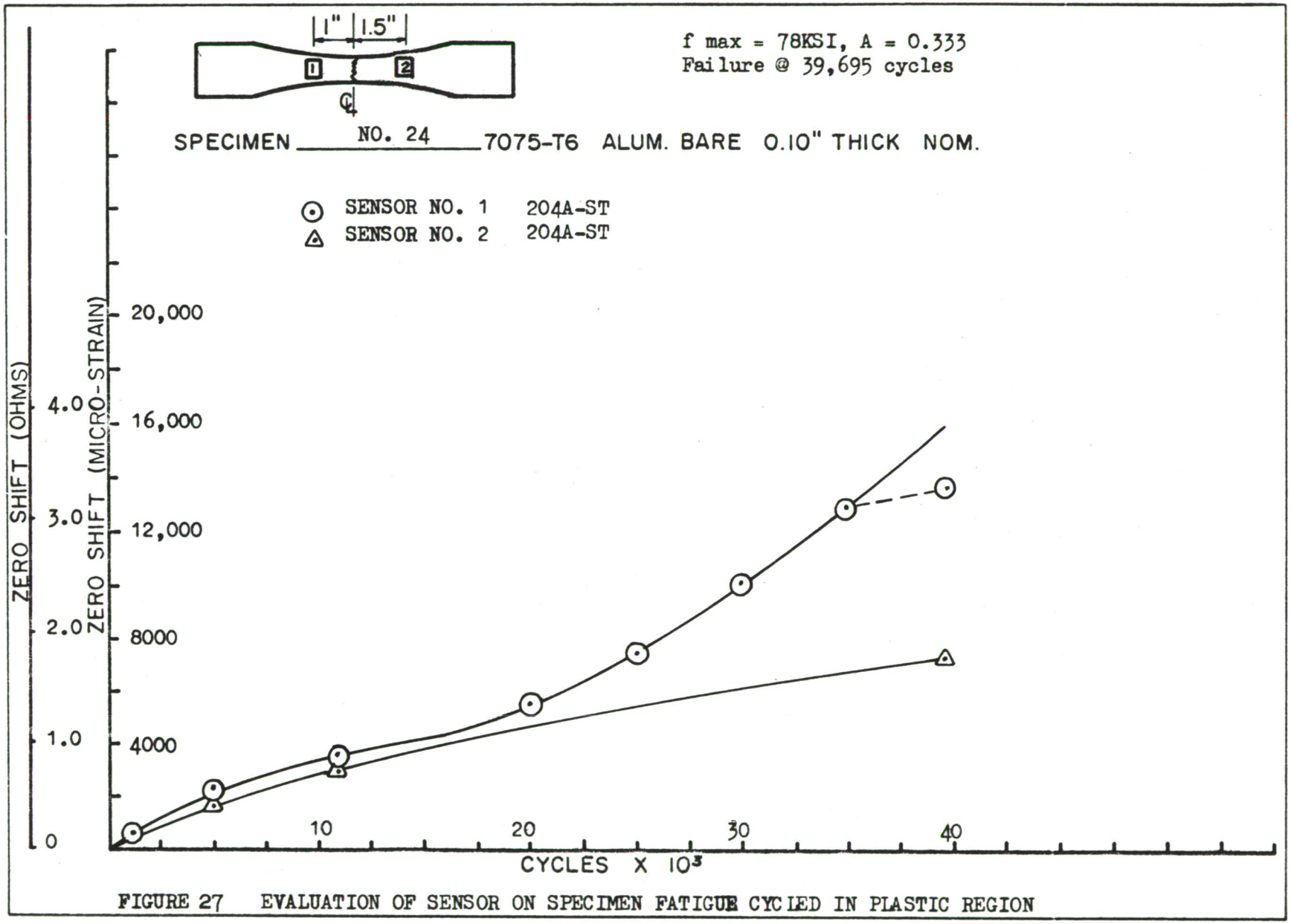

FIGURE 27 EVALUATION OF SENSOR ON SPECIMEN FATIGUE CYCLED IN PLASTIC REGION

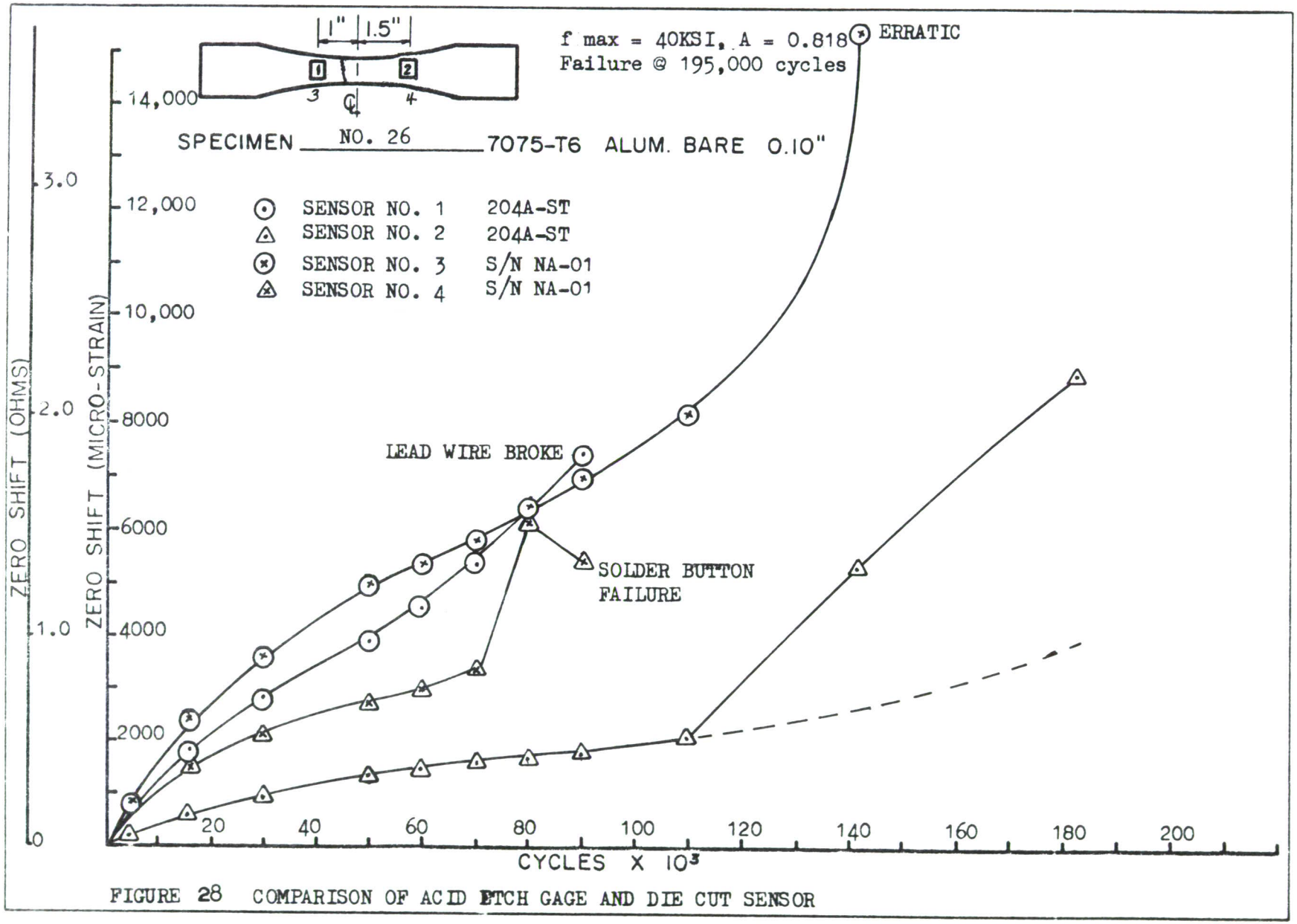

FIGURE 28 COMPARISON OF ACID ETCH GAGE AND DIE CUT SENSOR

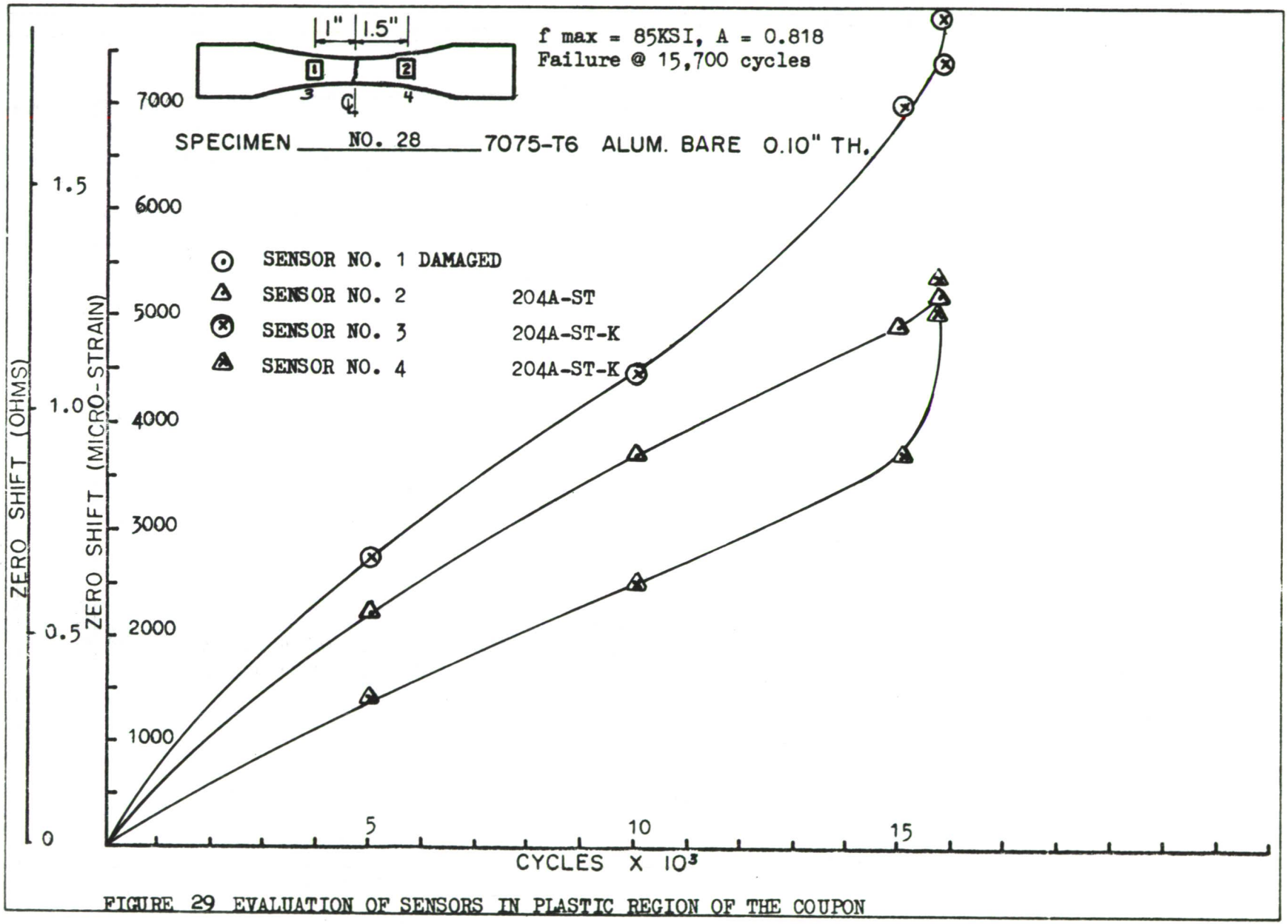

FIGURE 29 EVALUATION OF SENSORS IN PLASTIC REGION OF THE COUPON

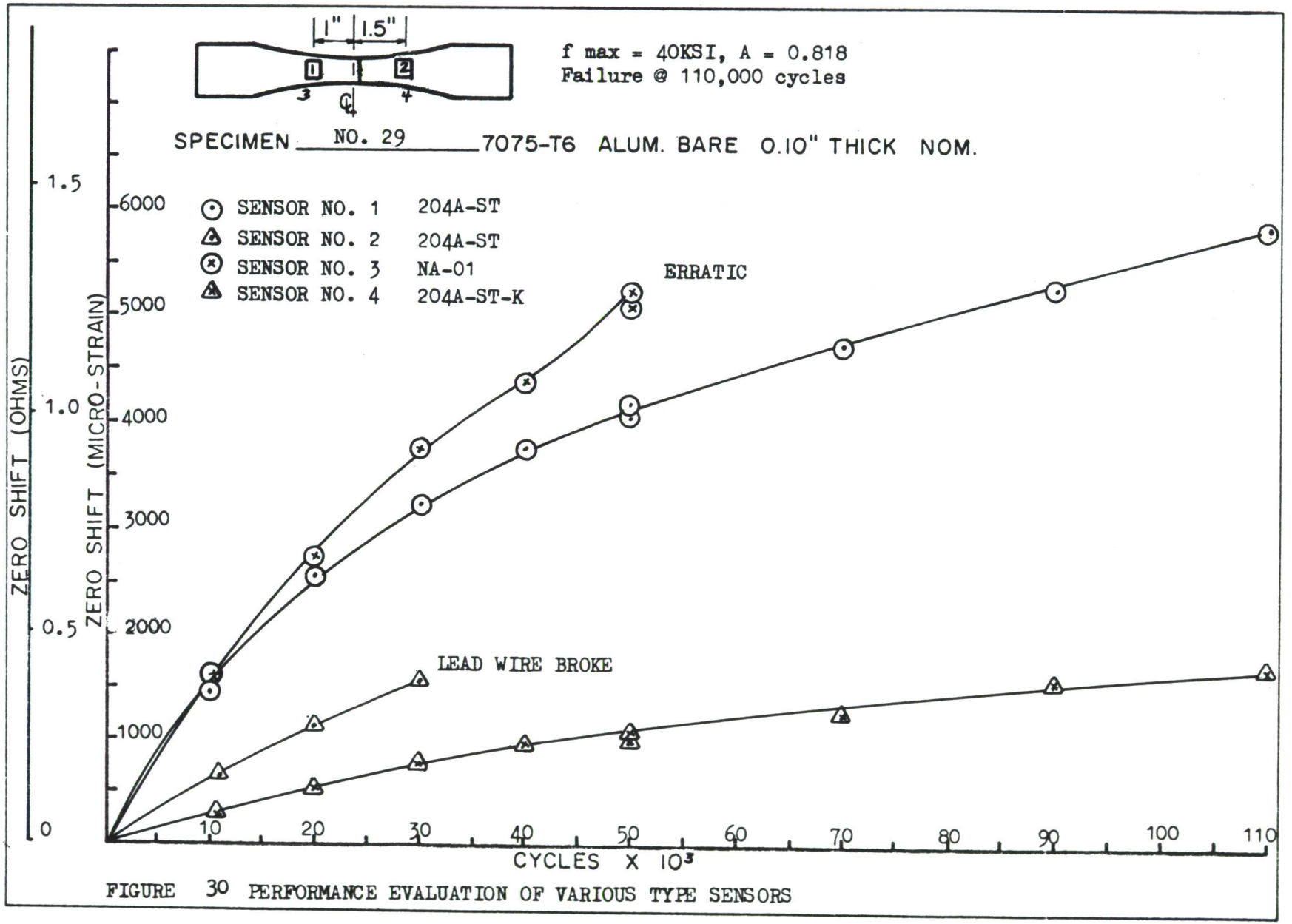

FIGURE 30 PERFORMANCE EVALUATION OF VARIOUS TYPE SENSORS

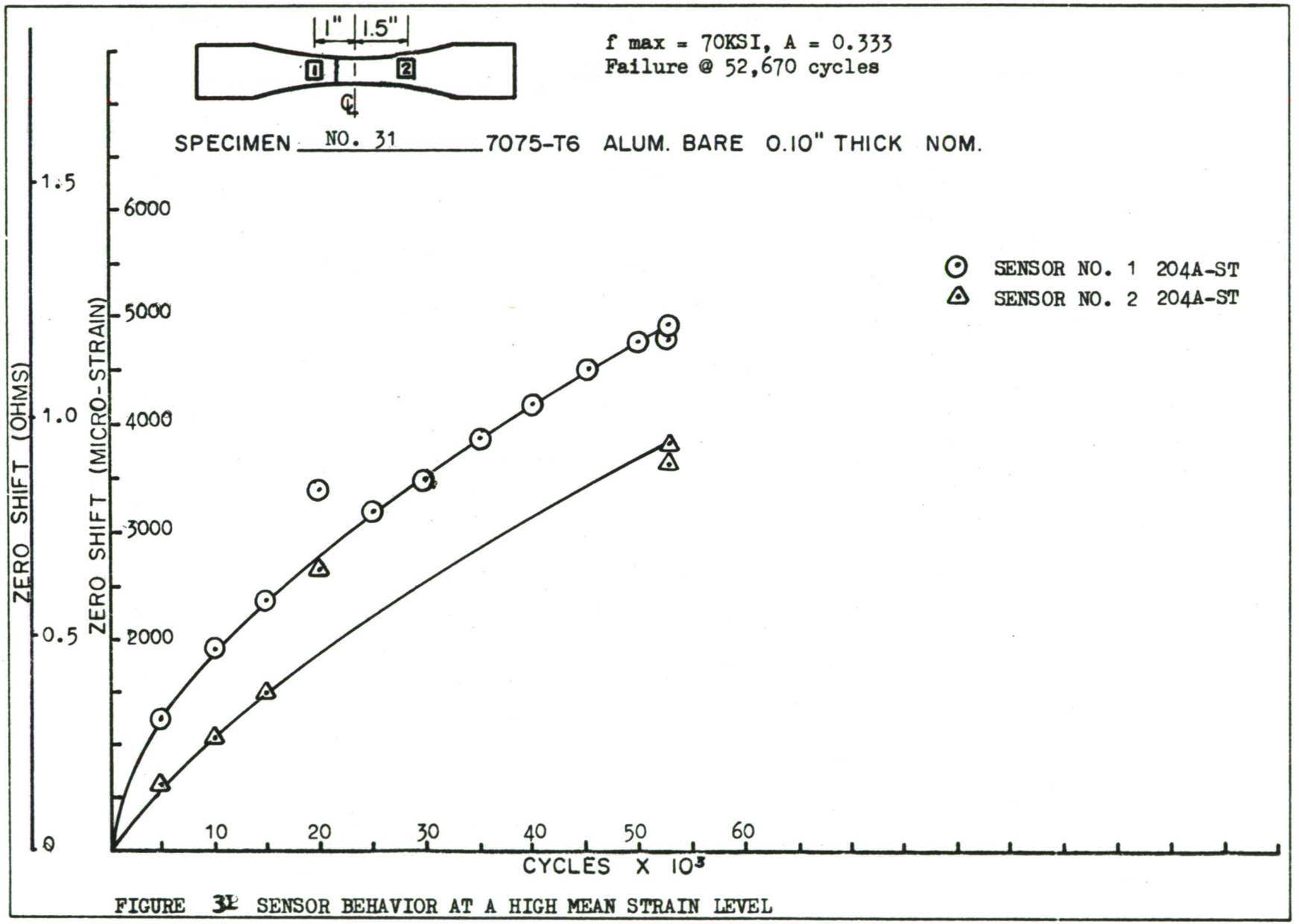

FIGURE 32 SENSOR BEHAVIOR AT A HIGH MEAN STRAIN LEVEL

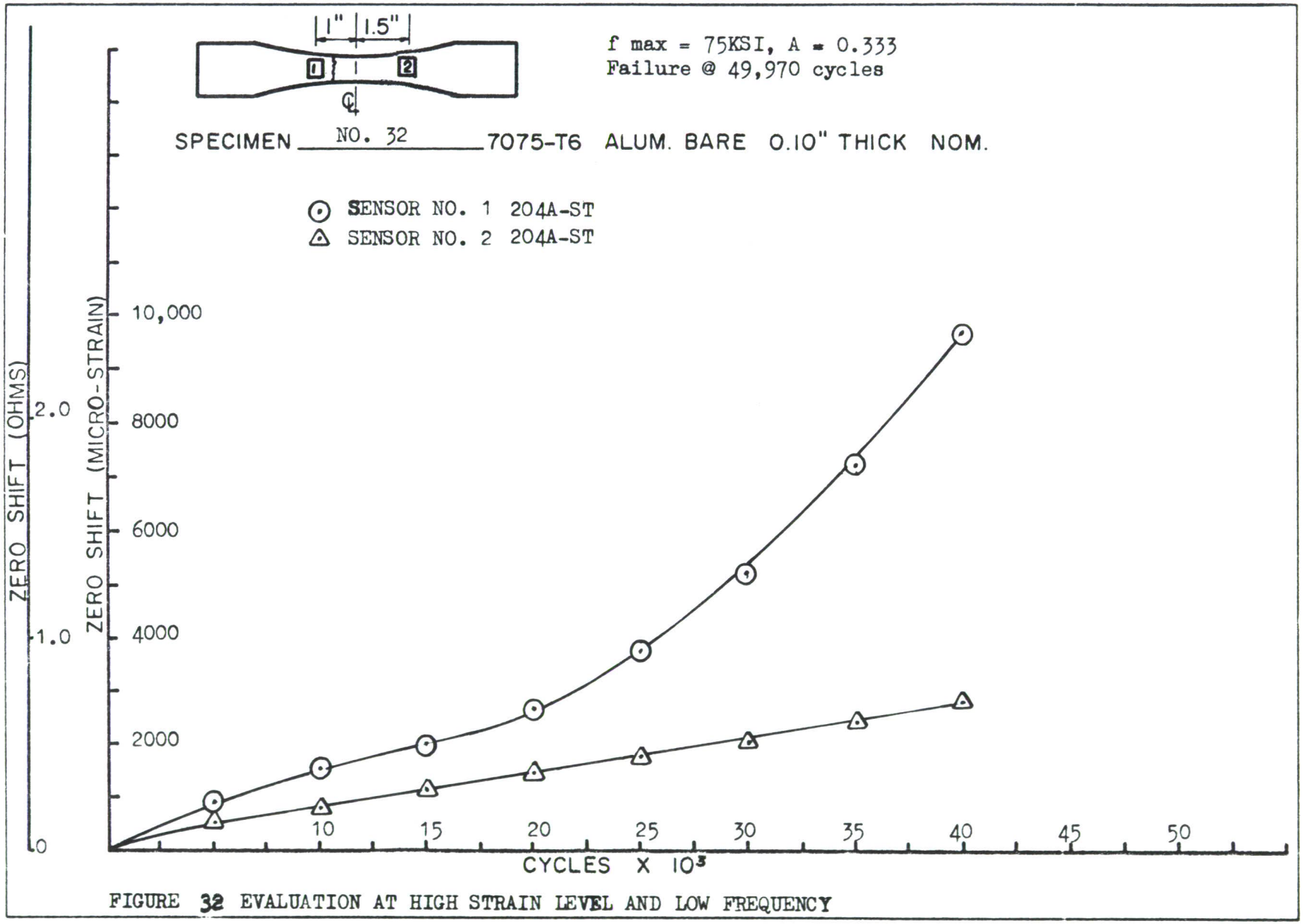

FIGURE 32 EVALUATION AT HIGH STRAIN LEVEL AND LOW FREQUENCY

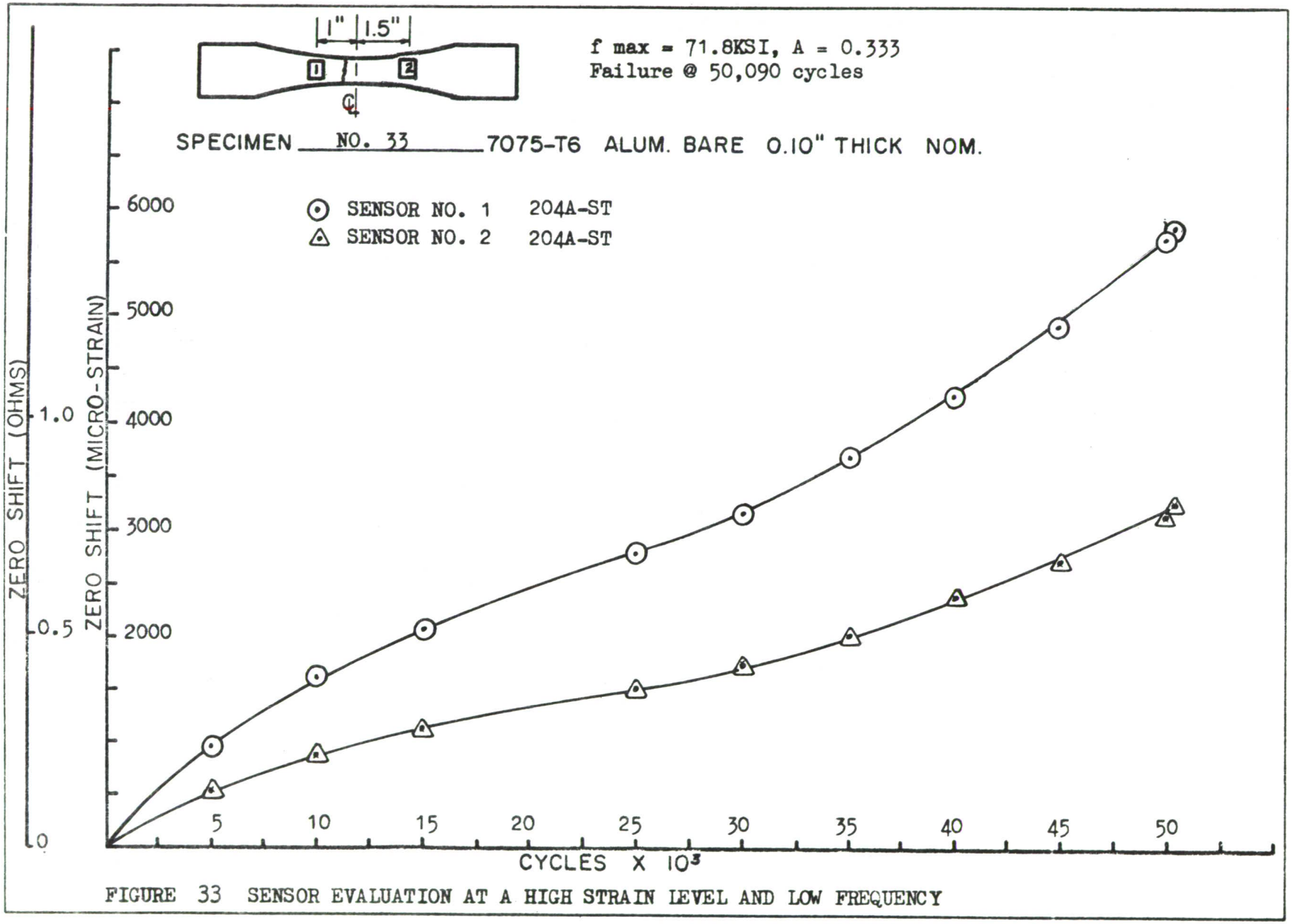

FIGURE 33 SENSOR EVALUATION AT A HIGH STRAIN LEVEL AND LOW FREQUENCY

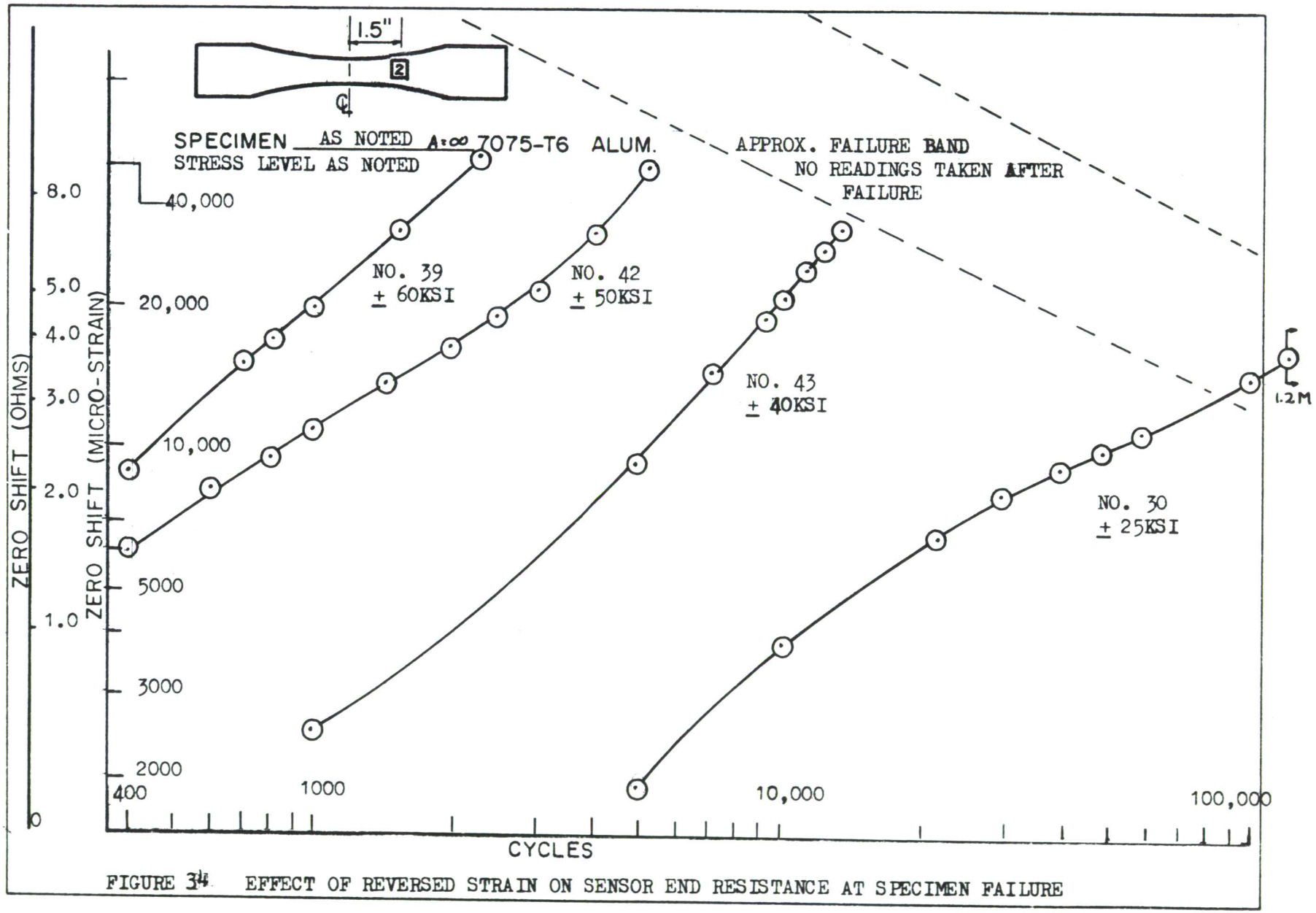

FIGURE 34 EFFECT OF REVERSED STRAIN ON SENSOR END RESISTANCE AT SPECIMEN FAILURE

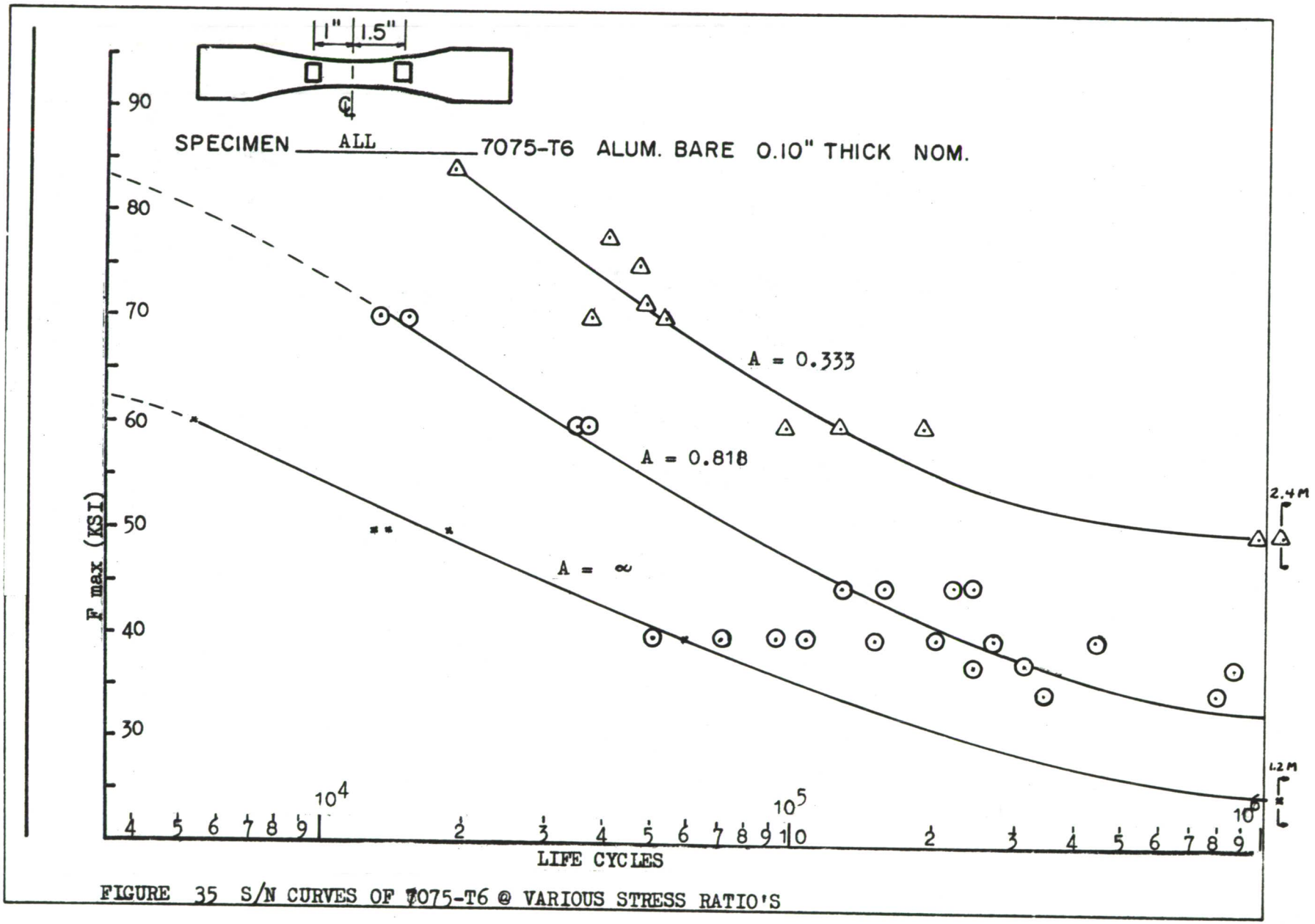

FIGURE 35 S/N CURVES OF 7075-T6 @ VARIOUS STRESS RATIO'S

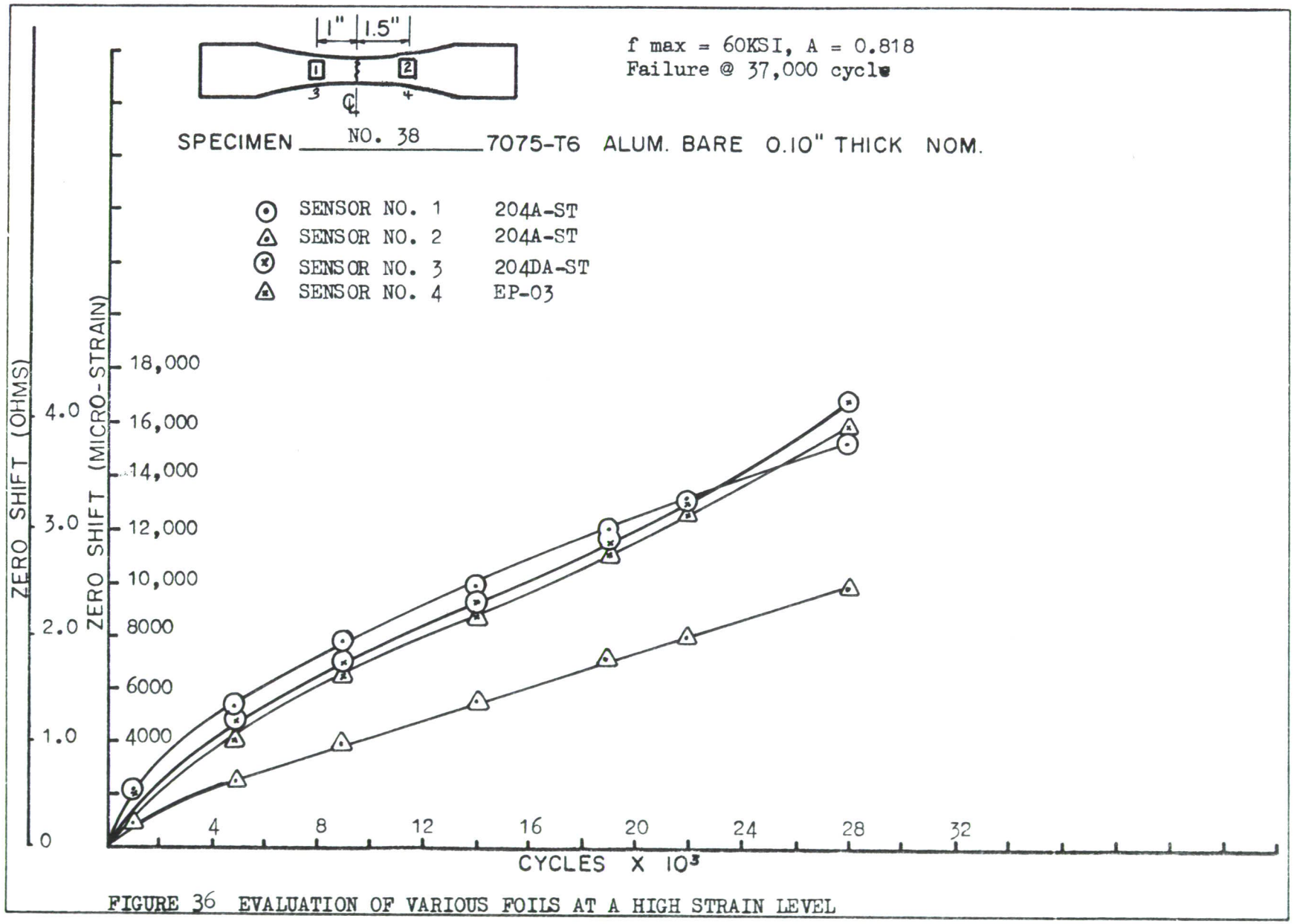

FIGURE 36 EVALUATION OF VARIOUS FOILS AT A HIGH STRAIN LEVEL

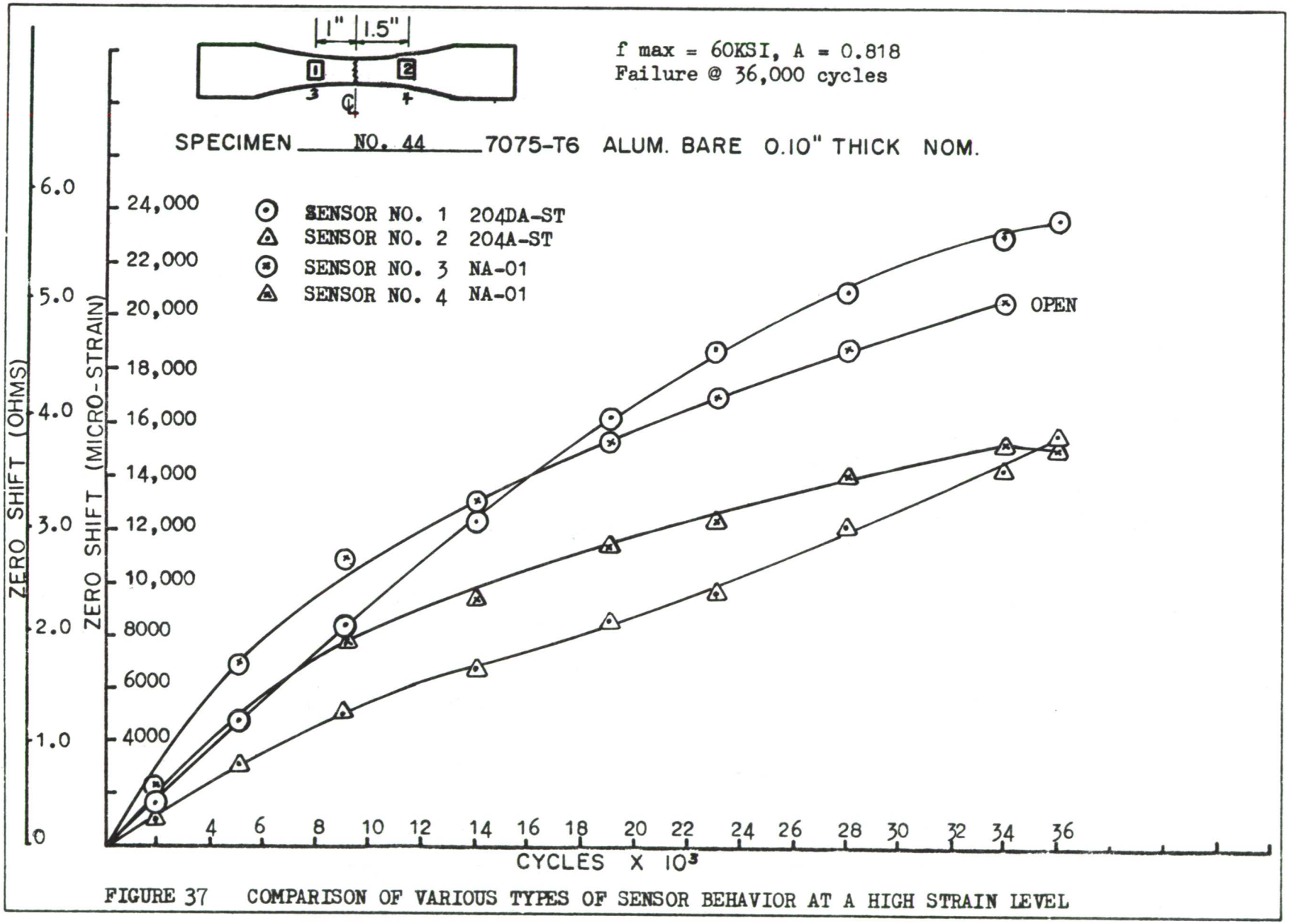

FIGURE 37 COMPARISON OF VARIOUS TYPES OF SENSOR BEHAVIOR AT A HIGH STRAIN LEVEL

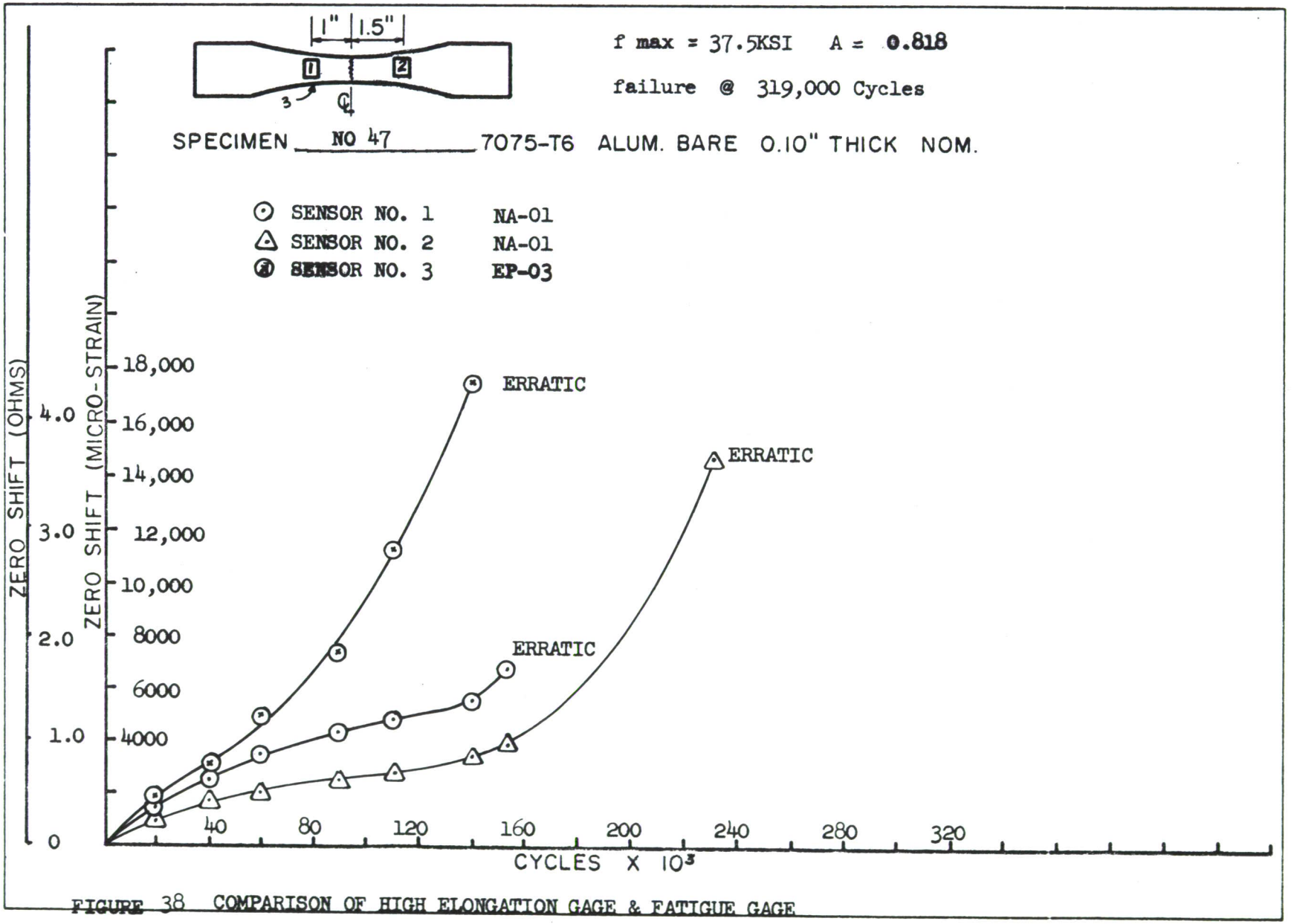

FIGURE 38 COMPARISON OF HIGH ELONGATION GAGE & FATIGUE GAGE

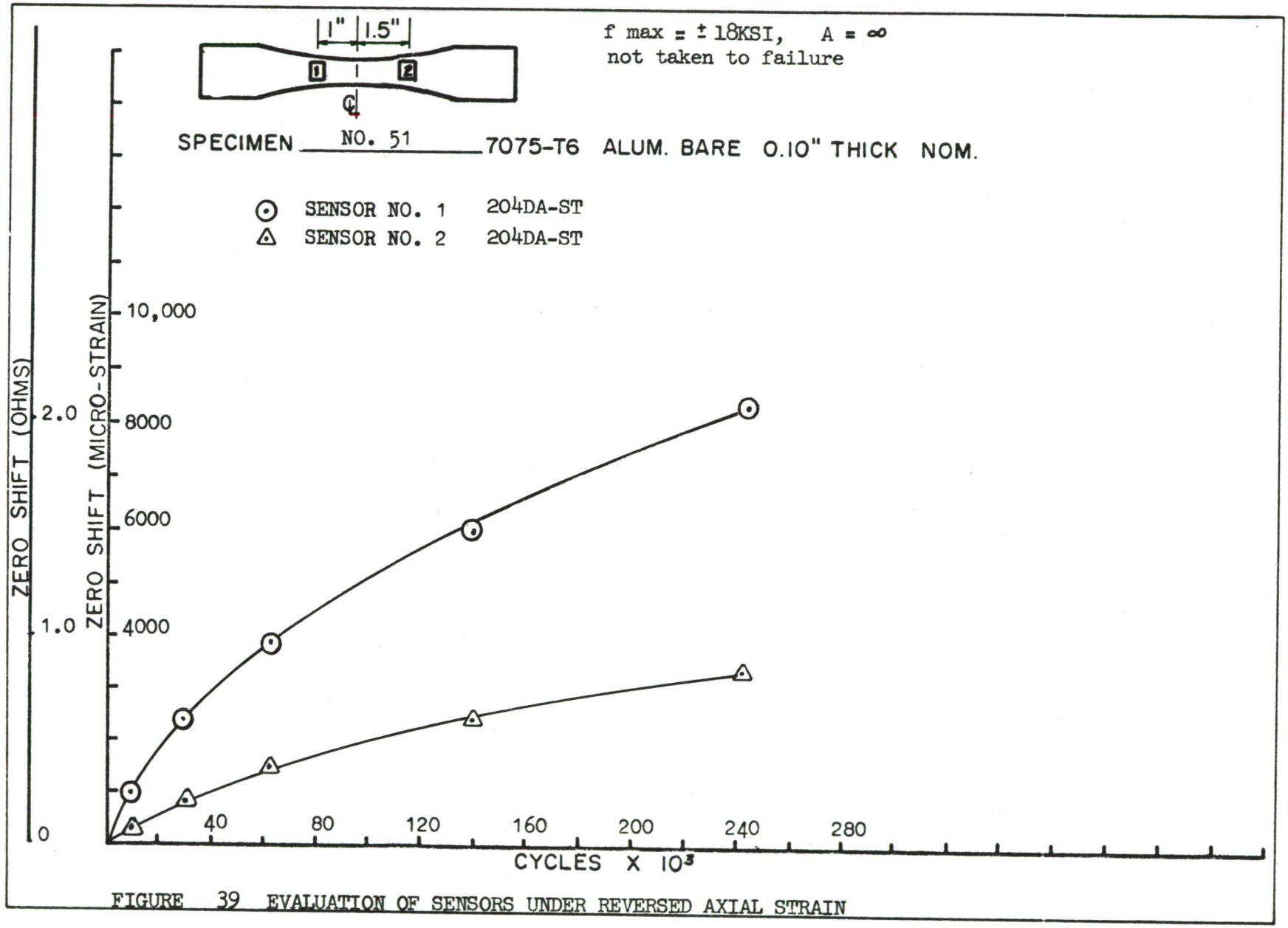

FIGURE 39 EVALUATION OF SENSORS UNDER REVERSED AXIAL STRAIN

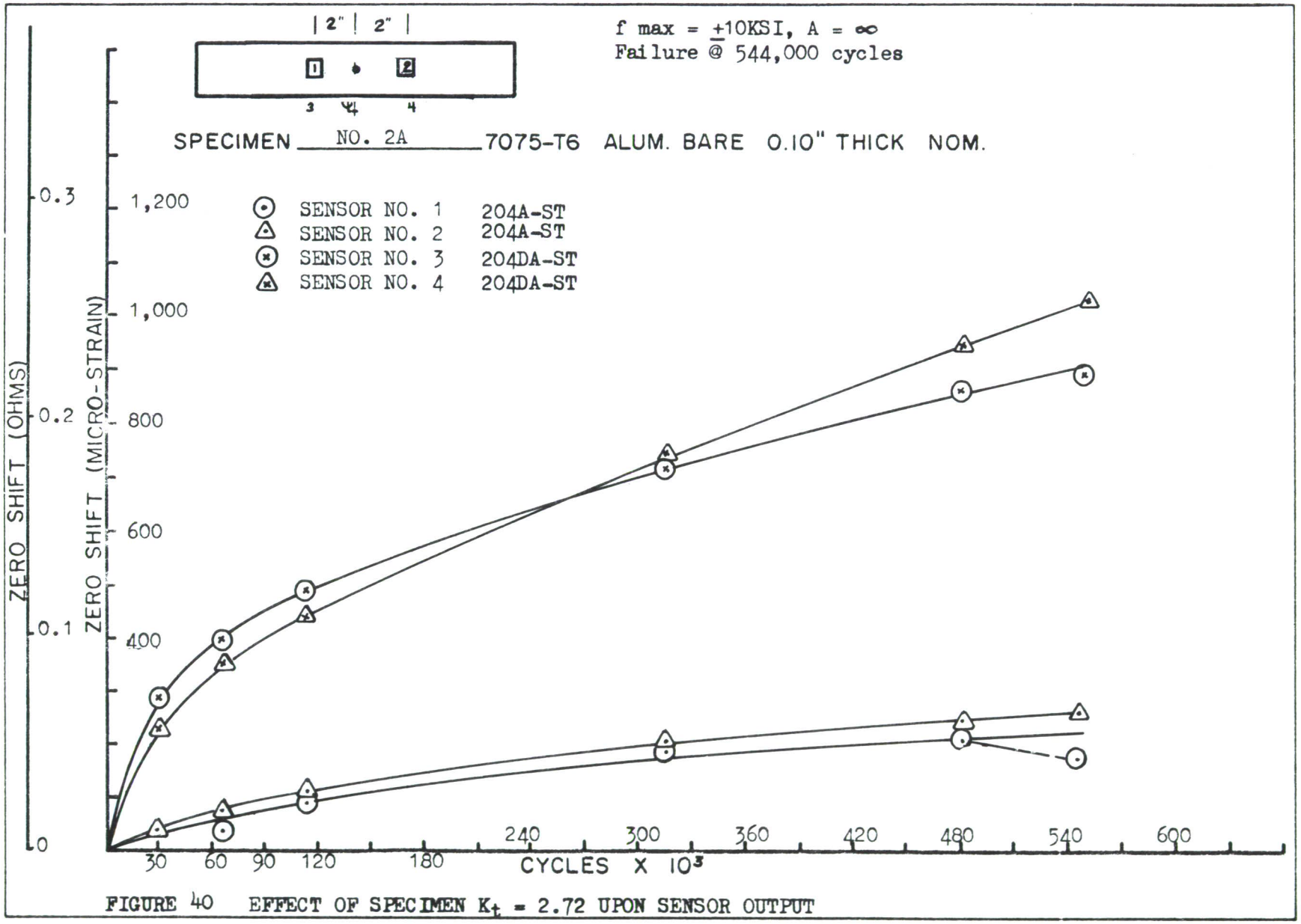

FIGURE 40 EFFECT OF SPECIMEN K_t = 2.72 UPON SENSOR OUTPUT

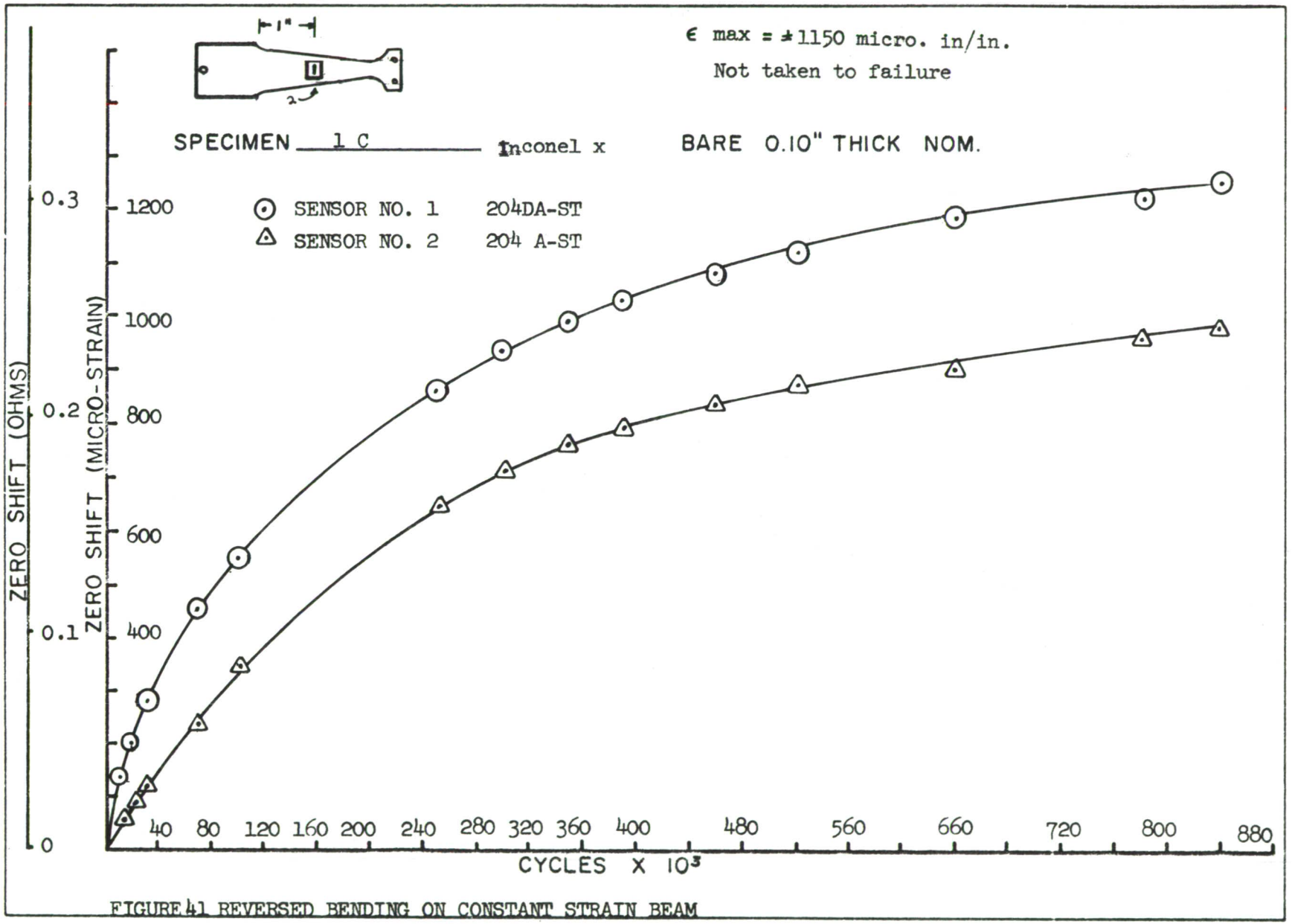

FIGURE 41 REVERSED BENDING ON CONSTANT STRAIN BEAM

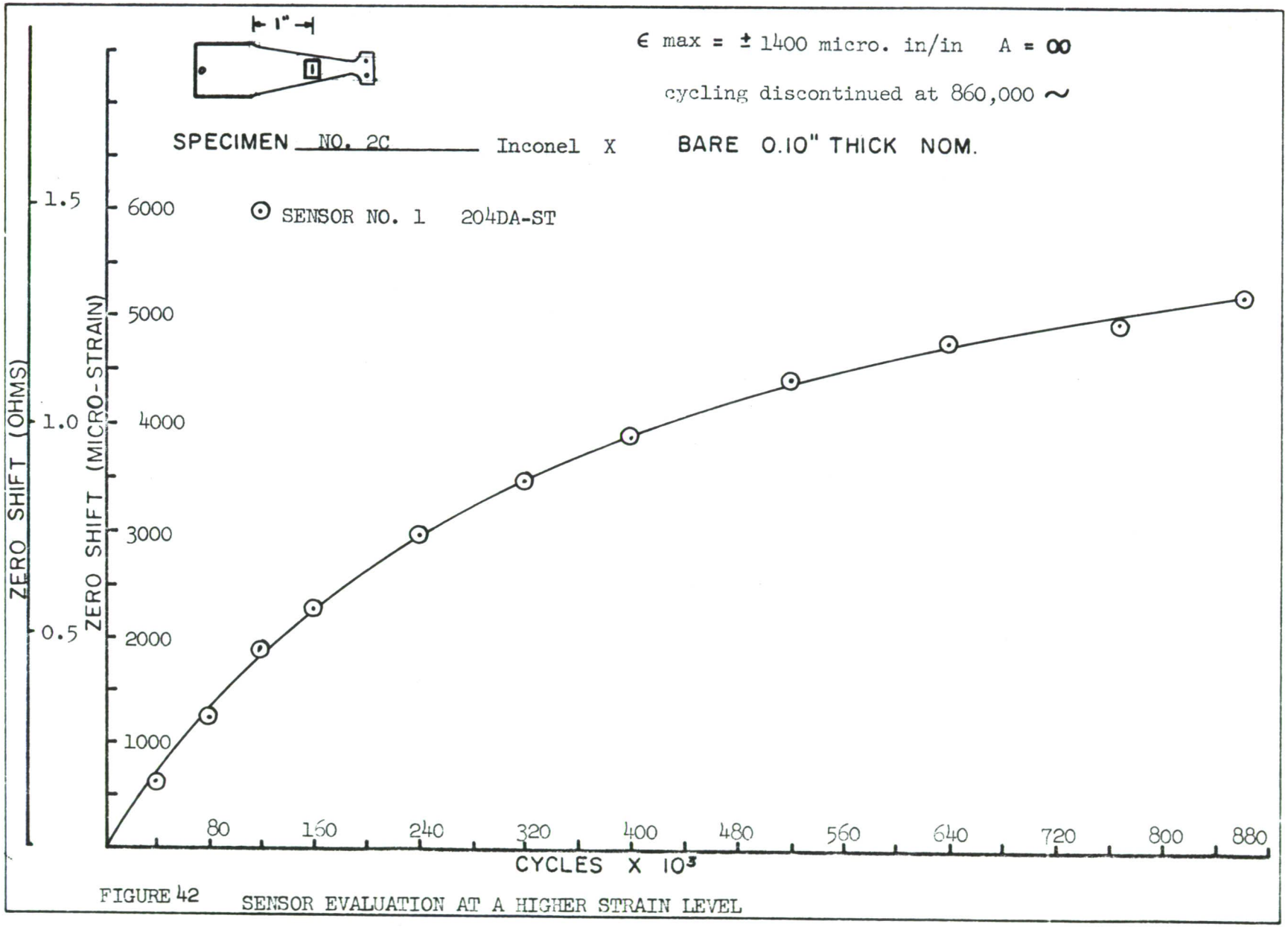

FIGURE 42 SENSOR EVALUATION AT A HIGHER STRAIN LEVEL

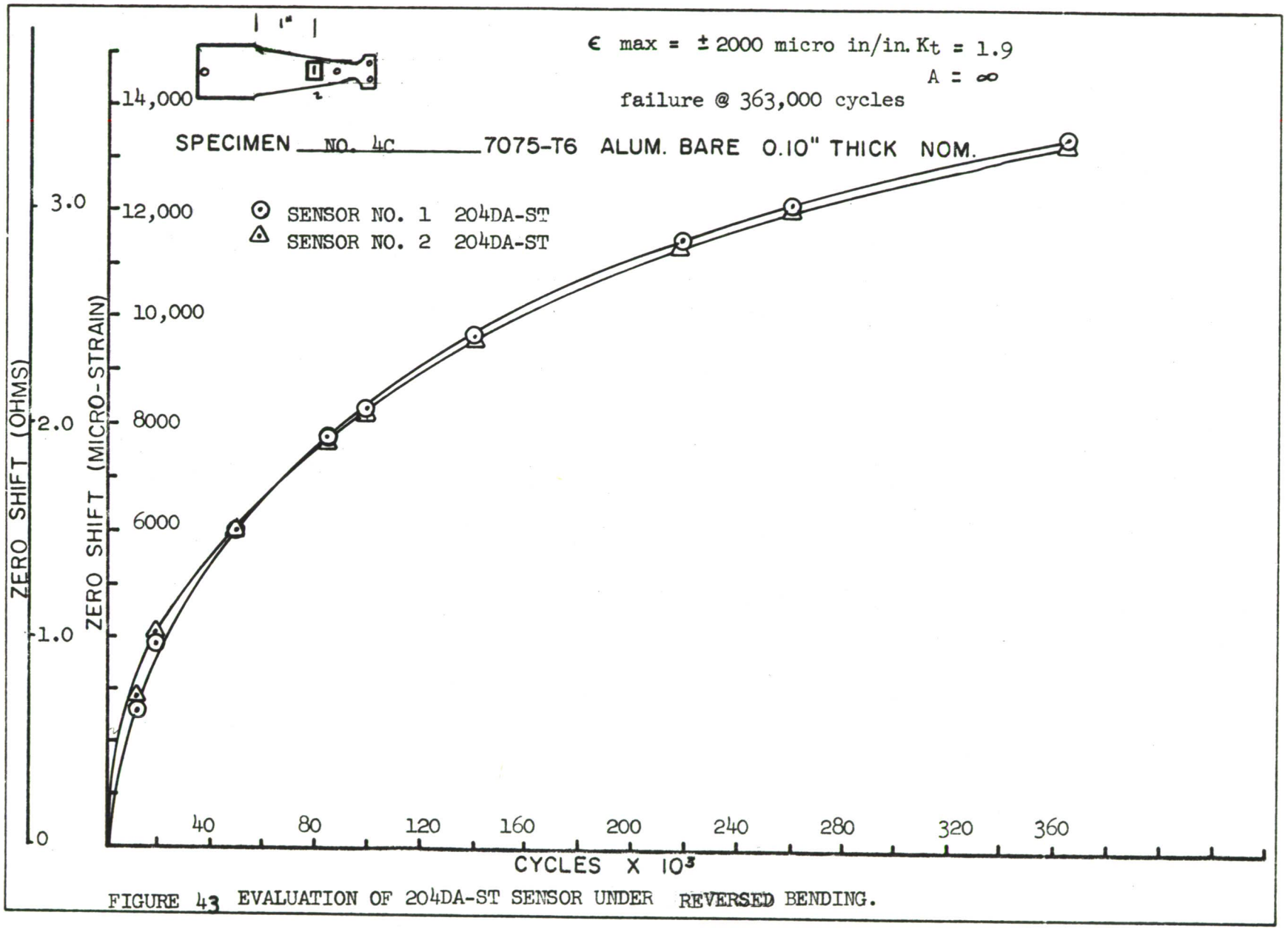

FIGURE 43 EVALUATION OF 204DA-ST SENSOR UNDER REVERSED BENDING.

4.1.2 THRESHOLD SENSITIVITY

The fact that a threshold sensitivity exists is advantageous, however, it would be desirable to have a more flexible one. For instance it would be undesirable for the sensor to indicate a zero shift response to repeated strain below the endurance limit of the structure under investigation. Ideally, the foil should possess characteristics shown in the diagram below, with the capability of shifting the threshold up or down to suit the fatigue characteristics of the structure under surveillance. Ideally the threshold would be considered as a particular point on the sensitivity curve.

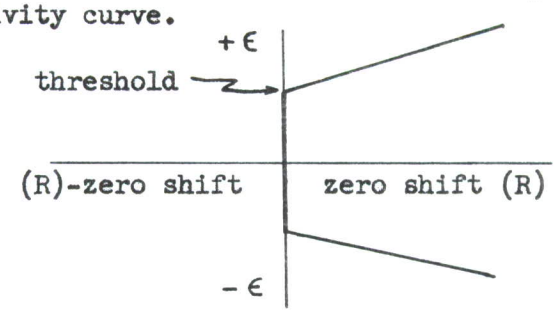

The following diagram shows by a graphical relationship the actual behavior characteristics of the foil in regard to tension/compression strains and threshold sensitivity.

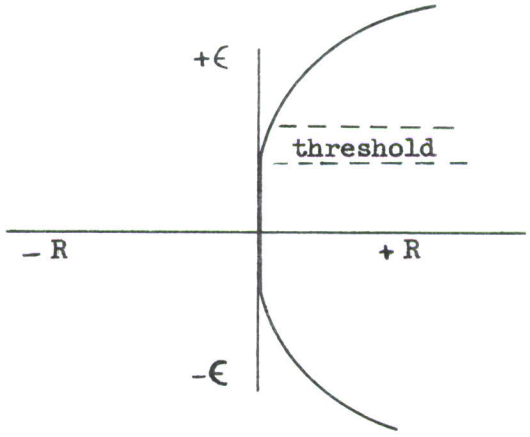

The exact strain level at which the foil will zero shift (threshold sensitivity) is a somewhat nebulous area since a sharp knee to the curve does not exist. The conventional method of obtaining stress-strain curves for a material is not practical for the .00018" thick foil, especially in compression. During a tension evaluation it was indicated that any shearing of the foil edges apparently introduces some work hardening resulting in non-repeatable results. In any event, the threshold could be more accurately defined by running statistical sensitivity checks on a number of sensors bonded to a coupon. The coupon was evaluated over a specified number of cycles at ± 500 micro-strain, than ± 800 micro-strain, and so on until a zero shift was obtained. The completely reversed strain level at which a 250 micro-strain zero shift was obtained within 50,000 cycles was specified as the threshold sensitivity.

It was determined that the threshold sensitivity of the foil could be varied over a range of 960 u in/in to 1200 u in/in by varying the degree of anneal. The values given represent completely reversed strain levels, however the total zero shift output is also a function of mean strain level. The sensor designated as the 204DA-ST has the lowest threshold level with no apparent deterioration in fatigue life. In structural areas with a $K_t = 4$, it was desired to lower the threshold still further to 600 u in/in. One of the experimental techniques investigated involved mounting the sensor on a concave curved shim so that upon bonding to a specimen the sensor would see a tensile prestrain. The purpose was to shift the zero of the sensor lower on the sensitivity curve, which effectively shifts the sensitivity curve to a new lower position. Basically, the technique can be represented as follows:

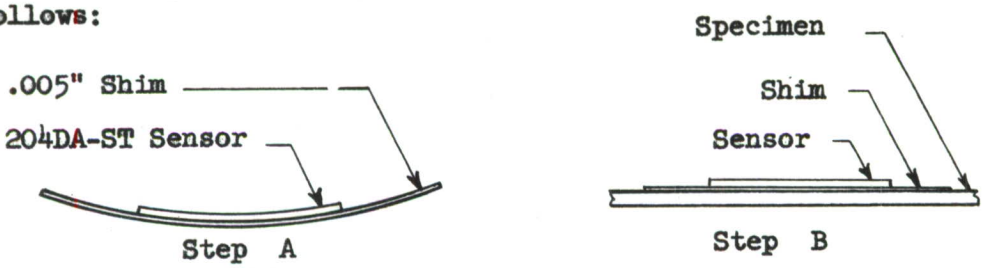

Although the radius of curvature of the .005 aluminum shim could be accurately maintained, the method produced inconsistant results. The outputs of a tension shim sensor as shown in Specimen 9A data, reflects very little improvement in sensitivity. Measurements with an SR-4 indicator before and after bonding to the structure indicated that 500 ± 50 u in/in tension residual strain could be obtained which should have shifted the zero half way down the curve as indicated in the following diagram.

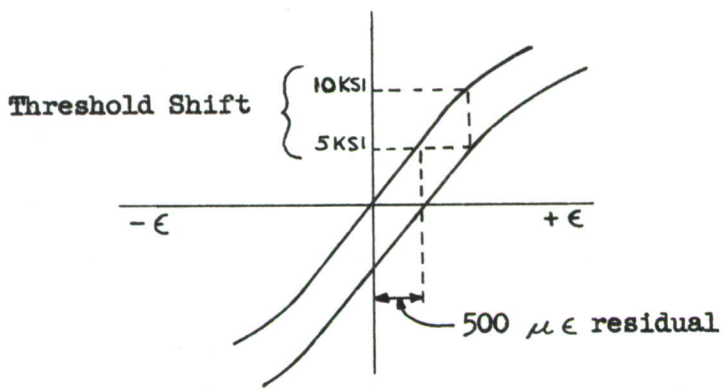

If one desired to work in the area of a stress concentration; a hole, or rivet area appears as the most promising, particularly if a spiral grid sensor could be used. Generally speaking, the strain pattern around a notch, hole, or other stress concentrations does not lend itself readily to a strain measurement due to the difficulty of aligning the sensitive axis of the strain gage grid with the direction of principal strains. A hole in a tensile coupon similar to that shown in the following diagram, creates both tension and compressive strains in areas adjacent to the hole, making conventional strain measurements somewhat hazardous.

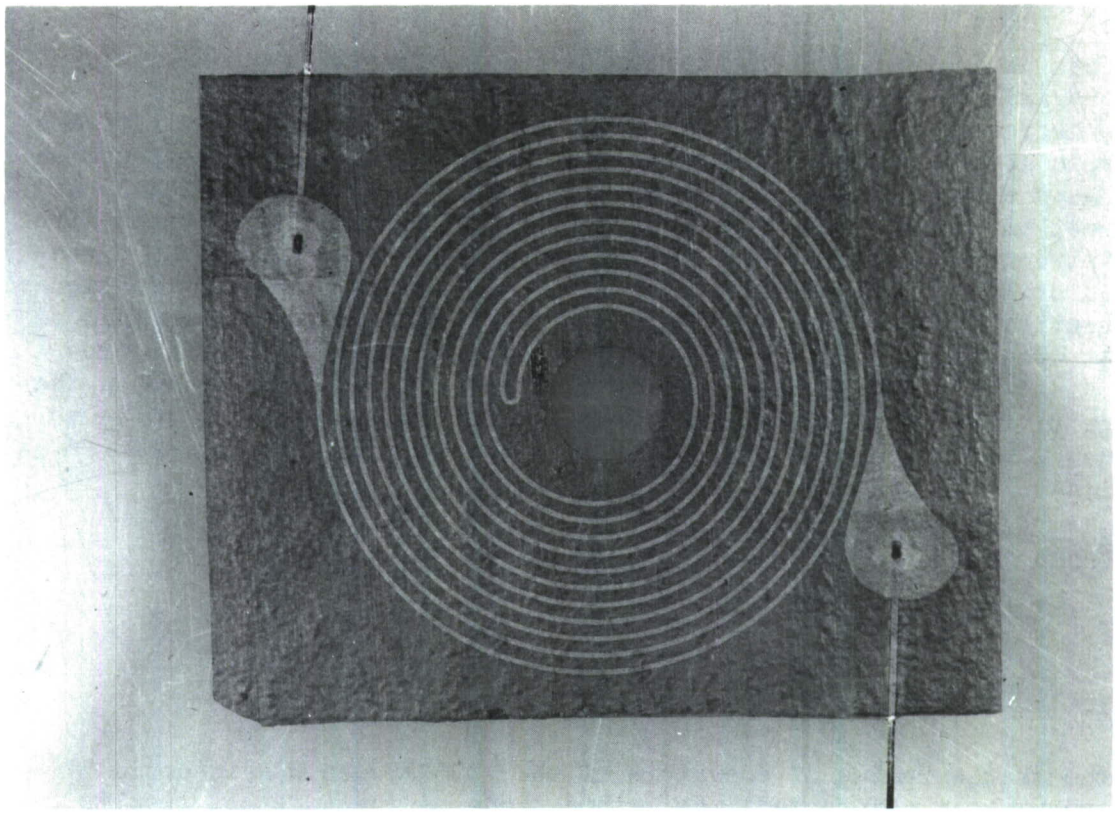

FIGURE 44A BALDWIN SPIRAL GRID FATIGUE SENSOR FOR USE AROUND RIVETS.

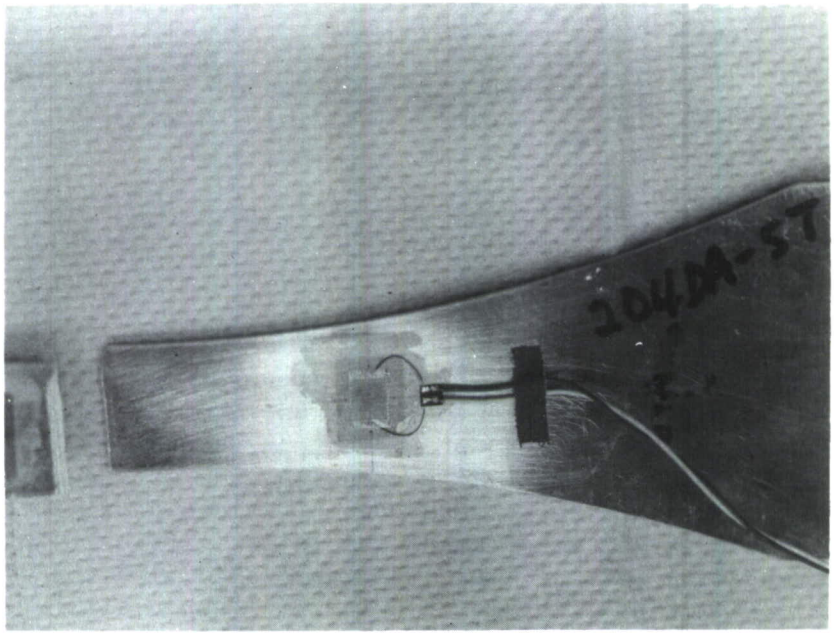

FIGURE 44B TYPICAL SENSOR INSTALLATION ON 7075-T6 ALUMINUM SHOWN AFTER SPECIMEN FAILURE. SENSOR BONDED WITH EPY-150 AND MOISTUREPROOFED WITH GW-1.

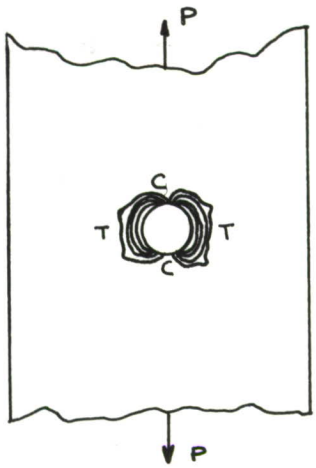

The behavior of the annealed foil in the fatigue sensor is such that repeated strains of either tension or compression or both, will cause an <u>increase</u> in sensor resistance. Thus, the center hole spiral grid construction is readily adaptable for use around rivets, drain holes, etc. This feature makes it attractive for use directly in the stress concentration since the strain level in adjacent nominal areas might be less than the threshold sensitivity of the standard axial fatigue sensor. With this philosophy in mind, an annealed constantan foil sensor was fabricated by Baldwin-Lima-Hamilton according to Lockheed specifications.

The first evaluation of this spiral grid was somewhat disappointing as evidenced by the data from Specimens 6A, 9A, 10A. The size and construction of the sensor as shown in Figure 44A indicates that the design could be improved. It is suspected that the strain pattern on the coupons tested, extended outward from the hole no further than two or three strands of the sensor grid. A review of the strain pattern indicates that the stress gradient around the hole can be pictorially represented as shown below.

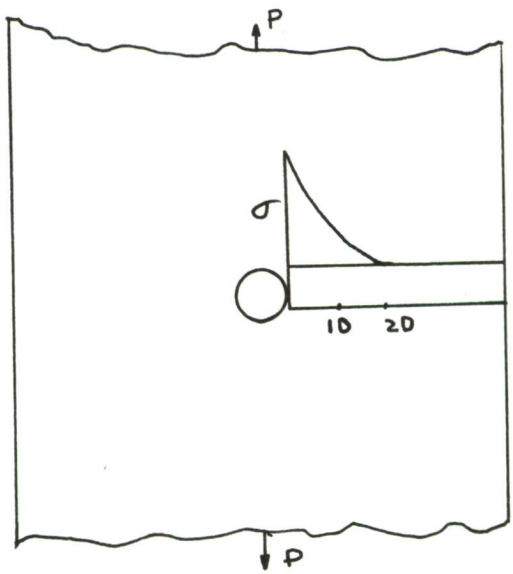

The diagram indicates that the stress is relatively high at the hole edge, but quickly reduces to nominal area stress within 2 hole diameters. The revised grid was selected with reduced spacing between the concentric strands so that all strands are within one hole diameter of the hole edge. The 0.325 inch diameter center hole of the grid was selected as a "happy medium" to fit the usual run of rivets, unfilled holes, or spot welds.

Attempts to improve the threshold sensitivity of the axial sensor prompted an evaluation of commercially available post yield gages such as the Baldwin "PFA" type or the Micro Measurement EP-03 type. As previously mentioned all "high elongation"or "post yield" strain gages will have the same characteristic high zero shift with repeated strains, as the foils which are promoted as fatigue gages.

The selection of the ideal foil and sensor then becomes one of the best combination of high sensitivity, low threshold, and high fatigue life. The evaluation of the EP-03 on Specimen 47 at a relatively low strain level indicates that although it has a high output it goes supersensitive long before specimen failure. Previous comparisons on Specimen 38 and 44 had indicated the EP-03 had a slightly higher output than either the 204DA-ST or the NA-01. A closer review of data and a microscopic examination of the gage indicates that the high output of the EP-03 is the result of a large number of stress concentrators rather than a softer foil.

Of all the foils and configurations of sensors evaluated, it appears that the type 204DA-ST shows the optimum behavior characteristics. Extensive checks have been made to confirm the improvements in threshold sensitivity and output of the 204DA-ST over the 204A-ST. The data shows conclusively that a desirable improvement has been made particularly at the lower strain levels where it is most needed. A review of the date from Specimen 2A and other tabulated data over a wide strain range regarding the two types of sensors under consideration indicates that the double annealed foil has the higher output with no apparent sacrifice in fatigue life. Below is shown the relative percentage increase in output of the 204DA-ST over the 204A-ST over all investigated strain ranges, as taken from statistical averages.

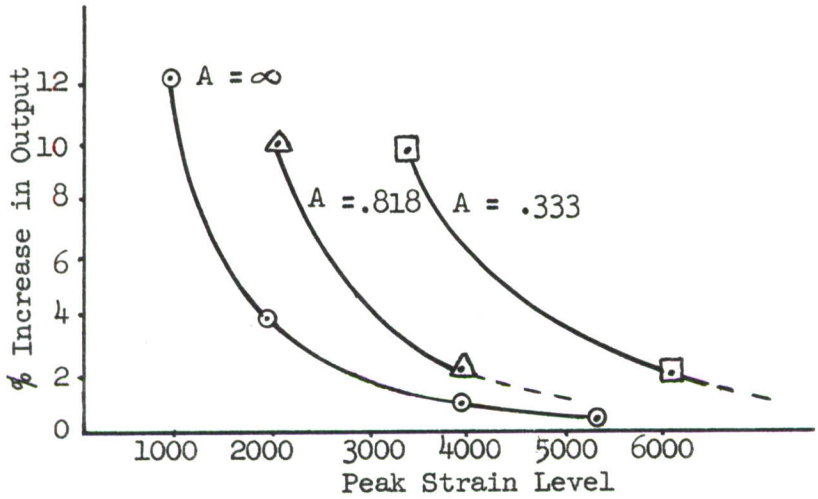

4.1.3 WEATHEROMETRY TESTS

In order to evaluate the performance characteristics of the sensor, under weather exposure, two (2) specimens were instrumented and then subjected to a simulated weather environment for one year. An Atlas weatherometer with a 17-3 cam was used in this test. This program allowed the weatherometer to simulate rain for three minutes at seventeen minute intervals with alternate sunshine supplied by carbon arc electrodes. According to specifications supplied by Atlas Electric Devices Company, 300 hours of weatherometer exposure is equivalent to one year exposure of actual weather in the central portion of the north temperate zone. After Specimen 40 was subjected to one year of typical weather the sensors were given a quality control check and then evaluated in fatigue.

When this data is compared with data from a coupon (Number 101) which had been exposed to actual Georgia weather for 12 months, it is apparent that a valid simulation of weather was obtained. If the data from Specimen 40 is compared with data from Specimen No. 21 also cycled at an f max of 45KSI, it can be seen that when specimen fatigue life is reduced by weather exposure the end resistance of the sensor is also reduced.

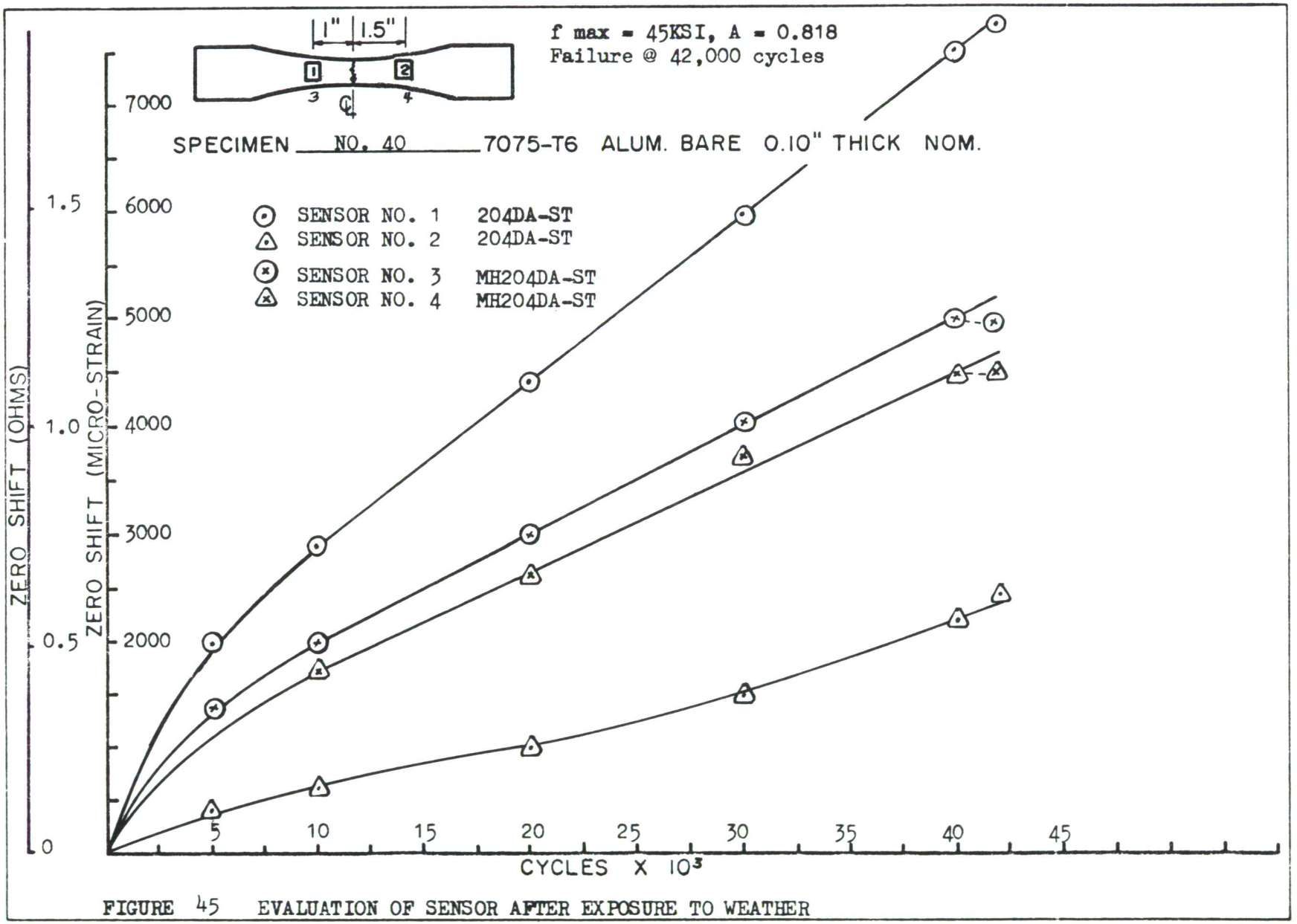

FIGURE 45 EVALUATION OF SENSOR AFTER EXPOSURE TO WEATHER

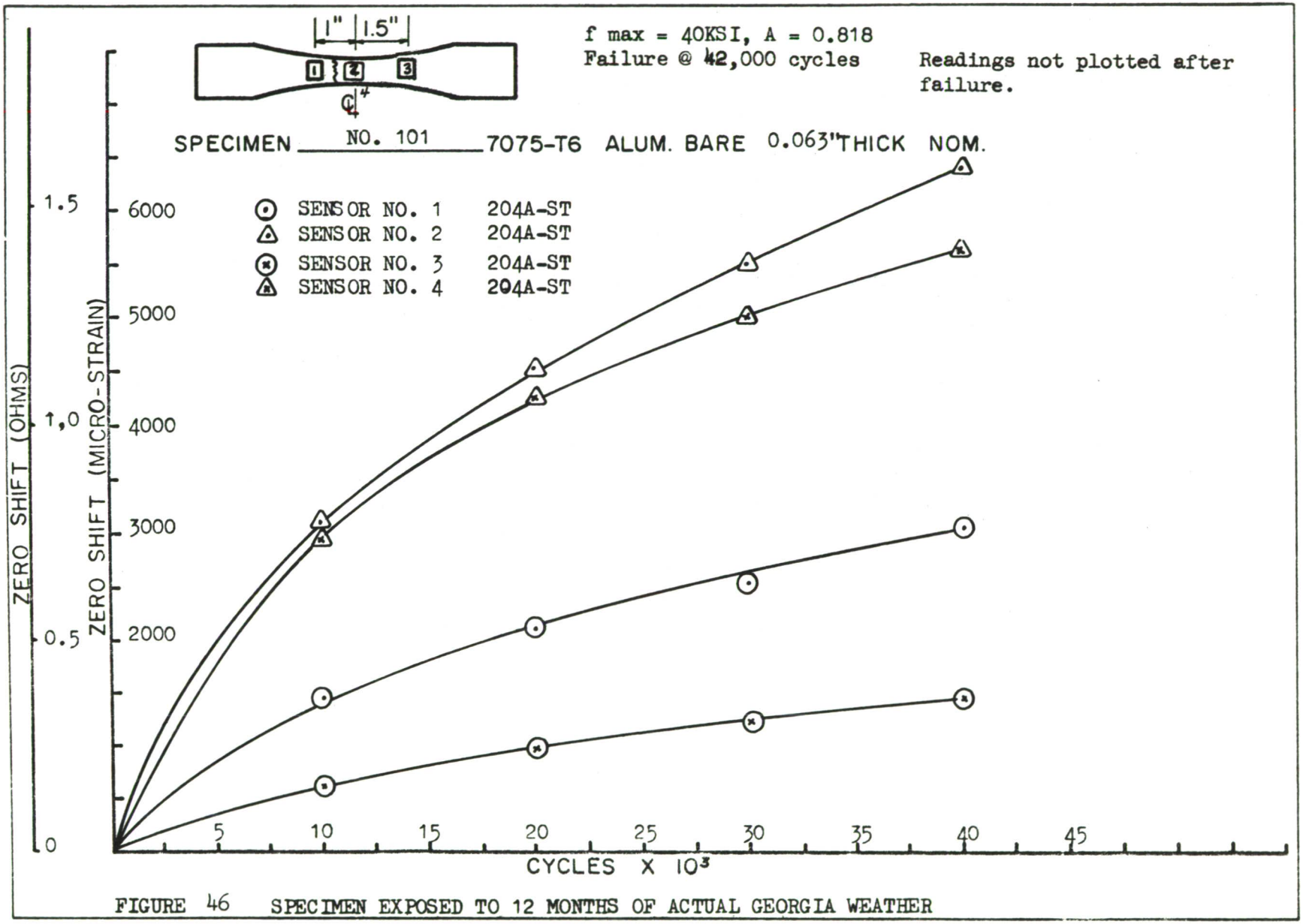

FIGURE 46 SPECIMEN EXPOSED TO 12 MONTHS OF ACTUAL GEORGIA WEATHER

4.1.4 ELEVATED TEMPERATURE TESTS

In order to optimize an elevated temperature fatigue sensor, two different foils and three different backings were investigated. A comparison is made with a standard anneal and a double anneal constantan in combination with a glass fiber, epoxy resin, and an asbestos backing. The constantan foil limits the useful elevated temperature service of the sensor to approximately 450°F. Karma would have been useful above 700°F, however, the Karma has not produced the desired results in regard to sensitivity. Data from specimen T-2 indicates that the resistance change of the annealed Karma foil (Type MH304AE) is very insensitive and erratic. Further comparisons of the various sensors used on specimen T-2 indicates the double annealed foil in combination with the fiber glass backing, has a considerably higher output than the same foil in a softer asbestos backing. The specimen was not taken to failure since the test was conducted at room temperature and would have operated for a large number of cycles at the 90KSI stress level. The evaluation of sensors on specimen T-2 indicates that the type MH204DA-ST was optimum for further evaluations at the elevated temperature of 400°F.

During the evaluation of the optimized MH204DA-ST fatigue sensor at 400°F on coupons T-3, T-4, T-5, and T-6, several irregularities were noted. The data was random, non-repeatable and look suspicious when it did not follow the characteristic curves established during room temperature tests. A review of literature regarding fully annealed (soft) foils indicated that work hardened foils might be re-annealed at 400°F if a very long time period were allowed. Reference 11 states that the fatigue induced zero shift in strain gages can be partially reversed by heating. These investigators discovered that the fatigue induced resistance increase in foil strain gages will be approximately 20% retro-acted at 250°F in 120 hours and approximately 70% more in 90 hours at 400°F.

Two (2) of the type MH204DA-ST fatigue sensors, which had been work hardened at room temperature to a fatigue induced resistance increase of 2.4% (12,000 microstrain), were subjected to a 90 hour heat soak at 400°F. The data from these two sensors indicated that the so called "irreversible" resistance (Ref. 6) increase could be reversed approximately 30% by a prolonged heat soak.

Although the number of samples tested is insufficient to determine the exact degree of retroaction possible, the samples are adequate to conclude that this phenomena is present.

As a possible solution, encapsulation and a variation in the alloy, is suggested although a modified karma foil has been rejected as insensitive. In any event, development of a satisfactory elevated temperature fatigue sensor appeared beyond the scope of the program. The present sensor does not appear feasible since the behavior characteristics are such that the fatigue data obtained is rendered useless by a prolonged heat soak.

A check of three (3) type 204DA-ST room temperature fatigue sensors was initiated to determine if re-annealing could occur at a lower temperature. The three sensors selected had been exposed to fatigue induced work hardening and had indicated a zero shift or resistance increase of approximately 2% (10,000 microstrain). The sensors were then subjected to a 40 hour heat soak at 250°F.

Readings after the 40 hour exposure indicated that none of the fatigue induced resistance increase was retro-acted. In fact, the only measurable variations in readings reflected a slight increase in resistance readings. This might be expected since the temperature coefficient of resistance of low temperature solder may be slightly increased by a prolonged heat soak.

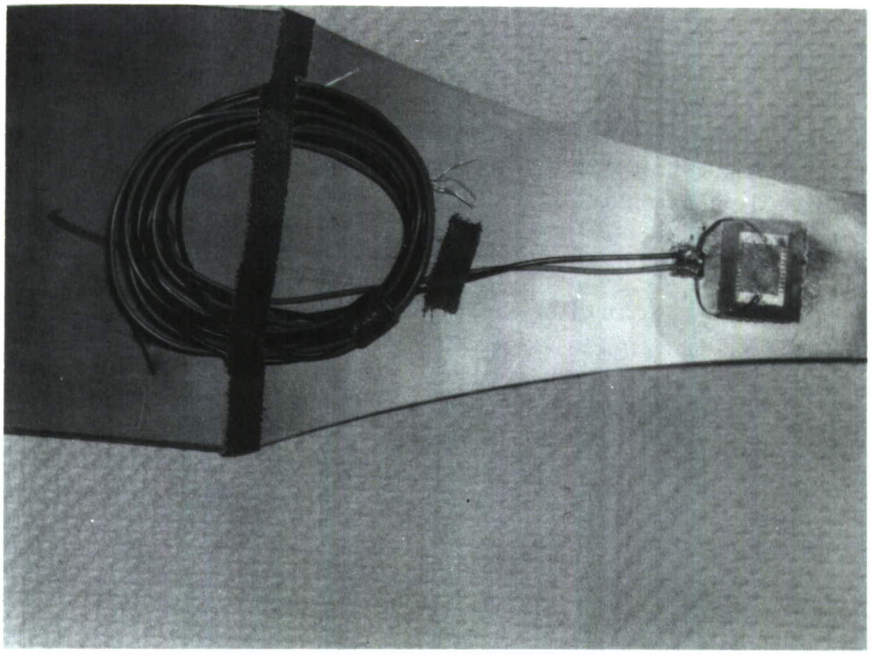

FIGURE 47 A TYPE HA204DA-ST FATIGUE SENSOR INSTALLED ON TITANIUM.

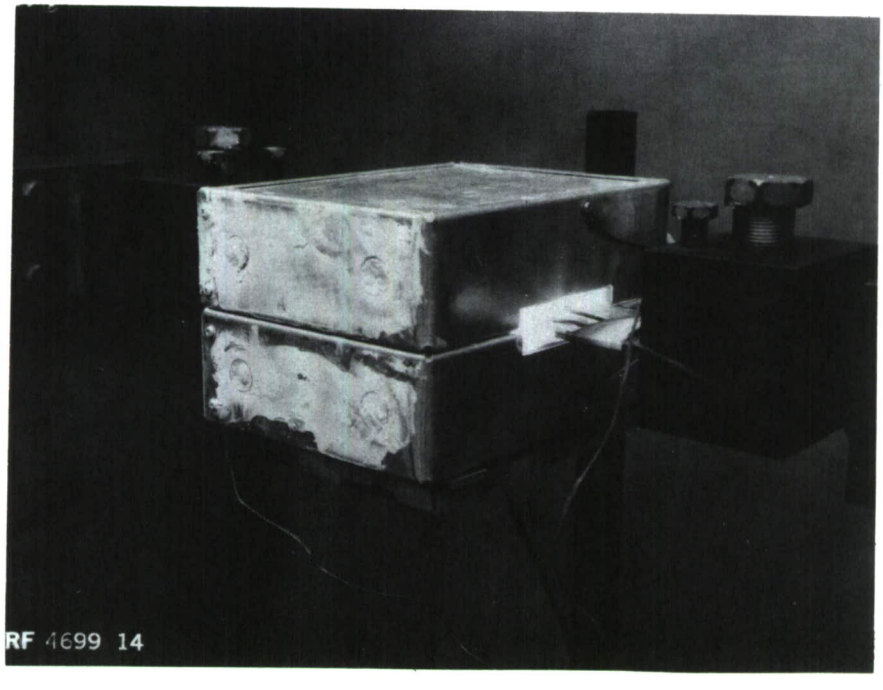

FIGURE 48 ELEVATED TEMPERATURE EVALUATION IN PROGRESS.

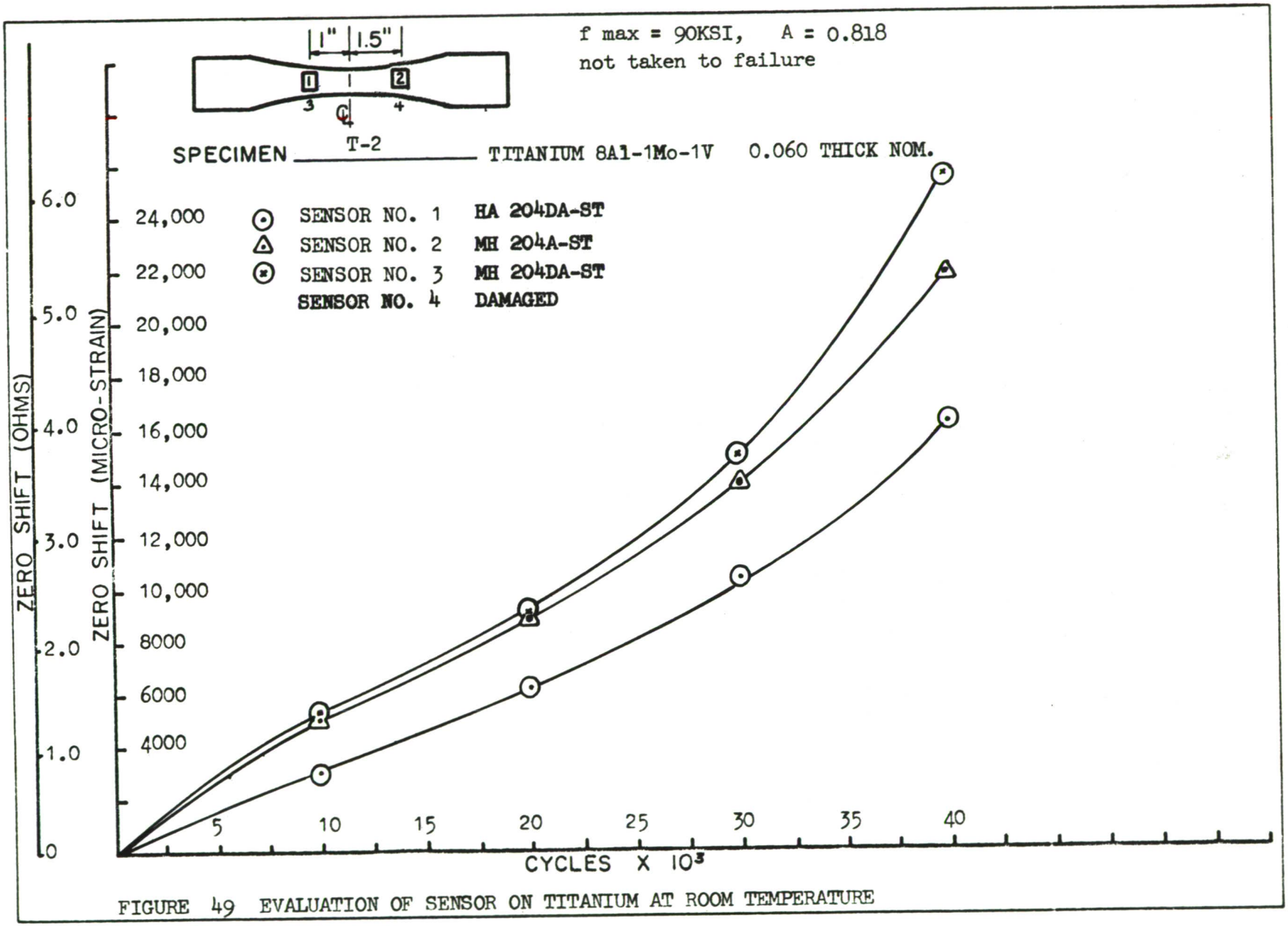

FIGURE 49 EVALUATION OF SENSOR ON TITANIUM AT ROOM TEMPERATURE

4.1.5 LOW TEMPERATURE TESTS

Since a high altitude aircraft structure may be subjected to temperatures of -65°F for extended time periods the performance capabilities of the sensor in this environment was evaluated. During laboratory testing it was elected to use LN_2 rather than CO_2 to provide the necessary environment of -65°F. The low temperature tests also permitted an evaluation of the sensors coefficient of thermal expansion and resistance over a much wider range. The tests conducted at stress levels of 45KSI and 60KSI indicate that the fatigue life of the material is significantly increased at the lower temperatures. Coupon No. 38 & No. 44 at 60KSI stress level and room temperature had a life of 37,000 and 36,000 cycles respectively while coupon No. 52 at the same stress level and -65°F showed a life of 179,000 cycles. However the sensor end resistance on coupon No. 44 and No. 52 were very nearly the same even with the wide spread in fatigue life.

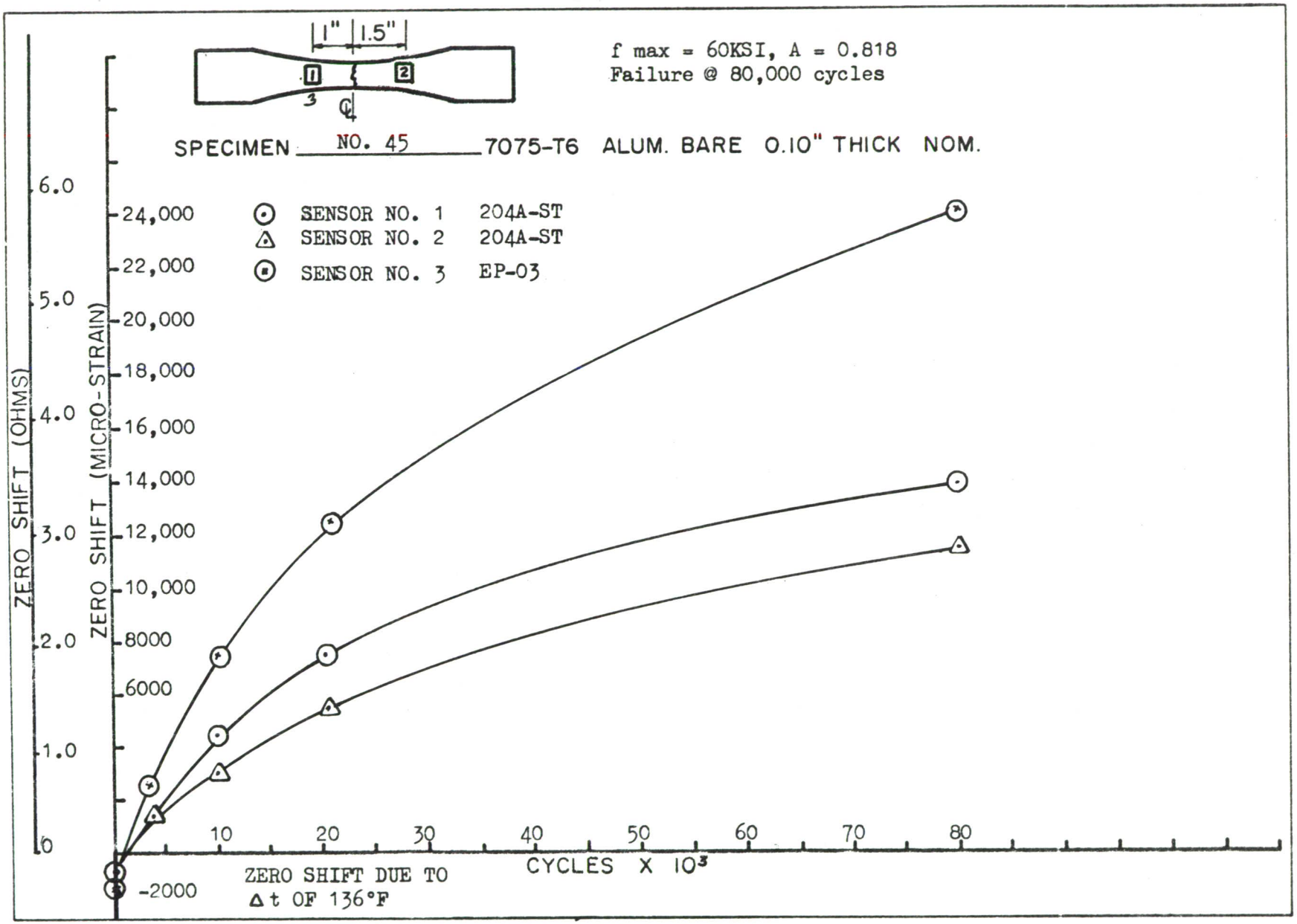

FIGURE 50 LOW TEMPERATURE EVALUATION OF SENSOR BEHAVIOR

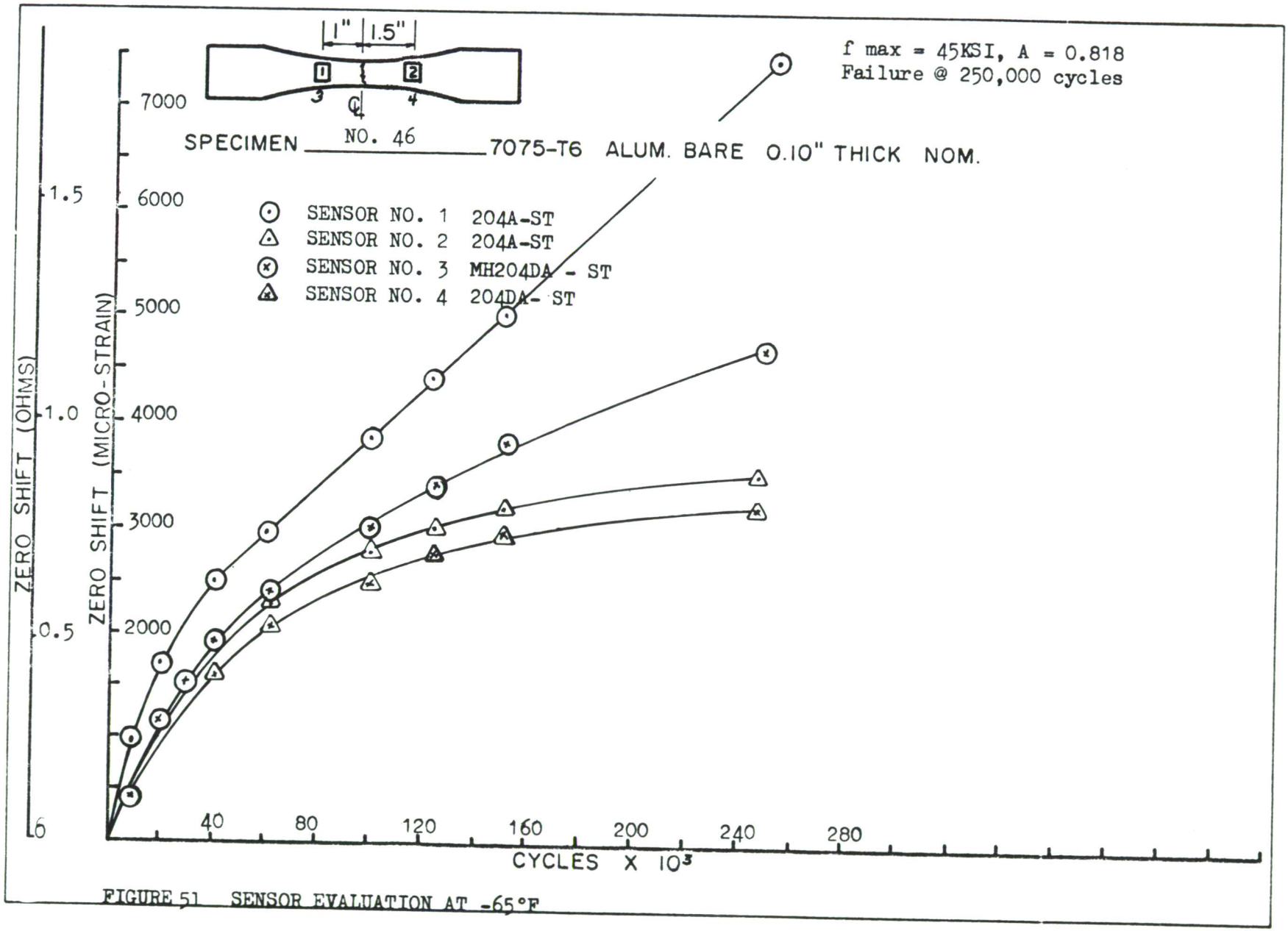

FIGURE 51 SENSOR EVALUATION AT -65°F

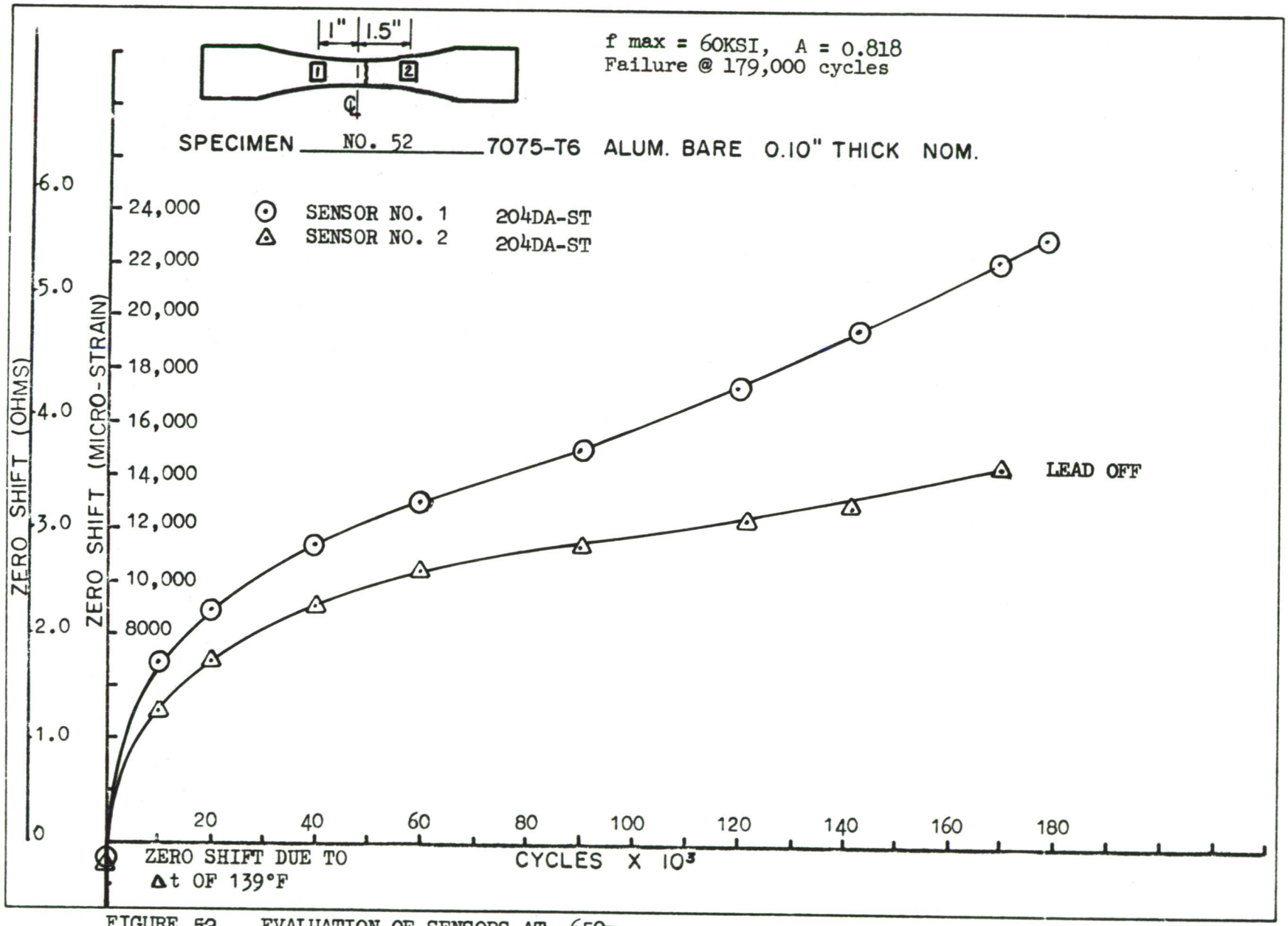

FIGURE 52 EVALUATION OF SENSORS AT -65°F

4.1.6 EVALUATION OF FATIGUE SENSORS AT TWO LOAD LEVELS

Although Miner's theory neglects the concept that high strain levels applied during early cycles results in differences in fatigue damage than when applied during later stages; it is generally recognized in industry that the order in which high stress levels are applied will affect the fatigue life of a material. It was therefore desirable to evaluate the effect of this phenomena versus the capabilities of the fatigue sensor, since previous testing had been done at constant amplitude. It would, of course be desirable to have the sensor indicate a narrow band width of resistance at specimen failure regardless of the order of cyclic load application. For the two level tests, a constant mean load of 38.5KSI was selected for both load levels, with the 70KSI maximum load level having a stress ratio of 0.818 and the other load level of 51.3KSI a stress ratio of 0.333. Graphically, the spectrum can be represented as shown below:

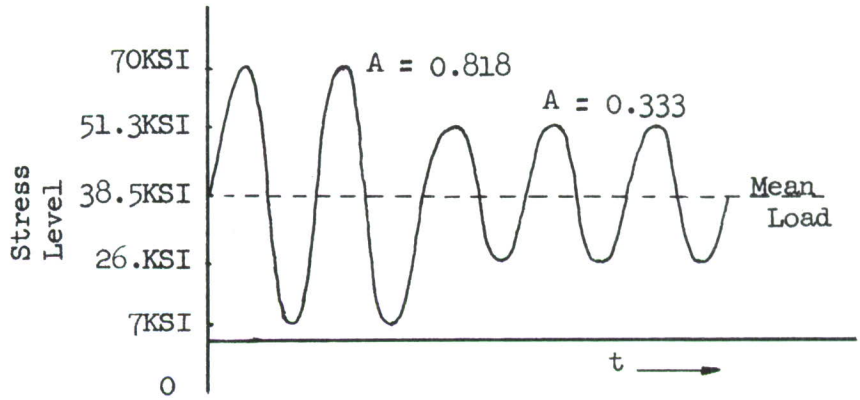

Two types of sensors were evaluated in this regard, that is the 204A-ST and the 204DA-ST. In all cases, the preferred behavior was exhibited by the 204DA-ST fatigue sensor. The consistant high output of the double annealed sensor at a wide range of cyclic strain levels reinforced it as the optimum of all foil sensors evaluated.

The number of cycles representing a given portion of specimen fatigue life at a particular stress level was selected from baseline data taken from the S/N curves shown in Figure 35. In Specimen No. 48 for example, 6000 cycles and 7000 micro-strain zero shift represents approximately 50% of the fatigue life of the coupon at 70KSI and A = 0.818, as determined from the S/N curves. At 51.3KSI and A = 0.333, half life of the specimen approximates 300,000 cycles and a sensor zero shift of 1200 ue, when a point is selected from baseline data as shown by the S/N curves. When these two conditions are imposed on one specimen, the order in which they are imposed has a decided effect upon the specimen fatigue life. It can also be noted that considerable spread exists in the end resistance of the sensor, if the data from Specimen No. 48 is compared with that of Specimen No. 49.

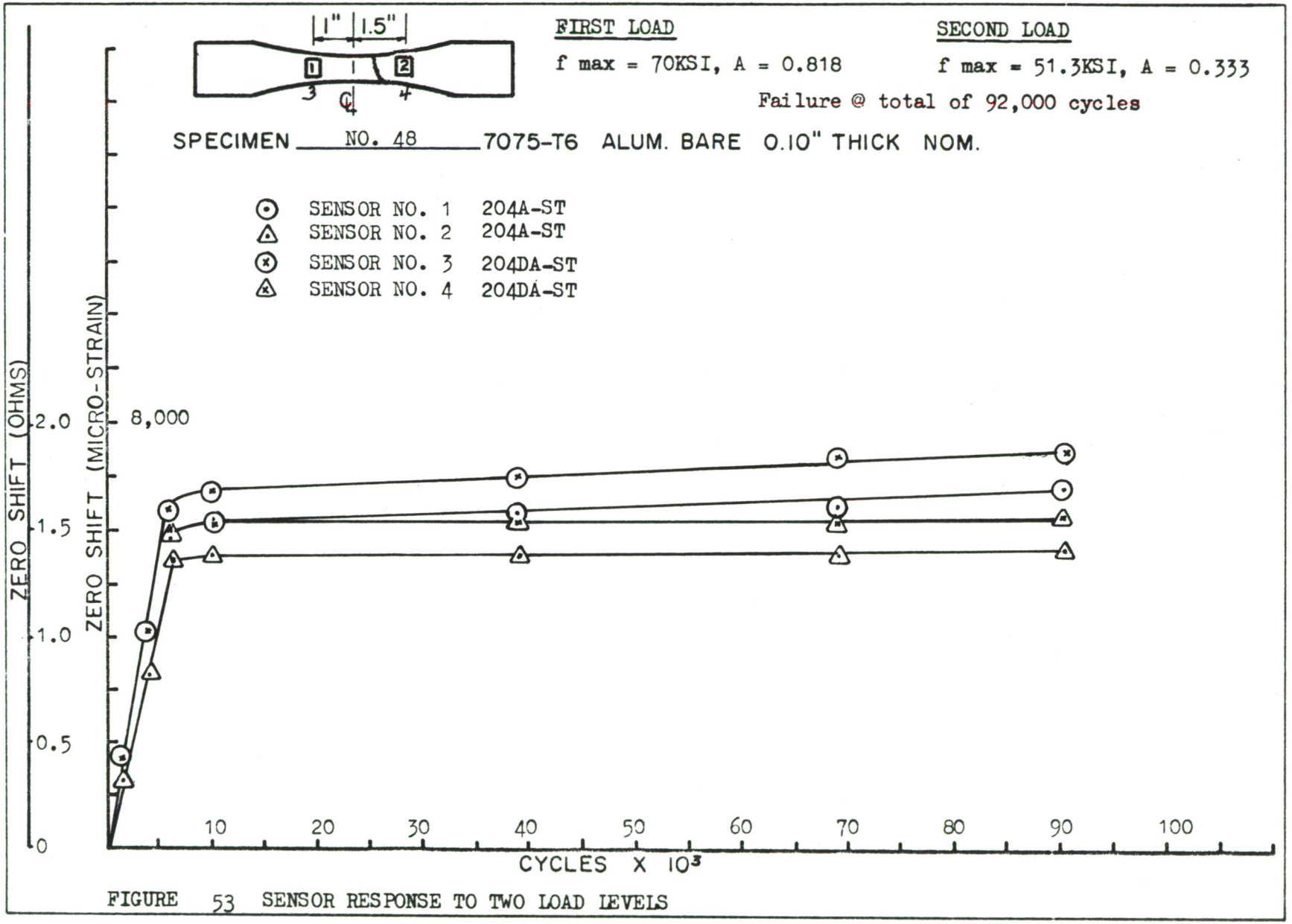

FIGURE 53 SENSOR RESPONSE TO TWO LOAD LEVELS

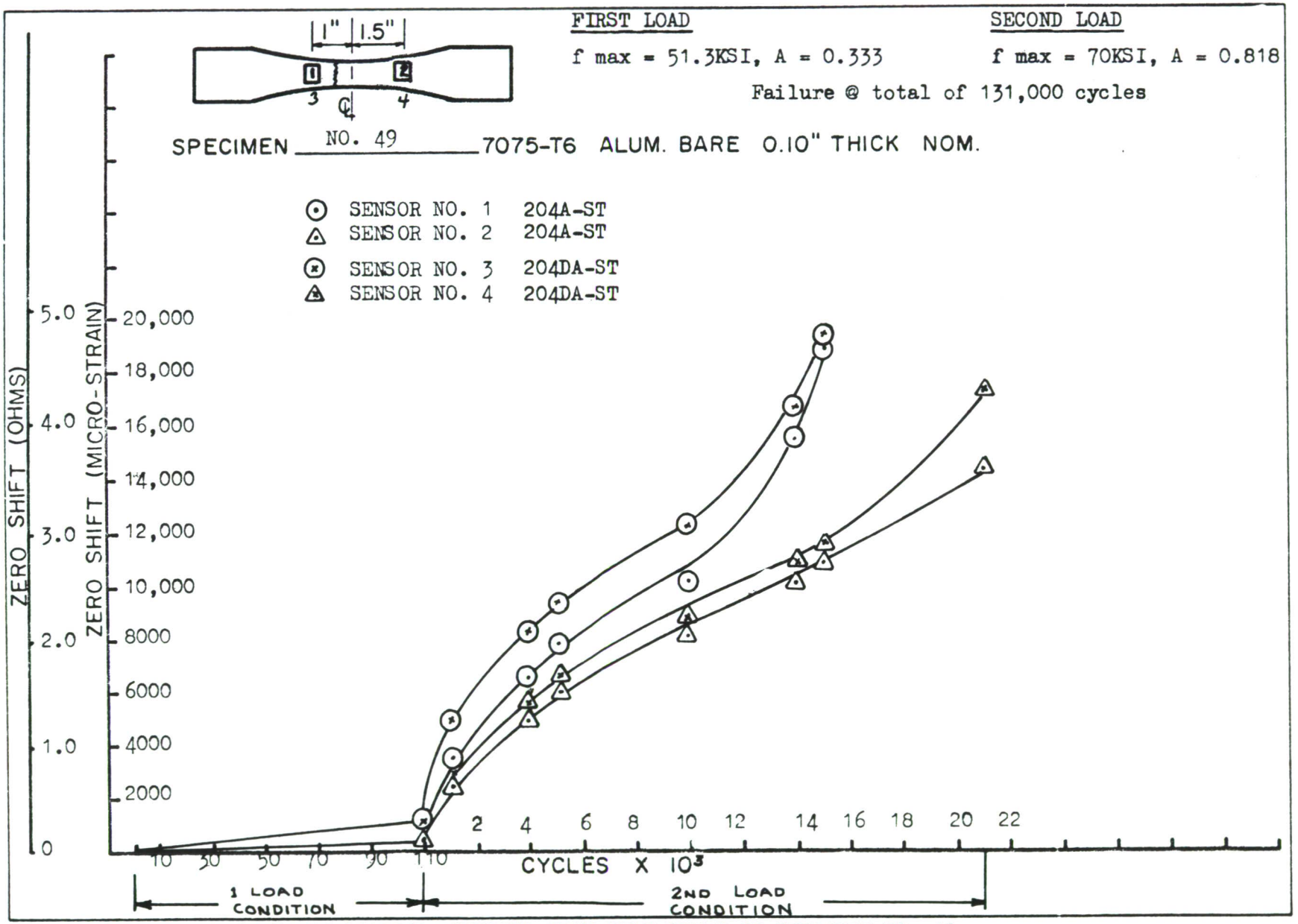

FIGURE 54 ORDER OF LOADING REVERSED FROM THAT SHOWN IN SPECIMEN NO. 48

4.1.7 SONIC FATIGUE TESTS

The type 204DA-ST was the only sensor evaluated in a sonic environment and then only at room temperature. No attempt has been made to correlate data or predict failure; the investigations were merely to determine the feasibility of using in a sonic environment. The sensors were installed mid-span on 2 foot square honeycomb panels which were then edge mounted and subjected to a random sonic environment. The panels were constructed of 1/2 inch honeycomb between .020 inch face sheets, with fibre glass reinforced ends. The panels were then tested to failure, with stops at intervals to permit reading the strain gages and fatigue sensors. Basically, it was determined that the sensor would respond to peak strains over 1000 micro in/in and would endure the environment for the life of the panel. The output characteristics of the sensors on each of the panels are shown below. The number one panel was subjected to peak strains of 1000 u in/in and lasted six hours while number two panel experienced peaks of 1200 u in/in and lasted 2 3/4 hours. The diagrams are shown on a time base rather than cycles since a random spectrum was used.

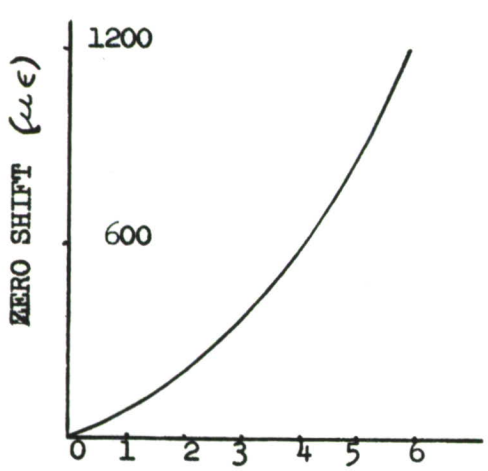

PANEL NO. 1

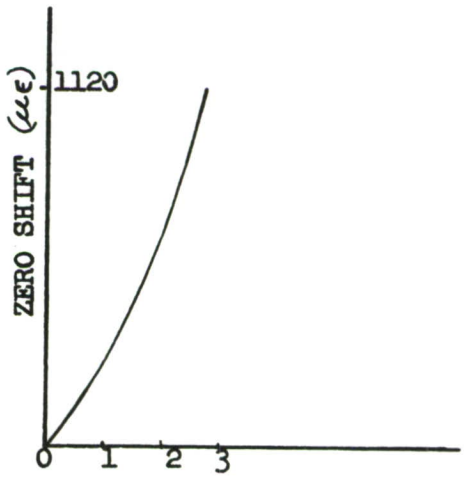

PANEL NO. 2

4.1.8. SUMMATION OF IRREGULARITIES

During the evaluation of sensors on some sixty odd coupons, several irregularities were noted which indicated examination in further detail would be warranted.

The following is a list of peculiarities which developed during the program and a discussion of their significance to the overall problem of developing a fatigue damage indicating system. It should be emphasized that these are considered irregularities rather than significant problems, however, their evaluation will assist in the selection and optimization of the sensor. Since these irregularities were observed and recorded, a side investigation to remove some of the mystery appeared to be a necessity.

Sensor Failure - Only two (2) modes of sensor failure, prior to specimen failure, have been observed. These are solder joint and grid cracking (supersensitivity) failures. These modes of failure are clearly associated with the accelerated method of evaluating sensors on coupons. This difficulty has not been encountered at the slower cyclic rates and lower stress levels used on the C-130E panels or on the C-141 empennage laboratory specimen. However, in utilization on flight aircraft which might endure a service life of 10 years, it is advisable to select the grid which is least susceptible to this grain boundary cracking. Consequently, in optimizing the sensor, it is only natural to lean toward the foil grid which is least sensitive to fatigue cracking and had withstood the more severe mode of testing.

Sensor Installation Technique - Since a number of jumper lead failures have been experienced, some effort has been directed toward correcting techniques which precipitate the mode of failure labeled "solder connections." Human nature being what it is, a solder technique is necessary which will tolerate some degree of sloppiness yet still produce reliable data. The most critical area and the one in which all breakdowns have occurred is from the jumper wire to the sensor solder tab, or the solder button. The fatigue life of the connection has been improved by flattening the end of the round #34 gage jumper wire so that a greater area of the wire is in contact with the thin foil. Since initiating this technique, no further jumper wire failures have been experienced. The soldereze wire is preferred over tinned copper ribbon since it is insulated and can readily be bent into a stress relief bow. In general, it is felt that the installation techniques can be simplified to the degree that a "run of the mill" technician can make an acceptable installation. Of the two modes of sensor failure mentioned above, one is basically controlled by the manufacturer and the other by the user.

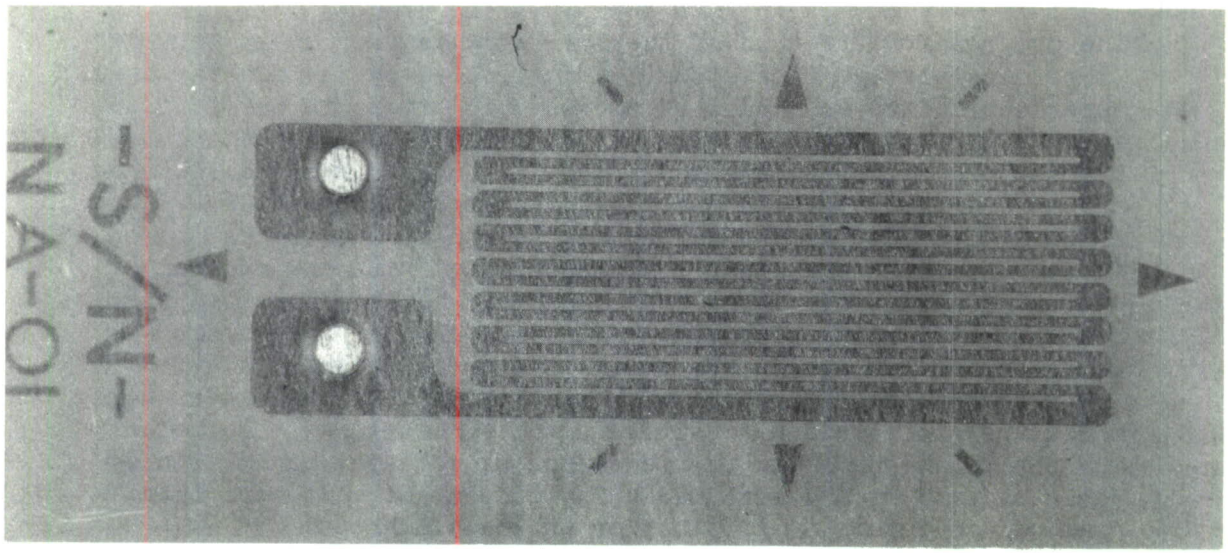

FIGURE 55 TYPICAL ACID ETCHED ANNEALED FOIL GAGE USED AS A FATIGUE SENSOR.

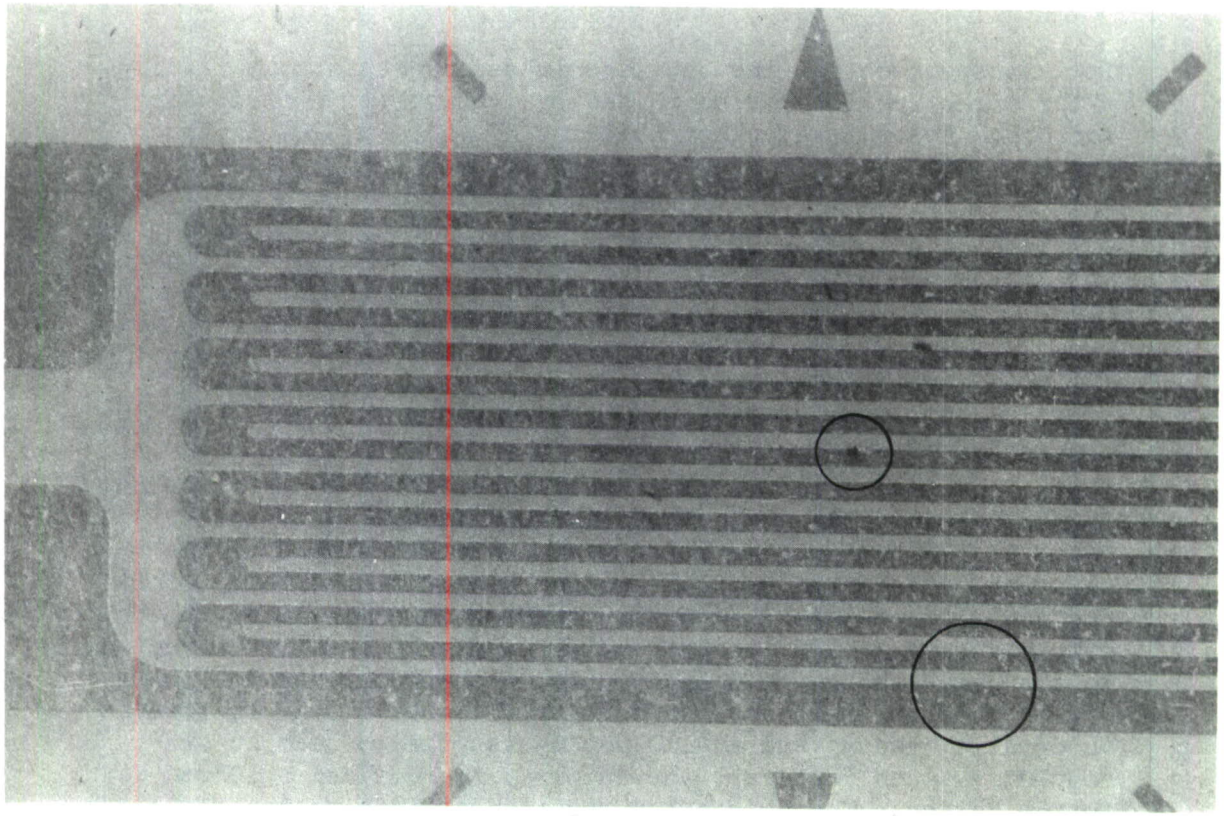

FIGURE 56 CIRCLES INDICATE IRREGULARITIES IN THE FOIL STRANDS PRODUCED BY THE ACID ETCHING PROCESS VISIBLE AT A MAGNIFICATION OF 24X.

The progressive fracture of the foil strands previously termed "supersensitivity" is a situation controlled by the manufacturer. Supersensitivity is caused by microscopic cracks in the foil strands, starting at the edge of the strand and propagating across. The crack starts and follows along grain boundaries and apparently is accelerated if the strand edge has been exposed to acid. As the number and length of the cracks increase so does the electrical resistance, with any movement of the strands producing a "make and break" circuit across the crack resulting in an erratic resistance change. Microphotos of these fatigue cracks are shown in Figures 62 through 63. The grid strand or strands which had failed were located by using miniature probes and a sensitive wheatstone bridge. The sensor was positioned under a 30X stero-zoom microscope and the resistance of each strand measured. The suspect strands were then examined in detail at 1000X under the metallograph.

Effect of Rest Period on Sensor Resistance - The decrease in sensor reading after a rest period is clearly a peculiarity associated only with accelerated coupon testing. This peculiarity has not been observed on typical aircraft structure tests conducted at lower cyclic rates.

It is suspected that the decrease in sensor resistance reading after a rest period may be caused by a number of contributing factors. Refer to specimen numbers 20, 21, 28, 29, 31, etc. One possibility is strain relaxation of the sensor material. It should be noted that the sensor material is being repeatedly strained beyond its elastic limit, while the aluminum when stressed to 70,000 psi would probably not experience relaxation. Another possibility is that the sensor material may generate heat within itself as a result of the high frequency cycling. In any event it does not appear to be a problem, but is simply a peculiarity which will be noticed if one uses a sensitive instrument to measure zero shift.

It is felt that irregularities such as sensor 4 on specimen No. 26 must be investigated. This discrepancy was fully investigated by our Chemical Metallurgical group and pinpointed as an inferior connection of the solder button to the foil. This particular type gage (S/N NA-01), makes use of a solder button, note Figure 55, which is apparently fused or otherwise connected to the gage tab by the manufacturer. At approximately 80,000 cycles the button connection had deteriorated enough to present an erratic reading and at 110,000 cycles the connection was completely open, however, the jumper wire remained soldered to the button. The original purpose of evaluating the NA-01 gage was to make a comparison between it and the die cut gage type 204A-ST. However, when failures occur they should be investigated to remove any mystery.

Although some irregularities were also brought about by the accelerated method of coupon testing it is believed the advantages of this method offset the disadvantages. While the complexities and stress concentrations which exist on modern aircraft structure cannot be easily duplicated on a standard laboratory coupon, the evaluation of the sensor on coupons has permitted the following:

1. Determination of sensor behavior characteristics under the extremes of fatigue loadings, i.e. from the plastic region of the aluminum (85KSI) to some fatigue operational levels on aircraft structures. The coupon is also adaptable for testing at a wide variety of stress ratios such as $A = \infty$, $A = 1$, $A = 0.818$, $A = 0.333$.

2. Determination of the effects of fatigue loading conditions can be separately isolated and individually evaluated.

3. The higher cyclic loading frequencies possible with a small coupon permits the failure of a structure in an abbreviated time period.

However, it is still recognized that the feasibility of a fatigue damage indicating system rests upon its practicality for utilization on aircraft structure and as such would be subjected to combined environments, lower strain levels and lower frequencies.

4.1.9 METALLURGICAL INVESTIGATIONS

A side evaluation effort was directed toward removing some of the mystery from irregularities which developed during the evaluation of sensors on Specimens No. 26,29, and 37. These curves of sensor output indicate that the gage has gone "supersensitive" which must be considered a gage failure, because its erratic operation renders the data useless. Since it might be possible for a solder joint failure to behave like microcracks in the gage grid, further attempts to isolate this "supersensitivity" mode of failure were conducted on a constant strain beam. Figure 58 shows an S/N NA-01 gage which was bonded to the beam and cycled at a strain level of $\pm$ 1500 micro in/in until complete gage failure. The coupon was cycled at 30 cps using a Sonnatag SF-2 machine and a Tektronix scope operating in the AC mode for monitoring the output of the gage. Figure 57 illustrates a sequence of Polaroid photographs of the oscilloscope presentation of gage output. In Photo No. 1, the output wave shape of the gage at 20,000 cycles indicates the gage is operating normally. In Photo No. 2 at 105,000 cycles, the first signs of deterioration can be noted. In Photo No. 3 and 4 at 120,000 cycles, and 130,000 cycles, respectively, the distortion on the tension side has increased. In Photo No. 5 at 149,000 cycles, the output signal on the tension half cycle is erratic while the compression half cycle is still a normal wave form. This leads to the conclusion that the grid has failed rather than the solder joint. In a further attempt to isolate the failure the jumper wire was resoldered, however, the erratic signal still persisted. If failure had occurred, at the sensor tab, "hash" on the scope trace would have been evident on the compression half cycle as well as the tension cycle. It is suspected that fracture of the grid strands has occurred at the grain boundaries which produces an erratic electrical continuity on the tension half cycle. Further investigations with probes designed for measuring the resistance of each individual grid strand indicated that the 500% plus increase in resistance of the sensor was distributed among particular strands.

The tedious time consumming job of pin pointing and photographing the grid strand microcracks were explored both with an Electron microscope and a Metallograph. Of the two instruments, a carbon arc Model 2400 American Optical Metallograph with a magnification capability of 1500X proved the most practical.

A sampling of some typical photos resulting from grain studies and metallographic examination of both the die cut foil and the acid etch foil are shown in Figures 60 through 72. Figures 65 and 66 show a typical surface and edge condition of the acid etch foil. Although all irregularities can not be definitely identified, it appears that the black spots may be carbonized oil particles, since the foil is often rolled in oil solution while hot and under pressure. The "pock" marks shown in Figure 68 may be due to dirt or other contaminates encountered during the rolling process. The jagged edge shown in Figure 69 is probably the result of the ferric chloride acid preference for grain boundaries, since the masking does not cover the edges of the strand. This strand edge can be compared with that of the die cut gage in Figure 70 since both are shown at a magnification of 500. It should be noted that the acid undercuts the strand edge resulting in a sharp knife like edge as shown in the sectional cut below:

Acid Etch

Die Cut

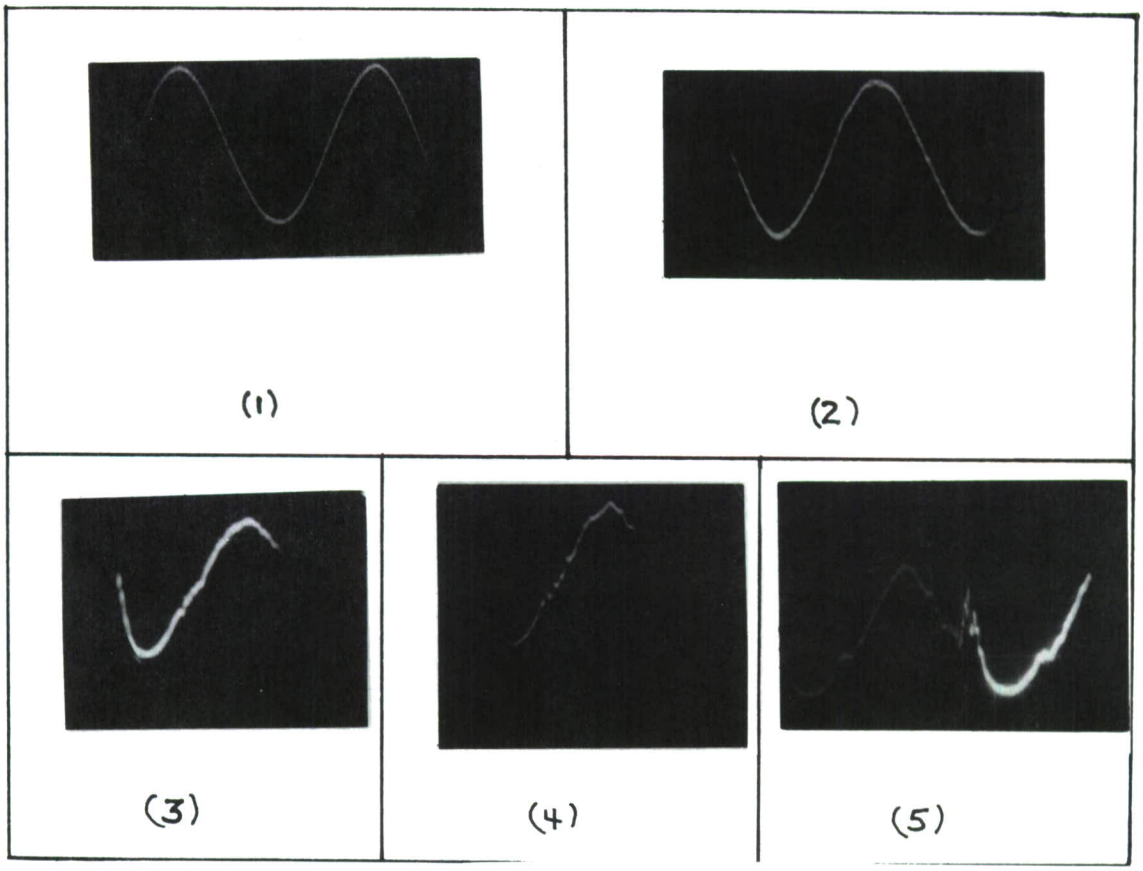

FIGURE 57 SEQUENCE OF OSCILLOSCOPE TRACES SHOWING THE PROGRESSIVE STAGES OF SENSOR GRID FAILURE OF GAGE IN FIGURE 58

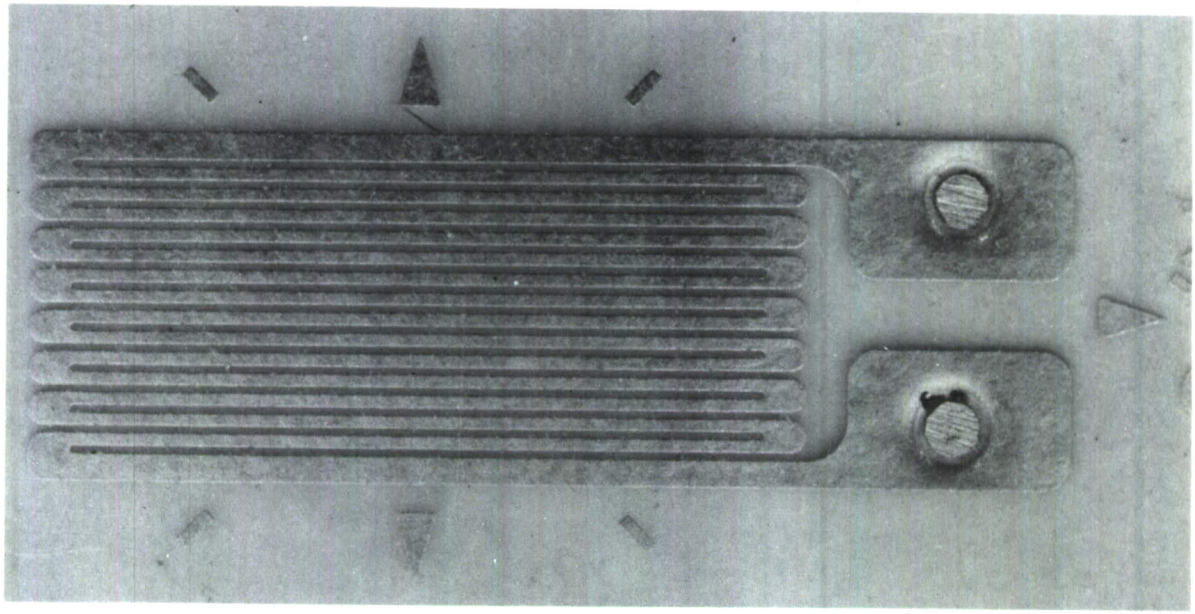

FIGURE 58 S/N NA-01 GAGE AS RECEIVED FROM THE MANUFACTURER PRIOR TO INSTALLATION ON THE CONSTANT STRAIN BEAM OF FIGURE 59

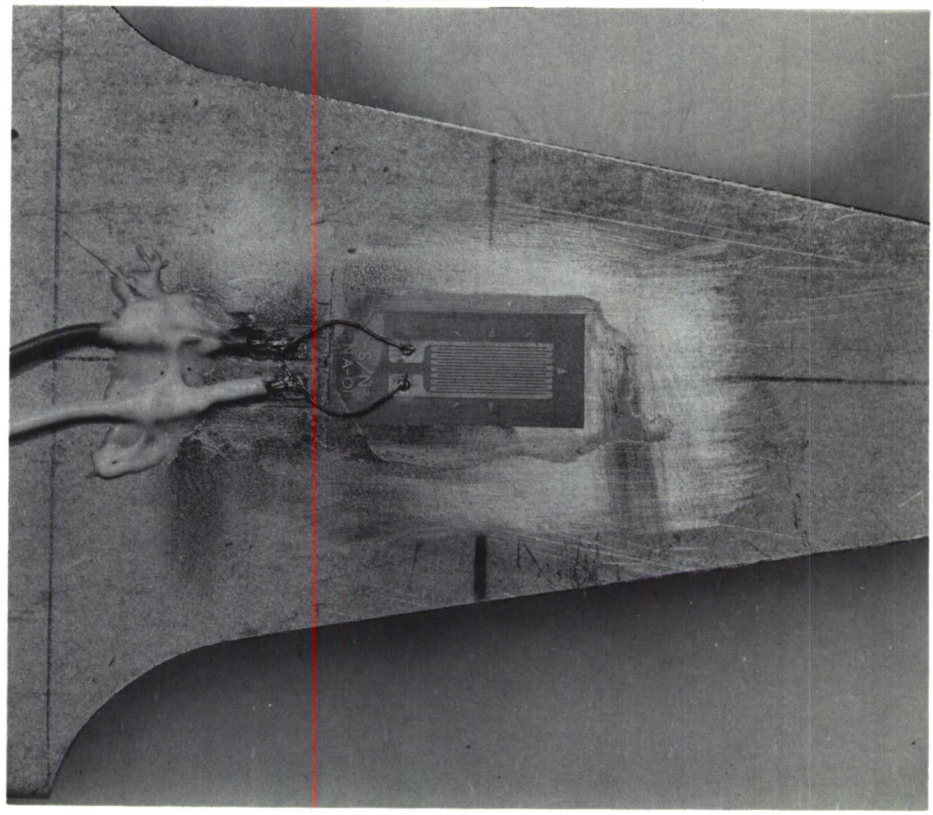

FIGURE 59 S/N GAGE MOUNTED ON BENDING SPECIMEN AND EVALUATED AT ± 1500 MICRO IN/IN UNTIL GAGE FAILURE. PHOTO 2.2 TIMES ACTUAL SIZE.

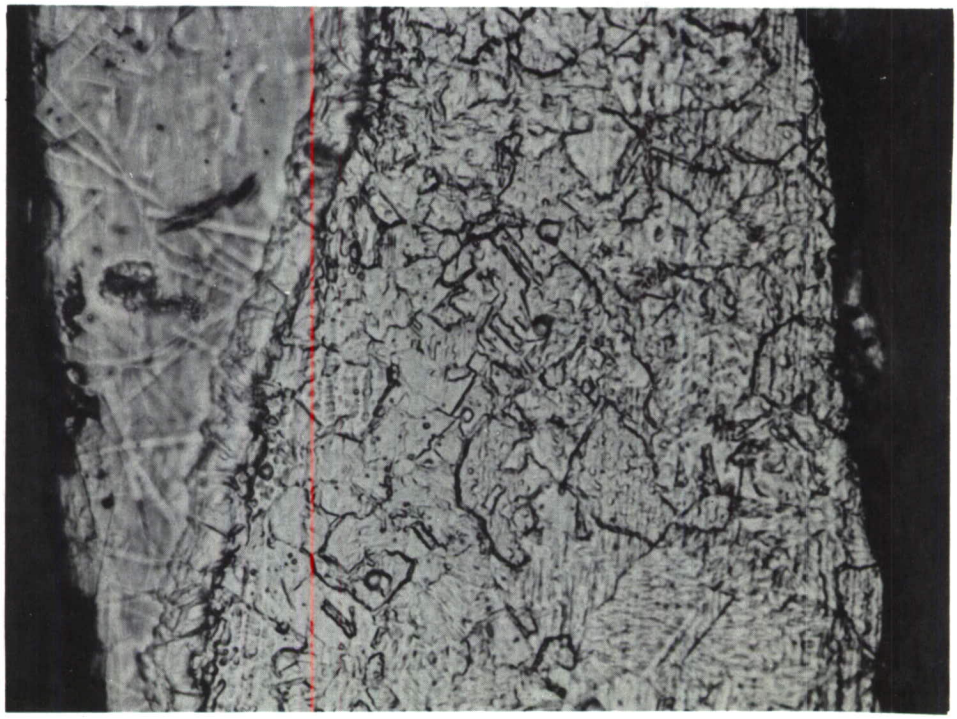

FIGURE 60 S/N NA-01 STRAND AT 1000X AFTER PARTIAL REMOVAL OF EPOXY ENCAPSULATION. ARMSTRONG EPOXY STRIPPER USED FOR REMOVAL OF EPOXY.

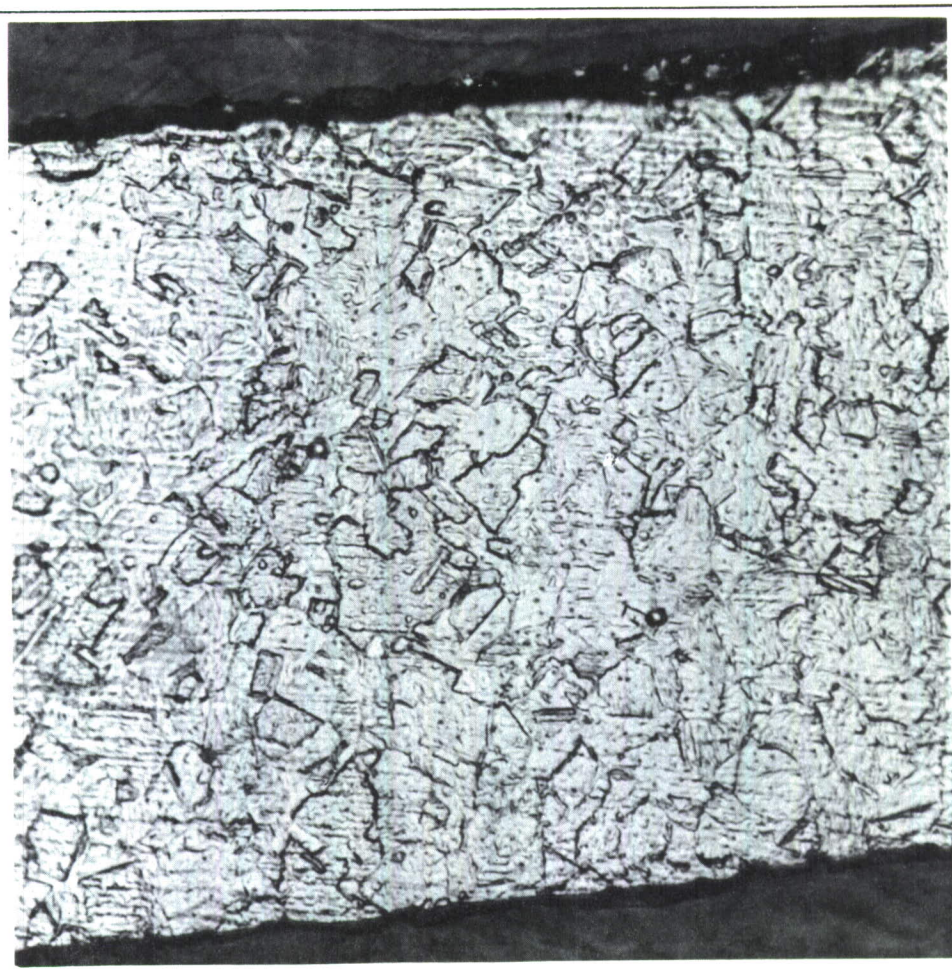

FIGURE 61 A STRAND SECTION OF THE NA-01 S/N GAGE AT A MAGNIFICATION OF 1000X. NOTE THE SEVERITY OF UNDERCUTTING OF STRAND EDGE DUE TO ACID ETCH PROCESS OF FABRICATION.

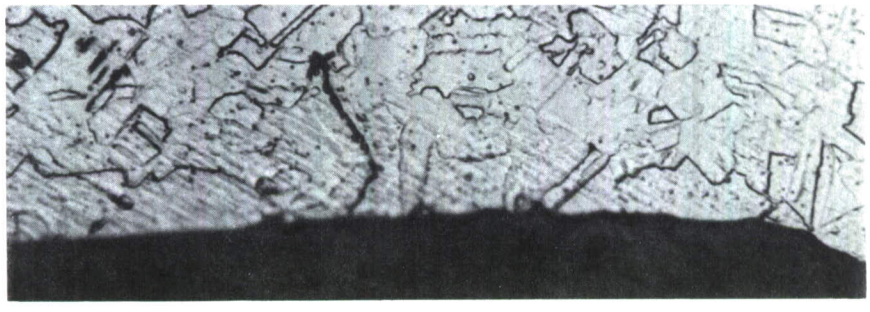

FIGURE 62 A STRAND FAILURE IN THE GAGE SHOWN IN FIGURE 59 NOTE THE MICROSCOPIC CRACK NEAR THE END LOOP. THE SURFACE HAS BEEN SLIGHTLY ETCHED TO HIGHLIGHT THE GRAIN STRUCTURE.

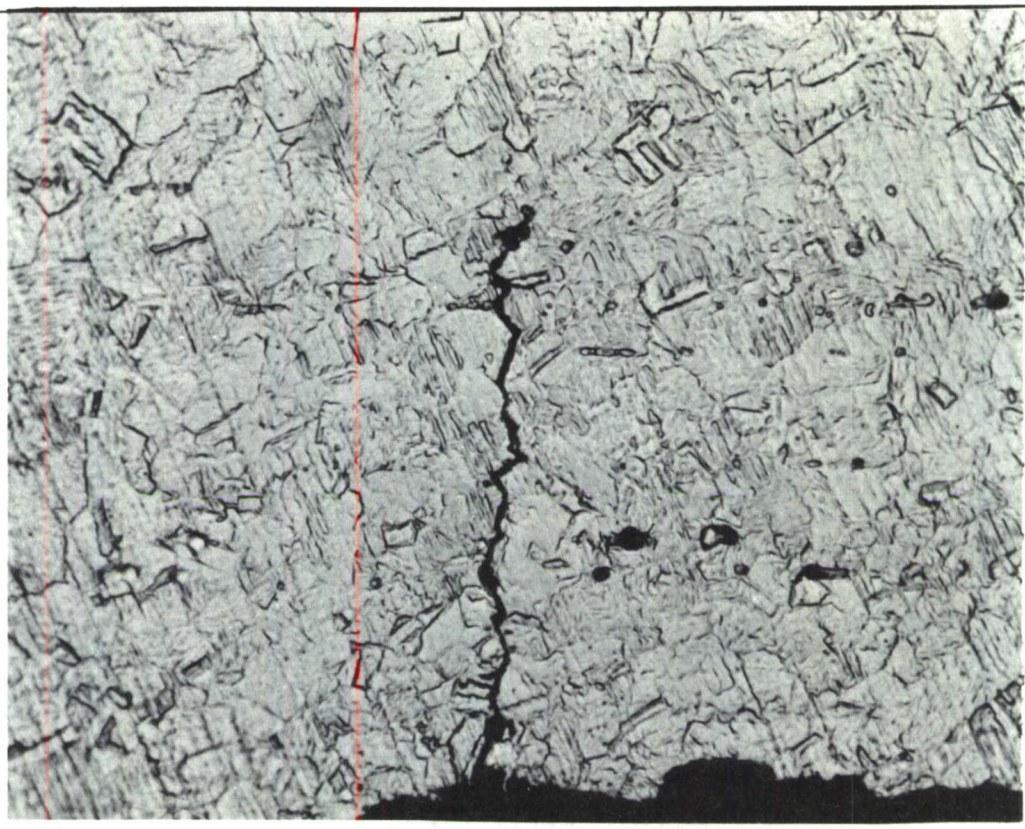

FIGURE 63 MICRO PHOTO AT 1000X OF THE NO. 1 SENSOR USED ON SPECIMEN NO. 47. CRACK APPARENTLY ORIGINATED NEAR END LOOP AND FOLLOWED GRAIN BOUNDARIES.

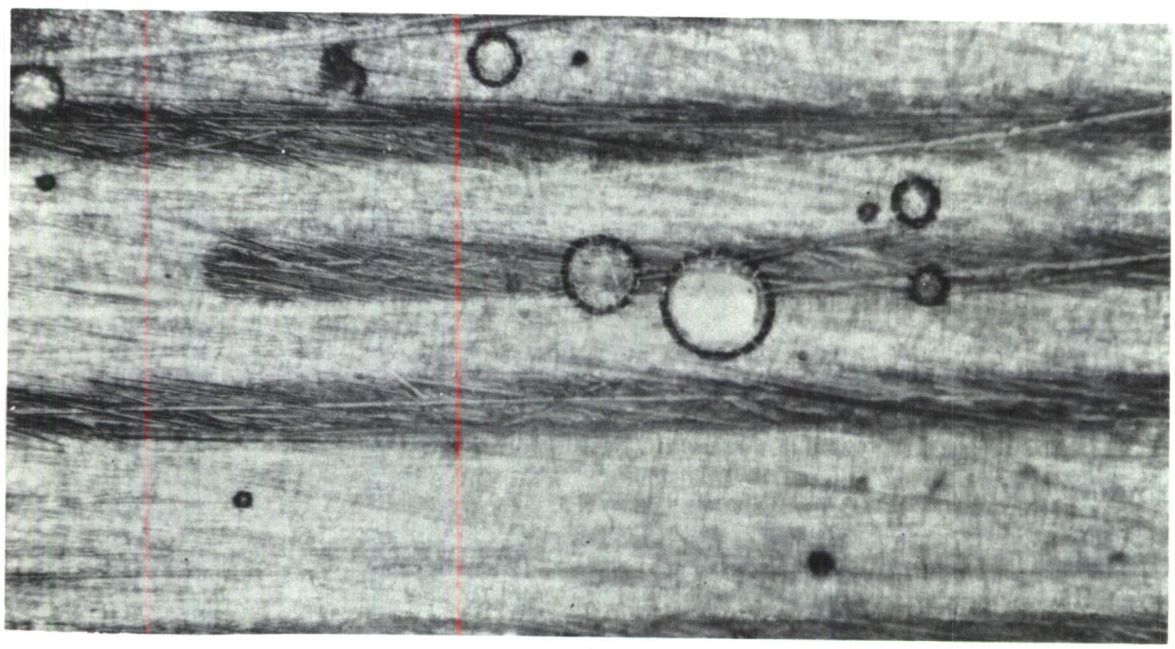

FIGURE 64 S/N GAGE AS RECEIVED FROM THE MANUFACTURER. PHOTO TAKEN AT 100X OF THE BONDING SIDE OF THE GAGE. SHOT WAS TAKEN THROUGH THE EPOXY AND SHOWS BUBBLES IN THE EPOXY AT VARIOUS DEPTHS.

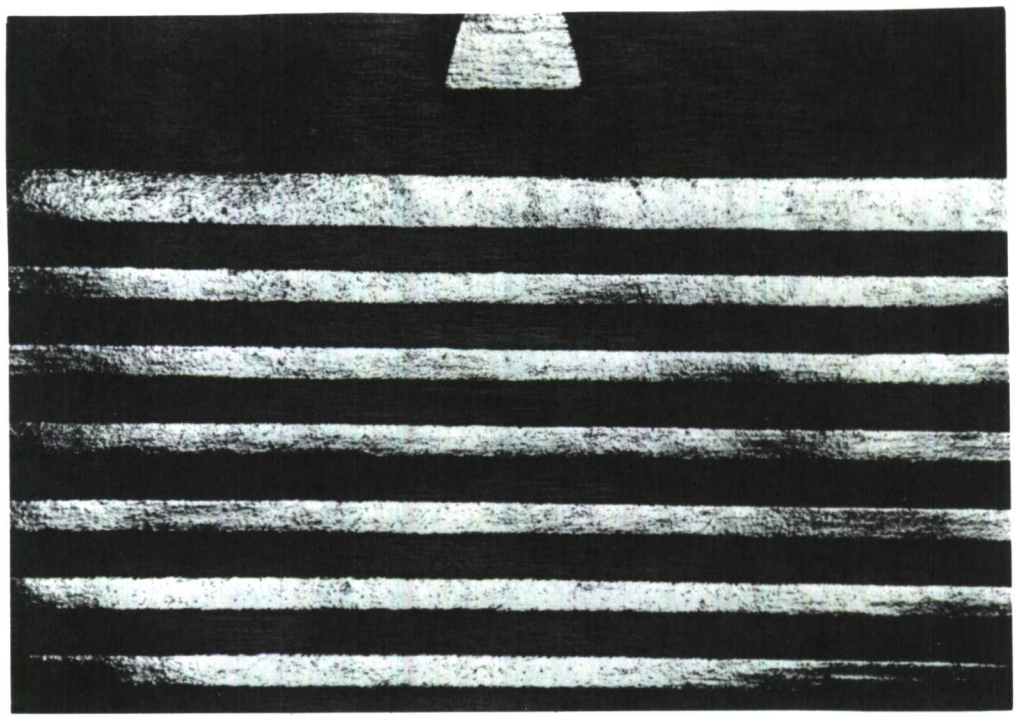

FIGURE 65 VIEW OF UNENCAPSULATED STRANDS OF FATIGUE GAGE AT A MAGNIFICATION OF 50X. OBLIQUE LIGHTING USED TO HIGHLIGHT IRREGULARITIES OF THE SURFACE. GAGE IN AS RECEIVED CONDITION WITHOUT ENCAPSULATION.

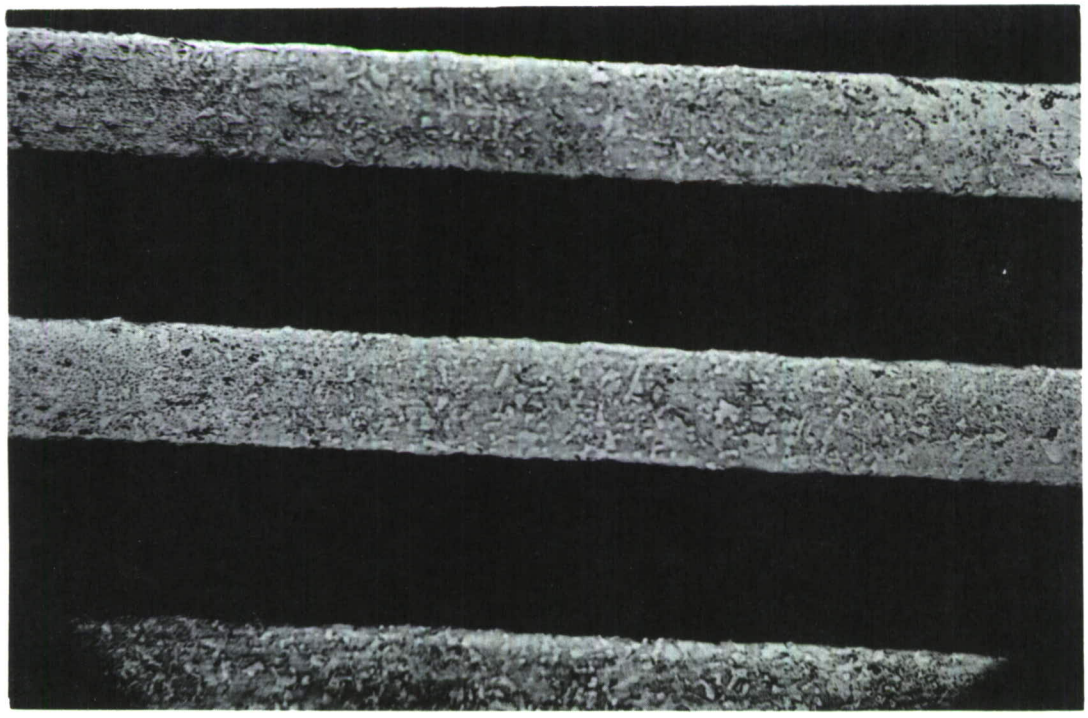

FIGURE 66 VIEW OF SAME GAGE AS ABOVE AT A MAGNIFICATION OF 200X. GAGE IN "AS RECEIVED" CONDITION.

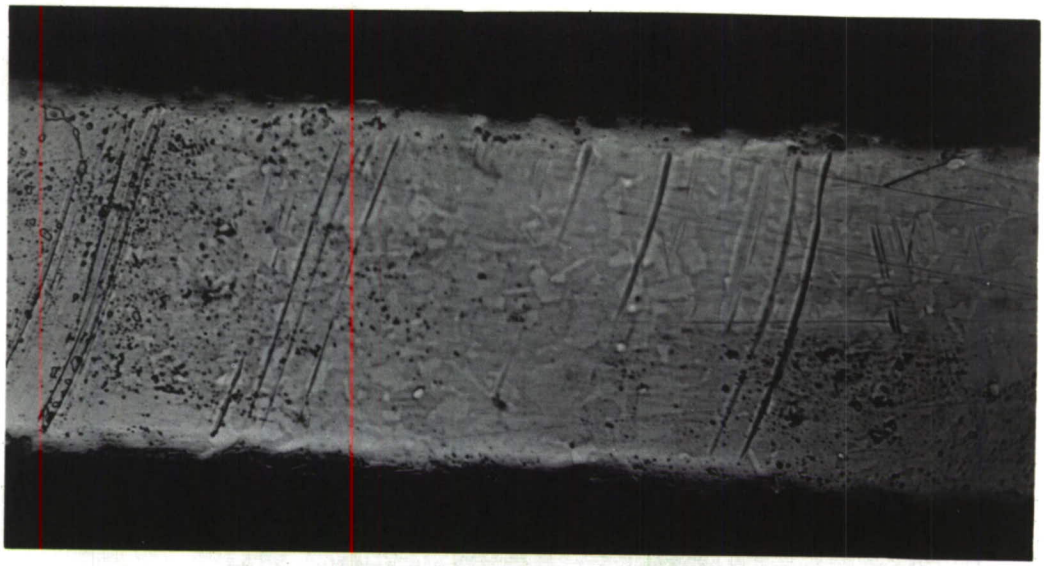

FIGURE 67 STRAND PHOTO AT 500X OF WHAT APPEARS TO BE AN UNDESIRABLE AREA OF THE STRAND CONDUCTOR. THIS STRAND SHOWS A VARIATION IN FOIL THICKNESS, TRANSVERSE SCRATCHES, AND GRAIN EFFECT IN THE FLAT ROLLED SURFACE PLANE.

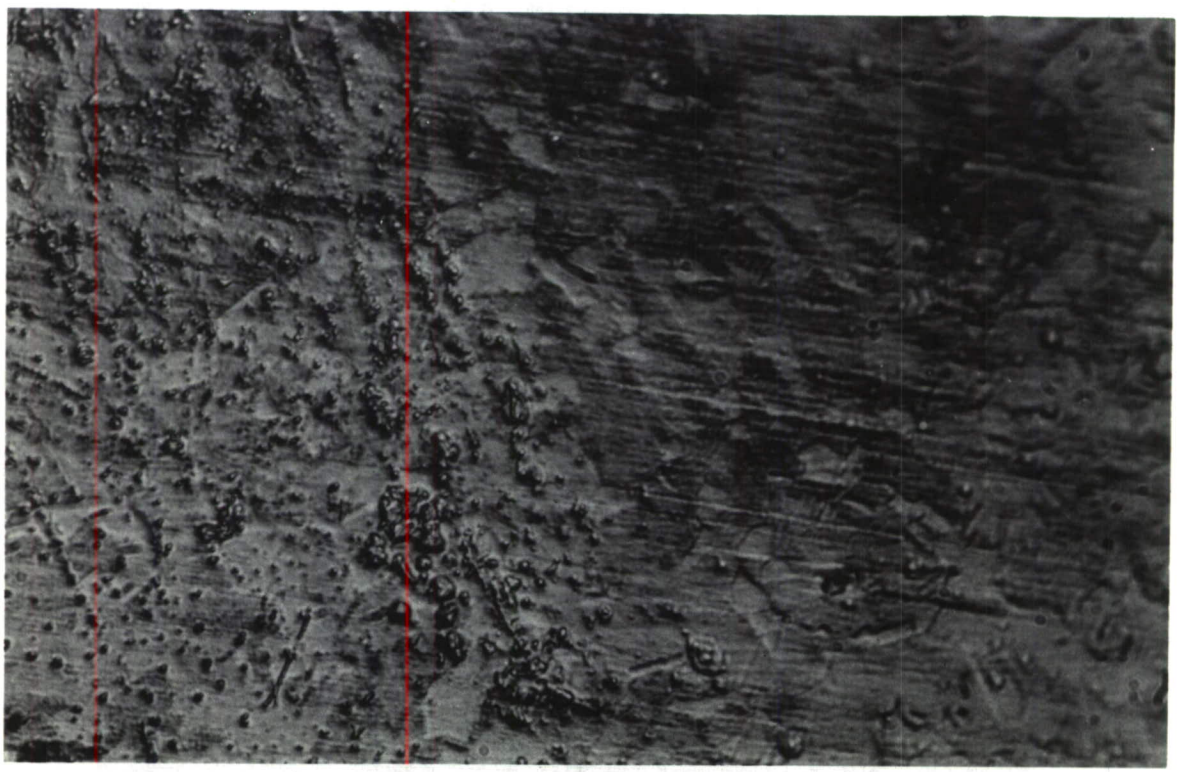

FIGURE 68 VIEW OF THE SAME STRAND AT 1000X. NOTE THE CHANGE IN FOIL THICKNESS. ALSO THE APPEARANCE OF GRAIN EFFECT, ALTHOUGH AN ACID ETCH WAS NOT USED TO HIGHLIGHT THE GRAIN.

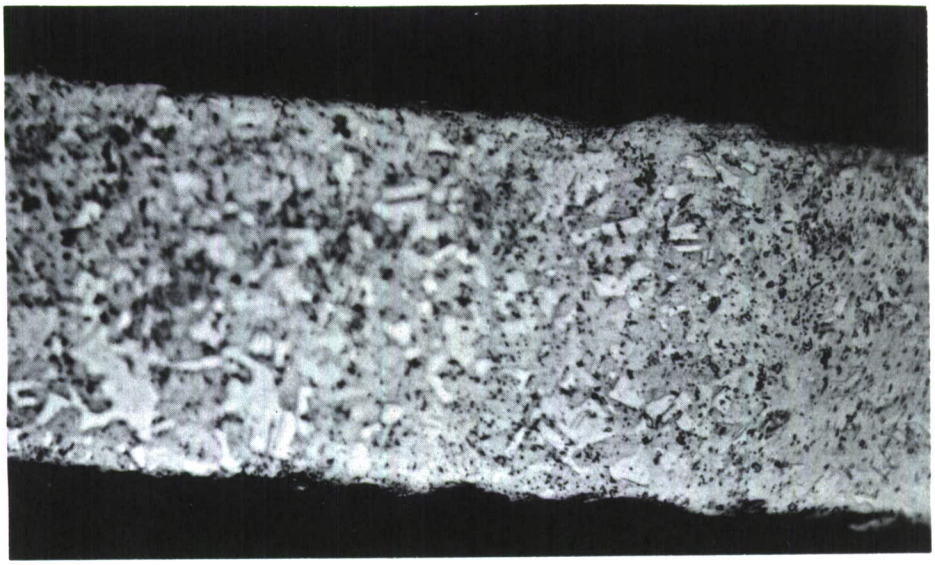

FIGURE 69 PHOTO OF FATIGUE GAGE STRAND AS RECEIVED FROM THE MANUFACTURER. EPOXY ENCAPSULATION REMOVED BY ARMSTRONG EPOXY STRIPPER. BLACK SPOTS MAY BE CARBONIZED OIL, SINCE OIL IS SOMETIMES USED IN THE FOIL ROLLING PROCESS. PHOTO MADE AT 500X.

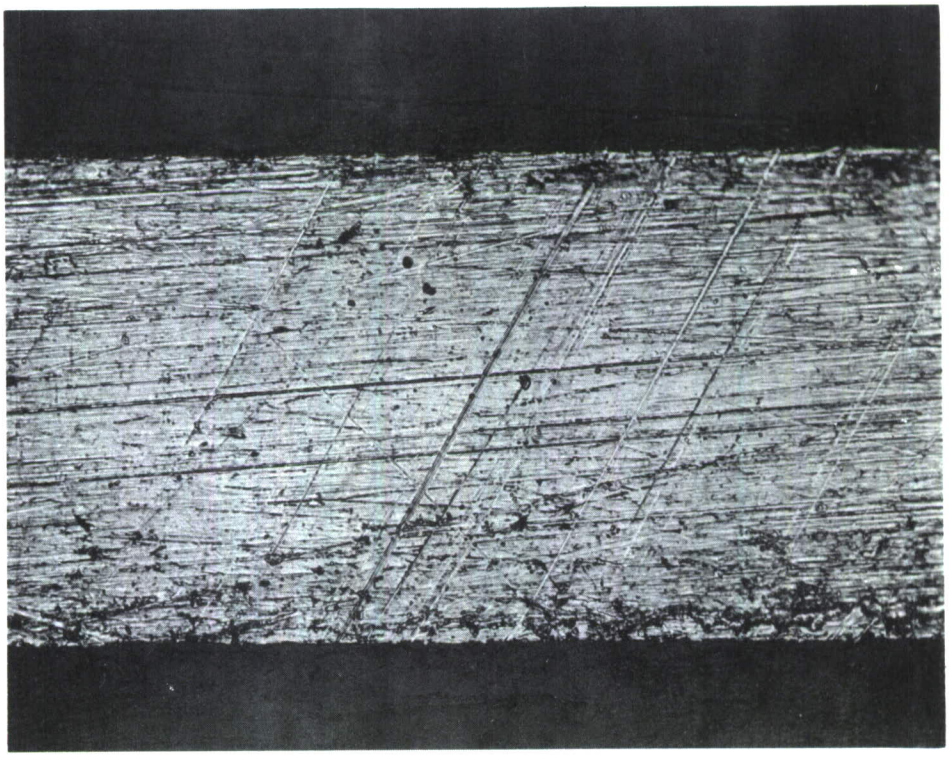

FIGURE 70 VIEW OF AN UNDESIRABLE STRAND SECTION OF A 204DA-ST SENSOR AS RECEIVED FROM THE MANUFACTURER. ALTHOUGH THE 500X MAGNIFICATION SHOWS TRANSVERSE SCRATCHES, IT ALSO INDICATES THE SHARP EDGE POSSIBLE BY DIE CUTTING.

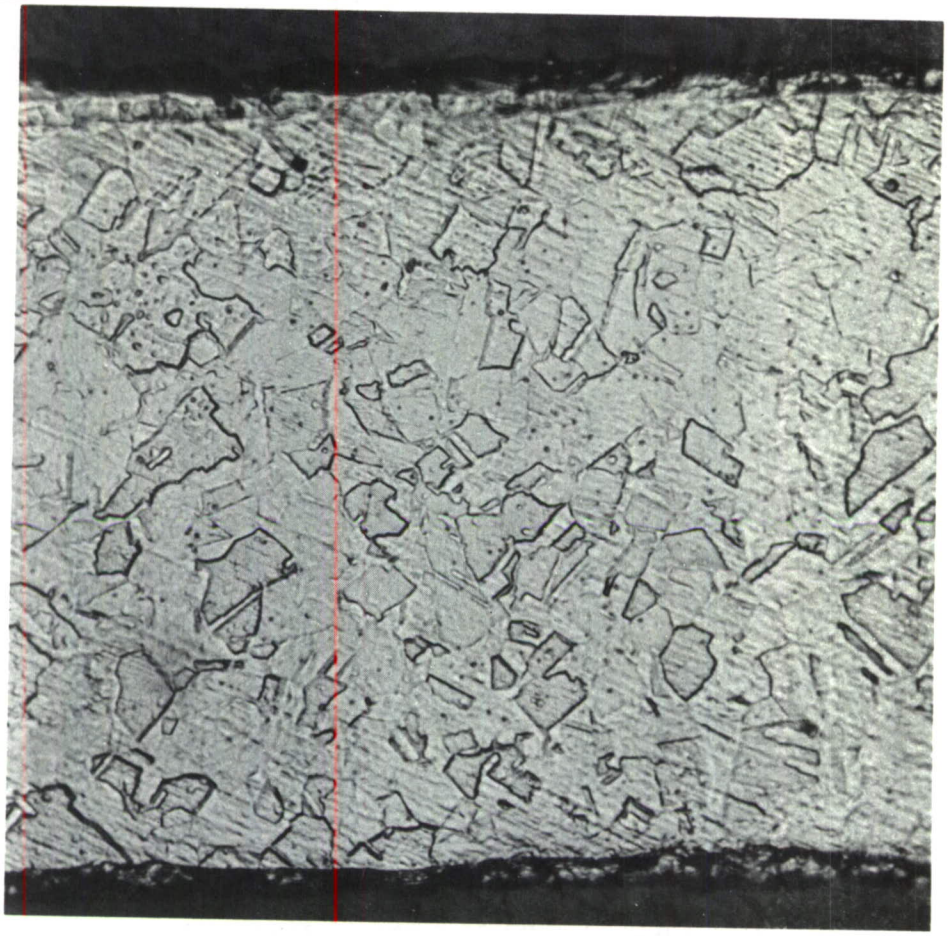

FIGURE 71 PHOTO TAKEN AFTER A FATIGUE INDUCED FAILURE OF AN NA-01 GAGE. POSSIBLE MICROSCOPIC CRACK IN LOWER LEFT CORNER. CARAPELLAS REAGEANT USED TO HIGHLIGHT GRAIN STRUCTURE.

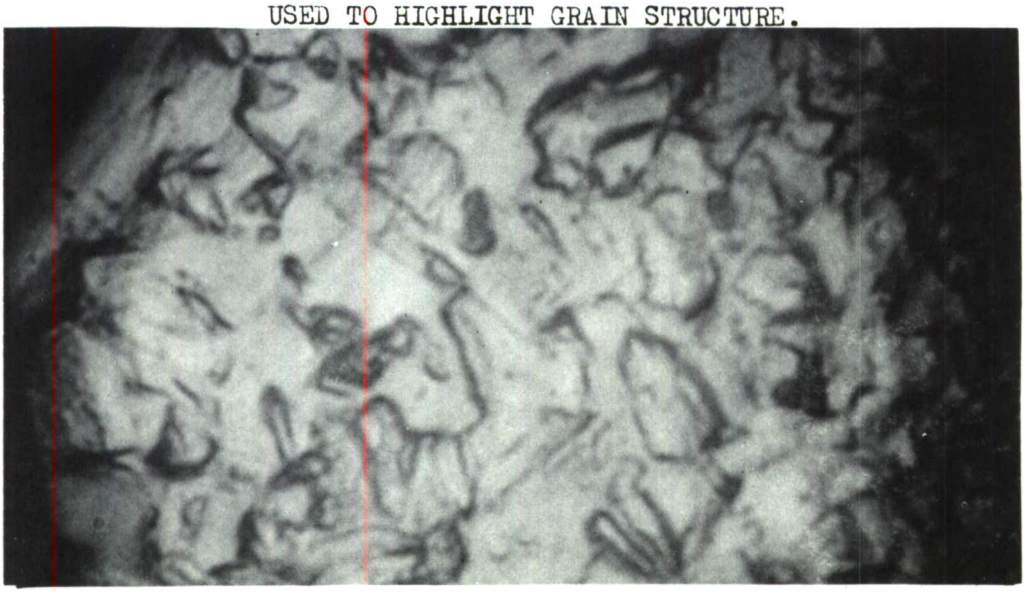

FIGURE 72 DIE CUT FOIL STOCK AT 1500X. SURFACE ETCHED WITH CARAPELLA REAGENT TO OBTAIN RELIEF EFFECT. SUB-GRAIN STRUCTURE IS VISIBLE.

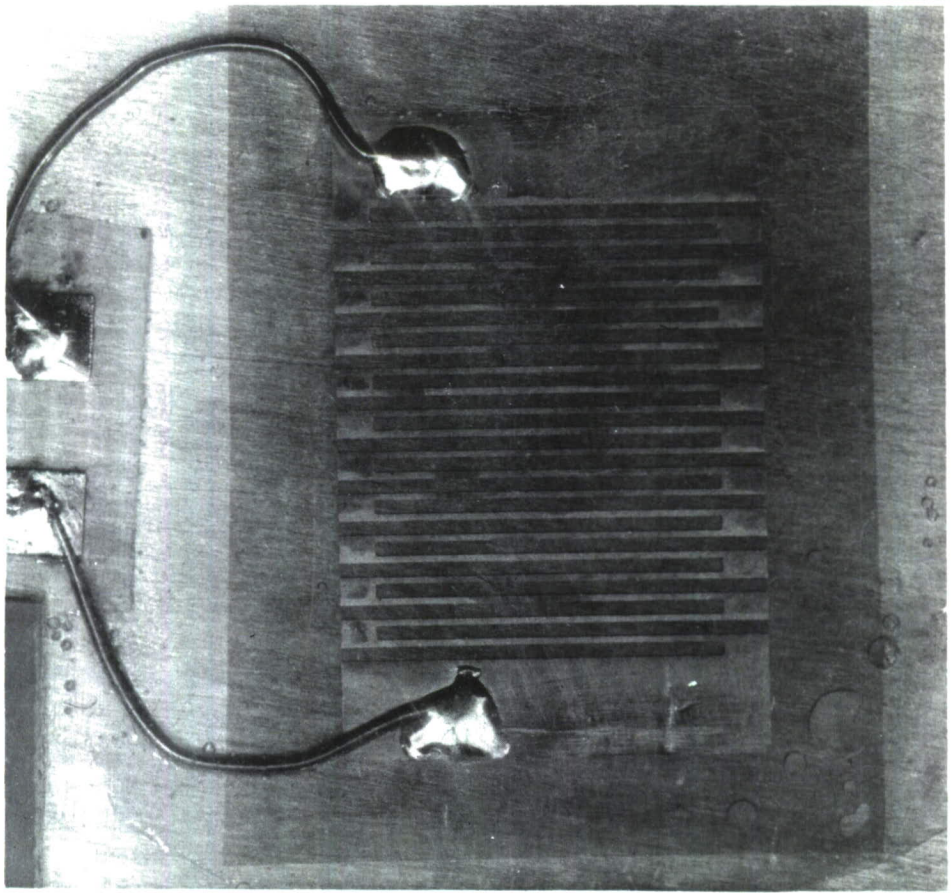

FIGURE 73 AVERAGE INSTALLATION OF A 204A-ST FATIGUE SENSOR SHOWN APPROXIMATELY 8 TIMES ACTUAL SIZE. ALTHOUGH EXCESSIVE SOLDER WAS USED ON END TABS, SENSOR ENDURED 1,200,000 AT ± 2100 U IN/IN ON COUPON NO. 30.

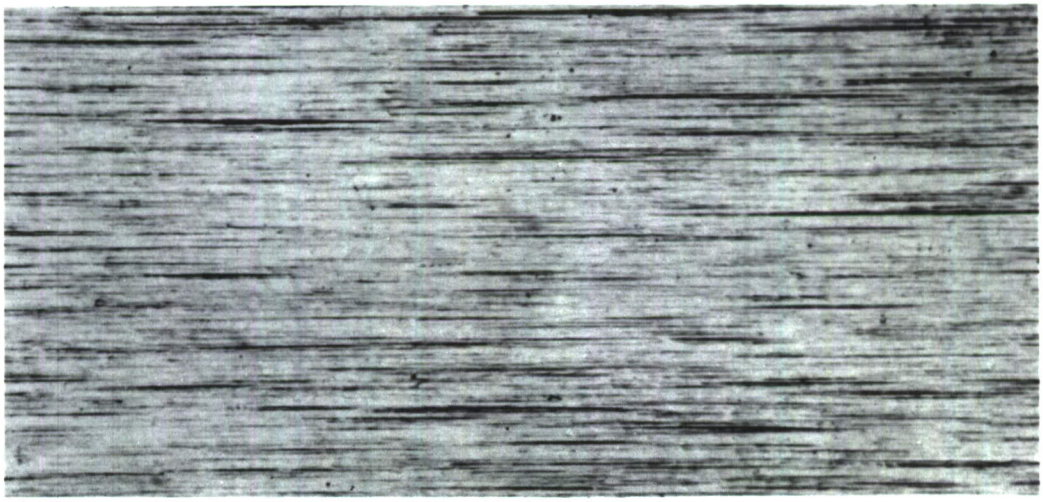

FIGURE 74 MICRO PHOTO OF FOIL STOCK AS USED IN THE 204A-ST SENSOR SHOWN AT 500X. THE LINES ARE FINISH MARKS.

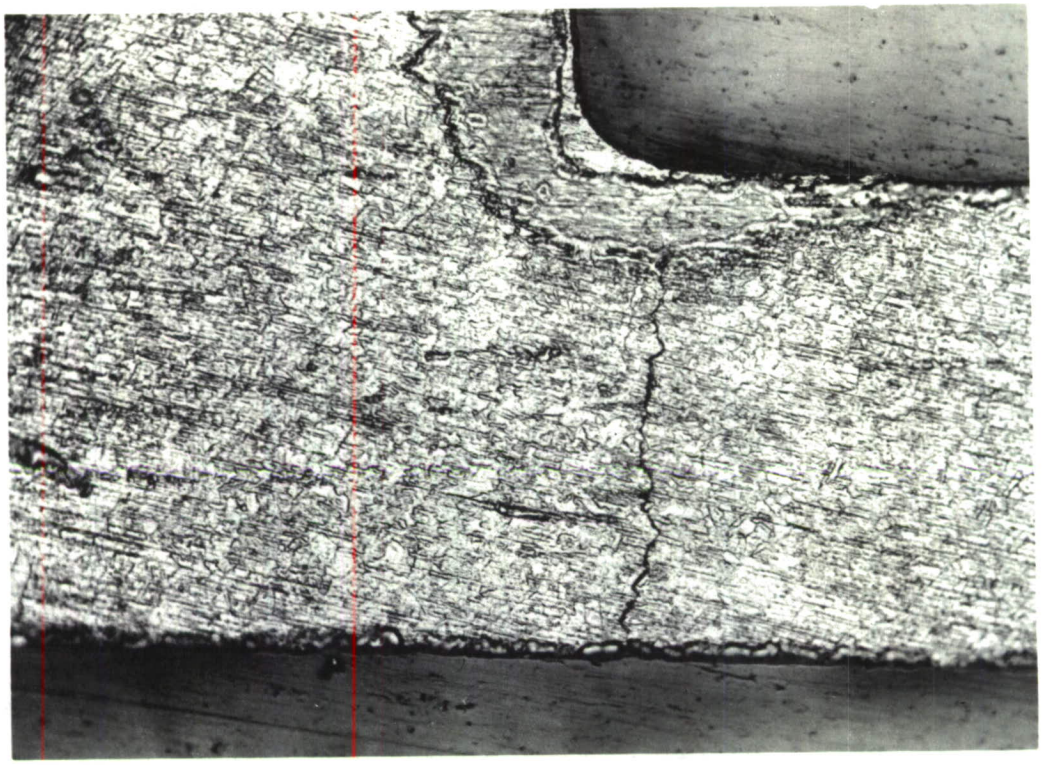

FIGURE 75 TYPE 204A-ST SENSOR WHICH ENDURED OVER TWO MILLION CYCLES AT 4000 MICROSTRAIN BEFORE FAILURE. NOTE RADIUS AT STRAND END LOOP. MAGNIFICATION IS 500X.

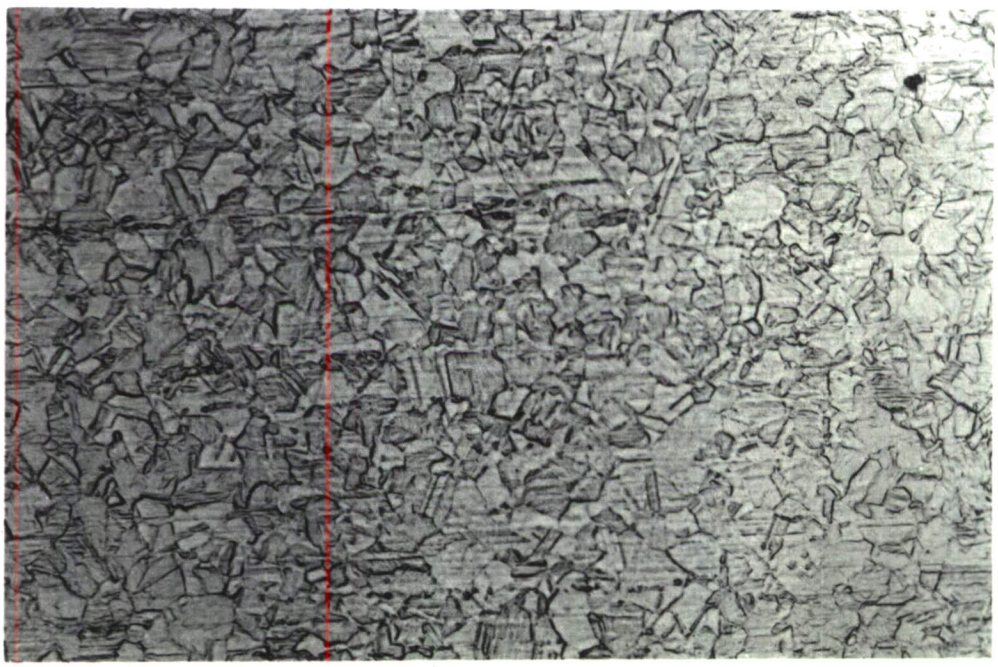

FIGURE 76 GRAIN STRUCTURE OF A 204DA-ST AT 1000X. SLIGHT ETCH WITH CARAPELLAS REAGENT TO EMPHASIS GRAIN.

4.1.10 DISCUSSION OF POSSIBLE ERROR SOURCES

Thermal Output Characteristics of the Sensor

The temperature coefficient of resistance (T.C.R.) of the sensor is a function of:

1. Strain level to which it is exposed.
2. The amount of cold work the alloy has received.
3. The amount of heat treatment the alloy has received.
4. Minute changes in trace element composition.

Number two (2) is by far the most significant for the fatigue sensor application. The sensor foil has been fully annealed to produce a dead soft metallurgical condition, however, the side effect is to increase its temperature sensitivity. The strain gage manufacturer normally heat treats the foil to take advantage of self temperature compensating possibilities. By varying the degree of heat treatment, the resistance-temperature behavior of the constantan foil can be varied so as to create the effect of self temperature compensation of a gage installation on any of a large number of structural materials. For fatigue sensor application, the high T.C.R. of the annealed foil must be endured since any attempt at making it self compensated would destroy its more desirable "zero shift" characteristic.

In order to determine the temperature sensitivity of the foil for various degrees of work hardening from dead soft to full hard, a temperature effects survey was conducted. The curve shown in Figure 77 indicates the variation of temperature coefficient of the foil (bonded to 7075-T6 aluminum) at the various stages of fatigue induced work hardening. Maximum temperature error occurs during initial usage and is quickly reduced until it is nearly self-compensating for aluminum. The curve shown represents data sampled over a four week period and a temperature span of 30°F. In order to more closely define the temperature sensitivity for the early stages of work hardening, nine channels of sensors on Specimen C were selected for a temperature survey. It was estimated that the sensors had been work hardened about 1% after 2500 simulated flight hours, since most were showing a 0.1 ohm resistance change. Testing of Specimen C had been discontinued for two weeks due to specimen modifications, so day-to-day readings were taken of the nine sensors over the two week span. Inside building temperatures varied from 64°F to 82°F representing an excursion of 18°F. From the curve in Figure 77 it can be seen that there is a rapid decrease in the temperature coefficient of resistance as well as a decrease in scatter.

From the series of readings, it can be concluded that maximum error would occur in the early stages of the fatigue life of a structure. The T.C.R. of the foil in the sensor becomes more and more self compensated on aluminum as fatigue damage is accumulated. The net result would be to reduce the indicated cumulative strain error due to temperature as the aircraft structure approached the most critical portion of its fatigue life. It would not be practical to compensate for temperature effects in the active sensor, by installing a dummy sensor in the opposite arm since the T.C.R. of the active arm will change with work hardening while the compensating sensor would show no change in T.C.R. For application on service aircraft, it may be necessary to apply a temperature correction factor to obtain a true initial zero.

Temperature Induced Mechanical Strain

Another question that might arise is the possible error which may be introduced by extreme variations in temperature cycles producing mechanical strain in the sensor. Although the aircraft structure itself is designed thermally stress free; a thermal cycle produces a mechanical strain in the sensor which is a function of the mismatch of the thermal coefficients of expansion of the two materials. A ground-air-ground cycle could conceivably produce a temperature variation of from -65°F to +150°F or a ΔT of 215°F. Temperature variations and the expansion mismatch of the two materials (constantan 8.7 ppm/°F versus aluminum 12.7 ppm/°F) could result in an apparent strain cycle, the magnitude of which would be 4 ppm xΔT. Therefore, a total temperature variation of 215°F would produce a maximum strain differential of 860 microstrain.

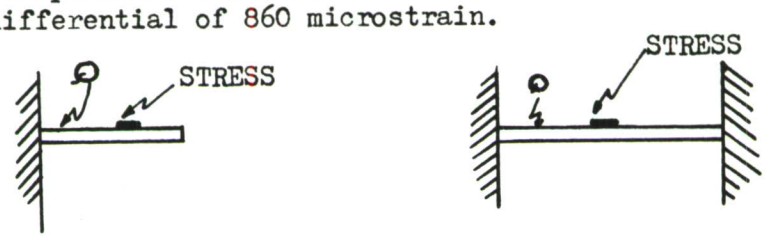

STRAIN
NO STRESS

STRESS
NO STRAIN

Consider the case shown above in which heat is added to a coupon that can freely expand and also one which cannot expand. In both cases, the sensor will be stressed due to the mismatch in expansion coefficient of the two materials even though one specimen is restrained and the other is not. The question now becomes one of whether the threshold sensitivity of the foil has been exceeded or not. The threshold was previously established as 1000 microstrain so no hardening or "zero shift" of the sensor should occur, **as long as the temperature variation does not exceed 250°F.**

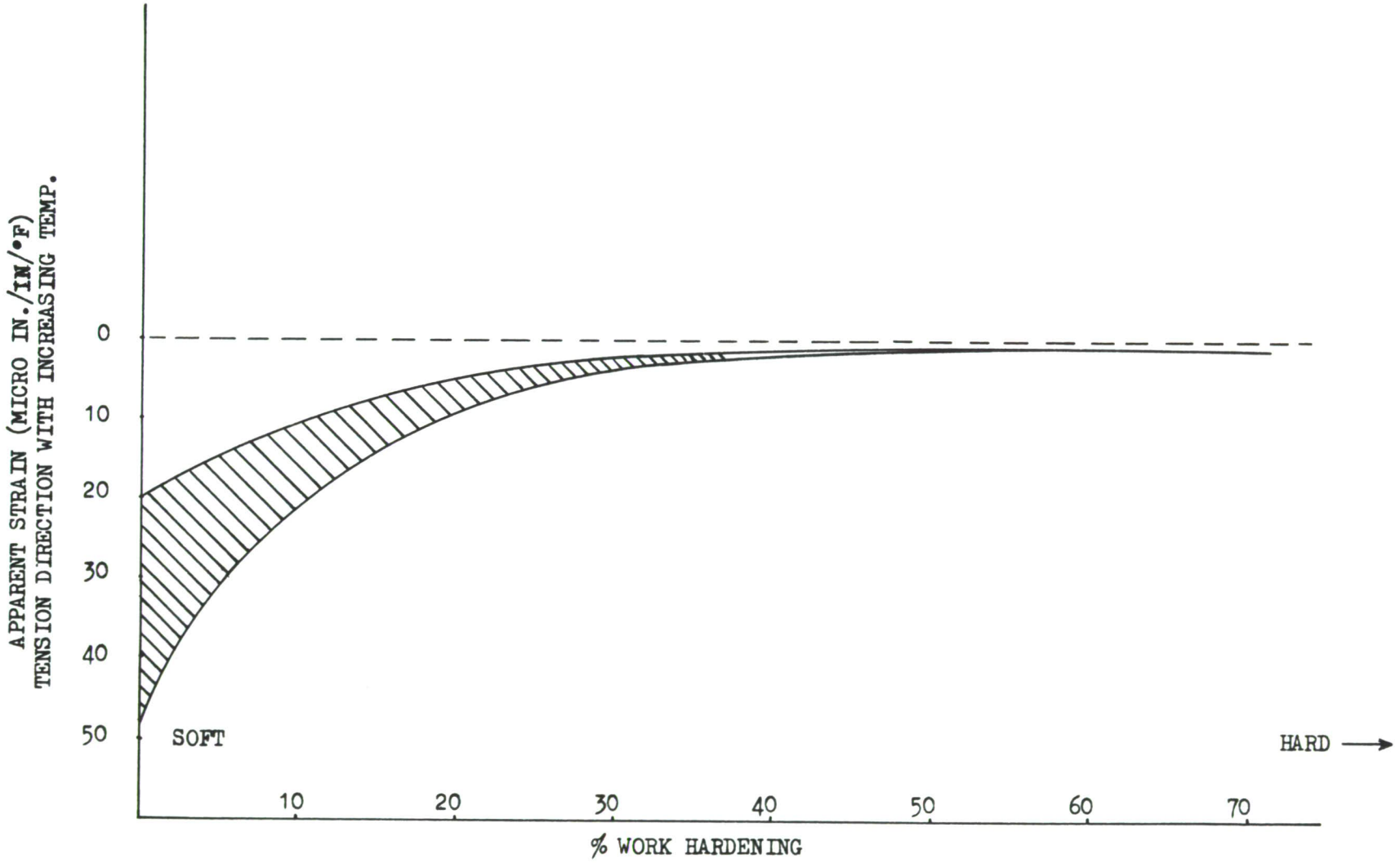

FIGURE 77 TEMPERATURE EFFECTS SURVEY OF 204A-ST SENSORS BONDED TO 7075-T6 ALUMINUM

One might also consider the mismatch between constantan and an elevated temperature aircraft material such as titanium. If 5.7 ppm is used as the linear coefficient of thermal expansion for titanium over a working range of -65°F. to + 400°F, the apparent mismatch of constantan to titanium is approximately (-3 ppm/°F). In this instance a ground-air-ground cycle could produce a ΔT of 465°F or a maximum strain differential of 1395 micro strain. However, to be exact, the coefficient of linear expansion of the entire gage composite (backing, adhesive, foil, etc.) should be determined as an individual case before reaching a conclusion regarding the error present.

Frequency Effect on Resistance Change of the Sensor

Several specimens were instrumented and cycled over a range of frequencies and strain levels. Initially it was felt that the frequency of applied cycles might alter the end resistance of the sensor. The tabulated specimen data in the Appendix indicates that the sensor is not frequency sensitive over cyclic rates of 5 cps up to 30 cps. Refer to data regarding specimens No. 20, 22, 24, 28, 31, 32, 33 in Table III of the Appendix.

Nuclear Radiation

It is realized that nuclear radiation would have a slight effect on electrical and dimensional changes in the adhesive layer of the fatigue sensor installation, however, for aircraft usage the effect should be considered negligible.

The foregoing represents a review of possible error sources to be considered in the application of fatigue sensors for long term aircraft usage. The fact that these errors can be pinpointed and controlled now will go a long way toward eliminating surprises during service usage.

4.2 PHASE II TYPICAL AIRCRAFT STRUCTURE TESTS

Maneuver loadings of cargo type aircraft are characterized by near symmetry of the varying load component about a constant mean load level. If one considers a typical stress-time history of an aircraft wing upper surface, the average sample would be composed of half cycles about some mean level, as shown in the diagram below.

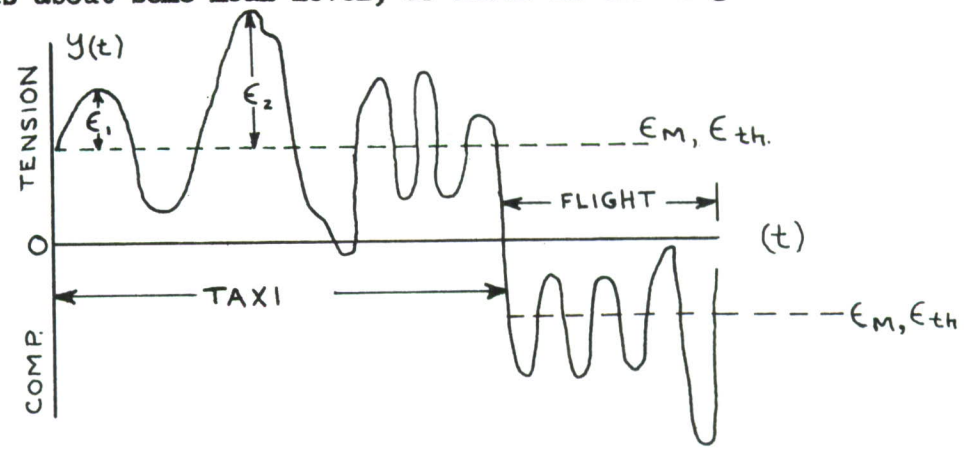

A fatigue sensor bonded to the wing surface would experience strain excursions proportional to the varying peak stress amplitudes. The totalization and storage capabilities of the sensor will cause it to register all strain excursions exceeding its threshold level. The cyclic frequency or direction of strain does not affect the resistance change; only the number and amplitude of the cycles above the threshold is considered by the sensor.

The Palmgren-Miner theory assumes that fatigue damage accumulates in a linear fashion, although many laboratory evaluations are in conflict with this hypothesis. For the proposed application of fatigue sensors to an aircraft structure a true linear relationship of sensor resistance to fatigue damage is not necessary. However, for the purpose of this analysis the relationship will be considered linear. That is, the change in resistance ΔR is proportional to fatigue damage D.

$$\Delta R \cong D \qquad (1)$$

The ΔR of the sensor as related to number and amplitude of the strain excursions can be expressed as,

$$\Delta R \cong \left(\frac{\epsilon_M}{\epsilon_{th}}\right)^b \left[\sum_0^{N-1} \epsilon_1 + \epsilon_2 + \ldots\ldots \epsilon_N\right] \qquad (2)$$

where

ϵ_M = mean strain level — b = constant

ϵ_1, ϵ_2 = peak strain amplitudes — ϵ_{th} = threshold strain level

N = number of peaks

Equation (2) is intended only to show a relationship in its simplest form and fits experimental curves best for a stress ratio of A = 0.818, however, it will not fit at all for a ratio of A = α

There is considerable similarity between the equation (2) and that for fatigue damage advanced by Bendat (Ref. 13) in which he states that,

$$D = \sum_{o}^{m-1} \frac{k}{2} | S_i |^{b} \qquad (3)$$

where

m = number of half cycles
b, k = constants of the material in relation to S-N diagram
S = peak stress amplitude

The factor 1/2 comes from considering the damage to be associated with a half cycle.

4.2.1 C-130E WING PANELS

Generally speaking, aircraft structural fatigue failures occur due to tensile stresses at some geometric discontinuity. Engineering prediction of the when and where of such failures require the development of methods, statistical data, and instrumentation which takes into consideration the complex interplay between stress distribution, number of load occurrences and material behavior. Pinpointing just where failure will occur is of secondary importance if one can forecast when the general service life of a structure will be expended. The feasibility of obtaining an indication of the degree of exposure to normal operational cyclic loads experienced in subsonic transport type wing structure has been reinforced by the results collected during the C-130E wing panel tests. By correlating loadings and strain reading with fatigue sensor zero shift, it is apparent that the sensor responds to repeatedly applied strain excursions above a particular strain level. Regardless of whether one wants to call the sensor output, accumulated strain or accumulated fatigue damage, the structure's relative degree of exposure can be monitored.

The C-130E wing panels selected for fatigue sensor evaluations are full scale duplicates of panels in service on the C-130E aircraft. In an attempt to improve the fatigue life of these fatigue critical panels minor structural modification have been made prior to a laboratory evaluation. Development tests were then conducted to evaluate these design modifications of the wing station WS 120 fuel filler cap panels as well as the WS 1.5 access door area panels. The original or "AS IS" panels are designated as Design I, with any redesign designated as Design II or III. The test conditions and the design goals of all five (5) of the C-130E wing panels are discussed in detail in ER-7853, Volume I, which is herein designated as Reference 4. The Design I, II and III WS 120 panels were tested and instrumented in exactly the same manner except for the following changes.

1. Fatigue Sensor 5019 was relocated on the redesigned panels to its alternate location as the result of a riser being extended. See Figure 88.

2. Many of the structural changes are so minor that they are not shown on the drawing, illustrated in Figure 88. Also the fatigue sensors are located in areas which would not be influenced by local stress redistributions, resulting from minor modifications.

3. The Design III WS 120 panel was instrumented with both the 204A-ST and the 204DA-ST as "mirror images" of each other in order to substantiate improvements claimed for the 204DA-ST sensor.

One complete pass is the equivalent of 5,000 flight hours as established by the eight load conditions and developed by a computer analysis. The eight load conditions were obtained from in-flight load recorders of C-130 aircraft subjected to representative mission profiles. By noting the number of load conditions completed prior to specimen failure the fatigue life of the panel in terms of flight hours may be approximated. Figures 78 and 79 show that the Design I panel had a life of 8,000 simulated flight hours while the Design II panel had a life of 15,000 simulated flight hours. Since the anticipated life of the Design I panel was 40,000 flight hours initial sensor readings were made on an infrequent basis, consequently only a few data points were obtained prior to panel failure at 8,000 simulated flight hours. The zero shift resistance change of the sensors was measured at the end of the load conditions designated in the curves of Figure 78 through Figure 81.

It is apparent from the curves, that load conditions # 6, # 7 and # 8 caused the maximum fatigue damage while conditions 1 through 5 were below the endurance limit of the material in the foil sensor. As to whether or not this also represents the endurance limit of the structure is not precisely known. In any event, it appears that the sensor can be used to establish the fatigue allowables from panel to panel as can be readily seen from the readings as both panels approach failure. A comparison of stress survey readings between the Design I and Design II Filler Cap panels, indicates a minor redistribution of stresses for the Design II panels. It is concluded that a small reduction in strain levels may have increased the fatigue life of the panel resulting in approximately the same sensor end resistance upon failure of both panels. An encouraging point in this phase of the investigation was that failure of both panels occurred at very nearly the same value of sensor resistance reading, although one panel endured approximately twice as many simulated flight hours as the other. In a practical application one could periodically monitor the sensor readings to see if the previously established fatigue damage allowables were being approached.

On the C-130E W.S. 120 panels, initial failure consisted of cracks at several distributed points rather than total failure across the panel. Previous sensor data obtained from clean coupons has indicated that the general location of failure might be determined by a change in rate of sensor zero shift. However, the fatigue sensor data obtained from the typical complex aircraft structure was so evenly distributed that the exact location of failure was difficult to forecast. The notable exception to this is the curves for sensors 5019 and 5020 on the W.S. 120 redesigned panel. These sensors were in the vicinity of the failure which may be responsible for the variation in the rate of change in sensor readings. It appears that an unsymmetrical distribution of load occurred in the panel which caused premature failure in the area of sensor number 5019. This local failure apparently occurred near the end of the second pass and the redistribution of load following this failure increased the rate of fatigue damage accumulated by sensor 5020. From the data available, it can be concluded that the degree of allowable exposure to repeated load cycles can be forecast, although forecasting point of failure is more difficult.

The C-130E Filler Cap panel Design III was instrumented to substantiate improvements claimed for the 204DA-ST sensor. Sensor locations 5011, 5012, 5017, 5018 were instrumented with the type 204A-ST sensor and the companion locations 5013, 5014, 5019, 5020 were instrumented with the type 204DA-ST fatigue sensor. Since the strain gage data from the stress survey was very similar to that obtained on the first two designs, a tabulation of survey data is not shown. The basic structural change in the panel consisted of the deletion of some fastener holes around the filler neck. The panel was subjected to approximately 25,000 simulated flight hours before the cracks became extensive enough to constitute a failure.

In comparing the two types of sensors on the Design III panels with data from previous tests it can be concluded if one allows for the percentage increase of sensitivity of the 204DA-ST foil, the sensor end resistance is very nearly the same upon specimen failure.

Two (2) C-130E W.S. 1.5 access door panels were also instrumented with strain gages and fatigue sensors, and evaluated under a similar loading spectrum. Since the data obtained and the conclusions reached were the same as for the previous three (3) panels a detailed review is not included. The outputs of the fatigue sensors and general shape of the curves were quite similar for both sets of the W.S. 120 panels and the W.S. 1.5 panels. This is to be expected since the sequence of repeated loads and strain amplitudes as shown by the stress surveys were closely related. The loading spectrum as applied to both sets of panels is characterized by the same flight conditions, with only the amplitude of loading changed.

C-130E W.S. 120 FUEL FILLER CAP PANEL LOAD AND STRAIN DATA

The following data was obtained during the stress survey prior to fatigue cycling the panel. The strain readings show the stress distribution in the panel for the applied loads and since they are located adjacent to the fatigue sensor, they will also show strain levels for the sensor.

STRAIN READINGS (u in/in) AT VARIOUS LOADS DESIGN I

Strain Gage Channels	0 Load Counts	100 Load* Counts	200 Load Counts	300 Load Counts	400 Load Counts	539 Load Counts
1001	0	190	400	590	780	1020
1002		180	370	540	730	960
1003		230	470	720	950	1240
1004		200	430	660	880	1150
1005		210	450	680	900	1200
1006		200	430	650	860	1140
1007		190	400	620	840	1100
1008		70	130	200	290	360
1009		-60	-150	-220	-280	-400
1010		230	420	620	860	1140
1011		220	480	730	980	1300
1012		220	470	730	970	1280
1013		220	480	740	990	1300
1014		220	480	740	990	1300
1015		230	440	690	910	1200
1016		200	450	690	920	1210
1017		220	470	710	960	1240
1018	0	210	440	680	900	1200

*The strain data is recorded directly in microinches per inch with no sign indicating positive (+) or tension strains, and the negative sign indicating compressive strains. The load counts represent potentiometer settings on the loading console with one count equal to 132.94 pounds tension load.

STRAIN READINGS (u in/in) AT VARIOUS LOADS — DESIGN II

Strain Gage Channels	0 Load Counts	*100 Load Counts	200 Load Counts	300 Load Counts	400 Load Counts	539 Load Counts
1001	00	190	400	590	800	1080
1002	30	210	390	580	770	1020
1003	00	220	360	680	900	1200
1004	00	200	420	610	800	1070
1005	20	260	500	710	940	1260
1006	10	220	470	680	900	1220
1007	00	150	330	480	640	860
1008	40	70	140	180	230	320
1009	-10	-50	-110	-180	-230	-300
1010	10	200	410	580	780	1040
1011	20	260	520	740	960	1300
1012	10	240	490	700	920	1240
1013	10	240	500	720	960	1280
1014	00	240	490	700	920	1240
1015	20	210	430	620	840	1120
1016	00	200	410	610	820	1090
1017	20	260	510	730	960	1290
1018	10	200	430	620	830	1120
1019**	10	480	970	1440	1920	2600

*Load counts are potentiometer settings on the loading console with one (1) count equal to 132.94 pounds. Consequently the total load applied to the specimen at a setting of 100 counts is 13,294 pounds tension. No sign on the strain reading is positive or tension, the negative sign indicates compressive strain.

** Miniature gage added between fasteners at filler cap.

NOTE: A strain survey was also conducted on the Design III W.S. 120 Fuel Filler Cap panel, but since the strain readings were essentially the same as for the Design II panel the tabulation is not shown.

LOADING SPECTRUM APPLIED TO C-130E FILLER CAP PANELS

Load Condition	Mean Load (Lbs.)	Variable Load (Lbs.)	Cycles/Pass (5000 Flt. Hrs.)
1	50700	± 20,900	12,600
2	50700	± 29,300	796
3	64400	± 26,100	3,446
4	64400	± 43,900	5
5	71900	± 26,300	11,334
6	- 900	± 66,200	508
7	-10200	± 75,000	382
8	-20300	± 92,600	268

A typical loading spectrum is shown below, with the positive sign indicating tension loads. Variable loads are plus and minus values.

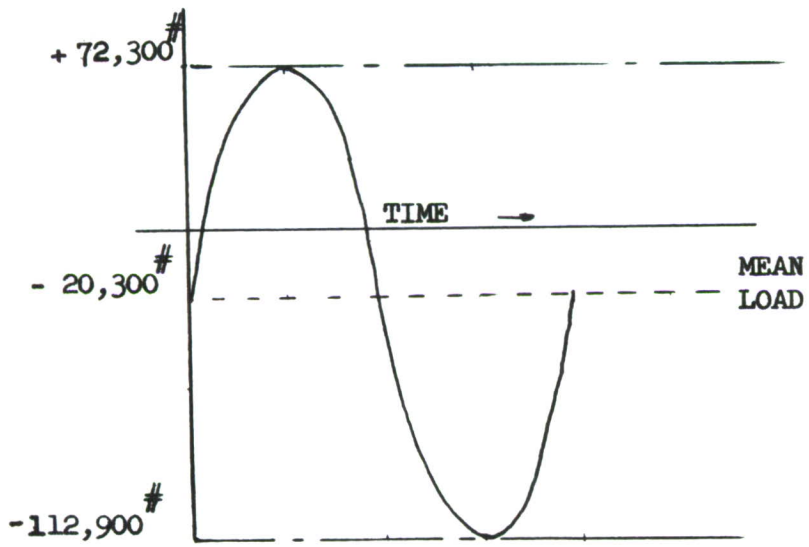

LOAD CONDITION # 8

C-130E ACCESS DOOR PANEL W.S. 1.5 LOADING SPECTRUM

The following is the loading spectrum applied to both the "AS IS" panel and the "REDESIGN" panel.

Load Condition	Mean Axial Load (Lbs.)	Variable Load (Lbs.)	Cycles/Pass (5,000 Flt. Hrs.)
1	113,000	± 46,640	12,600
2	113,000	± 65,430	796
3	143,650	± 58,180	3,446
4	143,650	± 97,790	5
5	160,260	± 58,560	11,334
6	- 2,000	±147,630	508
7	- 22,800	±167,232	382
8	- 45,340	±206,430	268

The loading conditions, 1 through 5, represent taxi loads while loads 6 through 8 represent ground-air-ground cycles. The negative sign for the mean loads indicates compression while the variable cyclic load varies in the plus and minus direction. The cyclic loads are applied beginning with condition 1 and proceeding in numerical order through condition 8 then reversing the sequence, going back through 8 to 1. Cyclic load condition 8 is shown in the diagram below:

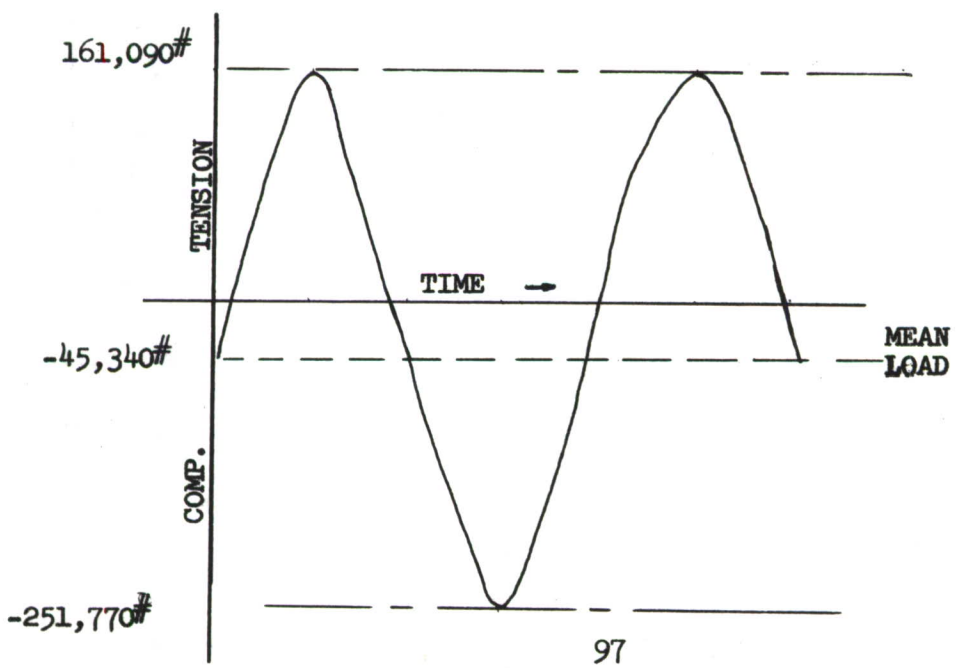

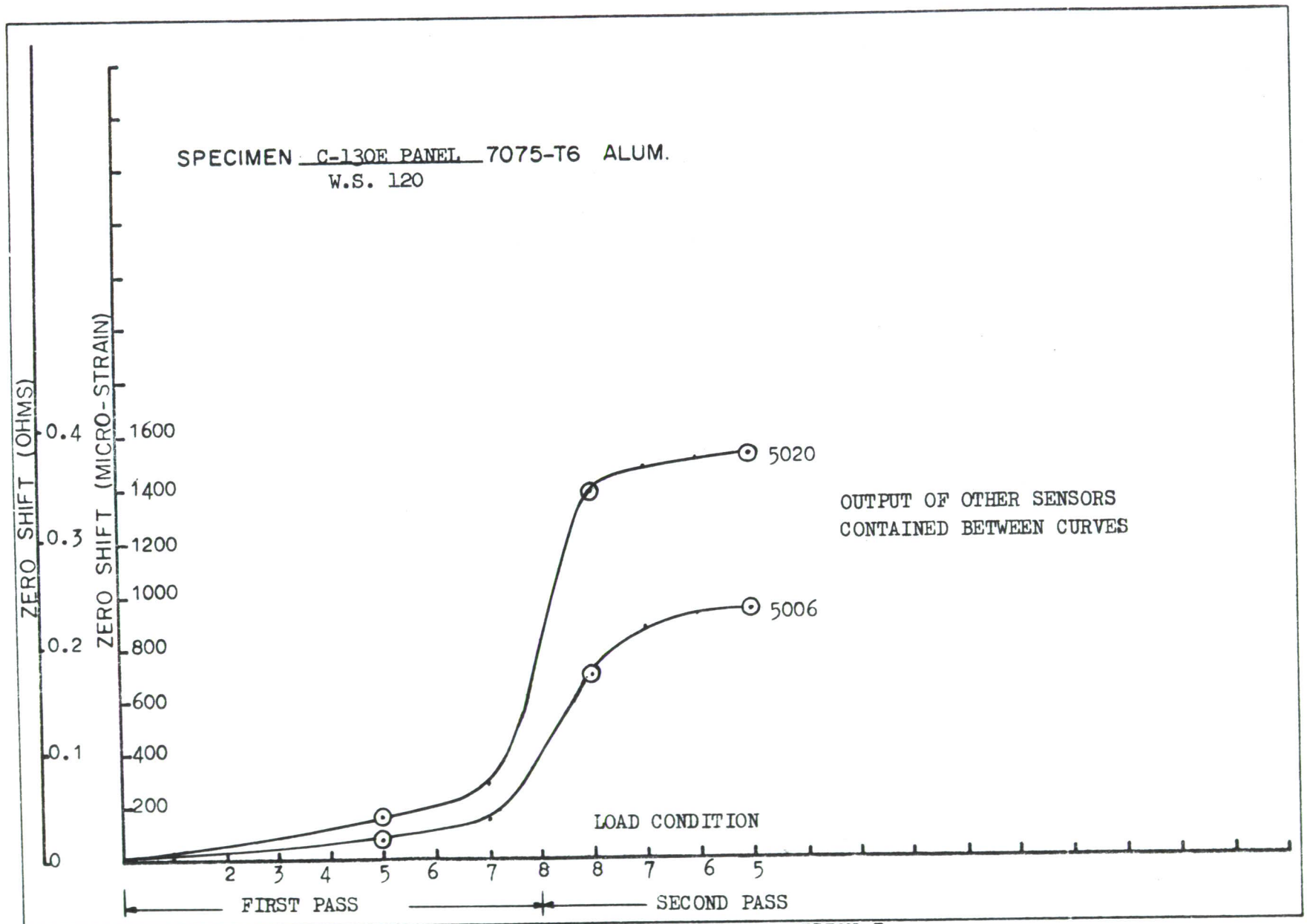

FIGURE 78 FATIGUE SENSOR READINGS ON C-130E FILLER CAP PANEL DESIGN I

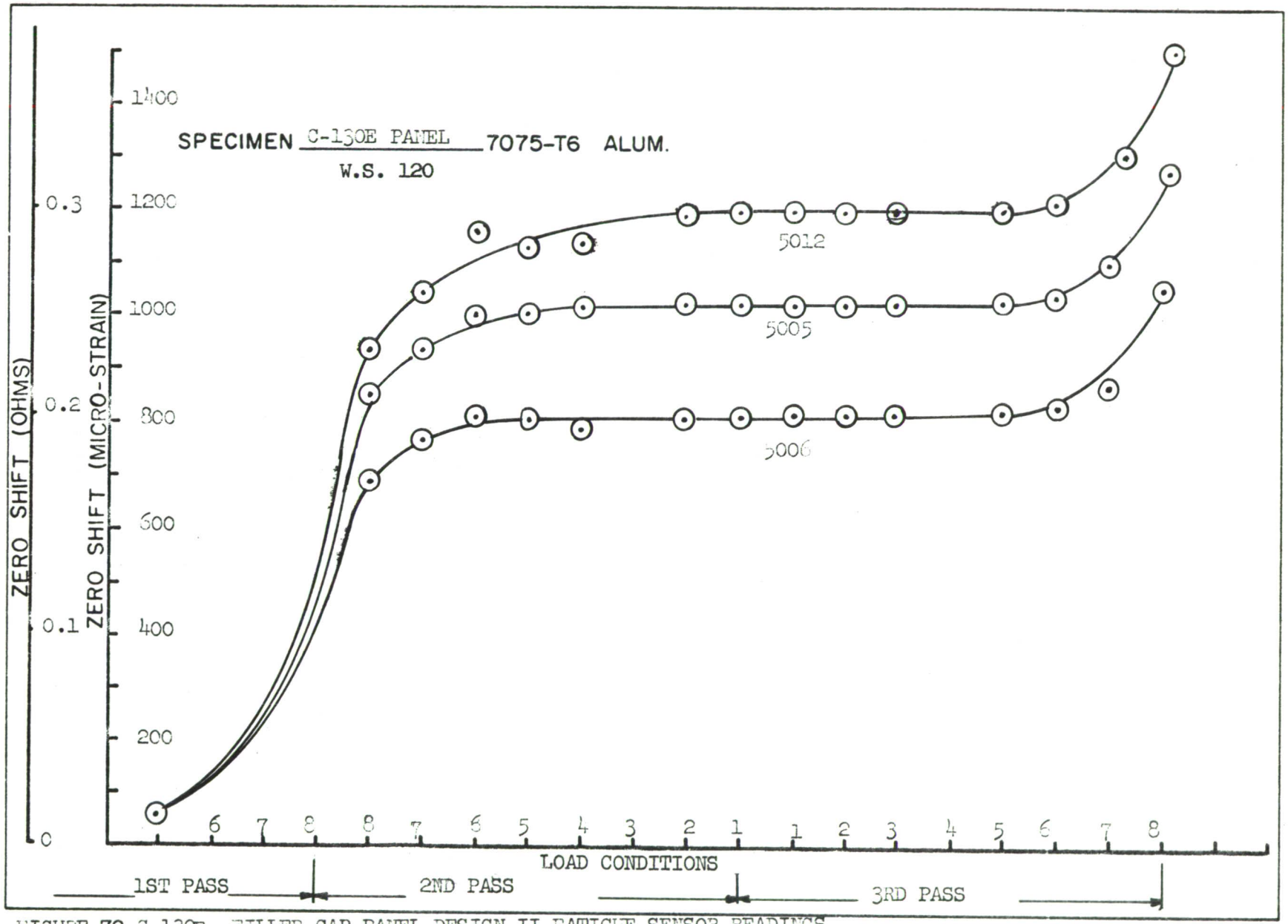

FIGURE 79 C-130E FILLER CAP PANEL DESIGN II FATIGUE SENSOR READINGS

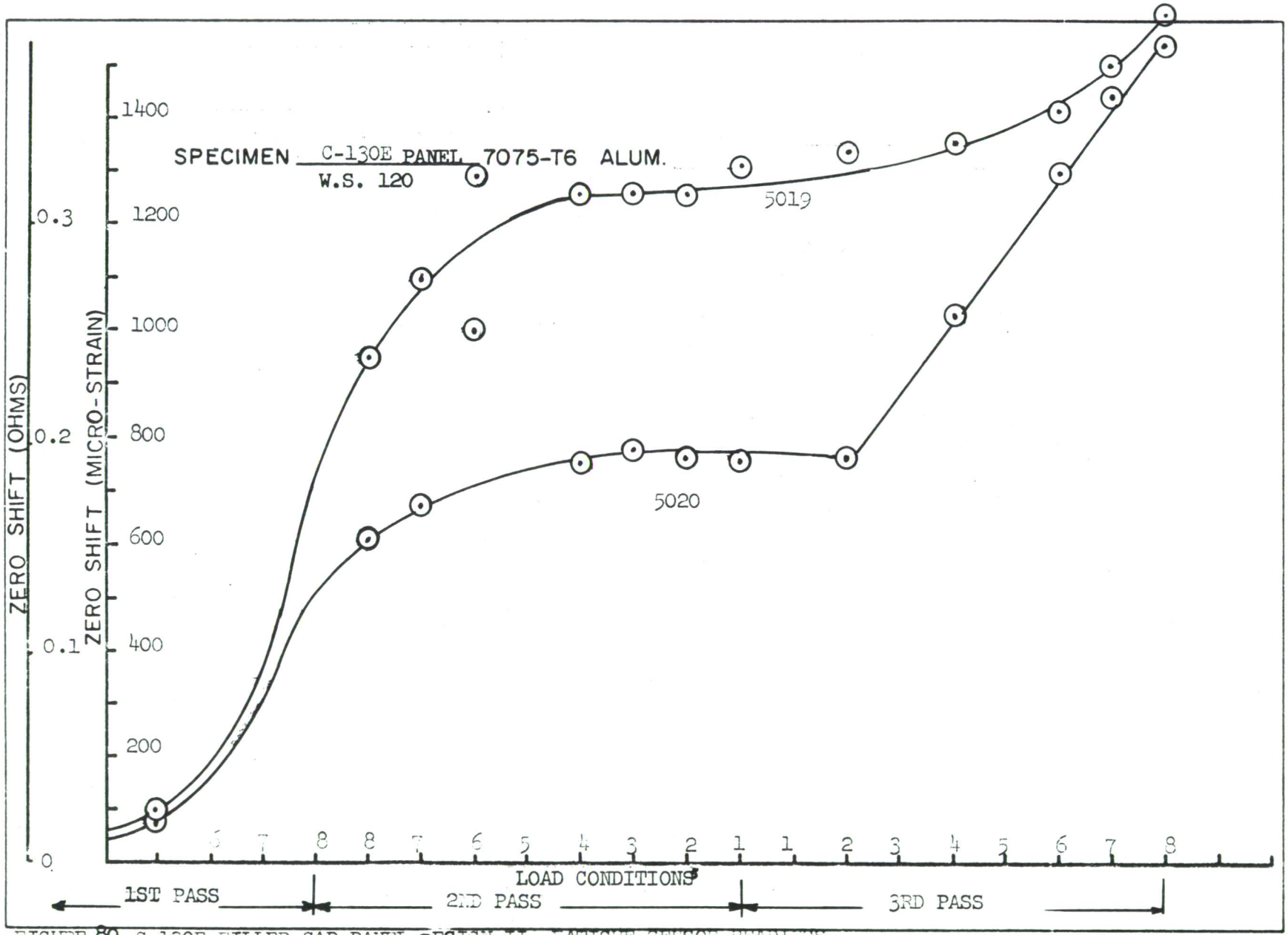

FIGURE 80 C-130E FILLER CAP PANEL DESIGN II FATIGUE SENSOR READINGS

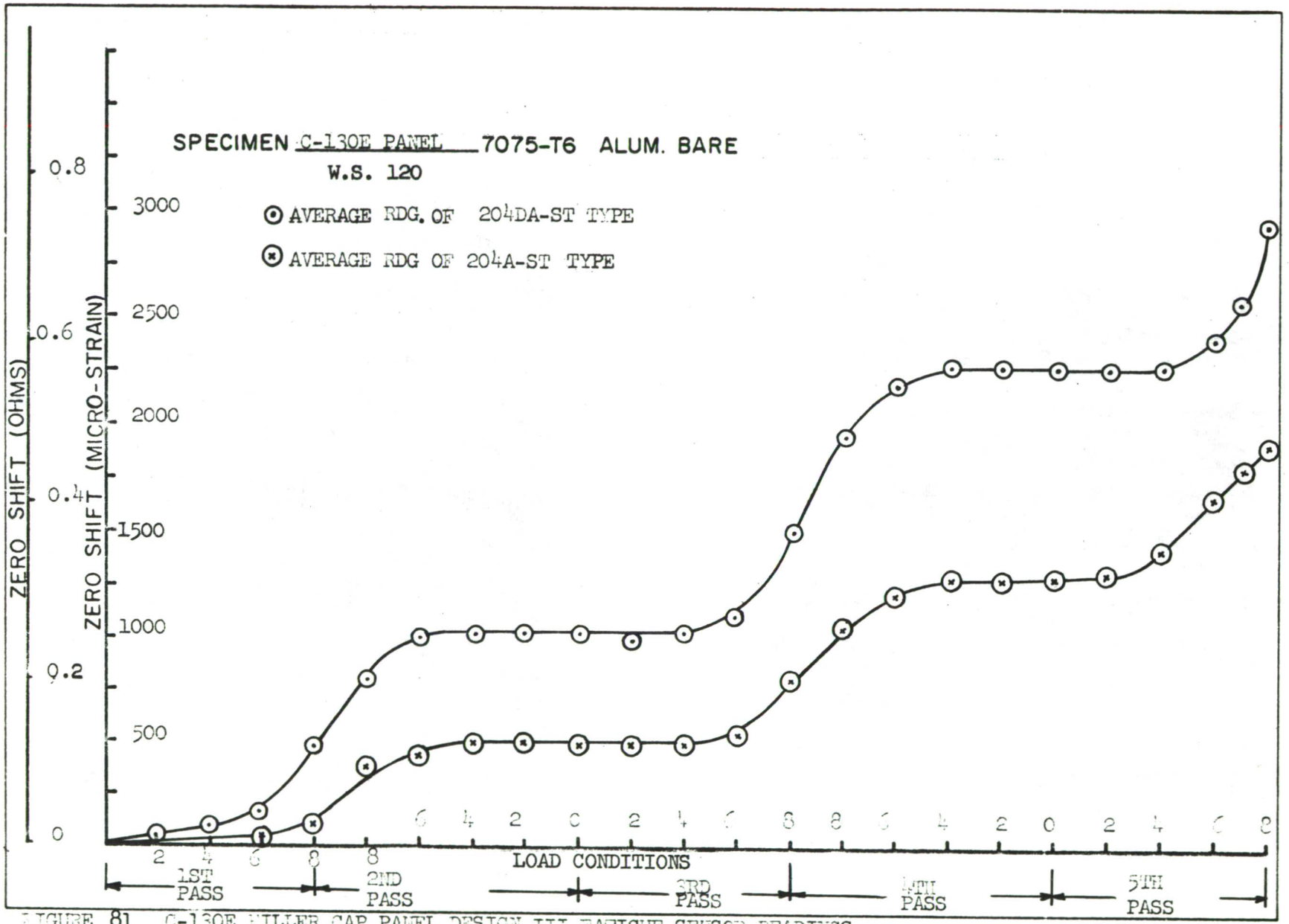

FIGURE 81 C-130E MILLER CAP PANEL DESIGN III FATIGUE SENSOR READINGS

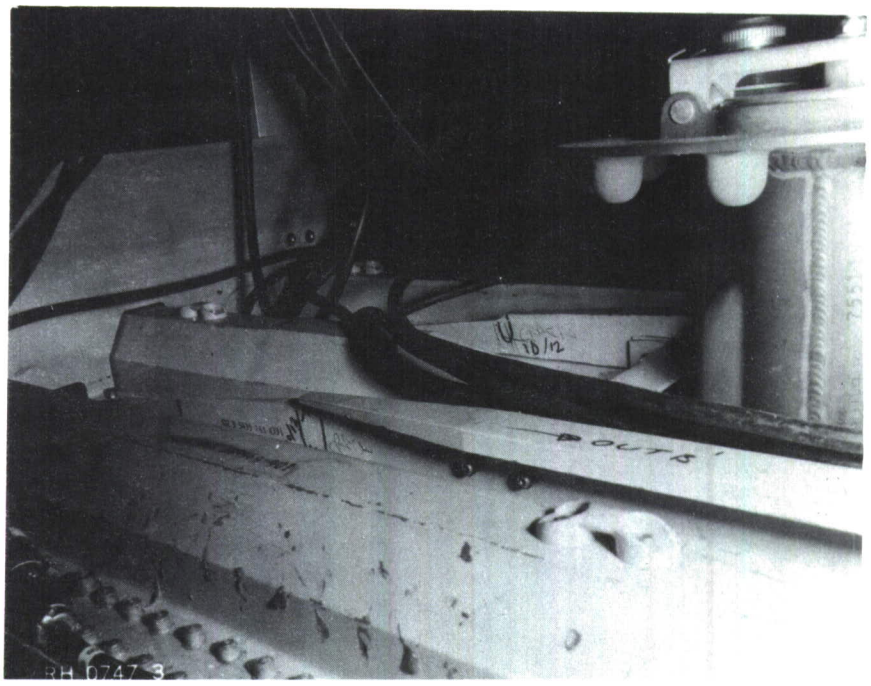

FIGURE 82 REDESIGN C-130E FILLER CAP PANEL SHOWING CRACKS IN THE RISER EXTENSION ADJACENT TO THE FILLER CAP

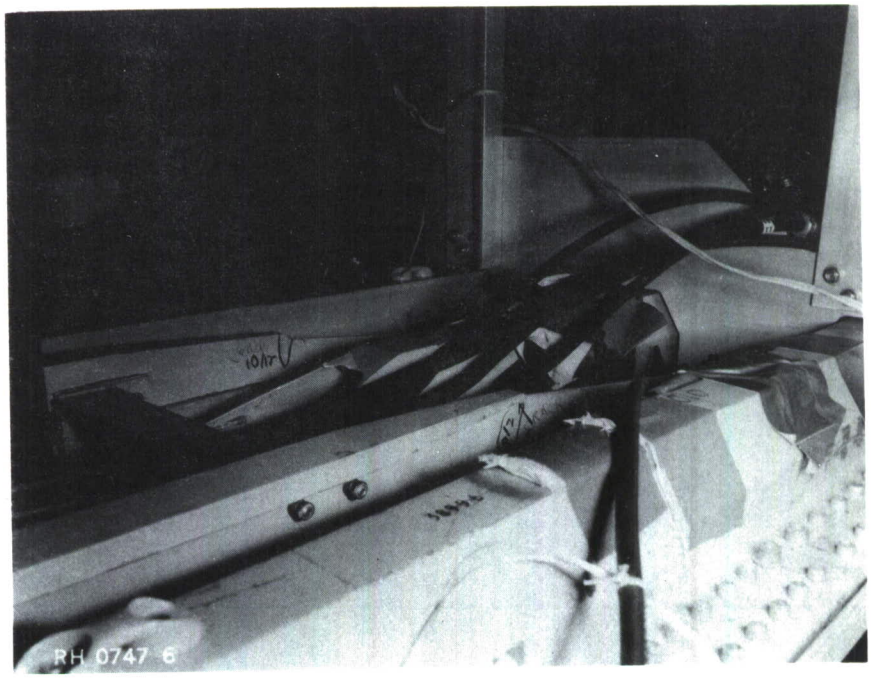

FIGURE 83 OTHER END OF RISER SHOWING CRACKS OF A SIMILAR NATURE

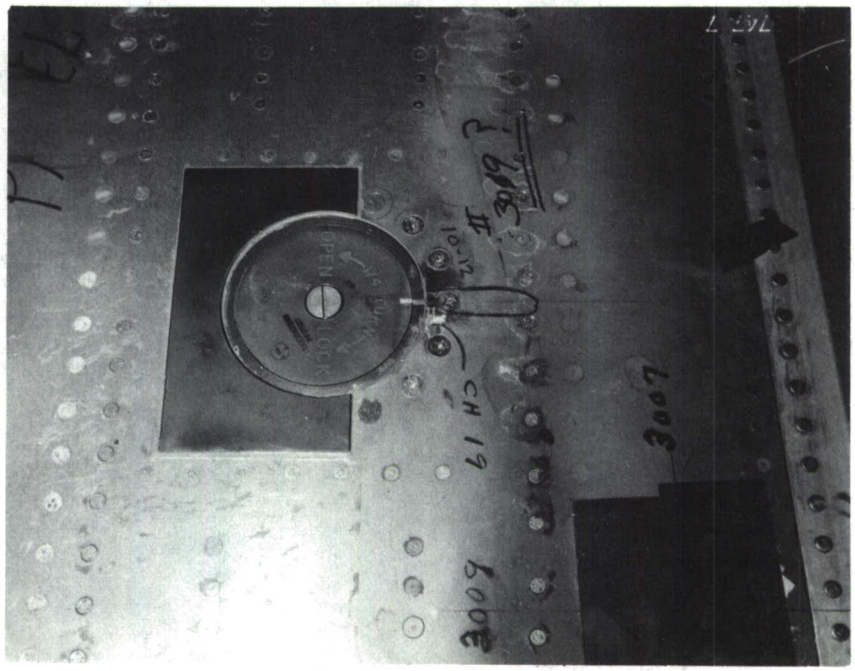

FIGURE 84 REDESIGN C-130E FILLER CAP PANEL SHOWING A CRACK EXTENDING OUT FROM A RIVET

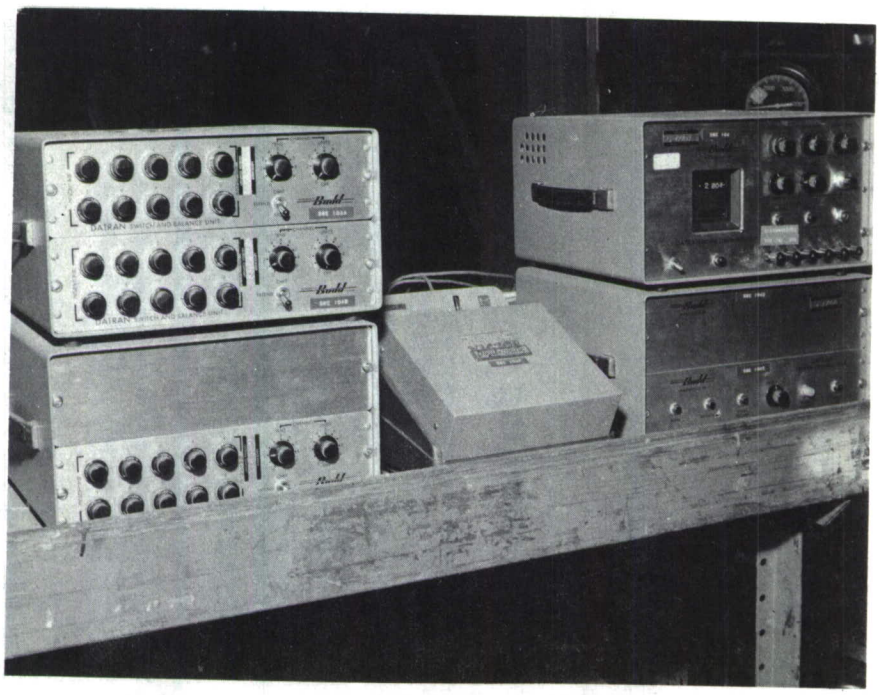

FIGURE 85 EQUIPMENT USED FOR RECORDING STRAIN GAGE OUTPUTS DURING THE STRESS SURVEY

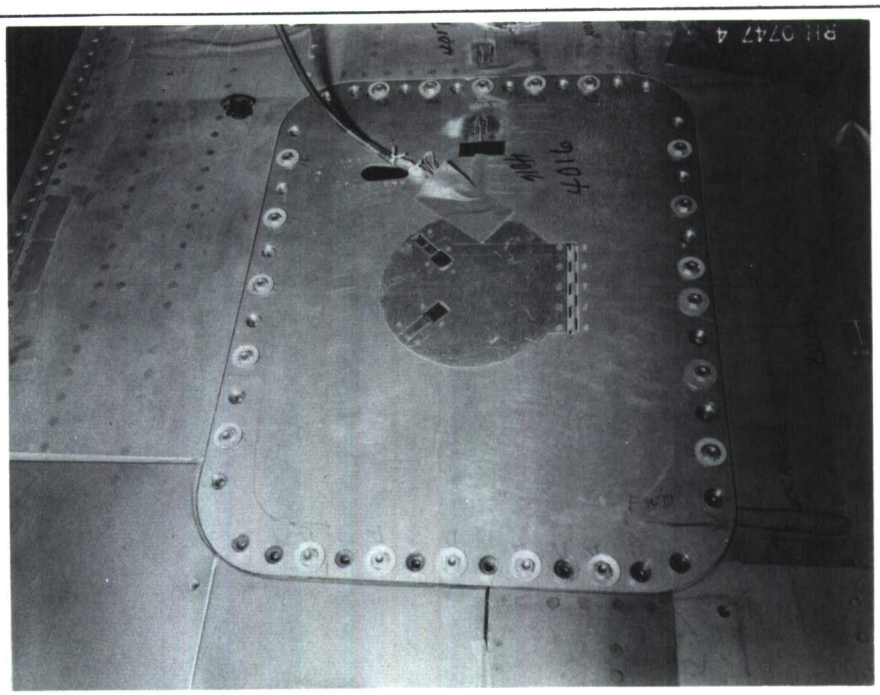

FIGURE 86 REDESIGN C-130E W.S. 1.5 PANEL SHOWING FATIGUE CRACK AT ONE CORNER OF THE ACCESS DOOR

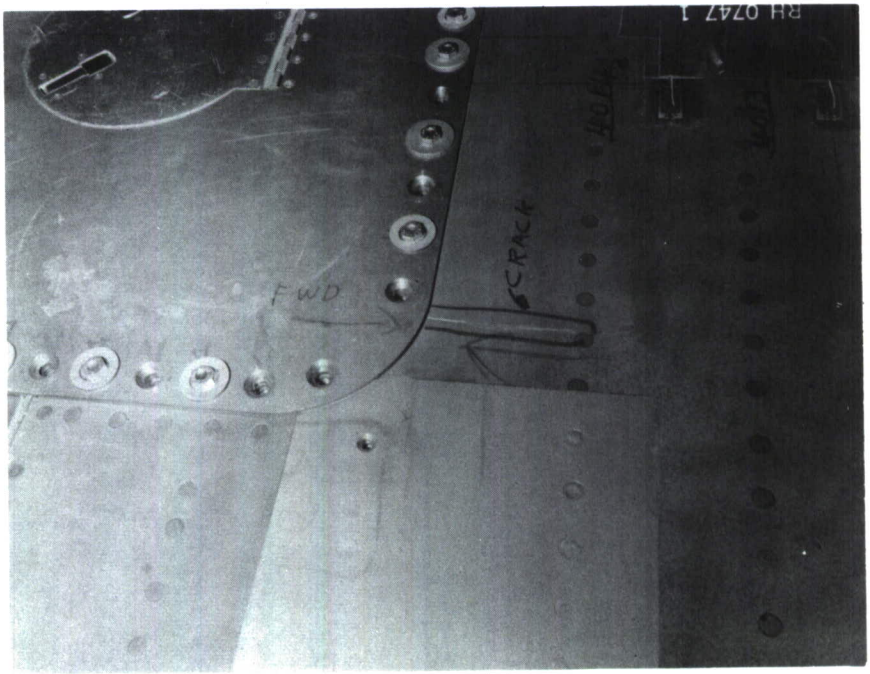

FIGURE 87 CLOSE UP VIEW OF CRACK WHICH RUNS FROM DOOR FASTENER TO THE RIVET

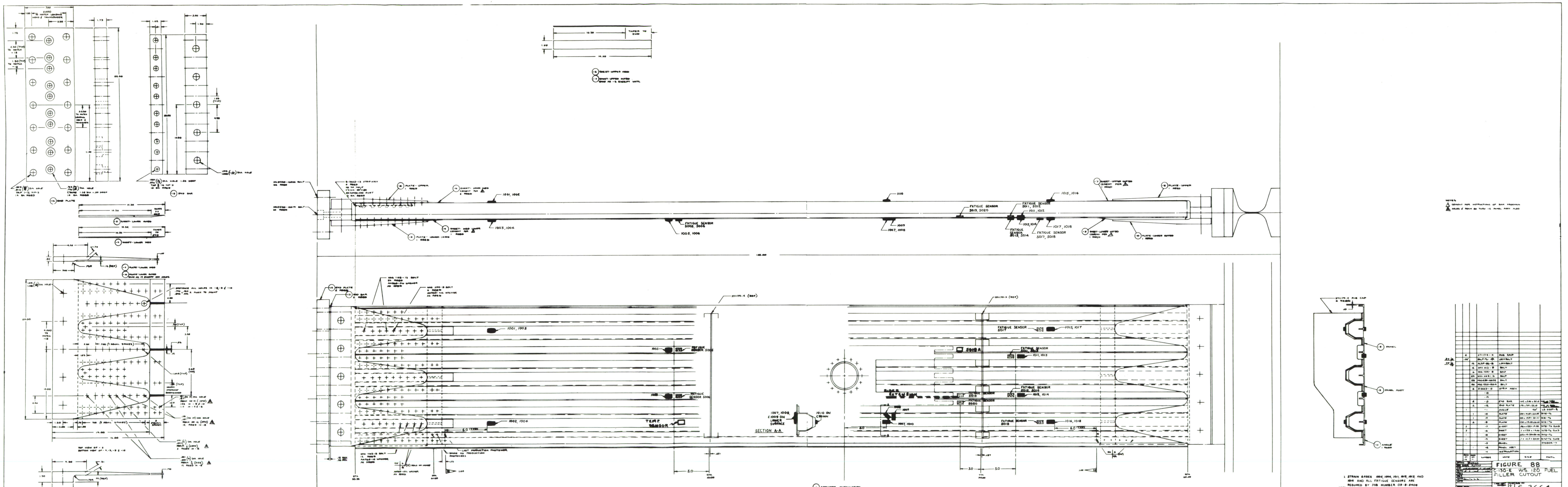
SECTION A-A
TEMP SENSOR
FATIGUE SENSOR
STRAIN GAGE
PANEL ASSY
ANGLE
PLATE : UPPER
PLATE : LOWER
SHIM PLATE
SPAR CAP
FIGURE 88
T-38E WS 120 FUEL
FILLER CUTOUT
S-3664

4.2.2 C-141A AFT FUSELAGE - EMPENNAGE SPECIMEN C

The evaluation of the laboratory fatigue structure consisted of an instrumented specimen as shown in Figure 90. The specimen was instrumented with strain gages and 40 channels of fatigue sensors located as shown in the expanded view diagram. The structure was then cycled with servo loaders according to an established mission profile for this type of aircraft (Ref. 3). The specimen was instrumented prior to accumulating any simulated flight hours and prior to optimizing the fatigue sensor. However near the end of 12,000 simulated flight hours the sensors indicated very little zero shift even though some pressurization failures had occurred. A review of the situation indicated that the cyclic strain level was near or even below the threshold sensitivity of the sensor. A second look at the fatigue sensor locations also indicated that a more judicious selection of locations by a stress analyst would have provided nominal areas with higher strain levels and subsequent higher output from the fatigue sensors. The original selection of sensor location came by way of an instrument engineer and at a time when the threshold sensitivity of the 204A-ST was not precisely known. The follow on coupon test phase indicated a lower threshold for the double annealed foil, so it was decided to install the type 204DA-ST at fuselage station 1398, which is in the aft end of the pressure vessel.

The following is a brief tabulation of readings obtained from the 3 sensors installed at the pressure door at F. S. 1398. The zero reading was taken 8 Mar. 66 with the status of the specimen at G. A. G. condition 2 of pass 7, or approximately 18,000 simulated flight hours.

Channel Number	Zero Bal. 8 Mar. 66	End of Pass 8 (4 May 66)
C-1	0	155 Micro-strain
C-2	0	80 Micro-strain
C-3	0	90 Micro-strain

It should be noted that each pass is the equivalent of 3000 flight hours, so a zero shift of 155 microstrain /pass would approximate a total cumulative strain reading of 3100 microstrain for the total program of 20 passes. Zero shifts of this magnitude will indicate the structures exposure to cumulative strain excursions in considerably more detail than that initially obtained. Even from a short run program it appears that these improvements in threshold sensitivity and sensor location techniques will enhance the practicality of fatigue sensor usage on laboratory specimens.

The fatigue cycling of Specimen "C" was on gust condition 7 of pass 9 when the pressure door blew out causing extensive damage to the door and back up structure. Since considerable time will be involved in repairs, before cycling can continue, no further sensor readings will be obtained during the present contract. The following readings were taken just after the pressure door failure, and represents the status at approximately 25,000 simulated flight hours.

Channel Number	Zero Bal. 8 Mar. 66	After Cond. 7 Pass 9(13 May 66)
C-1	0	230 Micro-strain
C-2	0	180 Micro-strain
C-3	0	195 Micro-strain

4.2.3 C-141A SPECIMEN "B" WING FUSELAGE

During the program it became evident that specimen "C" would spend considerable time on an inactive status, consequently it was decided to install some sensors on specimen "B". This activity would allow an evaluation of the more sensitive 204DA-ST sensor on typical aircraft structure and would supply some data in case specimen "C" remained inactive. The three sensors (type 204DA-ST) were installed on the upper surface at the wing root just prior to the start of the fifth pass. Therefore, fatigue sensor data will be obtained from the 12,000th simulated flight hour until termination of the program. The test loading spectrum as extracted from ER-4946 (Ref. 4) constitutes one complete pass or 3000 simulated flight hours. The total program, as presently defined, consists of 20 passes or 60,000 simulated flight hours. Therefore, only one-fifth of the specimen fatigue life had been expended prior to installation of the sensors. One pass is designed to be representative of all phases of aerodynamic or ground loadings since it considers taxi conditions, ground-air-ground cycles, gust and maneuver conditions. Although the specimen was cycled on odd shifts, the permanent zero shift of the fatigue sensors were recorded at convenient intervals such as completion of taxi, G.A.G. or gust conditions. The following is a brief tabulation of the readings obtained during, and at the completion of pass five. Readings are in micro-strain corrected for temperature.

Channel Number	Zero 27 Dec. 65	After Load 1D	After Load 4D	After Load 4C
B-1	0	140	175	240
B-2	0	125	130	140
B-3	0	40	80	190

Inspections after pass five revealed cracks in the splice plate at W.S. 415 of the left wing. The fatigue sensors above are located near the splice plate at W.S. 77 of the left wing. The sensitivities and sensor outputs obtained above are more encouraging than those obtained from the original instrumentation on specimen C. The maximum zero shift of 240 micro-strain for only one pass indicates ten passes would have put it in the vicinity of 2400 micro-strain representing more useful data since a higher resolution is obtained. The loads 1A through 1D represent taxi conditions and the sensors indicate more damage for this condition. Taxi loads would be expected to do more damage to the wing upper surface, especially at W.S. 77. Strain gages located in similar areas on the right wing indicated peak strains on the order of 2000 micro inches/inch, so the sensor is being operated well above its threshold limit.

After repairs to W.S. 415 of the left wing fatigue cycling was resumed and had progressed to approximately 17,000 simulated flight hours. The readings shown below are in micro-strain corrected for temperature.

Channel Number	Zero Bal. 27 Dec. 65	After Cond. 3A Pass 6 (16 May 66)
B-1	0	310 Micro-strain
B-2	0	195 Micro-strain
B-3	0	285 Micro-strain

Since these sensors have been subjected to hydrostatic pressure they were checked for leakage to ground. The resistance to ground for all three channels exceeded 1K megohms.

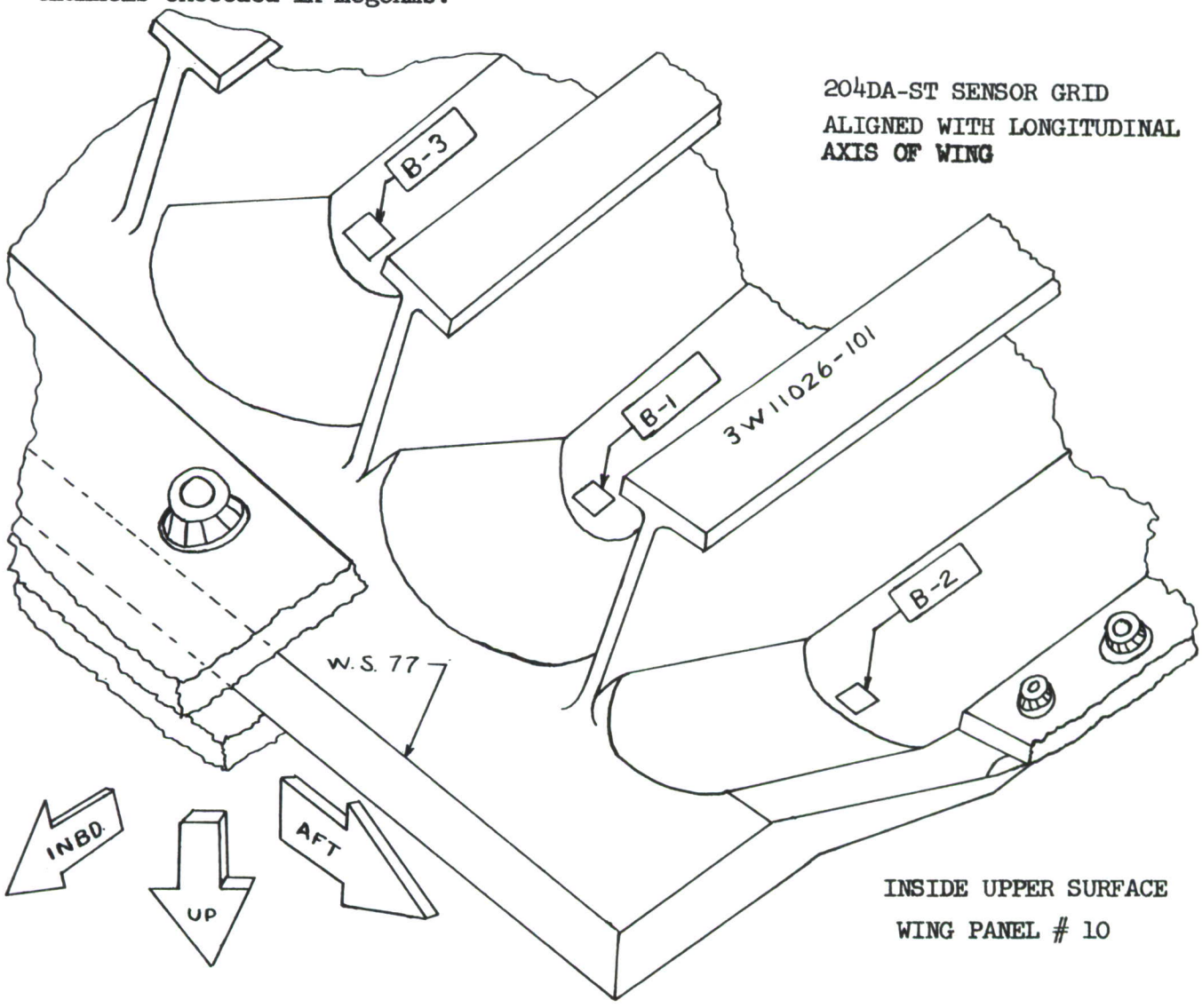

FIGURE 89 SENSOR INSTALLATION ON C-141 SPECIMEN "B"

C-141A WING-FUSELAGE FATIGUE PROGRAM

SPECIMEN "B"

TEST LOADING CONDITIONS

CONDITION		NO. CYCLES	FUSELAGE PRESSURE (PSIG)
1A		19,120	0
1B		874	0
	Taxi		
1C		3.0	0
1D		3.0	0
2A		820	0
	G.A.G.		
2B		830	0 at Min. to 8.60 at Max.
		49.3	0
4A	Mean	1,242	0 to 8.6
3A	Mean	378	0 to 8.6
3A		1,840	2.45
		14	6.45
		69	8.60
3B		181	2.45
		1.0	6.45
		2.0	8.60
	Gust		
3C		2.5	2.45
		.5	8.60
4D		424	2.45
		85	6.45
		7,976	8.60
4A		764	2.45
		68	6.45
		4,064	8.60
4B		149	2.45
		2.0	6.45
	Gust and Maneuver	50	8.60
4C		1.0	2.45
		2.0	8.60

FIGURE90 - EMPENNAGE
FATIGUE SENSOR LOCATION

Notes

1. **All sensors located internal, none are on outside surfaces.**

2. **Cable routing out of tail cone for specimen C.**

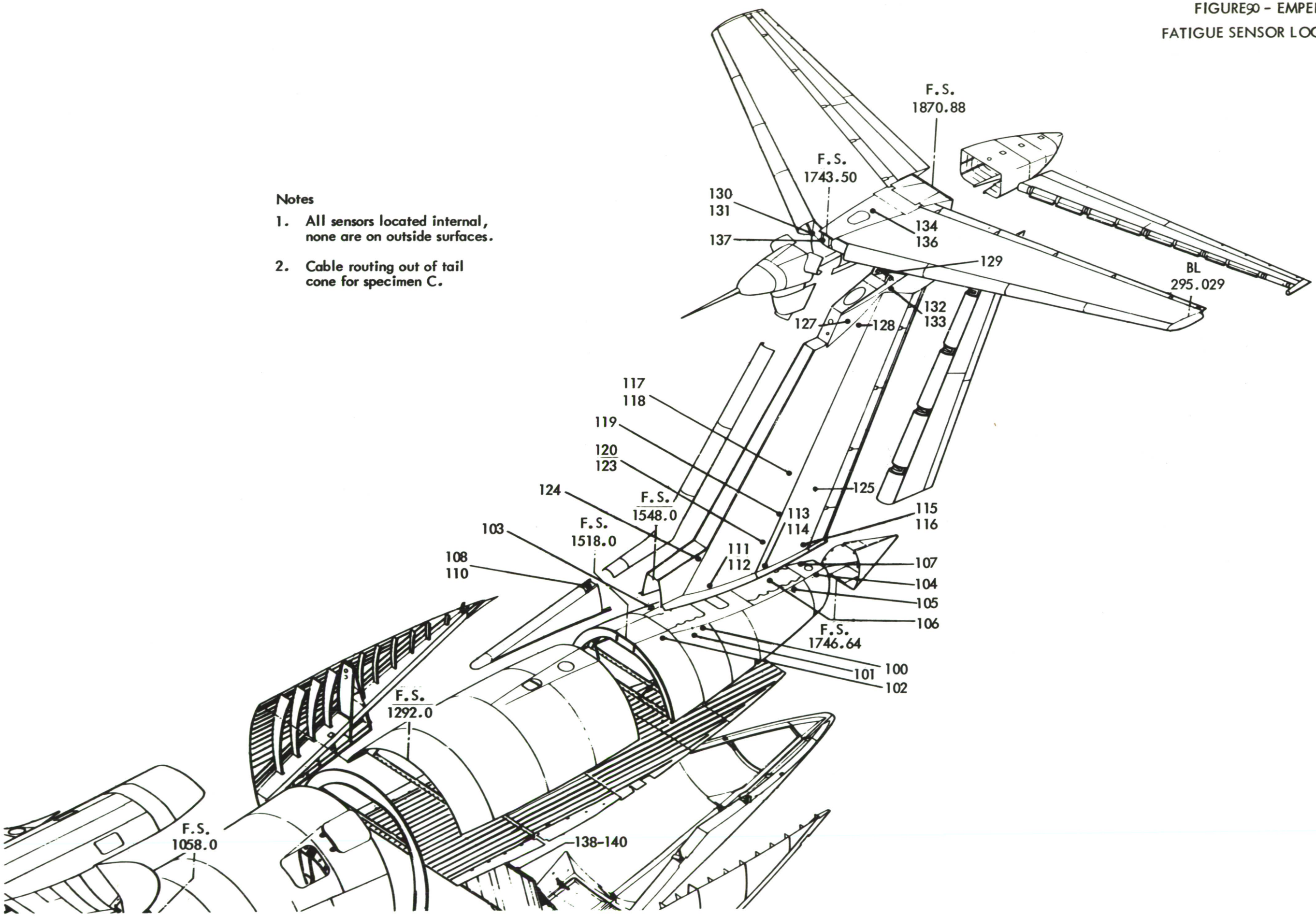

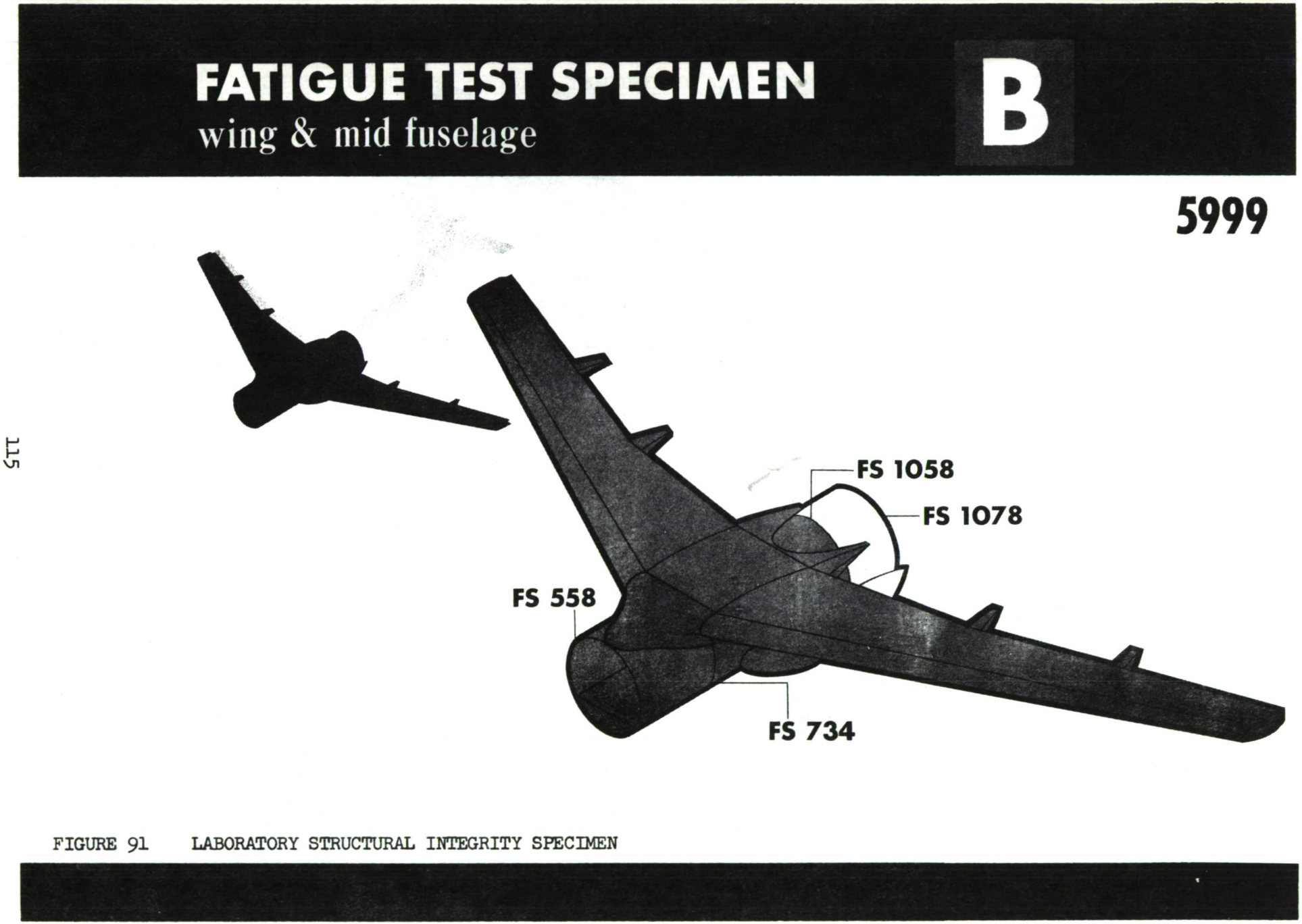

FIGURE 91 LABORATORY STRUCTURAL INTEGRITY SPECIMEN

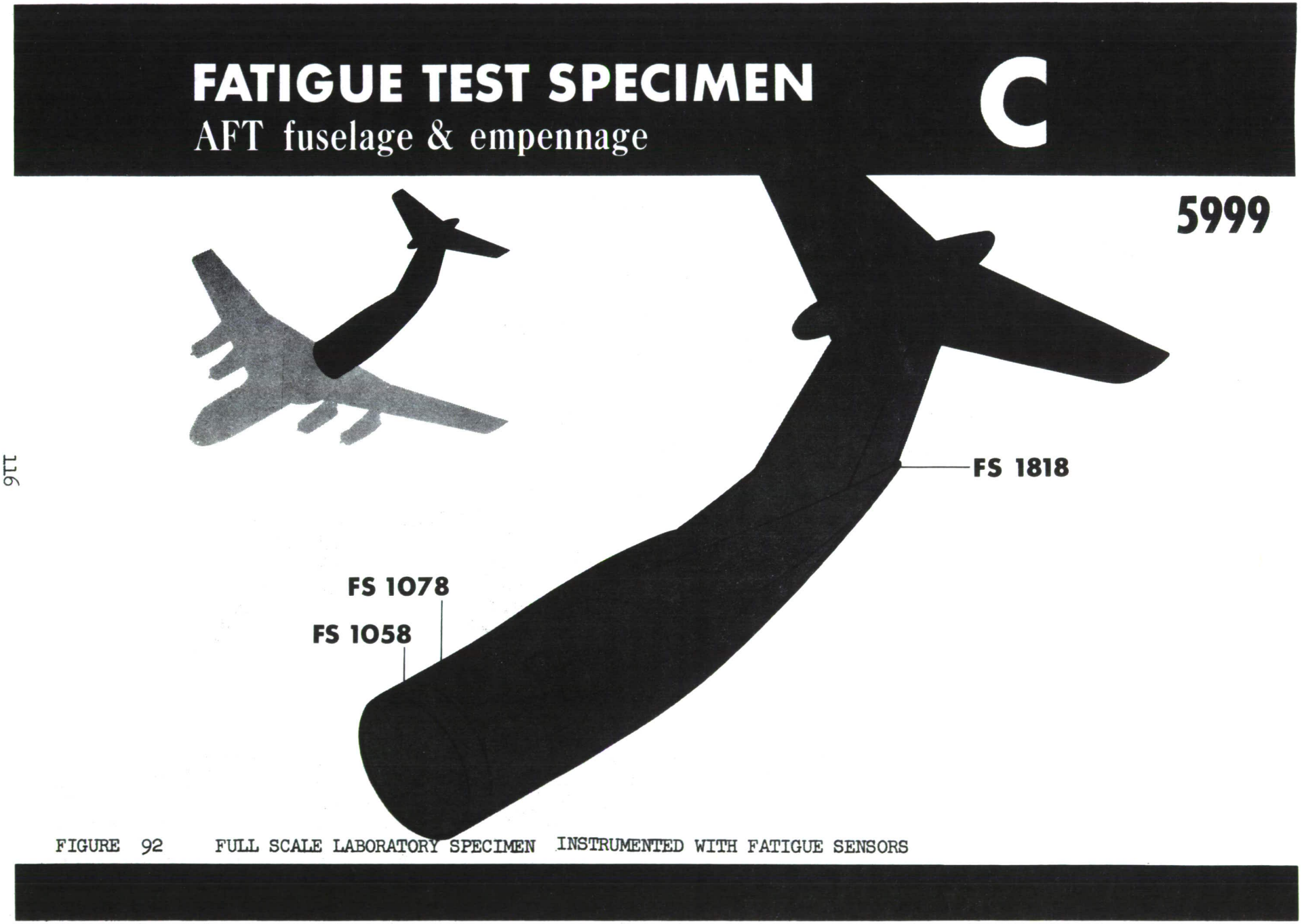

FIGURE 92 FULL SCALE LABORATORY SPECIMEN INSTRUMENTED WITH FATIGUE SENSORS

4.2.4 $K_t = 4$ SPLICE JOINTS

For practical application of a fatigue damage evaluation system to an aircraft, all possible fatigue damage sources should be considered. In some areas of an aircraft structure aerodynamic loadings are transferred across a splice joint representing a $K_t = 4$, resulting in nominal area strains of less than 600 micro inches/inch. In lieu of an adequate and reliable method of lowering the sensor threshold sensitivity to this level, it appeared necessary to actually work in the area of the stress concentration.

In order to evaluate the capability of determining the fatigue status of a structure having a $K_t = 4$ a revised spiral grid sensor was installed around selected fasteners of a splice joint. The specimens selected were (1) a C-141 aft fuselage skin panel with a flush riveted splice joint and (2) a double row titanium riveted lap joint splice. The C-141 skin panel was fabricated of 7079-T6 alclad .056 inches thick and flush riveted. Two sensors were installed around rivet heads as shown in the sketch below:

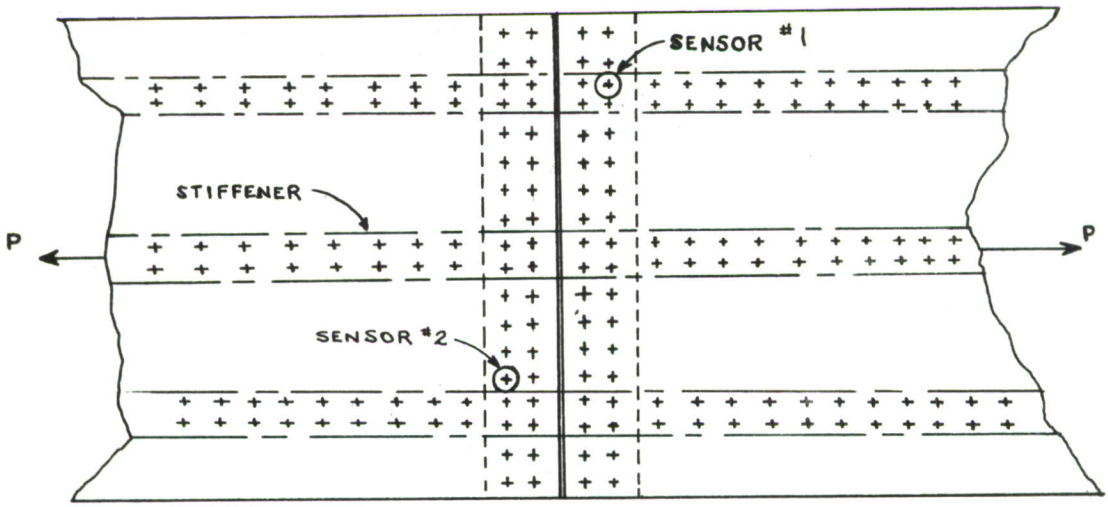

Constant amplitude cyclic loading about a tension mean load was then applied producing nominal peak strains of approximately 600 micro inches/inch. The panel was cycled at 5 cps. using servo loading equipment with sensor readings taken during panel inspection periods under no load conditions. A minor crack occurred in a stringer after 63,000 cycles; this was locally repaired and cycling continued with zero shift readings ($\mu\epsilon$) taken as shown in the chart on the following page.

SENSOR NO.	AFTER 26,320 ~	AFTER 36,340 ~	AFTER 63,000 ~	AFTER 98,880 ~
1	130	160	205	280
2	160	210	260	345

SENSOR NO.	AFTER 126,625 ~	AFTER 162,750 ~	AFTER 166,480 ~
1	350	365	400
2	395	405	430

After 166,480 cycles the cracks became so extensive that repairs resulted in considerable delays, consequently sensor readings were discontinued.

Substantiating evaluations of the original spiral grid versus the revised grid on coupons as shown in Figure 14 confirms an improvement in both threshold sensitivity and total output. The spiral grid sensors were installed as "mirror images" of each other around the unfilled hole. Although the number of specimens evaluated were insufficient to determine an exact percentage improvement, it can be concluded that the spiral grid concept for use in the proposed **areas** is a valid one. It should also be noted that the foil in this sensor is not fully annealed and that an even larger output could be expected if the sensor were composed of a softer foil.

4.3 PHASE III BREADBOARD MODEL

The breadboard model was designed to demonstrate feasibility of the fatigue damage concept. This equipment was submitted to the AF Flight Dynamics Laboratory for their evaluation. Basically the equipment consisted of an (1) instrumented constant moment beam, and (2) associated electronic equipment. The power equipment to fatigue cycle the beam is supplied by AFFDL and is the NAS 942 standard strain gage fatigue tester.

4.3.1 TEST SPECIMEN AND INSTRUMENTATION

Originally the NAS 942 constant strain beam and test machine were designed to evaluate strain gages and not to produce a specimen failure. It should be noted that the NAS 942 fatigue tester is a constant amplitude machine rather than constant load so that once a crack starts the load is relieved and the crack does not propagate as rapidly as it would under constant load. Consequently, specimen fatigue lives obtained by using this equipment will not correspond to published S-N curves. The beam used in this program was a modified NAS 942 standard, and a theoretical stress concentration (K_t) was designed into the beam to force a failure at a selected location. The beam was instrumented with fatigue sensors as shown in Figure 93, then cycled at ± 1500 micro strain until failure. Sensor readings are taken at convenient intervals under no load conditions. The stress concentrator representing a K_t of 1.9 as determined from Ref. 1, simulates a rivet filled hole. Since the specimen should now fail at the concentrator, the specimen root radius that was required by NAS 942 has been deleted to simplify fabrication. The mathematical considerations indicate that the 7075-T6 aluminum material should dissipate the 871 inch lbs./sec. of energy with no significant temperature rise in the specimen.

4.3.2 ELECTRONIC BREADBOARD

The breadboard model of the electronic equipment contains nine (9) channels of all the functional elements shown in Figure 94. This capacity is adequate to evaluate the quality of the seven sensors on the specimen as well as indicate their output in regard to the fatigue status of the specimen.

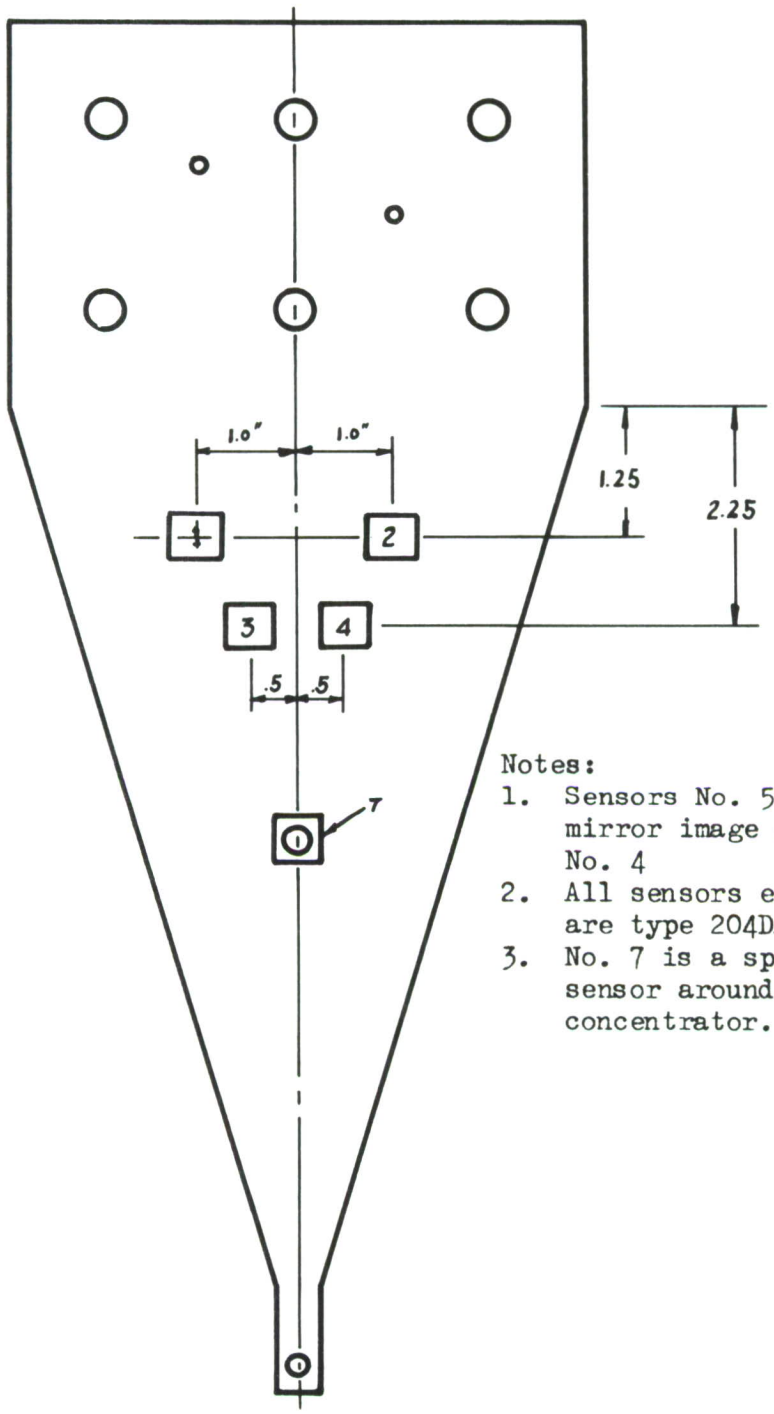

Notes:
1. Sensors No. 5 & No. 6 are mirror image of No. 3 & No. 4
2. All sensors except No. 7 are type 204DA-ST.
3. No. 7 is a spiral grid sensor around stress concentrator.

FIG. 93 INSTRUMENTATION OF CONSTANT STRAIN BEAM (NAS 942). THEORETICAL $K_t = 1.9$

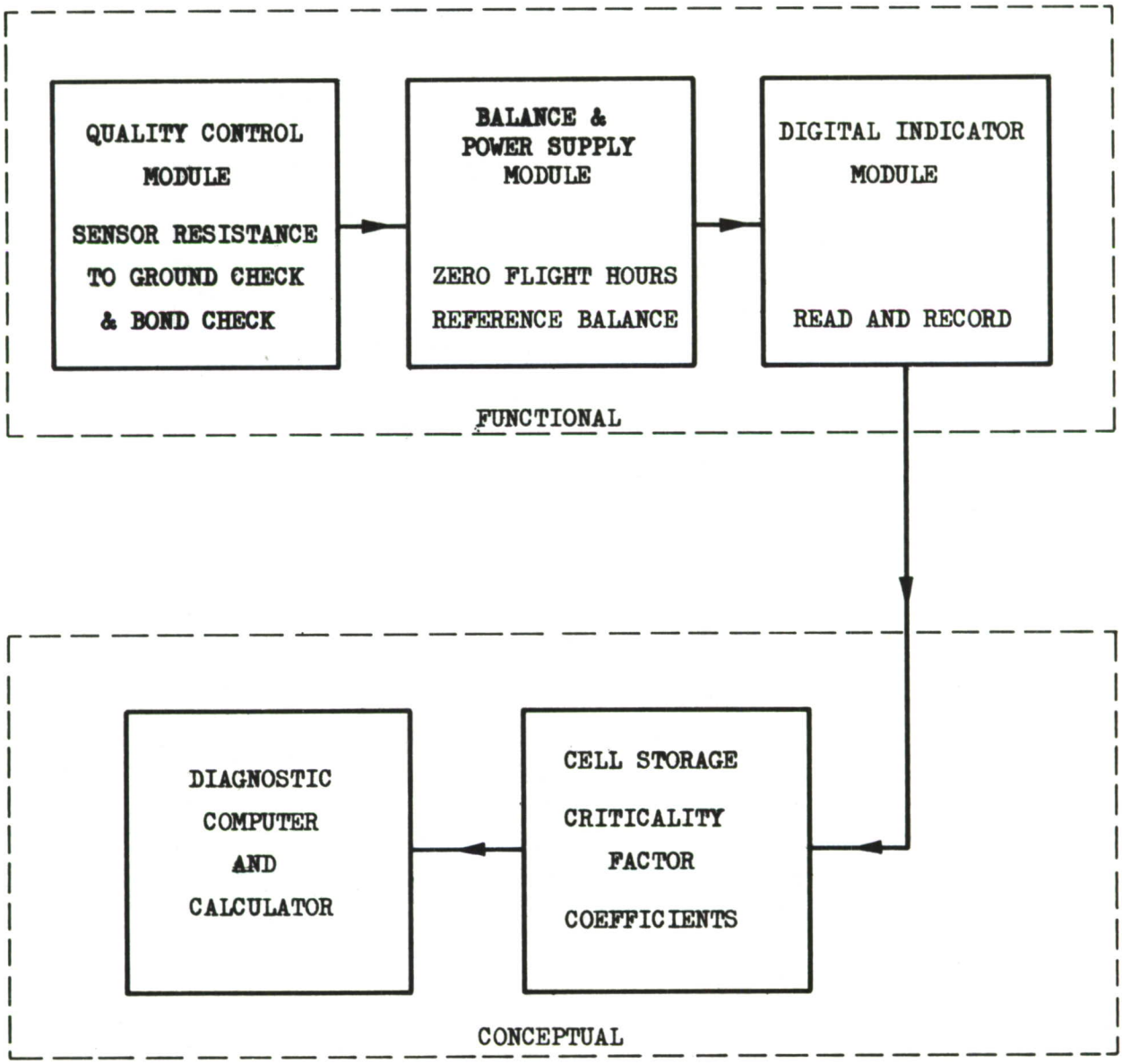

FIGURE 94 BLOCK DIAGRAM OF ELECTRONIC EQUIPMENT

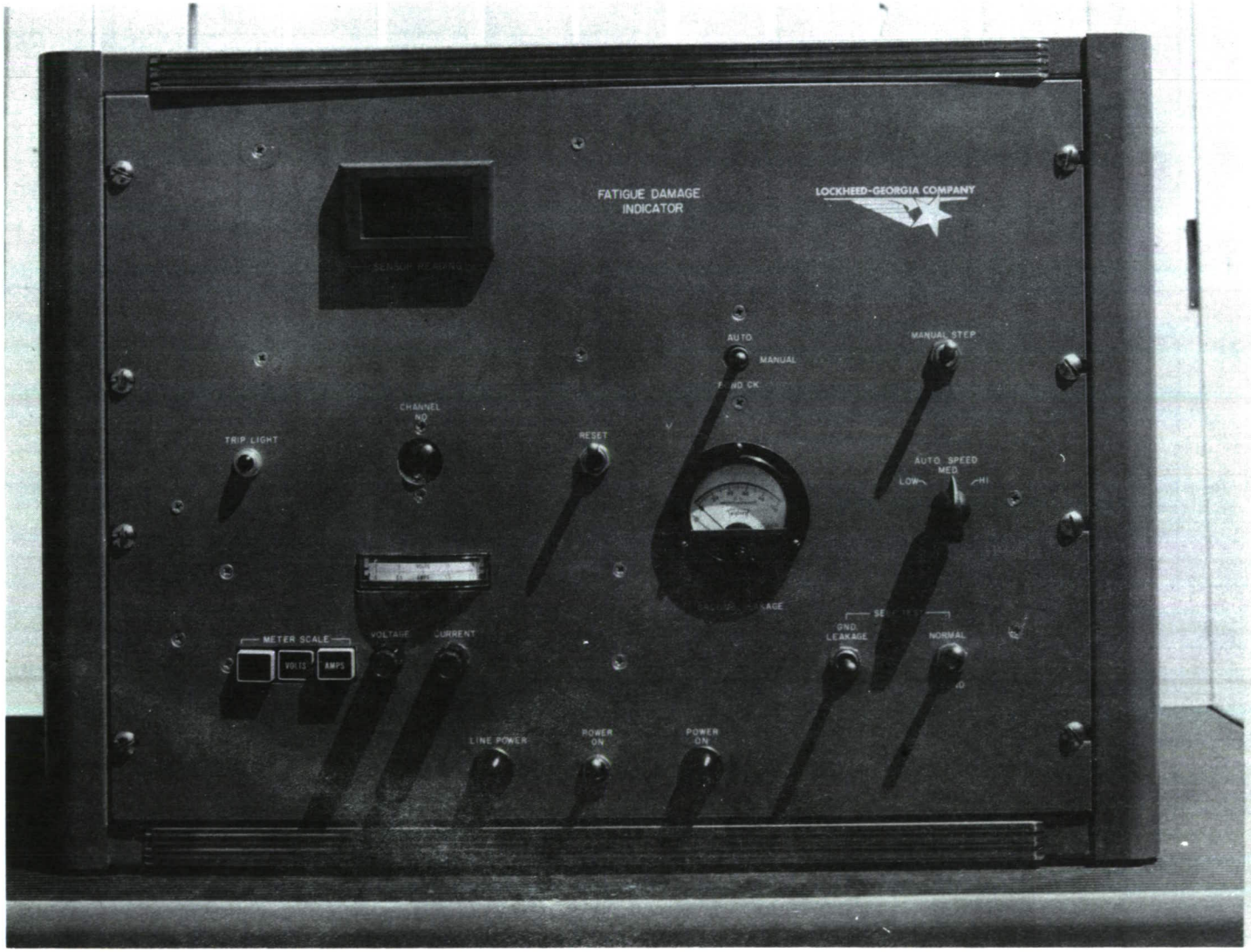

FIGURE 95 ELECTRONIC PHASE OF THE FATIGUE EVALUATION SYSTEM

4.3.3 MATHEMATICAL CONSIDERATIONS REGARDING THE MODIFIED NAS 942 BEAM

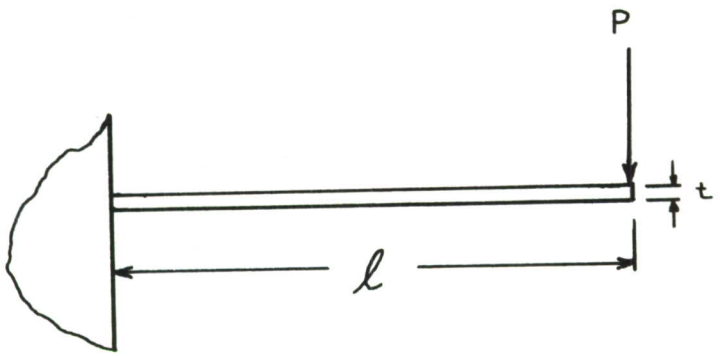

Test Conditions: (t) thickness = 0.125" (F) cyclic freq. = 30 cps.
(y) beam defl. zero to peak = 1.2" (ℓ) length = 10.0"
(ϵ) strain = ?

$$\epsilon = \frac{yt}{\ell^2}$$

$$\epsilon = \frac{(1.2")(0.125") \times 10^6}{(10)^2}$$

$$\epsilon = 1500 \text{ u in/in}$$

Hooke's Law says: $f = E \times \epsilon$

Where:

f = stress (psi)
E = modulus of material
ϵ = strain (u in/in)

$f = 10.4 \times 1500$
$f = 15{,}600$ psi

FORCE TO DEFLECT BEAM (1.2in)

$$P = f \frac{wt^2}{6\ell}$$

$$P = (15{,}600 \text{ psi}) \frac{(6")\ (.125)^2}{(6)\ (10")}$$

$P = 24.20$ lbs.

Where:

w = width of beam at root (in.)
P = force (lbs.)

WORK DONE ON THE BEAM

Pav. = 1/2 (Pmax - Po)
Pav. = 1/2 (24.20 - 0) = 12.10 lbs per half cycle

W = Pav. (y) (2)

W = (12.10 lbs X 1.2 in) 2

W = 29.04 in. lbs per cycle

Where:
W = work (in. lbs.)
Pav. = average force (lbs.)
y = defl. (in)

ENERGY DISSIPATED

Energy = (F) (W)

Energy = 30 X 29.04 = 871.20 in. lbs/sec.

Since 6600 in.lbs./sec. = 1 H.P. then,
H.P. required = $\frac{871.20}{6600}$ = 0.132 H.P.

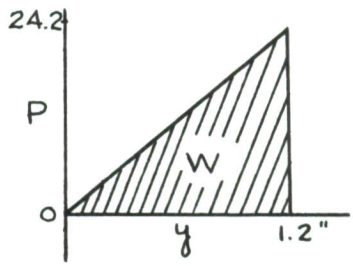

BEAM ACCELERATION

$G = 0.0511\ D\ F2$
$G = (.0511)\ (2.4")\ (30)^2$

Where:
G = number of gravities of acceleration
D = peak to peak defl. (in)
F = freq. (cps)

G = 110.5 g's at beam tip

SECTION V

SUMMARY AND CONCLUSIONS

5.1 SENSOR OPTIMIZATION

The one factor which became the most dominant during this feasibility study was that the sensor constitutes the heart of the system and that no amount of expensive instrumentation connected to its terminals can compensate for an inferior or inadequate detecting element. For this reason, a major effort has been directed toward the development of installation techniques as well as a manufacturer's inspection system to maintain quality control. Considerable study and research has also gone into the problem of selecting the most optimum material, method of fabrication and configuration of the fatigue sensor. The resulting grid pattern and particular type of construction was selected with the following main objectives in mind.

1. For long term installation (10-15 years) precision die cut foil sensors as opposed to acid etched foil were selected to avoid the possibility of installing sensors still containing an acid residue. An occasional lack of neutralization after post etching sometimes results in reactivation of the acid which presents itself as a slow change in resistance. Metallurgical studies also indicated that the acid etch process caused stress concentrators in the strand edges resulting in a decreased fatigue life.

2. The resulting grid configuration of the selected 204DA-ST type uses a thick foil which is less crack sensitive; the large side tabs distribute lead wire imposed stresses, and the open face grid permits a pre-use inspection.

3. All of the commercially available post yield or high elongation strain gages will exhibit the same fatigue induced behavior characteristics, however, they have not been optimized for a high fatigue life.

A general review of curves from the coupons tested illustrates several significant characteristics regarding the sensors behavior and capabilities.

1. Sensors of the same type which were bonded on opposite sides of a coupon as "mirror images" of each other produced duplicate curves of resistance versus cumulative strain cycles. This characteristic is indicative of the repeatability of the foil and the consistancy of manufacturing techniques.

2. Sensors may be located some distance away from where specimen failure will occur, and still register a resistance change proportional to the strain cycles required to produce a failure.

This leads to the conclusion that cumulative strain allowables for a structure may be determined although the sensor is remotely located from where failure will occur. This effect is illustrated in the diagram shown below:

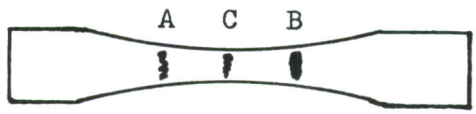

The maximum strain amplitude in the typical coupon shown above is less in areas A and B than C however, the accumulated strain amplitude at A or B required to produce a failure at C is very closely related from coupon to coupon.

In the introduction it was stated in a general way that the fatigue sensor should have (1) High output (2) Low threshold sensitivity and (3) High fatigue life. The laboratory evaluations of a variety of foils and configurations indicated that these three desirable characteristics are controlled by the following.

1. High output - Normal output can be increased by increasing the number of stress concentrators, and sacrificing fatigue life.

2. Low threshold sensitivity - Controlled by the manufacturer, since this is governed by the degree of foil anneal.

3. High fatigue life - Determined by grid configuration, construction and severity of stress concentrations.

When all behavior characteristics are evaluated objectively and considered for application to subsonic transport aircraft, the type 204DA-ST fatigue sensor appears as the most valid selection. It should be reiterated that some of the aerodynamic and environmental variables induced during coupon tests were extreme or exaggerated cases to emphasize that these variables must be considered when evaluating the end resistance of the sensor. The simulated aerodynamic mission profile of aircraft subjected to laboratory structural integrity tests contains an average of all variables, which should result in a small band width of sensor end resistance upon structural failure.

VARIABLES WHICH PRODUCE ZERO SHIFT IN THE SENSOR	VARIABLES WHICH INFLUENCE THE FATIGUE LIFE OF A STRUCTURE (BESIDES AMPLITUDE & NUMBER OF STRAIN CYCLES.)
(1) Amplitude and number of strain cycles. It should be noted that the sensor makes no distinction regarding direction of strain (tension or compression) or whether strains are bending or axial.	(1) Stress ratio (2) Temperature environment (3) Order of strain cycles (4) Corrosion (5) Initial pre-stress (6) Stress concentrations

The significance here is that the metallurgical condition of a structure can be varied by means other than by repeated loads. The sensors "zero shift" resistance is a measure of the mechanically induced fatigue damage within the sensor, but its validity as a fatigue damage indicator depends on the users ability to relate fatigue damage in the sensor to fatigue damage in the structure. If the sensor develops micro-cracks (super-sensitivity) then the user has forever lost this relationship.

The preponderance of evidence from coupon testing indicates that any variable which reduces the normal fatigue life of a coupon, also reduces the end resistance of the sensor by a proportional amount. In other words, the fatigue sensor resistance at specimen failure is not a constant, so therefore a calibration of the structure, imposing statistical loading averages of the flight should be utilized.

It is inadvisable to attempt any correlation of coupon data with fatigue damage of a flight aircraft structure. Although the fatigue sensor looks like a strain gage, it does not possess the versatility of a strain gage primarily because it lacks the convenient calibration of a strain gage i.e. Gage Factor.

As a result of the sensor evaluation on coupons as well as typical aircraft structure, the following guidelines have been formulated for application of the sensor to aircraft structure as an aid to assessing its fatigue status.

1. The structures history of accumulated aerodynamic loadings can best be determined by locating each sensing point in higher strain areas free from stress concentrations.

2. The number and location of the sensing check points on the structure should be sufficient to reliably evaluate the aircrafts degree of exposure to repeated load occurrences. Therefore, all critical fatigue sources should be instrumented.

3. Sensors should be applied to the aircraft structure prior to accumulating any flight time. A vehicle which had expended some unknown portion of its fatigue life would not be a suitable candidate for the fatigue evaluation system.

4. To minimize effect of temperature variation, periodic data should be recorded under controlled ambient conditions or else a temperature correction factor should be applied.

5. At the present time the sensors have been successfully evaluated for sub-sonic aircraft over a temperature range of -65°F to + 150°F. Sensors should be used within these temperature limits until further data, regarding temperature extremes, becomes available.

5.2 THE ELECTRONIC EQUIPMENT

The electronic equipment constitutes the final element which makes possible a "quick look" electro-structural inspection system. The ground based roll-a-round console would be composed of modules shown in the block diagram of Figure 94. The system is designed to be air transportable but not qualified for airborne usage. Since the fatigue sensors themselves are storage devices and have a memory capacity, it is not necessary to have the console continuously connected to the sensor. Periodic readings of the sensors installed on an aircraft structure would indicate the structures degree of exposure to repeated loads. One console could service say 15 or more aircraft at a base, by using a zero flight hours reference program representing each aircrafts' structural fatigue condition prior to any flight time.

The bread board model contains all the functional elements shown in the block diagram of Figure 94 which is sufficient to demonstrate feasibility of the concept. A full scale system for practical field usage should also contain the blocks shown in the conceptual diagram.

5.3 STEPS TO OBTAIN UTILIZATION ON FLEET AIRCRAFT

The recommended steps to obtain utilization of a complete system, integrated into fleet aircraft is shown in Figure 96. The instrumentation of the wing or empennage laboratory fatigue specimen represents a natural progression to a more complex structure. Although evaluation of the fatigue sensors on test coupons has provided a means for determining the fatigue status of a similar coupon, this information cannot be readily transferred to a complex structure such as an airframe. In order to ascertain the fatigue life of a specific airframe, the sensors must be calibrated on typical structure. At this point, the system objective makes no attempt to indicate where fatigue failure will occur, but rather documents the totalized strain excursions incurred at predetermined locations when specimen failure does occur.

A calibration must be performed on the laboratory test article if one wants to correlate and determine the allowable level of fatigue damage to airframes on production aircraft. Fatigue sensors can be located in identical critical areas of production aircraft such that each production installation is a duplicate of the laboratory installation. Generally the areas that proved critical during laboratory fatigue testing of structural components would be instrumented on the structural integrity airplane. These locations represent areas of higher stress levels as predicted by theoretical stress analysis. The selected locations may also represent areas where aerodynamic or weight limitations have imposed a limited life design.

Once sufficient measuring points have been established to provide adequate airframe coverage, the specimen calibration would then consist of sensor readings versus simulated flight hours. This procedure will provide a common demoninator for comparing load histories of the lab article with the flight article. These values are recorded at selected intervals throughout the program and specifically when a structural failure occurs. The accumulated total of sensor readings are indicative of the total work done on the airframe and the individual sensor outputs will show the manner in which repeated loadings have distributed itself throughout the structure. The data obtained from the laboratory specimen will establish a tolerance or limit of accumulated strain allowables for this area of the aircraft. Therefore the cumulative readings of the sensor resistance change on service aircraft can be expressed in % of fatigue life since it will be referenced to the laboratory fatigue article. The calibrated output from the sensors will establish the allowable fatigue damage limits on all service aircraft of this type which are instrumented in an IDENTICAL manner.

5.4 SIMPLIFICATION OF FATIGUE DAMAGE ANALYSIS

Stress analysts converse in a language all their own and quite often the techniques of fatigue detection and analysis remain a secret to everyone except this elite group of scientists and engineers. If shopmen, inspectors, and field service personnel do not know the signs of fatigue and where to look for them, then the using industry is not receiving full value for the time and money devoted to research.

Our basic problem then becomes one of simplifying fatigue analysis and communicating in a language understood by all. If some common unit of measurement can be obtained which is definitive and can be understood equally well by the shopman, designer or stress analyst then considerable progress could be expected. The fatigue sensor system that was investigated in this program could simplify the work of an inspector or maintenance man by pinpointing suspect areas of the aircraft structure. Then the aircrafts limited time for inspection periods could be better utilized by a visual inspection of only the most critical areas. To reduce a structural inspection to its simplest terms the examiner may view the structure with regard to:

1. How tired is it? (mechanically induced)
2. How rotten is it? (metallurgical condition)

At the present time the fatigue sensor, with its companion electronic equipment will provide a qualitative index relative to the structures degree of tiredness. The effects of corrosion, fungus growth, chance effects, or other variables which influence the metallurgical condition of materials would be considered only to the extent that they affect the mechanical response of the structure.

A fatigue damage information system used on cargo aircraft operating in a fleet would be most suitable since it would provide comparison data regarding each aircrafts' fatigue status. For "long life" cargo aircraft the combined influence of many factors may reduce actual service fatigue life below the most conservative engineering and laboratory estimates. Some of the factors which may become apparent during fleet operation are:

1. Service loading variations, changing operational requirements,

2. Environmental conditions, fungi growth, corrosion,

3. Chance effects; such as installation stresses, misalignments, tool marks, and scratches not duplicated in laboratory test specimens,

4. Joint friction, non linear slippage characteristics, material alloy, heat treat, batch variations, and many others.

While this investigation has indicated the sensor considers only the major contributor to fatigue damage (cyclic stresses), it is very probable that fleet usage would reveal that a combination of sensors could reflect a change in mechanical response due to chance effects. It is anticipated that fleet usage will provide benefits which are not apparent now, and which could not be proven during laboratory tests on a modest number of specimens. Fatigue patterns and repetitive trends will be established among fleet aircraft which should quickly pinpoint any problem areas with a high degree of confidence.

FIGURE 96
PROGRESSIVE SEQUENCE OF ACTIVITIES
TO OBTAIN UTILIZATION ON SERVICE
AIRCRAFT

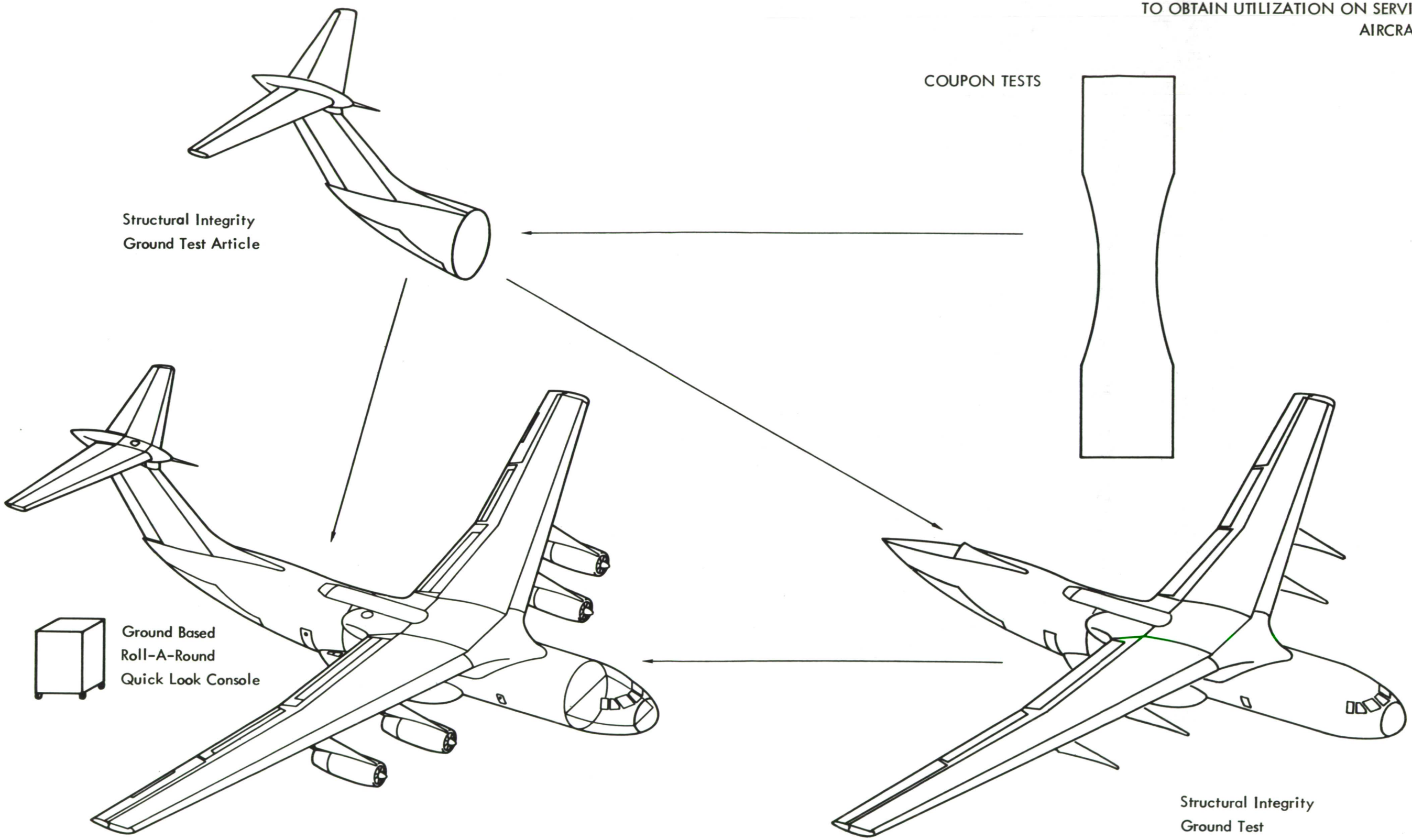

SECTION VI

REFERENCES

1. Petersen, R. E , Stress Concentration Design Factors, Wiley 1953.

2. Feltman, P., Brunel College of Advanced Technology, London W. 3, "The Electrical Resistivity of Metals Due to Plastic Deformation," Metallurgia, August 1964.

3. Chunn, F. L., C-141A Fatigue Airplane Test Procedure, Aft Fuselage Empennage (Specimen C), ER-4946, Volume III, May 1964.

4. Brown, S. K., C-130E Wing Fatigue Component Tests, Volume I, ER-7853, May 1965.

5. Wnuk, S. P., Jr., Baldwin-Lima-Hamilton Corporation, Performance Characteristics of Bonded Strain Gages Under Repeated Cyclic Strain, Paper presented at SESA, October 1964.

6. Harting, D. R., The Boeing Company, The S/N Gage: A Direct Means of Measuring Cumulative Fatigue Damage, Paper presented at SESA, October 1965.

7. Drew, D. A., "Supersensitivity of Foil Gages," Strain Gage Readings, Volume IV, No. III, August-September 1961.

8. Strength of Metal Aircraft Elements, MIL-HDBK-5, Armed Forces Supply Support Center, FSC 1500.

9. Bennett, John A., "New Data on Aluminum Fatigue," NBS Technical News Bulletin, January 1965.

10. Alcoa Aluminum Handbook, Aluminum Company of America, Pittsburgh, Pennsylvania.

11. Christof Rohrbach and Norbert Czaika, Studies on the Fatigue Behavior of Strain Gages, Materialprufung, 20 April 1961.

12. Brady, J. W. Investigation of Strain Gages for High Temperature Sonic Fatigue Environments, Lockheed Georgia Company ER-8292 March 1966.

13. Bendat, Julius S. Measurement Analysis Corporation, Probability Functions for Random Responses: Prediction of Peaks, Fatigue Damage, and Catastrophic Failures, NASA CR-33 April 1964.

14. Crichlow, W. J. et al., Lockheed California Co. An Engineering Evaluation of Methods for the Prediction of Fatigue Life in Airframe Structures, ASD-TR-61-434, AFSC, WPAFB, Ohio March 1962 (ASTIA AD 276249)

15. Shanley, FR., Fatigue Analysis of Aircraft Structures, RAND Corp. Paper No. RM1127, 31 July 1953; AD 210794

16. Langer, B.F., Fatigue Failure from Stress Cycles of Varying Amplitude, J. Appl. Mech., Vol. 4, pp. A-160 - A-162, December 1937

17. Marco, S.M. and Starkey, W.L., A Concept of Fatigue Damage. ASME Trans., Vol. 76, No. 4, pp 627-632, May 1954

APPENDIX I

INSTALLATION OF FATIGUE SENSORS

A. General

This procedure covers the installation, wiring, and checkout to be followed by the technicians in the fatigue sensor instrumentation of aircraft structure or laboratory test specimens.

B. Preliminary Preparation

Obtain adhesives, solvents, sensors and other materials necessary for the installation. Use only those materials which are not out of date. Sensors should be microscopically checked prior to use, but handling must be kept to a minimum.

C. Surface Preparation

1. Locate the area to be cleaned according to sketches or prints and define using a soft lead pencil; do not use ball point pens or scribe. Use magic markers or china marking pencil to define sensor location, in a manner suitable for photographing.

2. All foreign material such as dirt, paint, oxide, or scale must be removed by emery cloth (180 grit or finer) and the area washed by MEK or acetone. Perform further cleaning using cotton swabs with acetone until no discolorations can be detected on the swabs or cleaning tissue. If area must be touched, it should be recleaned with acetone. The area must be chemically clean, and the use of chemically pure solvents free from moisture is important to the cleaning operation. The area cleaned must be 3 - 4 times larger than the sensor.

D. Sensor Preparation

Use a strip of mylar silicone tape (or scotch tape) about 1" longer than the sensor to be mounted and at least 1/8" wider than the sensor. With tweezers place the sensor on the center of the tape, foil down. Place a terminal strip, metal down on the tape about 1/16" from the sensor. Wipe the back of the sensor and terminal strip with a Q-tip dampened with MEK or acetone. Do not allow sensor and tape to curl. Avoid stretching the tape during sensor handling, since the thin foil will stretch too, causing an out of tolerance resistance increase.

E. Epoxy Cement Preparation

Prepare the selected cement according to the instructions in the cement kit and apply it to the mounting surface, covering an area no larger than the area of the gage and terminal strip. The epoxy should be

buttered onto the surface about .001" thick. The date stamped on the package is the packaging date. Discoloration of adhesive indicates deterioration.

F. Sensor Mounting

The tape with the sensor and terminal strip adhering to it is now accurately positioned on the mounting area and the tape pressed down to hold the sensor in position. Excess adhesive should be removed from fluing area by moderate pressure with a finger on the tape over the center of the gage. Excessive pressure and rubbing will induce cold working in the foil resulting in an out of tolerance sensor. Now cover the tape above the gage and terminal strip, first with a small piece of thin teflon followed by a 1/16" thick piece of silicone gum rubber or neoprene. Hold it in place with a small strip of mylar tape. On top of this sandwich, place a metal pad of approximately the shape of the surface contour on which the gage is mounted. Apply a pressure to this plate with a squeeze clamp, negator spring, or other weight equal to 5 to 10 pounds per square inch. C-clamps are not permitted since their use tends to twist the sensor. Proceed now with the recommended curing cycle for the epoxy. After curing, if the installation is correct, the tape will peel off cleanly leaving the sensor bonded to the surface. Check the sensor with an ohmeter at this stage to see if the sensor grid has been opened or otherwise damaged,

G. Lead Attachment

The sensor anchor tabs may be cleaned by rubbing with a Q-tip which has been dipped into powdered aluminum oxide or fine powdered pumice of not more than 5 micron particle size. A red rubber pencil eraser or fibreglass brush may also be used to remove oxides. Avoid using tabs which are "necked down" the BLH type TL-18 or TL-25 is preferred. Cover grid with masking tape before soldering. After this has been done, the tabs must be tinned. This is done by first putting a small spot of Kester No. 44 flux on the tabs with a toothpick. A quick touch of a pencil type soldering iron using 1/8" tip and Kester No. 44 solder will tin a small spot on the tab. Preferably use a .020" diameter or .015" diameter wire solder. Avoid overheating the solder tabs. Jumper wire ends should be tinned and placed on the tab. Without additional solder, the wire should be touched with the iron to make the joint. The cables should be mechanically anchored to the test member about 3/4" to 1/2" away from the terminal strip to avoid undue strain on the terminals. The leads soldered to the tabs should be No. 34 soldereze wire. The enamel insulation is removed from the ends of the soldereze wire by dipping into the stripper 1/4" only. The stripped end of the round wire should now be flattened to obtain a better solder joint. For most installations, terminal strips cemented to the surface close to the gage tabs should be used to prevent lead tension from being transferred to the gage tabs. There should always be a little slack in the jumper or lead between the gage tab and the anchor point. Wash solder joints with a neutralizer to prevent corrosive action from fluxes.

Plastic identification sleeves are to be tied to both ends of the extension cable. The installation is now ready to be photographed and moistureproofed.

H. Checkout of Installation

The resistance of the sensor will be measured by a wheatstone bridge at the cable termination end and recorded in the installation record sheet. A strain indicator balance check is then made at the termination end of the extension cable, which must be within ± 5000 micro-inches per inch of mid scale of the indicator. Cold solder joints or a stretched sensor can throw an installation out of the acceptable range. Initial bond checks will be made by connecting an SR-4 indicator to the sensor terminals and applying enough pressure to the structure to obtain a deflection. A drift or non-return to zero condition will be considered as a poor bond. Before moistureproofing or waterproofing, the sensor resistance to ground will be checked with a five volt output megohmmeter. A resistance to ground reading of at least 1K megohms at the cable termination end is required. The leakage resistance of the sensor may be improved by the use of heat lamps, taking care not to exceed a surface temperature of 200°F. If these preliminary checks indicate a good installation, the sensor is ready for sealing.

APPENDIX II

TABLE I - TABULATION OF COUPON TESTS

7075-T6 BARE ALUMINUM (0.10" THICK) SEE FIGURE 1

COUPON NUMBER	NUMBER OF SENSORS	TYPE OF SENSOR	f MAX.	STRESS RATIO A	SPECIMEN LIFE CYCLES	MAX. STRAIN @ #1 POSITION #2 POSITION	TESTED IN MACH. NO.	REMARKS
1	4	204A-ST MH204A-ST	35KSI	+0.818	807,000	3000 u in/in 2700	11	Not Evaluated.
2	3	204A-ST MH204A-ST	45KSI	+0.818	21,000*	3950 3600	12	*Premature Failure Probably Caused by Misalignment in Test Equipment.
3	3	MH204A-ST 204A-ST	40KSI	+0.818	158,000	- - -	11	
4	4	204A-ST 204DA-ST	VAR.	+0.818	335,000	Variable	11	Threshold Sensitivity Check.
5	4	204A-ST 204DA-ST	40KSI	+0.818	46,000	3500 3150	11	
6	2	204A-ST	40KSI	+0.818	88,000	3500 3150	11	
7	2	204A-ST	40KSI	+0.818	69,000	3500 3150	11	
8	2	204A-ST	35KSI	+0.818	344,000	3000 2700	11	
9	2	204A-ST	35KSI	+0.818	3,335,000**	3000 2700	11	**Test Discontinued. Specimen Did Not Fail. Data Not Eval.
10	2	204A-ST	37.5KSI	+0.818	244,000	3250 2900	12	

COUPON NUMBER	NUMBER OF SENSORS	TYPE OF SENSOR	f MAX.	STRESS RATIO A	SPECIMEN LIFE CYCLES	MAX. STRAIN @ #1 POSITION #2 POSITION	TESTED IN MACH. NO.	REMARKS
11	2	204A-ST	37.5KSI	+0.818	881,000	3250 u in/in 2900	11	
12	4	204A-ST 204DA-ST	60KSI	+0.333	149,000	5300 4800	12	
13	4	204A-ST 204DA-ST	60KSI	+0.333	127,000	5300 4800	11	
14	4	204A-ST 204DA-ST	60KSI	+0.333	100,000	5300 4800	11	
15	4	204A-ST MH304AE	50KSI	+0.333	675,000	4400 4000	12	Test to Evaluate Threshold & Stability of Karma Sensors.
16	4	204A-ST MH304AE	50KSI	+0.333	1,082,000	4400 4000	11	Evaluate Output of Karma.
17	4	204A-ST MH204A-ST	50KSI	+0.333	2,473,000	4400 4000	12	Did Not Fail-Not Evaluated.
18	2	204A-ST	45KSI	+0.818	268,000	3950 3600	11	
19		U S E D I N M A C H I N E R E - C A L I B R A T I O N						
20	2	204A-ST	70KSI	+0.818	16,900	6250 5700	Slow Cycle	
21	2	204A-ST	45KSI	+0.818	145,000	3950 3600	4	
22	2	204A-ST	70KSI	+0.818	13,700	6250 5700	Slow Cycle	

COUPON NUMBER	NUMBER OF SENSORS	TYPE OF SENSOR	f MAX.	STRESS RATIO A	SPECIMEN LIFE CYCLES	MAX. STRAIN @ #1 POSITION #2 POSITION	TESTED IN MACH. NO.	REMARKS
23	2	204A-ST	±25KSI	∞	418,000	±2200 ±2000	5	
24	2	204A-ST	78KSI	+0.333	39,695	7000 6350	Slow Cycle	
25	2	204A-ST	70KSI	+0.333	35,960	6250 5700	Slow Cycle	Not Evaluated.
26	4	204A-ST S/N NA-01	40KSI	+0.818	195,000	3500 3150	11	
27	4	204A-ST 204A-ST-K	40KSI	+0.818	443,000	3500 3150	4	
28	4	204A-ST 204A-ST-K	85KSI	+0.333	15,702	7550 6850	Slow Cycle	Plastic Region of Aluminum.
29	4	204A-ST 204A-ST-K S/N NA-01	40KSI	+0.818	110,000	3500 3150	11	
30	2	204A-ST	±25KSI	∝	1,200,000	±2100 ±1900	5	
31	2	204A-ST	70KSI	+0.333	52,670	6250 5700	Slow Cycle	
32	2	204A-ST	75KSI	+0.333	49,970	6700 6100	Slow Cycle	
33	2	204A-ST	71.8KSI	+0.333	50,090	6400 5750	Slow Cycle	

COUPON NUMBER	NUMBER OF SENSORS	TYPE OF SENSOR	f MAX.	STRESS RATIO A	SPECIMEN LIFE CYCLES	MAX. STRAIN @ #1 POSITION #2 POSITION	TESTED IN MACH. NO.	REMARKS
34	4	204A-ST 204A-ST-K S/N NA-01	VAR.	+0.818	- - -	- - -	4	Threshold Sensitivity Check.
35	4	204A-ST HA204A-ST	50KSI	+0.333	950,000*	4450 4000	4	*Not Taken to Failure.
36	2	204DA-ST	±50KSI	∝	12,499	±4450 ±4000	Slow Cycle	Frequency Varied From 1 Cps to 5 Cps.
37	2	204A-ST	45KSI	+0.818	25,000	3950 3600	4	Weatherometry Not Eval.
38	4	204A-ST 204DA-ST EP-03	60KSI	+0.818	37,000	5300 4800	11	
39	2	204DA-ST	±60KSI	∞	4,407	±5300 ±4800	Slow Cycle	
40	4	204DA-ST MH204DA-ST	45KSI	+0.818	42,000	3950 3600	11	Weatherometry.
41	4	204DA-ST MH204DA-ST	45KSI	+0.818	347,000	3950 3600	4	
42	4	204DA-ST MH204DA-ST	±50KSI	∞	12,246	±4400 ±4000	Slow Cycle	
43	4	204DA-ST MH204DA-ST	±40KSI	∞	59,218	±3500 ±3150	Slow Cycle	
44	4	204DA-ST 204A-ST NA-01	60KSI	+0.818	36,000	5300 4800	11	

COUPON NUMBER	NUMBER OF SENSORS	TYPE OF SENSOR	f MAX.	STRESS RATIO A	SPECIMEN LIFE CYCLES	MAX. STRAIN @ #1 POSITION #2 POSITION	TESTED IN MACH. NO.	REMARKS
45	3	204A-ST EP-03	60KSI	+0.818	80,000	4400 4000	11	-65°F.
46	4	204A-ST 204DA-ST MH204DA-ST	45KSI	+0.818	260,000	3950 3600	11	Low Temperature.
47	3	S/N NA-01 EP-03	37.5KSI	+0.818	319,000	3250 2900	4	
48	4	204A-ST 204DA-ST	70KSI 51.3KSI	+0.818 +0.333	92,000	- - -	11	Two Load Level.
49	4	204A-ST 204DA-ST	51.3KSI 70KSI	+0.333 +0.818	131,000	- - -	4	Two Load Level.
50	4	204A-ST 204DA-ST	70KSI 51.3KSI	+0.818 +0.333	153,000	- - -	4	
51	2	204DA-ST	±18KSI	∞	- - -	±1550 ±1450	4	Not Taken to Failure.
52	2	204DA-ST	60KSI	+0.818	179,000	5300 4800	4	Low Temperature -65°F.
101	4	204A-ST	40KSI	0.818	42,000	----	11	12 Months Actual Weather Test.

7075-T6 Bare Aluminum (Kt = 2.72) See Figure 3

Coupon Number	Number of Sensors	Type of Sensor	f(max)	Stress Ratio A	Specimen Life Cycles	Tested in Machine Number	Remarks
1A	NOT	INSTRUMENTED	-	MACHINE	CALIBRATION	4	
2A	4	204A-ST 204DA-ST	± 10KSI	∞	544,000	2	
3A	2	204A-ST	25KSI	0.818	112,000	4	
4A	2	204A-ST	25KSI	0.818	32,000	2	
5A	2	204A-ST	20KSI	0.818	2,219,000	4	
6A	5	204A-ST Spiral Grid	22.5KSI	0.818	171,000	11	
7A	4	204A-ST	25KSI	0.818	29,000	12	
8A	5	204A-ST Spiral Grid					Not Tested
9A	5	204A-ST Spiral Grid	20KSI	0.818	No Failure @ 1,273,000	4	Test Discontinued
10A	4	204A-ST Spiral Grid	25KSI	0.818	50,000	11	
11A	4	208YA 204A-ST	25KSI	0.818	44,000	11	
12A	2	FASB-065-12 Spiral Grid	20KSI	0.818	No Failure @ 60,000	4	Test Discontinued

Titanium 8% Al - 1% Mo - 1% V .060 Thick See Figure 1

Coupon Number	Number of Sensors	Type of Sensor	f(max)	Stress Ratio A	Specimen Life Cycles	Tested in Machine Number	Remarks
T-1	2	HA204DA-ST	90KSI	0.818	Discontinued @ 25,000	11	Specimen Accidentally Buckled - Room Temp.
T-2	4	HA204DA-ST MH304AE	90KSI	0.818	Discontinued @ 40,000	4	Room Temperature
T-3	4	MH304AE MH204A-ST MH204DA-ST	90KSI	0.818	1,900,000	11	Random and Erratic @ 400°F
T-4	2	MH204DA-ST	100KSI	0.818			Accidently Overheated
T-5	2	MH204DA-ST	100KSI	0.818	88,000	4	Random and Erratic @ 400°F
T-6	2	MH204DA-ST	100KSI	0.818	90,000	11	

Inconel X, K_t = 1.00 - Aluminum, K_t = 1.9 See Figure 4

Coupon Number	Number of Sensors	Type of Sensor	Stress Ratio A	Specimen Life Cycles	ϵ max	Tested in Machine Number	Remarks
1C	2	204A-ST 204DA-ST	∞	Not Taken to Failure	± 1150 u in	SF-2	Inconel X, test discontinued at 840,000 cycles
2C	1	204DA-ST	∞	Test Discontinued @ 860,000	± 1400 u in	SF-2	Inconel X

(CONTINUED)

Coupon Number	Number of Sensors	Type of Sensor	Stress Ratio A	Specimen Life Cycles	ϵ max	Tested in Machine Number	Remarks
3C	- - -	Not Instrumented	∞	323,000	± 2000 u in.	SF-2	K_t = 1.9
4C	2	204DA-ST	∞	363,000	± 2000 u in	SF-2	K_t = 1.9

TABLE II SUMMARY OF FATIGUE SENSOR MATERIALS EVALUATED

The following represents a summary of fatigue sensitive foils evaluated for Phase I of AF Contract 33(615)-2505. Basically the standard 204A-ST was used on all coupon tests, however, the size and configuration of the coupon permitted the concurrent evaluation of additional sensors with a variety of backing and foils. Generally, the standard 204A-ST occupied the number 1 and number 2 positions, with any compared experimental sensors as a mirror image in the number 3 and number 4 position. The table shows the variety of backings and grid configuration which were tested in order to optimize the fatigue sensor and prevent overlooking any desired behavior patterns.

Manu. Desig. of Sensor	Tested on Coupon No.	Grid Foil Mat.	Grid Conf.	Grid Backing & Const.	(Approx) Threshold Sensit.	Remarks
Dentronic 204A-ST	3,5,6,7,8, etc.	.000188" ±2% Advance	1/4" Axial With Side Tabs	Cellulose Fiber, Epoxy Resin, Open Face	1200 ue	One Pass Fully Annealed
Dentronic 204DA-ST	5,40,41,46, 48,49,50	.000188 Advance	1/4" Axial With Side Tabs	Cellulose Fiber, Epoxy Resin, Open Face	1000 ue	Fully Annealed
Dentronic 204A-ST-K	29,28	.000188 Advance	1/4" Axial With Side Tabs	Cellulose Fiber, Epoxy Resin, Open Face	1200 ue	Same Anneal as 204A-ST Except a Slow Cool Down
Dentronic MH 204A-ST	1,T-3	.000188 Advance	1/4" Axial With Side Tabs	Glass Fiber, Epoxy Resin	1200 ue	Designed for Elevated Temperature Service
Dentronic MH 204DA-ST	40,41,T-3, T-4	.000188 Advance	1/4" Axial With Side Tabs	Glass Fiber, Epoxy Resin	1000 ue	Designed for Elevated Temperature Service
Dentronic HA 204DA-ST	T-1,T-2	.000188 Advance	1/4" Axial With Side Tabs	Asbestos	1100 ue	Designed for Elevated Temperature Service

Manu. Desig. of Sensor	Tested on Coupon No.	Grid Foil Mat.	Grid Conf.	Grid Backing & Const.	(Approx) Threshold Sensit.	Remarks
Dentronic MH 304AE	15,16,T-2, T-3	Modified Karma	1/4" Axial With End Tabs	Encapsulated	2200 ue	Designed for Elevated Temperature Service
Dentronic 208YA	11A	.00033 Advance	1/2" Axial With End Tabs	Mylar Backing	1200 ue	Requires a Polyester Adhesive
Dentronic 204A-ST Alum. Backed Residual	7A,11A	.000188 Advance	1/4" Axial With Side Tabs	.005 Alum. Shim Backing	Inconsistent	Philosophy Was to Shift the Threshold Sensitivity by Pre-Loading the Sensor Grid
MicroMeasurements S/N NA-01	26,29,32, 44,45	Advance Thickness Unknown	1/4" Axial With End Tabs	Encapsulated	1300 ue	
MicroMeasurements EP-03-250BG-120	45,38	Advance	1/4" Axial With End Tabs	Open Face Grid	1300 ue	Commercially Available Post Yield Strain Gage
BLH FASB-130-35-F	10A,1B,2B	Advance	1" Diameter Spiral With Center Hole	Bakelite Encapsulated	Not Applicable	Not fully annealed
BLH FASB-065 12-F	12A	Advance	1/2" Diameter Spiral With Center Hole	Bakelite Encapsulated	Not Applicable	

TABLE III TABULATION OF DATA

The recorded data as well as plotted graphs have been included in this report since in an open grid graph it is difficult to locate a point with the same precision that it can be recorded. The tabulated data also shows the effect of rest periods, temperature variations, strain readings with mean load applied, and other data which could not be logically displayed on a graph.

SPECIMEN NO. 3

f (max) = 40KSI A = 0.818 p (max) = 3928 lbs.
freq. = 1600 Cpm Sensors 1 & 2 were 204A-ST

Total No. of Cycles	Sensor 1 u in/in	Sensor 2 u in/in	Room Temp. °F	Remarks
0	11,000	11,000	76	
5,000	12,050	12,490	76	
15,000	12,900	13,620	76	
30,000	13,810	14,600	76	
40,000	14,110	14,860	76	
50,000	14,450	15,110	76	
60,000	14,700	15,270	76	
70,000	14,930	15,420	76	
85,000	15,150	15,550	76	
158,000	16,450	16,260	76	Specimen failed 1/2 inch from ℄ between sensors 1 and 2.

SPECIMEN NO. 5

f(max) = 40KSI, A = 0.818, P(max) = 3940 Lb.
Machine No. 11, Freq = 1600 Cpm
Sensors 1 & 2 were 204A-ST annealed constantan
Sensors 3 & 4 were 204A-ST double annealed constantan

Total No. of Cycles	Sensor 1	Sensor 2	Sensor 3	Sensor 4	Room Temp °F	Remarks
0	11,000	11,000	11,000	11,000	69.5	
10,000	12,990	12,115	13,090	12,410	69	
20,000	13,660	12,470	13,880	12,990	69	
30,000	14,285	12,815	14,610	13,445	69	
46,000	15,020	13,100	15,470	14,300	69	Rdg. taken after specimen failure. 1/2 inch from ℄ towards sensor 1.

SPECIMEN NO. 6

f(max) = 40KSI, A = 0.818, P(max) = 3944 Lb.
Machine No. 11, Freq = 1600 Cpm
Sensors were 204A-ST annealed constantan

Total No. of Cycles	Sensor 1 u in/in	Sensor 2 u in/in	Room Temp °F	Remarks
0	11,000	11,000	73	
5,000	11,560	11,265	73	
10,000	12,390	11,700	72.5	
20,000	13,485	12,270	72.5	
30,000	14,180	12,640	71.0	
40,000	14,675	12,860	70.5	
50,000	15,055	13,035	71	
80,000	15,810	13,510	69.5	
88,000	15,630	13,775	69.5	Rdg. taken after specimen failure. 1/4 inch from ℄ towards sensor 1.

SPECIMEN NO. 7

f(max) = 40 KSI, A = 0.818, P(max) = 3956 Lb.
Machine No. 11, Freq = 1600 Cpm
Sensors were 204A-ST annealed constantan

Total No. of Cycles	Sensor 1 u in/in	Sensor 2 u in/in	Room Temp °F	
0	11,000	11,000	70	
5,000	12,110	11,405	70	
10,000	12,700	11,650	70	
20,000	13,830	12,215	70	
30,000	14,700	12,555	69.5	
40,000	15,300	12,805	69.5	
50,000	15,970	13,080	70	
60,000	16,690	13,240	70	
69,000	17,015	13,090	69.5	Specimen failed, 1/2 inch from ℄ toward sensor 1.

SPECIMEN NO. 8

f(max) = 35KSI, A = 0.818, P(max) = 3444 Lb.
Machine No. 11, Freq = 1575 Cpm
Sensors were 204A-ST annealed constantan

Total No. of Cycles	Sensor 1 u in/in	Sensor 2 u in/in	Room Temp °F	
0	11,000	11,000	70	
10,000	11,500	11,245	70	
21,000	11,830	11,370	70	
40,000	12,110	11,520	70	
83,000	12,550	11,770	68.5	
120,000	12,820	11,840	69	
135,000	12,940	11,870	69	
200,000	13,340	12,035	69	
250,000	14,070	12,165	70	
310,000	15,000	12,250	70.5	
310,000	14,825	12,110	64.5	Rdg. taken 15 hours later.
344,000	15,445	12,255	67	Specimen failed, on center line.

SPECIMEN NO. 10

f(max) = 37.5KSI, A = 0.818
P(max) = 3686 Lb.
Machine No. 12, Freq = 1700 Cpm
Sensors- 204A-ST Type

Total No. of Cycles	Sensor 1 u in/in	Sensor 2 u in/in	Room Temp °F	
0	10,000	10,000	71	
5,000	10,740	10,180	71.5	
10,000	11,200	10,310	71.5	
20,000	11,860	10,610	71.5	
42,000	12,540	10,965	72	
60,000	12,885	11,200	72	
90,000	13,475	11,730	73	
120,000	14,040	12,190	72	
128,000	14,200	12,250	74	
175,000	14,930	12,950	74	
244,000	15,420	12,880	74	Specimen failed, 1/4 inch from ℄ toward sensor 2.

SPECIMEN NO. 12

f(max) = 60KSI, A = +0.333, P(max) = 5946 Lb.
Machine No. 12, Freq = 1700 Cpm
Sensors 1 & 2 were 204A-ST standard type
Sensors 3 & 4 were double annealed 204A-ST

Total No. of Cycles	Sensor 1 u in/in	Sensor 2 u in/in	Sensor 3 u in/in	Sensor 4 u in/in	Room Temp °F	
0	11,000	11,000	11,000	11,000	72	
10,000	11,255	11,200	11,620	11,280	73	
20,000	11,495	11,400	12,100	11,530	73	
30,000	11,670	11,570	12,395	11,710	73	
50,000	11,905	11,820	12,805	11,930	74	
70,000	12,160	12,190	13,200	12,130	74	
100,000	12,420	12,550	13,530	12,280	75	
149,000	13,050	13,970	14,300	12,725	76	Specimen failed, 1/2 inch from ℄ towards sensor 2.

SPECIMEN NO. 13

f(max) = 60KSI, A = +0.333, P(max) = 5946 Lb.
Machine No. 11, Freq = 1650 Cpm
Sensors 1 & 2 were standard 204A-ST
Sensors 3 & 4 were 204DA-ST

Total No. of Cycles	Sensor 1 u in/in	Sensor 2 u in/in	Sensor 3 u in/in	Sensor 4 u in/in	Room Temp °F	
0	11,000	11,000	11,000	11,000	72	
10,000	11,190	11,060	11,705	11,150	71.5	
20,000	11,350	11,130	12,140	11,270	72	
30,000	11,450	11,180	12,380	11,340	72	
50,000	11,670	11,285	12,900	11,500	72	
82,000	11,950	11,360	13,280	11,600	72	
120,000	12,270	11,475	13,715	11,755	73	
127,000	12,530	11,840	13,620	11,840	73	Specimen failed, on ℄. #2 rdg. was off scale when a rdg. was first attempted, however, a close examination of the gage disclosed that a lead wire had broken loose from the gage terminal. This was re-soldered.

SPECIMEN NO. 14

f(max) = 60KSI, A = +0.333, P(max) = 5772 Lb.
Machine No. 11, Freq = 1650 Cpm
Sensors 1 & 2 were standard 204A-ST
Sensors 3 & 4 were 204DA-ST

Total No. of Cycles	Sensor 1 u in/in	Sensor 2 u in/in	Sensor 3 u in/in	Sensor 4 u in/in	Room Temp °F	
0	11,000	11,000	11,000	11,000	72	
10,000	11,185	11,070	11,380	11,185	72	
20,000	11,370	11,210	11,730	11,400	72	
30,000	11,540	11,360	11,970	11,650	72	
50,000	11,760	11,585	12,290	12,090	74	
100,000	12,160	11,850	13,065	12,800	72.5	Specimen failed, 1/2 inch from ℄ toward sensor 2.

SPECIMEN NO. 20

f(max) = 70KSI, P(max) = 6734 Lb.
A = 0.818, Slow Cycle Machine,
Freq = 300 Cpm, Standard 204A-ST,
Sensors

Total No. of Cycles	Sensor 1 u in/in	Sensor 2 u in/in	Room Temp °F	
0	11,000	11,000	75	
5,000	20,410	18,430	77	
13,100	38,060	25,010	77	
13,100	37,990	24,630	62	Rdg. 15 hrs. later.
16,910	38,400	25,580	62	Specimen failed 1/4 inch from ℄ toward sensor 2.

SPECIMEN NO. 21

f(max) = 45KSI, A = 0.818, P(max) = 4347 Lb.
Machine No. 4, Freq = 1925 Cpm, Sensors were
standard 204A-ST and were located conventionally.

Total No. of Cycles	Sensor 1 u in/in	Sensor 2 u in/in	Room Temp °F	
0	11,000	11,000	71.5	
10,000	13,460	12,330	70	
30,000	15,940	14,030	71	
50,000	17,900	15,120	70	
50,000	17,670	14,910	66	Rdg. 63 hrs. after previous rdg.
70,000	20,230	16,090	67	
100,000	21,460	17,235	70	
145,000	26,460	20,550	71	Last rdg's taken after specimen failure. Specimen failed .35 inches from ℄ toward gage 2.

SPECIMEN NO. 22

f(max) = 70KSI, A = 0.818, P(max) = 6769
Slow Cycle Machine, Freq = 300 Cpm,
Instrumented with 204A-ST, conventionally
located.

Total No. of Cycles	Sensor 1 u in/in	Sensor 2 u in/in	Room Temp °F	
0	11,000	11,000	75.5	
5,000	19,425	18,380	71.5	
13,100	32,860	26,060	69	
13,700	31,270	26,270	68.5	Specimen failed, 1/4 inch from ℄ toward sensor 1. Last rdg's taken after specimen failure.

SPECIMEN NO. 24

f(max) = 78KSI, A = 0.818, P(max) = 7540 Lb.
Slow Cycle Machine, Freq = 300 Cpm
Sensors were 204A-ST

Total No. of Cycles	Sensor 1 u in/in	Sensor 2 u in/in	Room Temp °F	
0	11,000	11,000	69.5	
1,000	11,700	11,380	70	
5,000	13,280	12,665	72	
11,000	14,690	14,380	71	
20,000	16,590	LEAD OFF	73.5	
25,000	18,620	↓	74.5	
30,000	21,200		76.5	
35,000	24,060	RECONNECTED	79	
39,695	24,350	18,230	83	Specimen failed through center line. Rdg. taken after failure.

NOTE: Although electrical continuity was accidentally lost, the sensor still accumulates fatigue damage.

SPECIMEN NO. 26

f(max) = 40KSI, A = 0.818, P(max) = 3844 Lb.
Machine No. 11, Date 11-11-65, Freq = 1700 Cpm
Sensor 1 & 2 were standard 204A-ST
Sensor 3 & 4 were S/N NA-01
Used 100 ohm gage as compensating resistor for sensor 3 & 4.

Total No. of Cycles	Sensor 1 u in/in	Sensor 2 u in/in	Sensor 3 u in/in	Sensor 4 u in/in	Room Temp °F	
0	11,000	11,000	11,000	11,000	72.0	
5,000	11,580	11,160	11,800	11,410	70	
16,000	12,780	11,630	13,680	12,410	69	
30,000	13,760	11,970	14,860	13,120	68	
50,000	14,890	12,260	16,020	13,876	67	
60,000	15,540	12,400	16,340	14,080	71	3 & 4 drifting at this rdg.
70,000	16,405	12,535	16,720	14,330	73	
80,000	17,625	12,630	17,490	17,285	71	4 was drifting.
90,000	18,640	12,790	18,010	16,470	72	
110,000	OFF SCALE	13,025	19,160	ERRATIC	71.5	3 drifted slightly.
141,000	↓	16,660	26,290	↓	72	Specimen was overloaded. approx. 200 cycles between 110 & 141 thousand cycles. Overload amount was approx. 20% of maximum load.
182,000		20,000	ERRATIC		72	
195,000						

NOTE: At specimen failure of 195,000 cycles, all leads snapped off.
No readings attempted after specimen failure.

SPECIMEN NO. 28

f(max) = 85KSI, A = 0.818, P(max) = 8236 Lb.
Slow Cycle Machine, Freq = 300 Cpm
Sensor 1 & 2 were 204A-ST
Sensor 3 & 4 were 204A-ST-K

Total No. of Cycles	Sensor 2 u in/in	Sensor 3 u in/in	Sensor 4 u in/in	Room Temp °F	
0	11,000	11,000	11,000	74	
5,000	13,270	13,840	12,420	74	
10,000	14,630	15,470	13,520	74	
15,200	15,870	17,800	14,780	76	
15,700	16,300	18,980	16,400	80	Specimen failed through ℄.
15,700	16,100	18,560	16,090	73	Rdg. taken 16 hrs. later.

NOTE: Sensor 1 damaged prior to installation in fatigue machine, therefore it was not evaluated.

SPECIMEN NO. 29

f(max) = 40KSI, A = 0.818, P(max) = 3836 Lb.
Machine No. 11, Freq = 1700 Cpm
Sensor 1 & 2 were 204A-ST
Sensor 3 was 100 ohm Type NA-01
Sensor 4 was 204A-ST-K

Total No. of Cycles	Sensor 1 u in/in	Sensor 2 u in/in	Sensor 3 u in/in	Sensor 4 u in/in	Room Temp °F	
0	11,000	11,000	11,000	11,000	71	
11,000	12,440	11,600	12,520	11,270	70	
20,000	13,620	12,160	13,810	11,540	70	
30,000	14,340	12,570	14,810	11,755	70.5	
40,000	14,840	LEAD	15,410	11,920	71	
50,000	15,080	BROKEN	16,180	11,990	71	No. 3 drifted slowly.
50,000	15,170	FROM	16,070	12,110	72	Rdg. taken 30 min. later.
70,000	15,770	TAB	ERRATIC	12,345	72	
90,000	16,300		↓	12,595	72	
110,000	16,970			12,745	72	Specimen failure 1/8 inch from ℄ toward sensor 2.

SPECIMEN NO. 31

f(max) = 70KSI, A = 0.333, P(max) = 6741 Lb.
Slow Cycle Machine, Freq = 300 Cpm
Sensor 1 & 2 - Standard 204A-ST

Total No. of Cycles	Sensor 1 u in/in	Sensor 2 u in/in	Room Temp °F	
0	11,000	11,000	77	
5,220	12,240	11,642	77.5	
10,000	12,905	12,065	75	
15,000	13,365	12,500	75	Strain rdg. with mean load applied. No. 2 18,640 micro inches/inch. No. 1 21,200 micro inches/inch.
20,000*	14,420	13,810	75	
25,000	14,155	13,155	76.5	
30,000	14,500	LOOSE	77	
35,000	14,880	↓	78	
40,000	15,190		77	
45,200	15,580		76	
50,000	15,820	WIRE	75	
52,670	15,970	14,810	75	Specimen failed ½ inch from ℄ toward gage 1.
52,670	15,870	14,565	75	Rdg. taken 63 hrs. later.

NOTE: *Reading above may have been taken with some load still in specimen.
Loose wire on No. 2 sensor was re-soldered.

SPECIMEN NO. 32

f(max) = 75KSI, A = 0.333, P(max) = 7267 Lb.
Slow Cycle Machine, Freq = 300 Cpm
Sensor were 204A-ST

Total No. of Cycles	Sensor 1 u in/in	Sensor 2 u in/in	Room Temp °F	
0	11,000	11,000	75	
5,000	11,980	11,560	76	
10,000	12,545	11,875	77	
15,000	13,030	12,135	75	
20,000	13,710	12,420	76	
25,000	14,800	12,730	76	
30,000	16,300	13,010	74	
35,000	18,290	13,390	73	
40,000	20,820	13,750	73	
49,970	LEAD WIRES BROKE	LEAD WIRE BROKE		Specimen failed .8 inch from ℄ toward sensor 1.

SPECIMEN NO. 33

f(Max) = 71.8KSI, A = 0.333, P(Max) = 6918 Lb
Slow Cycle Machine, Freq. = 600 Cpm
Sensors were 204A-ST

Total No. of Cycles	Sensor 1 u in/in	Sensor 2 u in/in	Room Temp °F	
0	11,000	11,000	73	
5,000	11,990	11,520	74	
10,000	12,620	11,860	74	
15,000	13,100	12,140	74	
25,000	13,790	12,520	72	
30,000	14,240	12,760	73	
35,000	14,740	13,060	72.5	
40,000	15,310	13,405	73	
45,000	15,930	13,730	73	
50,000	16,765	14,190	73	
50,090	16,880	14,295	74	SPECIMEN FAILED .25 IN FROM ℄ TOWARD GAGE 1
50,090	16,760	14,140	66	RDG TAKEN 14HRS LATER

SPECIMEN NO. 35

f(Max) = 50KSI, A = 0.333, P(Max) = 4955 Lb
Machine No. 4, Freq = 1900 Cpm
Sensors 1 & 2 were 204DA-ST
Sensors 3 & 4 were HA 204DA-ST

Total No. of Cycles	Sensor #1 u in/in	Sensor #2 u in/in	Sensor #3 u in/in	Sensor #4 u in/in	Room Temp °F	
0	11,000	11,000	11,000	11,000	74	
10,000	11,070	11,055	11,065	11,035	74	
40,000	11,100	11,065	11,080	10,980	72	
180,000	11,285	11,185	11,260	11,045	72	
380,000	11,460	11,265	11,545	11,065	73	
600,000	11,810	11,415	11,930	11,110	70	
600,000	11,820	11,465	11,965	11,185	74	
700,000	12,305	11,595	12,515	11,200	75	
950,000	13,455	11,995	13,290	11,320	77	NOT TAKEN TO FAILURE

Object is to compare the effects of a variation in backings, at a low cyclic strain level.

SPECIMEN NO. 40 - AFTER COMPLETION OF WEATHEROMETRY EXPOSURE
f(max) = 45KSI, A = 0.818, P = 4446 lb
Mach #11, Freq. = 1675 CPM

Sensor	Type
1	204DA-ST
2	204DA-ST
3	MH204DA-ST
4	MH204DA-ST

Sensors were waterproofed with RTV and had teflon lead wires.

Total No. of Cycles	Sensor 1 microstrain	Sensor 2 uin/in	Sensor 3 uin/in	Sensor 4 uin/in	Room Temp °F	
0	11,000	11,000	11,000	11,000	69.5	
5,000	13,050	11,410	12,430	12,320	71	
10,000	13,880	11,605	12,955	12,745	72	
20,000	15,250	12,020	13,960	13,660	74	
30,000	17,050	12,710	15,200	14,775	72	
40,000	18,455	13,295	15,990	15,495	73.5	
42,000	18,710	13,520	15,860	15,510	72	Rdg. after specimen failed through center line.

SPECIMEN NO. 101
Net Area = .0614, f(max) 40SKI
P(max) = 2456 lb: A = 0.818
Machine No. 11; Freq. 1400 CPM
All Sensors 204A-ST

Total No. of Cycles	Sensor 1 uin/in	Sensor 2 uin/in	Sensor 3 uin/in	Sensor 4 uin/in	Room Temp. °F	
0	7,000	7,000	7,000	7,000	82	Rdg. after installation in machine
10,000	8,450	10,210	7,630	9,870	82	
20,000	9,170	11,620	7,980	11,120	82	
30,000	9,580	12,430	8,170	11,790	82	
40,000	10,110	13,580	8,380	12,620	82	
42,000	10,060	17,680	8,350	Open	82	Rdg. after specimen failed. #2 and #4 gages damaged due to failure through center line.

SPECIMEN NO. 38

f(Max) = 60KSI, A = 0.818, P = 5874 Lb
Machine No. 10, Freq = 1575 Cpm

Sensors	Type
1	204A-ST
2	204A-ST
3	204DA-ST
4	EP-03

Total No. of Cycles	Sensor 1 u in/in	Sensor 2 u in/in	Sensor 3 u in/in	Sensor 4 u in/in	Room Temp °F	
0	11,000	11,000	11,000	11,000	71.5	
1,000	13,210	12,020	13,060	12,950	74.5	
5,000	16,330	13,530	15,570	15,180	74.5	
9,000	18,950	15,080	18,130	17,750	74.5	
14,000	21,080	16,680	20,310	19,980	74	
19,000	23,210	18,370	22,830	22,550	74.5	
22,000	24,330	18,780	24,150	23,640	63	TESTING RESUMED 15 HRS LATER
28,000	26,580	20,990	28,050	27,020	63	
37,000						SPECIMEN FAILED AT ¢ NO RDGS TAKEN AFTER SPECIMEN FAILED

SPECIMEN NO. 44

f(Max) = 60KSI, A = 0.818, P = 5772 Lb
Machine No. 4, Freq = 1500 Cpm

Sensors	Type
1	204DA-ST
2	204A-ST
3	NA-01
4	NA-01

Total No. of Cycles	Sensor 1 u in/in	Sensor 2 u in/in	Sensor 3 u in/in	Sensor 4 u in/in	Room Temp °F	
0	11,000	11,000	11,000	11,000	67	
2,000	12,670	11,930	13,200	12,440	67	
5,000	16,340	14,410	18,290	16,050	67	
9,000	19,520	16,260	22,165	19,020	67.5	
9,000	19,420	16,180	21,950	18,860	71	RDG TAKEN 15HRS LATER
14,000	23,360	17,770	24,130	20,555	71	
19,000	27,400	19,680	26,520	22,540	72	
23,000	29,870	20,790	27,840	23,560	72	
28,000	31,920	23,420	29,840	25,240	72	
34,000	34,180	25,670	31,870	26,680	70	
36,000	34,830	27,015	OFF SCALE	26,430	71	SPECIMEN FAILED THROUGH CENTERLINE. RDGS WERE TAKEN AFTER SPECIMEN FAILED

SPECIMEN NO. 45 (Low Temperature Test)

f(Max) = 60KSI, A = 0.818, P = 5772 Lb.
Machine No. 11, Freq. = 1700 C pm
Sensors 1 & 2 were 204A-ST, Sensor 3 was EP-03

Total No. of Cycles	Sensor 1 u in/in	Sensor 2 u in/in	Sensor 3 u in/in	Spec. Temp °F	
0	11,000	11,000	11,000	71	
0	-9,940	-9,910	-9,220	-65	Determination of apparent strain due to temperature.
4,000	12,380	11,650	13,360	-65	204A-ST = 8 u/F°
10,000	15,520	14,090	18,630	-65	EP-03 = 13 u/F°
21,000	18,350	16,440	23,750	-65	Ran out of LN_2 @ 40,000 cycles
80,000	24,950	22,600	35,210	+45	Rdgs were taken after specimen failed through center line at 80,000 cycles.

During continuous cycling from 40,000 cycles to failure, temperature changed linearly from -65°F to +45°F.

SPECIMEN NO. 46 (Low Temperature Test)

f(Max) = 45KSI, A = .818, P = 4464 Lb.
Machine No. 4, Freq. = 2150 C pm
Sensors 1 & 2 were 204A-ST
Sensor 3 was MH204DA-ST
Sensor 4 was 204DA-ST

Total No. of Cycles	Sensor 1 u in/in	Sensor 2 u in/in	Sensor 3 u in/in	Sensor 4 u in/in	Spec. Temp °F	
0	11,000	11,000	11,000	11,000	+75	
0	9,840	10,230	9,930	10,190	-65	T.C.R. check in soft condition.
0	11,000	11,000	11,000	11,000	-65	Readjusted zero reading to 11,000.
5,000	11,630	11,490	11,440	11,470	-65	
11,000	12,080	11,810	11,730	11,740	-65	
20,000	12,710	12,340	12,250	12,200	-65	
30,000	15,370	14,720	14,680	14,270	-65	Rdg with mean load applied strain sensitivity check.

SPECIMEN NO. 46 (CONT'D)

Total No. of Cycles	Sensor 1 u in/in	Sensor 2 u in/in	Sensor 3 u in/in	Sensor 4 u in/in	Spec. Temp °F	
40,000	13,610	12,990	13,000	12,730	-65	
60,000	13,910	13,200	13,250	12,910	-65	
100,000	14,820	13,880	14,080	13,550	-65	
123,000	16,800	15,440	15,980	14,900	+72	Returned to room temp. to obtained T.C.R. after work hardening.
123,000	15,440	14,090	14,370	13,780	-65	
150,000	16,030	13,220	14,900	14,030	-65	
250,000	19,400	14,520	15,760	14,285	-65	Specimen failed through center line.

SPECIMEN NO. 47

f(Max) = 37.5KSI, A = +.818, Area = .0994 $\frac{\text{in}^2}{}$
P(Max) = 3723 Lbs., Machine No. 4, Freq. = 2100 C pm
Sensor No. 3 was an EP-03
Sensors No. 1 and No. 2 were NA-01

Total No. of Cycles	Sensor 1 u in/in	Sensor 2 u in/in	Sensor 3 u in/in	Room Temp °F	
0	7,000	7,000	7,000	75	
10,000	8,300	7,730	8,470	75	
20,000	8,720	7,970	8,970	75	
30,000	9,310	8,300	9,715	75	
40,000	9,480	8,410	10,090	75	
60,000	10,690	9,150	12,100	75	
90,000	11,260	9,510	14,510	71	
110,000	11,780	10,030	17,430	73	
110,000	11,750	10,050	17,300	76	Rdg. taken 4 hrs. later.
140,000	12,800	10,530	24,580	78	Rdg. on Sensor No. 1 drifted downward slightly.
157,000	13,570	10,920	ERRATIC	79	
230,000	OFF SCALE	21,450	ERRATIC	80	No. 2 rdg was erratic.
280,000	OFF SCALE	OFF SCALE	OFF SCALE	78	Rdgs taken 15 hrs after previous rdg.
319,000				78	Specimen failed through ℄

SPECIMEN NO. 48 - TWO LOAD CONDITIONS

1ST CONDITION

(Approx. 50% of total R and of total life at this f and A)

f(Max) = 70KSI, f(Mean) = 38.5KSI
A = +0.818, P(Max) = 6923 Lb.
Machine No. 11, Freq. = 1725 C pm
Sensors 1 & 2 were 204A-ST
Sensors 3 & 4 were 204DA-ST

Total No. of Cycles	Sensor 1 u in/in	Sensor 2 u in/in	Sensor 3 u in/in	Sensor 4 u in/in	Room Temp °F	
0	11,000	11,000	11,000	11,000	77	
1,000	12,520	12,470	12,830	12,730	77	
4,000	14,510	14,350	15,100	14,880	77	
6,000	16,890	16,440	17,410	17,050	77	

2ND CONDITION

f(Max) = 51.3, f(Mean) = 38.5KSI,
A = +0.333 P(Max) = 5073, Machine No. 11,
Freq. = 2100 C pm

0	16,890	16,440	17,410	17,050	77	
4,000	17,200	16,580	17,680	17,200	77	
32,000	17,400	16,640	18,070	17,260	77	
32,000	17,180	16,460	17,920	17,120	71	Rdg. taken 16 hours later
62,000	17,680	16,670	18,510	17,250	71.5	
86,000	17,865	16,830	18,690	17,295	72	Specimen failed 1/2 in. from ℄ toward sensor 2. Rdg. taken after specimen failure

SPECIMEN NO. 49 - TWO LOAD CONDITIONS

1ST CONDITION

(Approx. 10% of the total life at this f & A as determined from base line date, but 50% if compared with sensor reading & cycles)

f(Max) = 51.3KSI, f(Mean) = 38.5KSI,
A = +0.333, P(Max) = 5104 Lb,
Machine #4, Freq. = 1900 C pm
Sensors 1 & 2 were 204A-ST
Sensors 3 & 4 were 204DA-ST

Total No. of Cycles	Sensor 1 u in/in	Sensor 2 u in/in	Sensor 3 u in/in	Sensor 4 u in/in	Room Temp °F
0	11,000	11,000	11,000	11,000	74
20,000	11,130	11,040	11,370	11,110	75
40,000	11,170	11,050	11,520	11,150	74.5
60,000	11,210	11,130	11,610	11,170	74
85,000	11,260	11,190	11,690	11,215	75
110,000	11,320	11,220	11,830	11,260	75

2ND CONDITION

f(Max) = 70KSI, f(Mean) = 38.5KSI,
A = +.818, P(Max) = 6965 Lb.
Machine #4, Freq. = 2200 Cpm

Total No. of Cycles	Sensor 1 u in/in	Sensor 2 u in/in	Sensor 3 u in/in	Sensor 4 u in/in	Room Temp °F	
0	11,230	11,140	11,750	11,165	70	Rdg. taken 19 hrs. after previous rdg.
1,000	14,510	13,450	15,690	13,730	73	
4,000	17,660	15,980	19,310	16,350	72	
4,000	17,660	15,990	19,270	16,370	75.5	Rdg. taken 2 hrs. later
5,000	18,980	16,980	20,730	17,450	76	#1-Off scale with mean LD applied and #3 erratic with mean LD applied
10,000	21,380	18,590	23,100	19,180	77	
14,000	26,640	21,000	27,480	21,810	76	#1 drifted slightly
15,000	30,150	22,310	30,550	23,140	75	
21,000	OFF SCALE	25,380	OFF SCALE	28,860	77	Rdg. taken after specimen failed. Failure plane was .4 inc. from ℄ toward gage. No. 1 Sensor 1 & 3 damaged by failure.

SPECIMEN No. 50 - TWO LOAD CONDITIONS

1ST CONDITION

f(Max) = 70KSI, f(Mean) = 38.5KSI, A = +0.818
P(Max) = 6965 Lb., Machine No. 4, Freq. = 220 C pm
Sensors 1 & 2 were 204A-ST
Sensors 3 & 4 were 204DA-ST

Total No. of Cycles	Sensor 1 u in/in	Sensor 2 u in/in	Sensor 3 u in/in	Sensor 4 u in/in	Room Temp °F	
0	11,000	11,000	11,000	11,000	70	
1,000	15,590	14,700	15,680	14,100	75	
5,000	19,930	20,490	20,150	17,420	75	

2ND CONDITION

f(Max) = 51.3KSI, f(Mean) = 38.5KSI, A = +0.333
P(Max) = 5104, Machine No. 4, Freq. = 1900 C pm

0	19,770	20,420	20,040	17,290	76	New zero reading
2,000	19,800	20,630	20,100	17,320	75.5	
15,000	19,830	20,750	20,240	17,390	75	
80,000	19,930	20,760	20,700	17,560	74	
148,000	20,110	20,770	21,230	18,050	76	Rig. taken after Spec. failed. Spec. failed through ℄

SPECIMEN NO. 52 (Low Temperature Test)

f(Max) = 60KSI, A = 0.818, P = 5,964
Machine No. 4, Freq. = 2,300Cpm
Sensors were 204DA-ST conventionally located.

Total No. of Cycles	Sensor 1 u in/in	Sensor 2 u in/in	Spec. Temp °F	
0	11,000	11,000	+74	
0	9,930	9,840	-65	6 Hr. cold soak-apparent strain or ΔR due to mismatch in T.C.E. of two materials plus T.C.R. of sensor.
0	11,000	11,000	-65	- Adjusted zero's.
10,000	17,940	16,230	-65	
20,000	19,980	18,000	-65	
40,000	22,520	20,295	-65	
60,000	24,035	21,305	-65	
90,000	25,920	22,360	-65	
122,000	28,760	23,180	-65	
142,000	30,830	23,935	-65	
142,000	31,390	24,170	+62	Rdg. 19 Hrs. after previous rdg. at room temp.
142,000	30,890	23,540	-65	Rdg. prior to resuming test after 2 Hrs. cold soak.
170,000	33,180	25,720	-65	
179,000	34,040	LEAD	-65	Spec. failed at 179,000 cycles. One quarter-inch from $\not{c}$ toward sensor #2. Upon failure, lead wires of sensor #2 were snapped off.

SPECIMEN NO. 2A

Area = .2610, P = 2654 Lbs.
Machine No. 2, Freq. = 1700 Cpm
f(Max) ± 10KSI - Net
A = ∝
Sensor 1 and 2 are 204A-ST
Sensor 3 and 4 are 204DA-ST

Total No. of Cycles	Sensor 1 u in/in	Sensor 2 u in/in	Sensor 3 u in/in	Sensor 4 u in/in	Room Temp °F	
0	11,000	11,000	11,000	11,000	80	
31,000	11,000	11,020	11,280	11,240	79	
67,000	11,020	11,080	11,410	11,360	79	
114,000	11,080	11,120	11,490	11,440	80	
114,000	11,080	11,090	11,490	11,440	82	Rdg.17 Hr. later
316,000	11,190	11,210	11,730	11,755	82	
481,000	11,210	11,240	11,860	11,960	82	
544,000	11,180	11,270	11,900	12,060	80	Spec. failed-rdg after spec. failed

SPECIMEN NO. 9A

f(Max) = 20KSI, A = .818, P = 5848 Lbs
Machine No. 4, Freq. = 2375 Cpm

Sensor	Type
1	204A-ST
2	204A-ST
3	204A-ST
4	Shim MTD 204A-ST (Tension)
5	Spiral, 350 Ω, Concentric to Hole

Total No. of Cycles	Sensor 1 u in/in	Sensor 2 u in/in	Sensor 3 u in/in	Sensor 4 u in/in	Sensor 5 u in/in	Room Temp °F	
0	11,000	11,000	11,000	11,000	11,000	80	
83,000	11,000	11,000	11,010	11,010	11,010	80	
1,263,000	12,750	12,940	13,070	13,510	11,870	71	No failure test discontinued.

SPECIMEN NO. 4A

f(Max) = 25KSI, A = 0.818, P(Max) = 6537 Lb
Machine No. 2, Freq. = 1980 Rpm, Area = .2615
Thickness = .0969, Width = 3.000-.296 = 2.704
Sensor Type 204A-ST, K_t = 2.72

Total No. of Cycles	Sensor #1 u in/in	Sensor #2 u in/in	Room Temp °F	
0	5,000	5,000	81.8	A crack appeared on each side of the hole at 25,000 cycles
20,000	5,150	5,270	82.0	
28,000	5,180	5,290	82.0	
32,000	5,230	5,360	82.2	Specimen failed at 32,000 cycles

SPECIMEN NO. 7A

Net Area = .2595, f(Max) = 25KSI, P(Max) = 6487 Lb.
A = .818, Machine No. 12, Freq. = 1900 Rpm K_t = 2.72
Sensor No. 1 & 2 Type 204A-ST, Sensor No. 3 & 4 were located on the opposite side of the specimen from gages 1 & 2 and contained on aluminum foil backing in a pre-stressed tension condition

Total No. of Cycles	Sensor #1 u in/in	Sensor #2 u in/in	Sensor #3 u in/in	Sensor #4 u in/in	Room Temp °F	
0	7,000	7,000	7,000	7,000	70	
10,000	7,055	7,070	6,950	6,950	70	
18,000	7,060	7,070	6,910	6,910	70	A crack on one side of the hole was visible at this time
18,000	7,115	7,090	7,080	6,960	73	Reading taken 2 hours later
29,000	7,145	7,130	7,040	6,920	73	Failure through hole

SPECIMEN NO. 11A

Net area = .2607, f(Max) = 25KSI, P(Max) = 6517 Lb.
A = .818, Machine No. 11, Freq. = 1900 CPM
Sensor #1 & 2 = 208YA Type, Sensor 3 = Compression shim 204A-ST, Sensor 4 = 204A-ST

Total No. of Cycles	Sensor #1 u in/in	Sensor #2 u in/in	Sensor #3 u in/in	Sensor #4 u in/in	Room Temp °F	
0	11,000	11,000	11,000	11,000	76	
10,000	11,015	11,020	11,510*	11,040	76	*Lost bond on compression shim relieving prestrain
20,000	11,060	11,050	11,600	11,060	76	
30,000	11,075	11,070	11,620	11,080	76	
40,000	11,100	11,080	11,650	11,100	76	
44,000	11,170	11,090	11,650	11,135	76	Failed rdgs. taken after rupture

SPECIMEN NO. 10A

f(max) = 25KSI, A = .818, New Area = .2607 IN ^{2}
P(max) = 6517 lb., Machine No. 11 K_t = 2.72

Sensor No.	Type
1	204A-ST
2	204A-ST
3	Spiral Grid Center Hole
4	Spiral Grid Center Hole

Total No. of Cycles	Sensor 1 u in/in	Sensor 2 u in/in	Sensor 3 u in/in	Sensor 4 u in/in	Room Temp. °F	
0	11,000	11,000	11,000	11,000	77	
10,000	11,080	11,030	11,040	11,000	77	
15,000	11,135	11,045	11,140	11,090	77.5	
22,000	11,215	11,060	11,170	11,200	78	
22,000	11,290	11,140	11,180	11,180	79	Rdg. taken 2 hrs later
40,000	11,335	11,220	Open	Open	75*	
50,000	11,400	11,150	Open	Open	74	SPECIMEN FAILED, rdg's. taken after specimen failed

*Crack had formed outward from the hole causing a fracture and electrical discontinuity of the grid strand.

UNCLASSIFIED
Security Classification

DOCUMENT CONTROL DATA - R&D

(Security classification of title, body of abstract and indexing annotation must be entered when the overall report is classified)

1. ORIGINATING ACTIVITY *(Corporate author)*
Lockheed-Georgia Company
86 South Cobb Drive
Marietta, Georgia

2a. REPORT SECURITY CLASSIFICATION
UNCLASSIFIED

2b. GROUP

3. REPORT TITLE
Feasibility Study for the Development of a Fatigue Damage Indicator

4. DESCRIPTIVE NOTES *(Type of report and inclusive dates)*
Final Report

5. AUTHOR(S) *(Last name, first name, initial)*
Horne, Robert S.

6. REPORT DATE
January 1967

7a. TOTAL NO. OF PAGES

7b. NO. OF REFS
17

8a. CONTRACT OR GRANT NO.
AF33(615)-2505

b. PROJECT NO.
1347

c. Task No.
134702

d.

9a. ORIGINATOR'S REPORT NUMBER(S)
AFFDL-TR-66-113

9b. OTHER REPORT NO(S) *(Any other numbers that may be assigned this report)*
ER-7981

10. AVAILABILITY/LIMITATION NOTICES This document is subject to special export controls and each transmittal to foreign governments or foreign nationals may be made only with prior approval of the Air Force Flight Dynamics Laboratory (AFSC) Wright-Patterson Air Force Base, Ohio 45433, ATTN: FDTE.

11. SUPPLEMENTARY NOTES

12. SPONSORING MILITARY ACTIVITY
Air Force Flight Dynamics Laboratory
Wright-Patterson AFB, Ohio 45433

13. ABSTRACT

This report describes a feasibility study for the development of a fatigue damage indicator. Various fatigue sensing elements were evaluated and tested under simulated aerodynamic and environmental conditions. A fatigue sensor was optimized and integrated with an electronic system to function as an aid to fatigue damage assessment of an aircraft structure.

After determining the behavior characteristics of the optimized sensor on laboratory coupons, practical applications were made on C-130E wing panels. The data indicated that a structures degree of exposure to repeated load occurrences could be monitored and the accumulated strain necessary to produce a fatigue failure could be forecast. The electronic phase was designed as the final element of an electro-structural inspection system for determining the fatigue status of an airframe. The electronic hardware consists of a module for an automatic quality control checkout of all detecting elements and module for indicating the sensors change in resistance.

From the results obtained, it can be concluded that the system shows excellent promise as a method for determining the degree of exposure of an aircraft to repeated load occurrences. For "long life" transport aircraft, the system offers a much better means for determining the fatigue status of an airframe than simply stating the number of accumulated flight hours.

DD FORM 1 JAN 64 1473

UNCLASSIFIED
Security Classification

14. KEY WORDS	LINK A		LINK B		LINK C	
	ROLE	WT	ROLE	WT	ROLE	WT
(1) Instrumentation; Fatigue (2) Fatigue Damage Indicator (3) Fatigue Measurement (4) Aircraft Structural Fatigue						

INSTRUCTIONS

1. ORIGINATING ACTIVITY: Enter the name and address of the contractor, subcontractor, grantee, Department of Defense activity or other organization *(corporate author)* issuing the report.

2*a*. REPORT SECURITY CLASSIFICATION: Enter the overall security classification of the report. Indicate whether "Restricted Data" is included. Marking is to be in accordance with appropriate security regulations.

2*b*. GROUP: Automatic downgrading is specified in DoD Directive 5200.10 and Armed Forces Industrial Manual. Enter the group number. Also, when applicable, show that optional markings have been used for Group 3 and Group 4 as authorized.

3. REPORT TITLE: Enter the complete report title in all capital letters. Titles in all cases should be unclassified. If a meaningful title cannot be selected without classification, show title classification in all capitals in parenthesis immediately following the title.

4. DESCRIPTIVE NOTES: If appropriate, enter the type of report, e.g., interim, progress, summary, annual, or final. Give the inclusive dates when a specific reporting period is covered.

5. AUTHOR(S): Enter the name(s) of author(s) as shown on or in the report. Enter last name, first name, middle initial. If military, show rank and branch of service. The name of the principal author is an absolute minimum requirement.

6. REPORT DATE: Enter the date of the report as day, month, year; or month, year. If more than one date appears on the report, use date of publication.

7*a*. TOTAL NUMBER OF PAGES: The total page count should follow normal pagination procedures, i.e., enter the number of pages containing information.

7*b*. NUMBER OF REFERENCES: Enter the total number of references cited in the report.

8*a*. CONTRACT OR GRANT NUMBER: If appropriate, enter the applicable number of the contract or grant under which the report was written.

8*b*, 8*c*, & 8*d*. PROJECT NUMBER: Enter the appropriate military department identification, such as project number, subproject number, system numbers, task number, etc.

9*a*. ORIGINATOR'S REPORT NUMBER(S): Enter the official report number by which the document will be identified and controlled by the originating activity. This number must be unique to this report.

9*b*. OTHER REPORT NUMBER(S): If the report has been assigned any other report numbers *(either by the originator or by the sponsor)*, also enter this number(s).

10. AVAILABILITY/LIMITATION NOTICES: Enter any limitations on further dissemination of the report, other than those imposed by security classification, using standard statements such as:

(1) "Qualified requesters may obtain copies of this report from DDC."

(2) "Foreign announcement and dissemination of this report by DDC is not authorized."

(3) "U. S. Government agencies may obtain copies of this report directly from DDC. Other qualified DDC users shall request through

_____."

(4) "U. S. military agencies may obtain copies of this report directly from DDC. Other qualified users shall request through

_____."

(5) "All distribution of this report is controlled. Qualified DDC users shall request through

_____."

If the report has been furnished to the Office of Technical Services, Department of Commerce, for sale to the public, indicate this fact and enter the price, if known.

11. SUPPLEMENTARY NOTES: Use for additional explanatory notes.

12. SPONSORING MILITARY ACTIVITY: Enter the name of the departmental project office or laboratory sponsoring *(paying for)* the research and development. Include address.

13. ABSTRACT: Enter an abstract giving a brief and factual summary of the document indicative of the report, even though it may also appear elsewhere in the body of the technical report. If additional space is required, a continuation sheet shall be attached.

It is highly desirable that the abstract of classified reports be unclassified. Each paragraph of the abstract shall end with an indication of the military security classification of the information in the paragraph, represented as *(TS)*, *(S)*, *(C)*, *or (U)*.

There is no limitation on the length of the abstract. However, the suggested length is from 150 to 225 words.

14. KEY WORDS: Key words are technically meaningful terms or short phrases that characterize a report and may be used as index entries for cataloging the report. Key words must be selected so that no security classification is required. Identifiers, such as equipment model designation, trade name, military project code name, geographic location, may be used as key words but will be followed by an indication of technical context. The assignment of links, rules, and weights is optional.